The Role of Histone 3 Lysine 27 Trimethylation in Thymic Epithelial Cell Development and Function



Annina N. Grädel
Lincoln College
University of Oxford

A thesis submitted for the degree of
Doctor of Philosophy

Trinity 2018

Acknowledgements

Above all, I would like to thank my supervisor, Professor Georg Holländer, for his invaluable support and guidance throughout my DPhil. I am infinitely grateful to Georg for his wisdom, inspiration and encouragement. Many thanks also go to my co-supervisor Professor Christopher Schofield for supporting me with his expertise in epigenetics.

Many people have helped me with my thesis research over the last four years. I am especially grateful to Michael Morgan for the bioinformatics analysis of the sequencing data sets, and Ioanna Rota and Wei Wu for their assistance with experiments. Additionally, I thank Mary Deadman, Stefano Maio, Bergithe Oftedal, Fatima Dhalla, Kathrin Jansen, Adam Handel, Eleni Adamopoulou, Hector Barbosa and Emma Haberman for their advice and practical help in the laboratory, and Hong Ying Teh and Thomas Barthlott for their remote counsel from Basel. I want to acknowledge all the lab members of the Developmental Immunology Group, for being such a friendly and supportive bunch.

Many thanks go to Nadine, Carole, Ioanna, Almut, Lena and Giles for their incredible support and help with proofreading. A special thanks and a lot of gratitude goes to Carole and Nadine for all their invaluable help with typesetting this thesis.

A DPhil is a long journey, I am incredibly grateful to all my friends that have accompanied me along the way – with distraction, coffees, laughs and love: Carole, Lena, Nadine, Francesco, Giles, Maria, Almut, Leila, Elise, Derya, Ioanna, Alexandros, Eleni, Bernadette, Christoph and Jeremias.

I dedicate this thesis to my family, my parents, Claudia and Christoph, my sisters, Nadine, Lena and Carole, and my partner, Giles. Thanks to you everything is possible.

Abstract

Thymic epithelial cells (TEC) create the unique environment for the selection of T cells that are tolerant to self but reactive to foreign antigens. For this purpose, TEC express an almost comprehensive repertoire of self-antigens, through a process referred to as promiscuous gene expression (PGE). The precise molecular mechanisms that account for PGE remain incompletely defined although a subset of promiscuously expressed genes rely for their efficient expression on the presence of the Autoimmune Regulator (AIRE). This transcriptional facilitator preferentially controls the expression of genes that display the repressive histone mark H3K27me3 at their transcriptional start sites.

To address the question whether alterations in the H3K27me3 landscape influence TEC biology, mice with a TEC-specific loss of the H3K27me3 demethylases UTX and JMJD3 were generated. These mice demonstrated that a deficiency in UTX and JMJD3 reduced the frequency of immature medullary TEC (mTEC), while increasing the frequency of mature mTEC. Although the resulting gene expression changes were limited, AIRE-regulated genes were strongly enriched within the upregulated genes, supporting the hypothesis that H3K27me3 modifications serve as recognition marks for AIRE-regulated PGE. Placement of H3K27me3 marks is mediated by the polycomb repressive complex 2 (PRC2), which gets recruited to its target genes by cofactor JARID2. Mice with a TEC-specific deficiency of JARID2 were also generated and investigated. Despite its seemingly different functional role, a JARID2 deficiency had a similar impact on the mTEC phenotype as a loss of H3K27me3 demethylases UTX and JMJD3. The altered TEC compartment of both experimental animal models further altered the frequency of thymocytes undergoing negative selection in the medulla and mildly decreased the generation of single positive thymocytes. Taken together, this work shows that a TEC-specific loss of epigenetic modifiers of H3K27 methylation impacts on TEC differentiation and function.

Contents

List of Figures **ix**

List of Tables **xiii**

List of Abbreviations **xiv**

1 Introduction **1**

1.1 The immune system . . . 1

1.1.1 The innate immune system . . . 2

1.1.2 The adaptive immune system . . . 2

1.1.3 Disorders of the immune system . . . 4

1.2 The thymus . . . 4

1.2.1 Thymus Organogenesis . . . 4

1.2.2 T cell development in the thymus . . . 6

1.2.3 Thymic stroma . . . 8

1.2.4 Promiscuous gene expression (PGE) . . . 9

1.3 Introduction to epigenetic mechanisms . . . 11

1.3.1 Histone modifications and their consequences . . . 12

1.3.2 Lysine residue 27 of histone H3 (H3K27) methylation . . . 13

1.4 Epigenetic mechanisms in the regulation of PGE . . . 15

1.5 Hypothesis and Aims . . . 16

2 Materials and Methods **18**

2.1 Mice . . . 18

2.1.1 UTX and JMJD3 conditional knockout mice . . . 18

2.1.2 JARID2 conditional knockout mice . . . 19

2.2 Standard reagents . . . 19

2.3 Genotyping . . . 19

2.3.1 Extraction and amplification of genomic DNA . . . 19

2.3.2 Agarose gel electrophoresis . . . 21

2.4 Flow cytometry . . . 22

2.4.1 Cell preparation . . . 22

2.4.2 Staining for flow cytometry . . . 22

2.4.3 TNFα production assay 24
2.5 Immunofluorescence microscopy 25
2.6 RNA methods 25
2.6.1 RNA extraction and cDNA conversion 25
2.6.2 Real time quantitative PCR (qPCR) analysis 25
2.6.3 Reverse transcription PCR (RT-PCR) analysis 26
2.6.4 Bulk and single cell RNA sequencing (RNA-Seq) 27
2.7 ChIP-qPCR for histone marks 28
2.8 T cell receptor excision circles (TREC) assay 29
2.9 Statistical analysis 29
2.10 Analysis of sequencing data 30
2.10.1 Bulk RNA-Seq analysis 30
2.10.2 Tissue specificity 31
2.10.3 Histone ChIP-Seq analysis 31
2.10.4 Single cell RNA-Seq analysis 31

3 The role of the H3K27me3 demethylases UTX and JMJD3 in TEC biology 33
3.1 Introduction 33
3.2 *Utx*, *Jmjd3* and *Uty* mRNA expression in TEC 35
3.3 Mouse model with a TEC-specific KO of UTX and JMJD3 37
3.4 TEC with targeted UTX and JMJD3 deficiency 38
3.4.1 Loss of UTX and JMJD3 does not affect thymus cellularity or architecture 38
3.4.2 Loss of UTX and JMJD3 affects cTEC to mTEC ratio, mTEC maturation and AIRE expression levels 41
3.4.3 UTX- and JMJD3-deficient cTEC and mTEC^{hi} proliferate less . . 44
3.4.4 Brief summary of UTX- and JMJD3-deficient TEC 45
3.5 Transcriptional changes in mTEC^{hi} lacking UTX and JMJD3 47
3.5.1 952 genes are differentially expressed in mTEC^{hi} in the absence of UTX and JMJD3 47
3.5.2 Genes upregulated in UTX/JMJD3-deficient mTEC^{hi} are enriched for genes enhanced in their expression in the presence of AIRE . . 50
3.5.3 The expression of mTEC-specific NFκB signaling genes are unchanged in UTX/JMJD3-deficient mTEC^{hi} 52
3.5.4 Histone landscape of differentially expressed genes 53
3.5.5 Relationship of H3K27me3 marks in promoter with expression frequency and average expression levels in mTEC^{hi} 54
3.5.6 Brief summary of the RNA-Seq analysis of mTEC^{hi} from *Utx*$^{TEC-/-}$ *Jmjd3*$^{TEC-/-}$ mice 58

3.6 H3K27me3 landscape in TEC with a loss of JMJD3 and UTX 59
3.6.1 Absence of global changes in H3K27me3 marks in UTX- and JMJD3-deficient TEC 59
3.6.2 Feasibility of H3K27me3 ChIP on 10 000 mTEC^{hi} 59
3.6.3 ChIP-qPCR reveals increase in H3K27me3 levels at one gene up-regulated in UTX/JMJD3-deficient mTEC^{hi} 64
3.6.4 Brief summary of H3K27me3 ChIP in *Utx$^{TEC-/-}$ Jmjd3$^{TEC-/-}$* mTEC^{hi} 66
3.7 Thymocyte development in *Utx$^{TEC-/-}$ Jmjd3$^{TEC-/-}$* mice 66
3.7.1 Early thymocyte development and positive selection are unchanged in *Utx$^{TEC-/-}$ Jmjd3$^{TEC-/-}$* mice 66
3.7.2 TCRβ^{hi} thymocytes are reduced in *Utx$^{TEC-/-}$ Jmjd3$^{TEC-/-}$* thymi . 71
3.7.3 Semimature and mature SPCD8 are reduced in *Utx$^{TEC-/-}$ Jmjd3$^{TEC-/-}$* thymi 71
3.7.4 Negative selection is impaired in *Utx$^{TEC-/-}$ Jmjd3$^{TEC-/-}$* thymi . . 78
3.7.5 The generation of thymic T_{reg} cells is unaffected in the *Utx$^{TEC-/-}$ Jmjd3$^{TEC-/-}$* mice 84
3.7.6 Brief summary of thymocyte development in *Utx$^{TEC-/-}$ Jmjd3$^{TEC-/-}$* mice 87
3.8 Peripheral T cell compartment in *Utx$^{TEC-/-}$ Jmjd3$^{TEC-/-}$* mice 89
3.8.1 $CD8^+$ T cells are skewed towards memory phenotype in *Utx$^{TEC-/-}$ Jmjd3$^{TEC-/-}$* mice 90
3.8.2 Recent thymic emigrants in *Utx$^{TEC-/-}$ Jmjd3$^{TEC-/-}$* mice 92
3.8.3 Peripheral T_{reg} cells are unchanged in *Utx$^{TEC-/-}$ Jmjd3$^{TEC-/-}$* mice 94
3.8.4 Unchanged frequency of anergic $CD4^+$ T cells in *Utx$^{TEC-/-}$ Jmjd3$^{TEC-/-}$* 96
3.8.5 Brief summary of peripheral T cells in *Utx$^{TEC-/-}$ Jmjd3$^{TEC-/-}$* mice 97
3.9 Summary of the *Utx$^{TEC-/-}$ Jmjd3$^{TEC-/-}$* mouse model 98
3.10 Discussion 99
3.10.1 The role of UTX and JMJD3 in TEC development and maturation 101
3.10.2 The role of UTX and JMJD3 for AIRE-regulated PGE 102
3.10.3 H3K27me3 and PGE 103
3.10.4 Demethylase-independent functions of UTX and JMJD3 in the context of PGE 104
3.10.5 Conclusion 105

4 The individual roles of UTX, JMJD3 and UTY in TEC biology 106
4.1 Introduction 106
4.2 *Utx$^{TEC-/-}$*, *Jmjd3$^{TEC-/-}$* and male *Utx$^{TEC-/Y}$ Jmjd3$^{TEC-/-}$* mice 107
4.3 UTX- or JMJD3-single-deficient and male double-deficient TEC 109
4.4 Transcriptional changes in mTEC^{hi} from *Utx$^{TEC-/-}$*, *Jmjd3$^{TEC-/-}$* and male *Utx$^{TEC-/Y}$ Jmjd3$^{TEC-/-}$* mice 113

4.5 Thymocytes in *Utx*$^{TEC-/-}$, *Jmjd3*$^{TEC-/-}$ and male *Utx*$^{TEC-/Y}$ *Jmjd3*$^{TEC-/-}$ mice . . . 116
4.5.1 Changes in negative selection are mainly caused by UTX deficiency 117
4.6 Peripheral T cells in *Utx*$^{TEC-/-}$, *Jmjd3*$^{TEC-/-}$ and male *Utx*$^{TEC-/Y}$ *Jmjd3*$^{TEC-/-}$ mice . . . 120
4.7 Summary . . . 120
4.8 Discussion . . . 122

5 The role of JARID2 in TEC biology 126
5.1 Introduction . . . 126
5.2 Mouse model with a targeted loss of JARID2 expression . . . 127
5.2.1 Genomic excision of exon 3 of *Jarid2* . . . 127
5.2.2 *Jarid2* RNA expression . . . 128
5.2.3 *Jarid2* transcript variants . . . 130
5.2.4 The conditional *Jarid2* locus does not affect thymus biology . . . 131
5.3 TEC with a deficiency in JARID2 . . . 137
5.3.1 Loss of JARID2 in TEC does not affect thymus cellularity and architecture at 5 weeks of age . . . 137
5.3.2 Loss of JARID2 affects mTEC maturation and AIRE expression levels . . . 137
5.3.3 MHC-I expression is increased in JARID2-deficient mTEC . . . 139
5.3.4 Global H3K27me3 and H3K9me3 levels are unchanged in JARID2-deficient TEC . . . 142
5.3.5 Reduced total thymus cellularity and reduced mTEC cellularity at 16-18 weeks of age . . . 144
5.3.6 Brief summary of JARID2-deficient TEC . . . 146
5.4 Thymocyte development in *Jarid2*$^{TEC-/-}$ mice . . . 146
5.4.1 mSPCD8 are reduced in *Jarid2*$^{TEC-/-}$ mice . . . 147
5.4.2 Positive selection is unaffected . . . 147
5.4.3 Post selection maturation reveals partial block at DP^{dull} to immature SPCD8 stage . . . 149
5.4.4 Post selection maturation using MHC-I and CD69 expression confirms an equal reduction of SPCD8 across all their medullary developmental stages . . . 152
5.4.5 TNFα licensing of SPCD8 is unchanged . . . 155
5.4.6 Medullary negative selection is increased in *Jarid2*$^{TEC-/-}$ affecting both SPCD4 and SPCD8 thymocytes. . . . 158
5.4.7 T_{reg} cell generation in the thymus is unaltered, but there are more ICOS^{+} CD103^{+} cells within the recirculating T_{reg} cell population . 161
5.5 The peripheral T cell compartment in *Jarid2*$^{TEC-/-}$ mice . . . 164

5.5.1 Reduction in $CD8^+$ T cells in the lymph nodes of mice with a TEC-specific JARID2 KO . . . 167
5.5.2 $CD103^+$ $ICOS^+$ T_{reg} cells are unchanged in the periphery . . . 168
5.5.3 Fewer peripheral T cells in aged *Jarid2*$^{TEC-/-}$ mice . . . 168
5.6 Summary . . . 171
5.7 Discussion . . . 174
5.7.1 JARID2 as a negative regulator of mTEC maturation . . . 176
5.7.2 Negative selection is increased in *Jarid2*$^{TEC-/-}$ mice . . . 178
5.7.3 Conclusion . . . 179

6 Conclusions and Future Work **180**
6.1 Conclusions . . . 180
6.2 Future Work . . . 182
6.2.1 H3K27me3 ChIP-Seq in UTX/JMJD3-deficient TEC . . . 183
6.2.2 Transcriptomic analysis of TEC lacking JARID2 expression . . . 183
6.2.3 Assessment of changed central tolerance . . . 184
6.3 Final Remarks . . . 185

References **186**

A Appendix **200**

List of Figures

1.1 Schematic of thymus organogenesis 5
1.2 Schematic of T cell development in the thymus 6
1.3 Illustration of chromatin organization in the cell and the structure of a nucleosome 12
1.4 Illustration of histone methylation landscape at active (A) and inactive (B) genes 13
1.5 H3K27me3 is regulated by methyltransferase PRC2 and the demethylases UTX and JMJD3 14

3.1 Schematic representation of UTX, JMJD3 and UTY 34
3.2 *Utx*, *Jmjd3* and *Uty* mRNA expression in TEC subpopulations and in peripheral tissues 36
3.3 Schematic representation of genomic targeting to generate TEC-specific deletions of UTX and JMJD3 38
3.4 Efficient Foxn1-Cre driven genomic excision of floxed exons in TEC of $Utx^{TEC-/-}$ $Jmjd3^{TEC-/-}$ mice 39
3.5 Cellularity and architecture of $Utx^{TEC-/-}$ $Jmjd3^{TEC-/-}$ thymi is normal. . . 40
3.6 Unchanged TEC cellularity in $Utx^{TEC-/-}$ $Jmjd3^{TEC-/-}$ thymi. 40
3.7 Scheme of TEC maturation 41
3.8 Frequency of mature mTEC is increased in mice with TEC-targeted loss of UTX/JMJD3 expression 44
3.9 Increased MHC-I expression in UTX/JMJD3-deficient cTEC. 45
3.10 UTX- and JMJD3-deficient cTEC and $AIRE^{+}$ $mTEC^{hi}$ proliferate less. . 46
3.11 Clustering of $Utx^{TEC-/-}$ $Jmjd3^{TEC-/-}$ and WT $mTEC^{hi}$ 48
3.12 UTX/JMJD3 double deficiency causes gene expression changes of small amplitude in $mTEC^{hi}$. 49
3.13 Gene ontology analysis of downregulated (A) and upregulated genes (B). . 49
3.14 Enrichment of TRA in differentially expressed genes. 50
3.15 Enrichment of TRA in differentially expressed genes. 51
3.16 Enrichment of AIRE-enhanced genes is specific to upregulated genes. . . . 52
3.17 Genes upregulated in UTX/JMJD3-deficient $mTEC^{hi}$ are marked with higher levels of H3K27me3. 54

3.18 H3K27me3 levels are negatively correlated with expression frequency, but positively correlated with average expression. 55
3.19 Relationship of H3K27me3 levels with expression frequency and average expression of AIRE-dependent, -enhanced and -independent genes. 56
3.20 Relationship of H3K27me3 levels with expression frequency and average expression of genes up- or downregulated in UTX/JMJD3-deficient mTEC^{hi}. 57
3.21 Unchanged H3K27me3 levels in UTX/JMJD3-deficient TEC. 60
3.22 H3K27me3 ChIP on low input mTEC^{hi} samples. 62
3.23 Chromatin shearing optimisation and ChIP-PCR on 10k mTEC^{hi}. 63
3.24 H3K27me3 ChIP-qPCR on UTX/JMJD3-deficient mTEC^{hi}. 65
3.25 *Utx*$^{TEC-/-}$ *Jmjd3*$^{TEC-/-}$ thymi support normal early thymocyte development. 68
3.26 Scheme of progression of thymocytes through DN stages and subsequent positive selection. 69
3.27 Unchanged positive selection in *Utx*$^{TEC-/-}$ *Jmjd3*$^{TEC-/-}$ mice 70
3.28 Lower frequency of TCRβ^{hi} thymocytes in *Utx*$^{TEC-/-}$ *Jmjd3*$^{TEC-/-}$ mice. . 72
3.29 Post selection maturation of the SPCD8 and SPCD4 lineage according to the expression of TCRβ, CCR7, CD24 and CD69. 73
3.30 Lower frequency of semimature and mature SPCD8 in *Utx*$^{TEC-/-}$ *Jmjd3*$^{TEC-/-}$ mice 75
3.31 Unchanged maturation of SPCD4 in *Utx*$^{TEC-/-}$ *Jmjd3*$^{TEC-/-}$ mice 76
3.32 Post selectional maturation defined by cell surface expression of MHC-I and CD69. 77
3.33 Lower frequency of SM and higher frequency of M1 in SPCD4 maturation in *Utx*$^{TEC-/-}$ *Jmjd3*$^{TEC-/-}$ mice. 80
3.34 Schematic of thymocyte negative selection. 81
3.35 Decreased cortical negative selection and early medullary negative selection, increased late negative selection in *Utx*$^{TEC-/-}$ *Jmjd3*$^{TEC-/-}$ mice. 83
3.36 Increased frequency of ICOS^{+}CD103^{+} T$_{reg}$ cells in the thymus. 86
3.37 Scheme of intrathymic T$_{reg}$ cell generation and recirculation of peripheral T$_{reg}$ cells. 87
3.38 Frequency of recirculating T$_{reg}$ cells is unchanged, however there are more ICOS^{+} CD103^{+} cells within recirculating T$_{reg}$ cells. 88
3.39 Cellularity of spleen and lymph nodes is unchanged in *Utx*$^{TEC-/-}$ *Jmjd3*$^{TEC-/-}$ mice. 90
3.40 Splenic CD8^{+} towards a memory phenotype in *Utx*$^{TEC-/-}$ *Jmjd3*$^{TEC-/-}$. . . 91
3.41 The frequency of RTE is comparable for WT and *Utx*$^{TEC-/-}$ *Jmjd3*$^{TEC-/-}$ mice. 93
3.42 TREC in naïve CD4 and CD8 T cells from *Utx*$^{TEC-/-}$ *Jmjd3*$^{TEC-/-}$ mice. 94
3.43 Normal frequency and phenotype of T$_{reg}$ cells in lymph nodes of *Utx*$^{TEC-/-}$ *Jmjd3*$^{TEC-/-}$ mice. 95

3.44 Normal frequency and phenotype of T_{reg} cells in the spleen of *Utx*$^{TEC-/-}$ *Jmjd3*$^{TEC-/-}$ mice. 96
3.45 The frequency of anergic CD4$^+$ T cells are unchanged in lymph nodes in *Utx*$^{TEC-/-}$ *Jmjd3*$^{TEC-/-}$ mice. 97

4.1 Single deficiency in UTX and JMJD3 does not lead to a change in the expression levels of the other demethylase 108
4.2 *Uty* expression was unchanged in male TEC with a double deficiency in UTX and JMJD3 108
4.3 TEC differentiation and maturation are altered in mice with a TEC-targeted single deficiency of UTX and JMJD3 expression 111
4.4 TEC differentiation and maturation are altered in male mice with a TEC-targeted deficiency of UTX and JMJD3 expression 112
4.5 Differential gene expression assessed by qPCR in mTEC^{hi} from female *Utx*$^{TEC-/-}$ *Jmjd3*$^{TEC-/-}$, *Utx*$^{TEC-/-}$ and *Jmjd3*$^{TEC-/-}$ mice. 114
4.6 Differential gene expression assessed by qPCR in mTEC^{hi} from male *Utx*$^{TEC-/Y}$ *Jmjd3*$^{TEC-/-}$ mice. 115
4.7 Cortical negative selection in *Utx*$^{TEC-/-}$, *Jmjd3*$^{TEC-/-}$ and male *Utx*$^{TEC-/Y}$ *Jmjd3*$^{TEC-/-}$ mice. 118
4.8 Medullary negative selection in *Utx*$^{TEC-/-}$, *Jmjd3*$^{TEC-/-}$ and male *Utx*$^{TEC-/Y}$ *Jmjd3*$^{TEC-/-}$ mice. 119
4.9 CD8$^+$ T cells in the spleen are skewed towards memory phenotype in *Utx*$^{TEC-/-}$, but not in *Jmjd3*$^{TEC-/-}$ mice, and can be rescued in male mice . 121

5.1 Schematic representation of gene construct to generate a TEC-specific JARID2 KO 128
5.2 Efficient genomic excision in *Jarid2*$^{TEC-/-}$ TEC 129
5.3 *Jarid2* transcripts without exon 3 are expressed in TEC isolated from *Jarid2*$^{TEC-/-}$ mice 129
5.4 Transcript variants of *Jarid2* in TEC 130
5.5 No alternative *Jarid2* transcripts detected in WT and KO TEC 131
5.6 Total thymus and TEC cellularity is comparable between *Jarid2*$^{wt/wt}$ and *Jarid2*$^{fl/fl}$ 132
5.7 mTEC maturation is comparable between *Jarid2*$^{wt/wt}$ and *Jarid2*$^{fl/fl}$ . . . 133
5.8 Thymocyte maturation is comparable between *Jarid2*$^{wt/wt}$ and *Jarid2*$^{fl/fl}$. 134
5.9 Positive selection and the frequency of CD25$^+$ SPCD4 are comparable between *Jarid2*$^{wt/wt}$ and *Jarid2*$^{fl/fl}$ 135
5.10 Splenic T cells are comparable between *Jarid2*$^{wt/wt}$ and *Jarid2*$^{fl/fl}$ 136
5.11 Normal total cellularity and architecture of the thymus with a TEC-specific loss of JARID2. 138

5.12 TEC cellularity is comparable between WT, *Jarid2*$^{TEC-/-}$ and *Jarid2*$^{wt/TEC-}$ mice. 139
5.13 mTEC maturation is altered in JARID2-deficient TEC. 141
5.14 Decreased MHC-I expression in JARID2-deficient mTEC. 142
5.15 Unchanged global H3K27me3 and H3K9me3 levels in JARID2-deficient TEC. 143
5.16 Thymic cellularity reduced at 16-18 weeks of age. 144
5.17 mTEC cellularity is reduced at 16-18 weeks of age. 145
5.18 Reduction of mSPCD8 in thymi with TEC lacking JARID2. 148
5.19 Reduction of SPCD8 in post selection stages in *Jarid2*$^{TEC-/-}$ mice. 150
5.20 Lower frequency of TCRβ^{hi} cells due to reduced TCRβ^{hi} SPCD8 thymocytes in *Jarid2*$^{TEC-/-}$ mice. 151
5.21 Partial maturational block in the progression of thymocytes from DP^{dull} to immature CD8 stage in *Jarid2*$^{TEC-/-}$ mice. 153
5.22 Unchanged maturation of SPCD4 in *Jarid2*$^{TEC-/-}$ mice. 154
5.23 The Frequency of CD8 SM, M1 and M2 stages is reduced in *Jarid2*$^{TEC-/-}$ mice 157
5.24 Expression of selected genes relevant for late stage thymocyte maturation and thymic egress were unchanged in *Jarid2*$^{TEC-/-}$ mice 158
5.25 M1 and M2 SPCD8 educated on TEC with JARID2 KO are able to produce TNFα upon stimulation 159
5.26 M2 SPCD4 educated on TEC with JARID2 KO are able to produce more TNFα upon stimulation 160
5.27 Frequency of negatively selected cells in medullary wave 2 is increased in *Jarid2*$^{TEC-/-}$ mice 163
5.28 Gating strategy for identifying newly generated and recirculating T_{reg} cells 165
5.29 Increased population of ICOS^{+} CD103^{+} recirculating T_{reg} cells in the thymus of *Jarid2*$^{TEC-/-}$ mice 166
5.30 Cellularity of lymph nodes and spleen are unchanged in *Jarid2*$^{TEC-/-}$ mice 167
5.31 Changed ratio of CD4^{+} to CD8^{+} T cells in the periphery of *Jarid2*$^{TEC-/-}$ mice 169
5.32 Small reduction in the frequency of T_{reg} cells within the pool of peripheral CD4^{+} T cells in *Jarid2*$^{TEC-/-}$ mice 170
5.33 T cells are reduced in lymph nodes of 16-18 week old *Jarid2*$^{TEC-/-}$ mice . 172
5.34 The frequency of T_{reg} cells in lymph nodes of 16-18 week old WT and *Jarid2*$^{TEC-/-}$ mice is comparable 173

6.1 Hypothetical role of H3K27me3 in targeting or stabilising the AIRE protein complex 182

A.1 Basic gating strategies. 202

List of Tables

2.1 Composition of standard reagents. 20
2.2 List of primers for genotyping 21
2.3 Thermocycler condition for amplifying genomic DNA 21
2.4 Antibodies and lectin for flow cytometry 24
2.5 List of primers for qPCR and RT-PCR 27
2.6 Primers used for ChIP qPCR 28
2.7 Reagents for TREC assay 29

3.1 Gene expression in WT and UTX/JMJD3-deficient mTEC^{hi} 53

4.1 Summary of TEC phenotypic changes as a result of an absence of UTX, JMJD3 and/or UTY expression 113
4.2 Summary of gene expression changes 116
4.3 Summary of changes caused by a TEC-specific deficiency of UTX and JMJD3123

5.1 Summary of changes caused by a TEC-specific loss of UTX/JMJD3 compared to a TEC-targeted loss of JARID2 174

List of Abbreviations

AIRE . . . . . Autoimmune Regulator

APC . . . . . Antigen Presenting Cells

CCL # . . . . . CC-chemokine ligand #

ChIP . . . . . Chromatin Immunoprecipitation

CMJ . . . . . Corticomedullary Junction

cTEC . . . . . Cortical Thymic Epithelial Cells

DC . . . . . Dendritic Cells

dKO . . . . . Double Knockout

DN . . . . . Double Negative

DNA . . . . . Deoxyribonucleic Acid

DP . . . . . Double Positive

E # . . . . . Embryonic Day #

EED . . . . . Embryonic Ectoderm Development

EpCAM . . . . Epithelial cell adhesion molecule

ETP . . . . . Early T Lineage Progenitor

EZH2 . . . . . Enhancer of Zeste Homolog 2

fl or floxed . . . Flanked by LoxP Sites

gMFI . . . . . Geometric Mean Fluorescent Intensity

H3K# . . . . . Lysine at position # of histone 3

iNKT cell . . . Invariant Natural Killer T Cell

JARID2 . . . . Jumonji And AT-Rich Interaction Domain Containing 2

JMJD3 . . . . . Jumonji domain-containing protein 3

K # . . . . . Cytokeratin #

KO . . . . . Knockout

MHC . . . . . Major Histocompatibility Complex

mRNA . . . . . Messenger Ribonucleic Acid

mTEC . . . . . Medullary Thymic Epithelial Cells

PCR . . . . . Polymerase Chain Reaction

pMHC . . . . . Peptide Major Histocompatibility Complex

PGE . . . . . Promiscuous Gene Expression

PHD . . . . . Plant Homeodomain

PRC2 . . . . . Polycomb Repressive Complex 2

PTM . . . . . Post-Translational Modification

qPCR . . . . . Quantitative real-time PCR

RAG . . . . . Recombination Activating Gene

RNA . . . . . Ribonucleic Acid

S1PR1 . . . . . Sphingosine-1 Phosphate Receptor-1

SP . . . . . Single Positive

SUZ12 . . . . . Suppressor of Zeste 12

TCR . . . . . T-Cell Receptor

TEC . . . . . Thymic Epithelial Cells

TPR . . . . . Tetratricopeptide Repeats

TRA . . . . . Tissue-Restricted Antigen

T_{reg} cell . . . . Regulatory T cell

TSS . . . . . Transcriptional Start Site

UEA . . . . . *Ulex europaeus* agglutinin

UTX . . . . . Ubiquitously transcribed Tetratricopeptide repeat, X chromosome

UTY . . . . . Ubiquitously transcribed Tetratricopeptide repeat, Y chromosome

WT . . . . . Wild Type

Iubet igitur nos [...] noscere nosmet ipsos.

— M. T. Cicero

1 Introduction

Contents

1.1 The immune system 1
1.2 The thymus 4
1.3 Introduction to epigenetic mechanisms 11
1.4 Epigenetic mechanisms in the regulation of PGE 15
1.5 Hypothesis and Aims 16

1.1 The immune system

The immune system is the body's defence against disease. Apart from recognising and fighting microorganisms such as bacteria, viruses, parasites and fungi, it also mounts a response against foreign substances such as toxins and neoplastic cells. The immune system is made up of many different organs, tissues and cell types that work together to carefully orchestrate a defence reaction to eliminate harmful elements while minimising damage to the own body. It can broadly be divided into two branches, called innate and adaptive immunity.

1.1.1 The innate immune system

The innate immune system is evolutionarily ancient and is present in some form in all multicellular organisms [1]. The first line of defence of the innate immune system is the mechanical barrier provided by the skin and mucosal membranes that prevent pathogens from entering the body. The innate immune response triggered by pathogens that have bypassed the physical barrier involves different cellular components such as macrophages, granulocytes and natural killer cells, and humoral factors such as the complement system and interleukines. The innate immune system relies on a set of germline-encoded pattern recognition receptors to recognise pathogens through their key characteristics that set them apart from cells of the own body, for example double-stranded viral RNA or saccharide surface structures unique to bacteria [2, 3]. The innate immune system is extremely quick and reliably clears most infections.

The limitation of the innate immune system is the restricted number of germline-encoded receptors. Pathogens can evolve quickly and acquire strategies to evade the immune response, for example by changing their surface antigens to avoid detection by pattern recognition receptors.

1.1.2 The adaptive immune system

The adaptive immune system evolved later than the innate immune system and is found only in vertebrates [4]. Its main components are B and T lymphocytes (called B and T cells), which maximise their capacity to recognise different pathogens by using gene rearrangement processes to generate their receptors [5]. This process has the potential to create a sheer endless number of antigen receptors with different binding specificities thus allowing a reaction against any foreign entity [6]. The adaptive immune response is characterised by the clonal expansion of cells that have a receptor that is highly specific to the pathogen and thus generates a tailored response to the threat.

The antigen receptor of T cells is called the T cell receptor (TCR), which recognises antigens presented on the major histocompatibility complex (MHC) [6]. T cells can be divided into two functionally distinct subsets depending on the TCR co-receptor (CD4 or CD8) they express, which determines the class of MHC they interact with. MHC class I (MHC-I) molecules are recognised by $CD8^+$ T cells and are expressed on the surface of every nucleated cell and are loaded with peptides derived from intracellular proteins. Whereas MHC-II molecules are recognised by $CD4^+$ T cells and are expressed by professional antigen presenting cells (APC). MHC-II molecules generally present peptides derived from extracellular proteins that have been taken up from their surrounding. Additionally, APC also have the capacity to present intracellular proteins on MHC-II molecules through a process called cross-presentation [7]. In a healthy organism, these peptides are derived from self-proteins, however during infection, foreign peptide sequences originating from the pathogen will also be presented. In response to binding to their cognate antigen, T cells become activated, proliferate and acquire their effector functions for fighting the infections. To this end, $CD8^+$ T cells have the capacity to directly eliminate infected cells [8], while the main role of $CD4^+$ T cells is to assist other immune cells by secreting a distinct set of cytokines that orchestrate an immune response specific to the infection [9].

B cells recognise foreign antigens with the B cell receptor (BCR), which is the membrane-bound form of an antibody. Binding to its cognate antigen triggers the internalisation of the BCR and subsequent presentation of the antigen on MHC-II [10]. This is recognised by $CD4^+$ T cells, which provide B cells with the additional stimulation necessary to initiate secretion of antibodies that directly bind to the pathogen both neutralising it and marking it for destruction by phagocytes and the complement system [11, 12].

Unlike the innate immune system, the adaptive immune system can provide long-lasting immunity after an initial encounter, as specific antibodies as well as memory cells persist and are able to mount a rapid and specific response. This is the principle underlying the immune protection through vaccination.

1.1.3 Disorders of the immune system

The innate and adaptive immune systems complement each other's function and efficiently protect against disease. It is not surprising that complications arise if the immune system or parts of it do not function properly. A compromised immune system results in immunodeficiency, which is characterised by higher susceptibility to infections and cancers, and can be the result of a variety of perturbations ranging from inherited genetic diseases to acquired factors that weaken the immune system, such as cancer or malnutrition. Problems also occur when the immune response is deregulated and mounts a defence reaction against harmless targets. This is the case in autoimmune diseases and allergies, where the immune system initiates an immune reaction to structures of the own body or harmless foreign substances respectively.

1.2 The thymus

The thymus is the primary lymphoid organ responsible for the development of T cells. It is a bilobulated tissue located in the upper mediastinum, anterior to the heart. The thymus is structured into two anatomically and functionally distinct compartments: the cortex and the medulla. Developing T cells, called thymocytes, undergo a series of phenotypically well-characterized maturation steps during which they move first through the cortex and then through the medulla and interact with the unique stromal cells of these compartments. The main stromal cells in the cortex are cortical thymic epithelial cells (cTEC), and in the medulla medullary thymic epithelial cells (mTEC). TEC are highly specialized cells that provide the unique microenvironment necessary for the generation of functional T cells [13].

1.2.1 Thymus Organogenesis

The murine thymus originates from the ventral region of the third pharyngeal pouch where at embryonic day (E) 9.5 endodermal cells start forming the thymus primordium [14]. Signalling from the surrounding neural crest cells (NCC) and patterning through various

transcription factors orchestrate the outgrowth of the anlage and its eventual separation from the pharyngeal pouches at E12.5 [15]. At this point in development, it divides into two distinct structures, the parathyroid and the thymus, the latter beginning its descent to its location above the heart (Fig. 1.1).

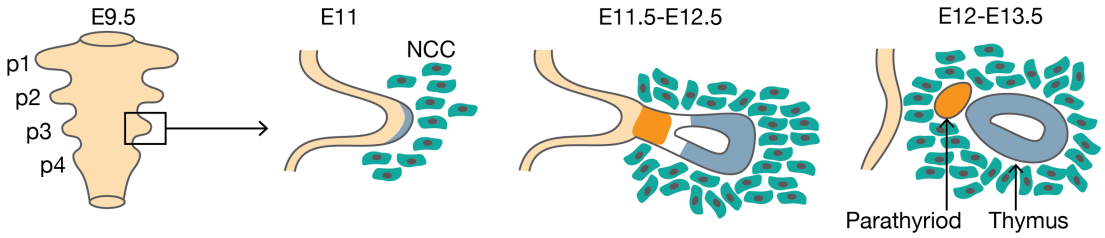

Figure 1.1: Schematic of thymus organogenesis. The thymus and parathyroid gland both originate from the third pharyngeal pouch [16].

A crucial step during thymus development is a significant increase in *Foxn1* expression at E11.25 in TEC [17, 18]. This transcription factor triggers their differentiation into fully functional TEC that orchestrate the development of a patterned and functional thymus. Haematopoietic precursors start to colonise the thymus at E11- E12 [19]. The interaction of TEC with the haematopoietic precursors then initiates receptor activator of NF-κB (RANK) signalling, which is essential for thymic epithelium development [20]. It triggers TEC lineage diversion into cTEC and mTEC [21]. As a consequence of increased signalling, the proportion of mTEC increases and medullary islets expand to form a continuous distinct compartment within the thymus [22]. In mice, growth of the thymus continues until around 5-7 weeks after birth, after which thymic involution commences and thymus size and T cell output starts to decline [23].

1.2.2 T cell development in the thymus

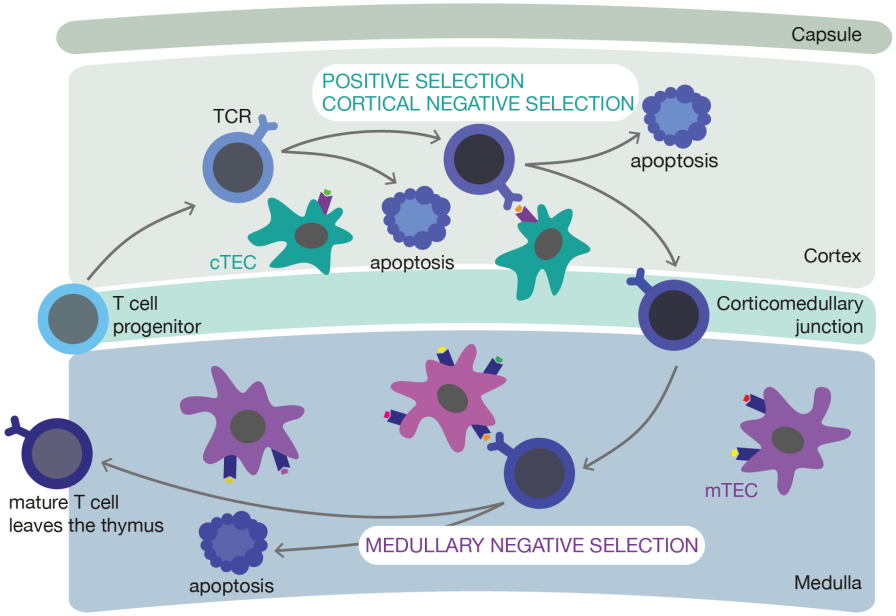

Figure 1.2: Schematic of T cell development in the thymus.

The function of the thymus is to support the development and selection of T cells [24] (Fig. 1.2). This begins with early T cell progenitors (ETP), originating from haematopoietic stem cells in the fetal liver or the bone marrow, seeding to the thymus by entering at the corticomedullary junction (CMJ) through interaction with P-selectin expressed by endothelial cells [25, 26]. ETP are characterised as double negative (DN) thymocytes as they lack the expression of the T cell co-receptors CD4 and CD8. Their differentiation and commitment to T cell fate depends on interactions with cTEC that express Notch ligand delta like 4 (DLL4) [25]. During these early steps of development, DN thymocytes move from the CMJ to the subcapsular region and start expressing the recombination activating genes (RAG) 1 and 2, which initiates the rearrangement of the TCR [27]. In a first step, the rearrangement of the β chain of the receptor is initiated and different segments of the variable (V), diversity (D) and joining (J) gene segments of this locus are combined, resulting in the creation of a TCRβ chain with unique antigen-binding capacity. The newly generated TCRβ chain associates with an invariant pre-TCR α chain, forming the pre-TCR [28]. If TCRβ gene rearrangement is successful and results in the formation of a

functional pre-TCR receptor capable of signalling, further rearrangement at the TCRβ locus is halted and cells begin to proliferate. These thymocytes are now fully committed to the T cell lineage and start to express CD8 and CD4 on their surface, thus adopting a double positive (DP) phenotype. Simultaneously, the rearrangement of the TCRα chain is initiated, which pairs with the β chain to form the αβTCR. DP thymocytes have a life span of 3-4 days after which they undergo apoptosis unless they receive signalling though their TCR. Signalling through the newly generated receptor is dependent on its capability to interact with peptides presented on major histocompatibility complexes (MHC) by cTEC and other stromal cells in the cortex. Subsequently, DP thymocytes differentiate into single positive (SP) CD4 or CD8 thymocytes, depending on whether their TCR recognises peptides on MHC-II or MHC-I. They also start expressing the chemokine receptor CCR7 and move to the medulla, as the ligands of this chemokine receptor, CCL19 and CCL21, are produced by mTEC [29]. In the medulla, thymocytes undergo further maturation and selection processes during which the TCR is probed for autoreactivity before they start expressing sphingosine-1 phosphate receptor-1 (S1PR1). This receptor mediates thymic egress by allowing the cells to follow a gradient of S1P, a molecule secreted at the blood vessels of the CMJ [30].

The gene rearrangement process at the α and β locus generates an incredible diversity of unique TCR specificities, which provides efficient protection against pathogens. However, since the rearrangement is a random process, only approximately 5 % of thymocytes carry a functional TCR that is capable of interacting with pMHC. Thus, the overwhelming majority of thymocytes will not receive the necessary survival signals and undergo apoptosis. This ensures that only T cells with a functional T cell receptor survive, a process called positive selection.

The random rearrangement process also results in thymocytes that carry TCR that are highly reactive to the self-peptides presented on MHC and are thus harmful as they have the potential to elicit autoimmunity. To exclude these cells from the pool of thymocytes, a process of negative selection is enforced, during which cells that interact with pMHC with high affinity are either deleted or, alternatively, are diverted to adopt a T regulatory

(T_{reg}) cell lineage [31, 32]. Negative selection is mediated by APC in the cortex and in the medulla. To select thymocytes on self-antigens to be encountered once these cells have exited from the thymus, mTEC express at a population level almost all antigens that constitute the "self", thereby achieving a comprehensive repertoire of peptides for negative selection [33]. The combination of positive and negative selection ensures that only functional and self-tolerant T cells are allowed to complete their intrathymic maturation and are rendered competent to exit to the periphery [34].

1.2.3 Thymic stroma

TEC are the main stromal cell type responsible for creating the microenvironment for thymocyte development and selection. Based on their phenotypic and functional characteristics, as well as their anatomical location, they can be classified as cTEC and mTEC. Both lineages originate from bipotent progenitor cells, that derive from the pharyngeal endoderm during embryogenesis [35, 36]. It is, however, still incompletely understood whether bipotent progenitor cells contribute to the maintenance of these two cell lineages in the postnatal thymus or whether this is mainly achieved by lineage-restricted progenitor populations [37, 38].

TEC form a mesh-like scaffold that provides optimal conditions for cell interactions with thymocytes that move through the distinct thymic compartments during the different stages of their development. In the cortex, cTEC provide the specialised microenvironment for the early steps of thymocyte development, including T cell lineage commitment of ETP and positive selection, while in the medulla, mTEC are central to mediating negative selection and T_{reg} cell generation.

Given that two of the central steps of T cell development (i.e. positive and negative selection) rely on the presentation of self-peptides in the context of the MHC molecule, it is not surprising that TEC are highly specialised APC with a sophisticated machinery to express, process and present antigens. To this end, cTEC express a proteasome with a composition that is unique to the thymus, called thymoproteasome, that includes

the subunit β5t. The thymoproteasome generates peptides that have high affinity for MHC-I and are pivotal for positively selecting the MHC-I restricted CD8 thymocyte lineage [39]. Similarly, cTEC express Cathepsin L and thymic-specific serine protease (TSSP) that generate peptides that are loaded onto MHC-II and are essential for CD4 lineage selection [40–42].

In the medulla, mTEC provide the specialised microenvironment for creating a self-tolerant T cell repertoire. This is dependent on the remarkable capacity of these cells to express at the population level almost all protein coding genes (described in 1.2.4 in more detail) and present them to developing thymocytes to impose negative selection of autoreactive cells [43]. This is most efficiently achieved by mature mTEC characterised by high levels of MHC-II and CD80 surface expression, which develop from immature MHC-II^{lo} CD80^{-} mTEC. Additionally, recent lineage-tracing and sequencing efforts have revealed more functionally distinct subpopulations within the MHC-II^{lo} CD80^{-} mTEC, which represent terminally differentiated cells and generate distinct niches for tolerance induction and thymocyte subset development [44, 45].

Other cell types in the thymus include dendritic cells (DC) and macrophages. DC assist TEC in thymocyte negative selection by presenting antigens that they have taken up from TEC [46–48]. Macrophages are involved in clearing apoptotic thymocytes that incur as a result of thymic selection processes [49].

1.2.4 Promiscuous gene expression (PGE)

For negative selection to be comprehensive, thymocytes need to be probed for their potential reactivity against all of the body's own proteins. To generate a complete molecular representation of "Self", mTEC take advantage of a process termed promiscuous gene expression (PGE). This practice allows an almost complete expression of all protein-coding genes and includes the expression of genes that characteristically are only expressed in specific tissues where they exercise a specific function that is of no physiological relevance in the thymus apart from thymocyte selection [43]. Antigens that result from

the expression of genes with a tissue-restricted expression pattern are called tissue-restricted antigens (TRA).

On the population level, TEC express approximately 92 % of protein coding genes, clearly surpassing the breadth of expression programmes of all other tissues in the body, which lies in average at 60-65 % [50]. A single TEC will however only express a small number of TRA at any given time, as TRA are only expressed in 1-3 % of mTEC [50, 51]. Restricting the number of TRA expressed per single TEC may be advantageous to avoid stress response and undesired effects through the expression of tissue-specific genes. The expression of TRA happens in "ordered stochasticity", which means that initially co-expression clusters of around 100-300 TRA are stochastically determined, but stay conserved across cell divisions [52, 53].

The precise molecular regulation mechanisms underlying PGE still remain incompletely defined. Of the approximately 20000 expressed genes, 4000 (2400 of which encode TRA) depend for their transcription in the thymus on the presence of a factor called Autoimmune Regulator (AIRE) [50, 54, 55]. AIRE is expressed in a subpopulation of mature mTEC and is essential for efficient negative selection [56]. Mutations in the *AIRE* gene in humans lead to a syndrome called autoimmune polyglandular syndrome 1 (APS-1) [57, 58], that is characterized by autoantibodies and destructive lymphocytic infiltrations in many organs [59, 60]. Similarly, mice with a loss of functional AIRE expression have reduced TRA expression and organ specific autoimmunity due to the incomplete negative selection of autoreactive T cells [54, 61].

AIRE enables the transcription of its target genes by interacting with a variety of proteins, that are involved in RNA transcription and processing, DNA damage repair and chromatin remodelling [62–64]. Most importantly it recruits the positive transcription elongation factor b (p-TEFb) and thus releases stalled RNA polymerase II (Pol-II) at inactive genes [65, 66]. It is, however, incompletely understood how AIRE gets recruited to its target loci. Given the broad and stochastic gene expression programme it controls and the lack of a sequence specific DNA binding capacity, it is unlikely that

AIRE acts as a classic transcription factor. Several epigenetic mechanisms including specific histone modifications [50, 67, 68] have been linked to the phenomenon of AIRE-regulated PGE [69]. This will be addressed in Chapter 1.4 after a short introduction to epigenetic mechanisms in Chapter 1.3.

AIRE is only responsible for the expression of 60-70 % of TRA and it remains unclear how the remaining tissue-restricted genes are regulated. Recently, the transcription factor FEZF2 has been discovered to control a large fraction of AIRE-independent genes [70], however, the exact role of this factor remains unclear as other groups were unable to reproduce the findings [71].

1.3 Introduction to epigenetic mechanisms

As the Greek origin of the word implies, epigenetics studies gene regulation mechanisms that lie "on top of genetics". It is defined as the study of changes in gene function that are mitotically and/or meiotically heritable and do not involve DNA sequence changes [72]. The importance of epigenetics is reflected in the fact that while all cells of an organism share the same DNA sequence, different tissues and cell types have very different phenotypes and functions, which are stably passed on to daughter cells upon cell division [73–75].

Epigenetics includes several layers of gene regulation such as DNA methylation, histone post-translational modifications (PTM), histone variants and non-coding RNA. These stable yet reversible modifications lead to changes in gene expression and thereby crucially define the phenotype and function of cells.

The DNA of eukaryotic cells is wrapped around histone proteins forming a complex called chromatin (Fig. 1.3). In the nucleus, regions with densely packed chromatin are called heterochromatin, which is gene-poor and contains repetitive sequences. Euchromatin is less densely packed and contains active genes. The basic packaging unit of chromatin is the nucleosome, which is composed of an octamer of histone protein pairs (H2A, H2B, H3 and H4) with DNA of 147 base pair length wrapped around it [76].

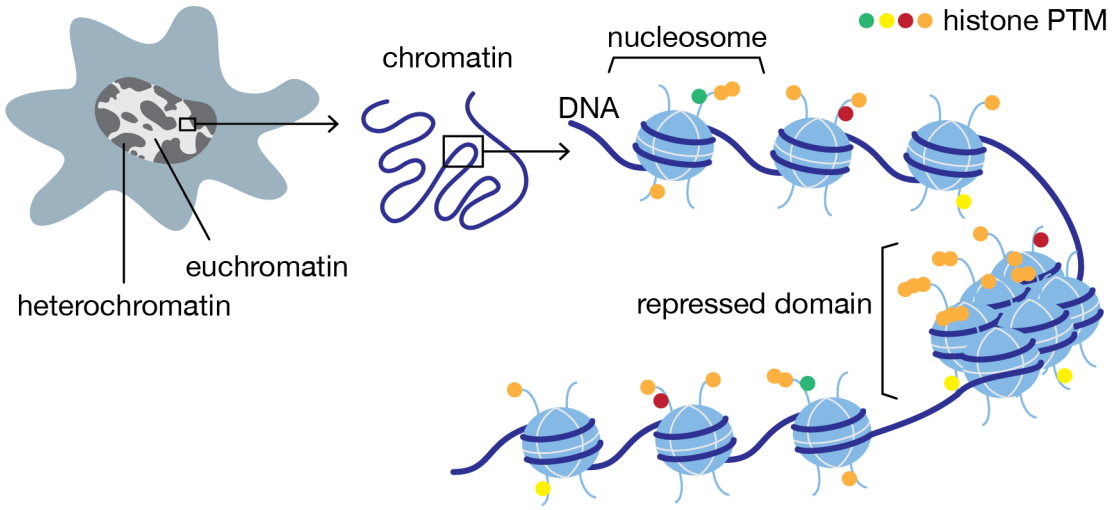

Figure 1.3: Illustration of chromatin organization in the cell and the structure of a nucleosome.

The storage of DNA as chromatin is not just a passive packaging system, but is highly dynamic and crucial for the regulation of gene expression. Chromatin compaction, nucleosome density, composition of the histone octamer and histone PTM all constitute determinants of gene activity.

1.3.1 Histone modifications and their consequences

The N-terminal tail of the histone proteins protrudes from the protein-DNA-complex and is accessible for PTM including methylation, acetylation, phosphorylation, and ubiquitylation [77]. The presence of a distinct combination of histone modifications at a specific genomic site is termed the "histone code" [78]. These PTM determine the structure of chromatin, identify distinct states of gene activity, since specific histone marks are recognized by "reader" molecules and consequently elicit a context-specific response [78, 79]. Histone marks are essential for regular cell differentiation and the maintenance of cell identity [80].

Histone modifications can be broadly divided into permissive and repressive histone marks that either allow or inhibit transcriptional activity. Examples for PTM that are characteristic for a permissive chromatin state are the trimethylation of histone 3 at lysine 4 (H3K4me3), which can be found around the transcriptional start site (TSS) of active

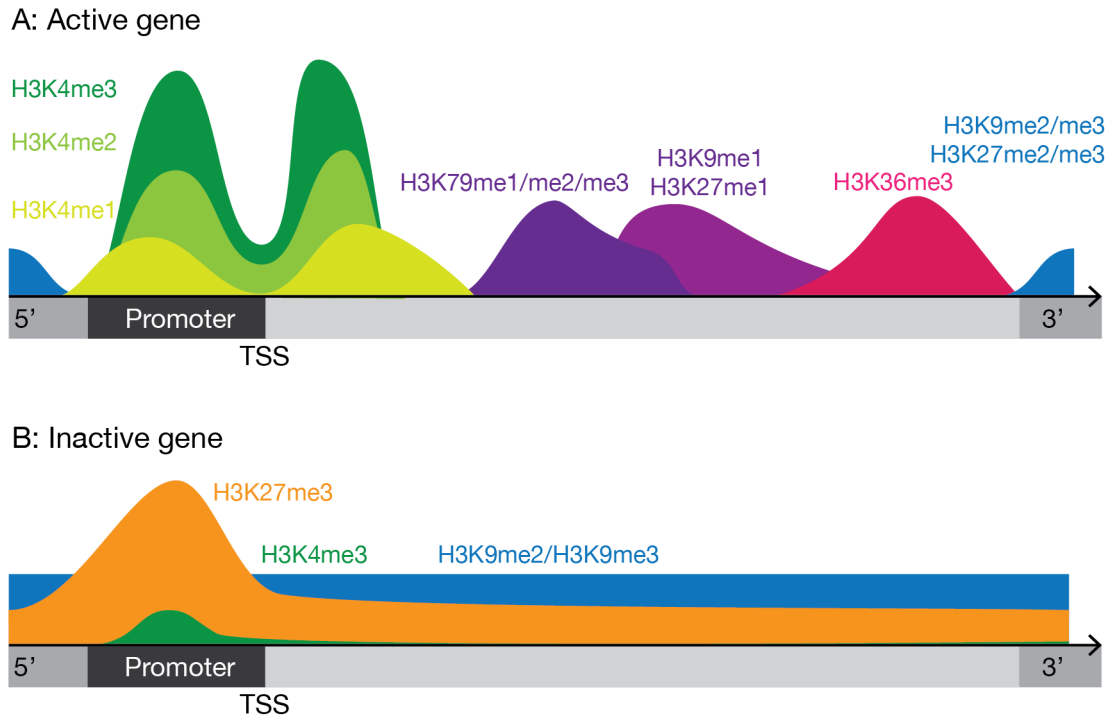

Figure 1.4: Illustration of histone methylation landscape at active (A) and inactive (B) genes [83].

genes [81], and methylated H3K79 and H3K36, which are important for transcriptional elongation [82]. On the other hand repressive histone marks include H3K27me3 and H3K9me3, which are characteristic for the promoters and gene bodies of silenced genes (Figure 1.4) [83, 84]. However, histone PTM elicit a context dependent response and thus do not always define the same transcriptional outcome. Promoters can also be marked by both permissive and repressive PTM; these genes are considered to be poised and can be rapidly turned on or off in response to developmental cues [85].

Enzymes classified as so-called "writers" and "erasers" catalyse the histone modifications and thus locally enforce or change transcription, for example, consequent to the addition or removal of methyl groups to lysine or arginine residues.

1.3.2 Lysine residue 27 of histone H3 (H3K27) methylation

H3K27me3 is a hallmark of the repressive chromatin state present at silenced genes. Chromatin immunoprecipitation (ChIP) analyses have shown that during differentia-

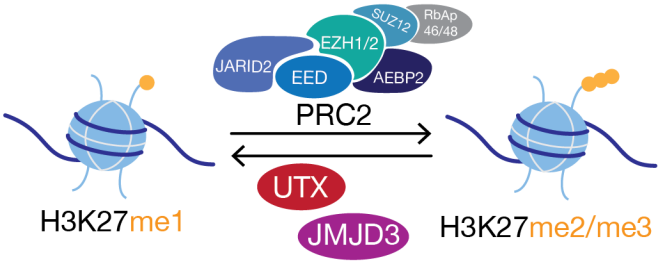

Figure 1.5: H3K27me3 is regulated by methyltransferase PRC2 and the demethylases UTX and JMJD3.

tion, H3K27me3 is lost at genes that get turned on, while H3K27me3 is reinforced at silenced regions [86] (Fig. 1.5). H3K27me3 is established by the polycomb repressive complex 2 (PRC2), which is composed of four core components: Enhancer of zeste 1/2 (EZH1/2), and suppressor of zeste 12 (SUZ12), embryonic ectoderm development (EED) and Retinoblastoma protein associated protein 46/48 (RbAp46/48). EZH1/2 is the enzymatically active component of the complex [87], which catalyses the addition of methyl groups to H3K27. PRC2 interacts with various cofactors that are essential for its proper function. One such cofactor is Jumonji AT-Rich Interaction Domain Containing 2 (JARID2) [88–90], a member of the Jumonji demethylase family, that lacks the catalytic activity for demethylation. Recent studies have highlighted the role of this protein in recruiting PRC2 to its targets and enhancing its methyltransferase function [89, 91]. In contrast to the core components, a deficiency in JARID2 does not lead to a global loss of H3K27me3, but causes a misplacement of these PTM. Defects in PRC2 core components and cofactors lead to severe problems in embryogenesis due to a failure to establish key developmental expression programmes [92, 93].

On the other hand, H3K27 methylation can be removed by the two H3K27me3 demethylases, Ubiquitously transcribed Tetratricopeptide repeat on chromosome X (UTX) and Jumonji Domain-containing protein 3 (JMJD3). They catalyse the removal of di- and trimethyl groups on histone H3 lysine 27, and thereby promote target gene activation [94–96]. Defects in these enzymes confer embryonic lethality due to the failure to initiate the appropriate gene expression programmes. Additionally, the removal of H3K27me3

can also happen in UTX/JMJD3-independent ways, for example in proliferating cells through the passive dilution of H3K27me3 by cell division.

The importance of regulating H3K27me3 levels extends beyond embryogenesis as PRC2 and UTX/JMJD3 play a role in many different cellular processes and tissues [97, 98].

1.4 Epigenetic mechanisms in the regulation of PGE

Effective thymocyte negative selection relies on a pansomatic, pandevelopmental expression programme in TEC. The large number and diverse nature of genes expressed suggests that epigenetic mechanisms may play an important role in regulating PGE. This is particularly plausible for gene expression regulated by AIRE, which stochastically induces a set of tissue-restricted genes that are usually silenced outside their specific tissue. An epigenetic mechanism is further supported by the fact that the expression of these tissue-restricted genes in the thymus is independent of their tissue-specific regulation mechanisms [99] and that inducing ectopic AIRE expression in different cell types does not cause the same transcriptional programme, suggesting that the distinct epigenetic landscape of different cell types might play a role [100].

AIRE possesses two plant homeodomains (PHD) [101], of which PHD1 falls into the category of histone "readers" as it is able to directly bind to unmethylated H3K4, a histone mark typically found in the promoter region of inactive genes [67, 68, 102]. Moreover, ChIP analyses reveal a distinct histone PTM landscape at the promoters of AIRE-regulated genes with a reduction of active histone marks (i.e. H3K4me3) and an increase of repressive marks (i.e. H3K27me3, H3K9me3) [50, 68, 103]. However, functional analyses of AIRE's binding with H3K4me0 revealed that dampening their interaction *in vivo* does not affect scope of AIRE-regulated PGE and that enforced demethylation of H3K4 in a cell culture system did not affect AIRE target genes [104]. This suggests that the interaction of AIRE with hypomethylated H3K4 does not fully account for AIRE targeting, but may rather be involved in the stabilisation of the AIRE complex at its target loci. Several interaction partners of AIRE are chromatin associated proteins, such

as the chromodomain helicase binding proteins (CHD) 4 and 6 [62, 64], which can interact with histone PTM that are characteristic for inactive chromatin including H3K4me0, H3K9me3 and H3K27me3 [105, 106]. It is therefore conceivable that AIRE targeting to the chromatin of its target loci is mediated by these interactions.

Studies have shown that local chromatin accessibility increases at target loci of genes encoding TRA when they are expressed [51]. Moreover, AIRE crucially depends on the chromatin remodeler BRG1 that facilitates accessibility and thus allows AIRE function [107]. Interestingly, this study has also shown that, after binding to its target gene, AIRE limits the transcriptional amplitude by reducing the accessibility of the loci thus ensuring safe levels of transcript expression.

An *in vitro* culture system has shown that H3K4 methylation at target genes increases in *Aire* transfected cells [68]. However it remains to be seen whether this also happens *in vivo*. Moreover, it is unclear whether repressive histone PTM such as H3K27me3 and H3K9me3 need to be locally removed in order to enable transcription or whether they are just overridden.

1.5 Hypothesis and Aims

The molecular mechanisms that control normal TEC development and function are to date only incompletely characterised. This especially concerns the extraordinary competence of TEC to effect PGE not least as the precise molecular mechanisms underpinning this extensive programme of gene expression are only partially defined. While it has been reported that gene loci encoding TRA are marked with repressive histone marks including H3K27me3, their functional role in PGE remains elusive.

The hypothesis that forms the basis of my thesis puts forth the notion that the presence of H3K27me3 influences TEC development and function. To address this contention the following objectives have therefore been defined:

(i) To assess the role of the **H3K27me3 demethylases UTX and JMJD3** for TEC biology. I will be investigating how a loss of UTX and JMJD3 impacts on TEC differentiation and the cells' capacity to perform PGE and promote normal thymopoiesis.

(ii) To characterise the importance of **JARID2, a cofactor of the methyltransferase complex PRC2**, for TEC development and function. I will probe the biological consequences of a loss of JARID2 expression targeted to TEC.

The first research objective will be addressed in Chapters 3 and 4 of this thesis, with the former investigating the impact of a TEC-specific double deficiency of UTX and JMJD3 and the latter differentiating in more detail the individual contribution of each of the two enzymes to the changes observed. The second research objective will be covered in Chapter 5.

2

Materials and Methods

Contents

2.1 Mice **18**
2.2 Standard reagents **19**
2.3 Genotyping **19**
2.4 Flow cytometry **22**
2.5 Immunofluorescence microscopy **25**
2.6 RNA methods **25**
2.7 ChIP-qPCR for histone marks **28**
2.8 T cell receptor excision circles (TREC) assay **29**
2.9 Statistical analysis **29**
2.10 Analysis of sequencing data **30**

2.1 Mice

2.1.1 UTX and JMJD3 conditional knockout mice

$Utx^{fl/fl}$ $Jmjd3^{fl/fl}$::FoxN1-Cre mice were a kind gift from Rémy Bosselut from the National Institute of Health, USA. The mice were generated by Catherine Baugé [108]. LoxP sites were inserted flanking exons 14-20 of *Jmjd3* and exon 24 in *Utx* covering the exons encoding the catalytic JmjC domain. The mice were crossed with mice carrying the FoxN1-Cre transgene to generate a deficiency in UTX and JMJD3 specific to *Foxn1* expressing cells.

2.1.2 JARID2 conditional knockout mice

Jarid2$^{tm1a(KOMP)Wtsi}$ mice were purchased from the KOMP Repository. They were created from the embryonic stem cell clone EPD018_2_A08, carrying the knockout first construct (Jarid2$^{tm1a(KOMP)Wtsi}$). The targeting vectors were generated by the Wellcome Trust Sanger Institute and the Children's Hospital Oakland Research Institute, as part of the Knockout Mouse Project (3U01HG004080). The mice carrying the knockout first construct (tm1a) were crossed with mice, expressing a *FLP1* recombinase gene under the direction of the *ACTB* promoter (B6;J-Tg(Actb-Flpe)9205Dym, The Jackson Laboratory) [109], to generate mice with the conditional allele (tm1c). Subsequently they were bred to mice carrying the FoxN1-Cre transgene [110], to obtain, mice with a specific excision of exon 3 in *Foxn1* expressing cells.

All mice used were on a C57BL/6 background and maintained according to UK Home Office regulation at the University of Oxford Biomedical Science facilities. For experiments mice were culled with ascending concentrations of carbon dioxide.

2.2 Standard reagents

The composition of standard buffers and cell media used in the following experiments are listed in Table 2.1.

2.3 Genotyping

2.3.1 Extraction and amplification of genomic DNA

Ear clips or sorted cells samples were digested in lysis buffer (see Table 2.1) and incubated for a minimum of 5 hours at 56 °C. DNA was precipitated adding an equal volume of isopropanol (VWR). The precipitated DNA was washed with 70 % ethanol (VWR) and finally resuspended in TE buffer.

Buffer/Media	Ingredients	Source	Final concentration
Fluorescence activated cell sorting (FACS) buffer	Phosphate-Buffered Saline (PBS)	Sigma	1x
	Fetal Calf Serum (FCS)	Sigma	2 %
Liberase Digestion Buffer	PBS	Sigma	1x
	Liberase	Roche	2.5 mg/ml
	DNase	Roche	10 mg/ml
Loading Dye (6x)	Glycerol	Sigma	30 %
	Bromophenol blue	Sigma	4 mg/ml
	Xylene cyanol FF	Sigma	4 mg/ml
Lysis buffer	Tris HCl pH 8.5	Merck	100 mM
	Ethylenediaminetetraacetic acid (EDTA)	Sigma	5 mM
	Sodium Dodecyl Sulfate (SDS)	Sigma	0.20 %
	Sodium Chloride (NaCl)	VWR	200 mM
	Proteinase K	Roche	100 μg/ml
Magnetic-Activated Cell Sorting (MACS) buffer	PBS	Sigma	1x
	EDTA	Sigma	5 mM
	Bovine Serum Albumin (BSA)	Sigma	0.20 %
Red Blood Cell (RBC) lysis buffer	Ammonium chloride (NH4Cl)	Sigma	8.26mg/ml
	Sodium Bicarbonate (NaHCO3)	Sigma	1.19mg/ml
	EDTA	Sigma	0.1mM
T cell media	RPMI	Sigma	1x
	FCS	Sigma	10 %
	Pen-Strep	Sigma	1x
	2-Mercaptoethanol	Sigma	50 μM
TREC lysis buffer	Tris HCl pH 7.8	Sigma	10 mM
	Proteinase K	Roche	100 μg/ml
Tris-EDTA (TE) buffer	Tris HCl pH 7.5	Merck	10 mM
	EDTA	Sigma	1mM

Table 2.1: Composition of standard reagents.

The DNA extracted from ear clip samples was amplified by polymerase chain reaction (PCR) using Taq polymerase (Sigma). PCR reactions were set up with the relevant primers (see Table 2.2) at a concentration of 0.2 µM each, 200 µM deoxynucleotides (dNTP, Sigma), 0.02 U/µl Taq polymerase (Sigma) and 1x Taq buffer (Sigma).

Genomic DNA extracted from sorted cell samples was analysed by PCR using LongAmp Taq polymerase (NEB) according to the manufacturer's recommendation. PCR reactions

contained primers at a concentration of 0.4 µM each, 300 µM dNTP (Sigma), 1 U/µl LongAmp Taq polymerase (NEB) and 1x LongAmp buffer (NEB).

Target	Forward primer	Reverse primer
Foxn1-Cre	TCTGATGAAGTCAGGAAGAACC	GAGATGTCCTTCACTCTGATTC
ACTFlp	CACTGATATTGTAAGTAGTTTGC	TACTTCTTTAGCGCAAGGGGTAG
Jarid2	GACTAGGCCCTGGATGTATCAAAGG	CTAGTGCGAAGTAGTGATCAGG
Utx floxed	GCTGGCACTGTTCATTGGGTTC	GGCATACTACCTAAGGGTAGGC
Utx excised	TGACTCAAAGCAGCAGGAGA	GGCATACTACCTAAGGGTAGGC
Jmjd3 floxed	GTGTCCTGGAACGTCGCTCG	GGCTGGAGGATGGCAGATG
Jmjd3 excised	CAGGGAGTCATTTGGGAGGT	GGCTGGAGGATGGCAGATG

Table 2.2: List of primers for genotyping. All primers were synthesized by Sigma.

Amplification of PCR reactions was done in a thermocycler (Applied Biosystems) using the programme detailed in Table 2.3. The annealing temperature (T_a) was adapted for each primer pair according to their melting temperature.

Step	Cycles	Temperature	Duration
1	1	94 °C	30 s - 10 min
2	30-35	94 °C	30 sec
		T_a	1 min
		72 °C (62 °C for amplification with LongAmp)	1 min/kb
3	1	72 °C (62 °C for amplification with LongAmp)	10 min
4	1	4 °C	Hold

Table 2.3: Thermocycler condition for amplifying genomic DNA.

2.3.2 Agarose gel electrophoresis

The resulting PCR reaction products were mixed 5:1 with loading dye (see Table 2.1) and resolved on agarose TAE gels (UltraPure Agarose (Life Technologies) in 1x TAE buffer (Ambion), 1:10000 GelRed Nucleic Acid Stain (Biotium)). Agarose concentration was chosen between 1.5-2.5 % according to expected PCR product size. As a reference a 1kb+ (Invitrogen) or 1kb (NEB) molecular weight ladder was run alongside the samples. DNA was visualised using a Gel Doc XR+ and Image Lab 4.0 Software (Biorad Laboratories).

2.4 Flow cytometry

2.4.1 Cell preparation

For TEC analysis, thymi were disintegrated by sequential enzymatic digestion combined with mechanical disruption through occasional pipetting. This entailed three digestion steps with 1.5, 1 and 0.8 ml Liberase digestion buffer (see Table 2.1) at 37 °C for 10 min each. The supernatant was collected into a Falcon tube (Corning) with 30 ml FACS buffer after each step. After washing and filtering through a 70 µm filter (Millipore), the samples were enriched for TEC by using AutoMACS depletion of $CD45^+$ cells. To this end, the samples were stained with anti-CD45 coated magnetic beads (Miltenyi) according to the manufacturer's instruction and run on the AutoMACS separator (Miltenyi) using the "DepleteS" programme.

For the analysis of haematopoietic cells, single cell suspensions were obtained by gentle mechanical disruption of thymi, spleen and lymph nodes between two frosted microscopy slides (Thermo Fisher). Spleen samples were subsequently incubated 1:4 with red blood cell lysis buffer (see Table 2.1) for 10 min at room temperature. All samples were washed in FACS buffer and filtered through a 70 µm filter (Millipore).

2.4.2 Staining for flow cytometry

Single cell suspensions were stained for surface antigens for 20-30 min at 4 °C with appropriate antibody panels. A list of the antibodies used for multicolour flow cytometric analyses can be found in Table 2.4. Splenocytes were incubated with Fc block (BD Biosciences) for 20-30 min at 4 °C before the surface antigen staining.

Where appropriate, intracellular staining was done for 1 h at 4 °C after fixation and permeabilisation with the FoxP3 transcription factor staining kit (eBioscience kit) according to the manufacturer's instructions. For the flow cytometric assessment of histone PTM, 10 % goat serum was added to the permeabilisation buffer and a 30 min blocking step was performed before adding the intranuclear antibodies.

Dead cells were identified either by staining the cells with DAPI (Thermo Fisher) immediately before analysis or by using the Fixable Aqua LIVE/DEAD Dead Cell Stain Kit (Life Technologies) before the surface antigen staining step according to the manufacturer's instructions.

Samples were analysed and sorted on a FACS Aria III (BD Bioscience). Sorting was done using high purity settings. Specifically, the "4-way purity" setting was used for bulk samples and "single cell purity" setting for single cell sorts. Data analysis was done using FlowJo (Tree Star).

Antibodies				
Antigen	**Clone**	**Isotype**	**Conjugate**	**Source**
AIRE	5H12	Rat IgG2c, κ	Alexa Fluor 488	Invitrogen
B220	RA3-6B2	Rat IgG2a, κ	BV605, PE	BD Biosciences
CCR6	29-2L17	Armenian Hamster IgG	PE	BioLegend
CCR7	4B12	Rat IgG2a, κ	BV421, PE	Biolegend
CD103	2E7	Armenian Hamster IgG	Alexa Fluor 647	BioLegend
CD11b	M1/70	Rat IgG2b, κ	Biotin	BioLegend
CD11c	N418	Armenian Hamster IgG	Biotin	BioLegend
CD19	1D3	Rat IgG2a, κ	Biotin	Invitrogen
CD24	M1/69	Rat IgG2b, κ	APC, FITC, PerCP-eFluor710	Biolegend
CD25	PC61	Rat IgG1, l	Biotin, PerCP-Cy5.5, BV605	BioLegend
CD25	PC61.5	Rat IgG1, l	eF450	eBioscience
CD28	37.51	Syrian Hamster IgG	(LEAF purified)	BioLegend
CD3ε	145-2C11	Armenian Hamster IgG	PerCP-Cy5.5	Invitrogen
CD3ε	145-2C11	Armenian Hamster IgG	(LEAF purified)	BioLegend
CD4	GK1.5	Rat IgG2b , κ	FITC, APC-Cy7	BioLegend
CD4	RM4-5	Rat IgG2a, κ	PE-eFluor610	Invitrogen
CD44	IM7	Rat IgG2b, κ	PE, PE-Cy7, PE-eF610	eBioscience
CD45	30-F11	Rat IgG2b, κ	Alexa Fluor 700	BioLegend
CD45RB	C363-16A	Rat IgG2a, κ	APC	BioLegend
CD49b	DX5	Rat IgM, κ	Biotin	BioLegend
CD5	53-7.3	Rat IgG2a, κ	PE-Cy7, PerCP-Cy5.5, PE-Cy5	BioLegend
CD55	RIKO-3	Armenian Hamster IgG	PE	BioLegend
CD62L	MEL-14	Rat IgG2a, κ	PE-Cy7	BioLegend
CD69	H1.2F3	Armenian Hamster IgG	PE-Cy5	BioLegend
CD73	TY/11.8	Rat IgG1, κ	PE	BioLegend
CD80	16-10A1	Armenian Hamster IgG	PE-Cy5	BioLegend
CD86	GL-1	Rat IgG2a, κ	PE-Cy7	Biolegend

CD8a	53-6.7	Rat IgG2a, κ	APC anti-mouse	BioLegend
EpCAM	G8.8	Rat IgG2a, κ	PerCP-Cy5.5	BioLegend
F4/80	BM8	Rat IgG2a, κ	Biotin	BioLegend
Fc Block (mouse)	2.4G2	Rat IgG2b, κ	-	BD Biosciences
Foxp3	FJK-16s	Rat IgG2a, κ	FITC, PE-eFluor610	eBioscience
FR4	12A5	Rat WI IgG1	APC	BD Biosciences
Gr-1	RB6-8C5	Rat IgG2b, κ	Biotin	BioLegend
H3	D1H2	Rabbit IgG	PE	Cell Signalling
H3K27me3	C36B11	Rabbit IgG	Alexa Fluor 488	Cell Signalling
Helios	22F6	Armenian Hamster IgG	PE, BV421	BioLegend
ICOS	15F9	Syrian Hamster IgG	PE-Cy5	BioLegend
ICOS	C398.4A	Armenian Hamster IgG	PE, Biotin	BioLegend
Isotype	RTK2071	Rat IgG1, κ	Alexa Fluor 647	BioLegend
Isotype	DA1E	Rabbit IgG	Alexa Fluor 488, PE	Cell Signalling
Ki67	16A8	Rat IgG2a, κ	Alexa Fluor 647	BioLegend
Ly51	6C3	Rat IgG2a, κ	PE, PE-Cy7	BioLegend
MHC II (I-A/I-E)	M5/114.15.2	Rat IgG2b, κ	BV421, FITC	Biolegend
MHC-I (H-2Dk)	28-14-8	Rat IgG2a, κ	PE	eBioscience
NK1.1	PK136	Mouse IgG2a, κ	Biotin	BioLegend
PD-1	29F.1A12	Rat IgG2a, κ	APC	BioLegend
Qa-2	695H19-9	Mouse IgG2a, κ	Biotin	Biolegend
Sca-1	D7	Rat IgG2a, κ	BV510	Biolegend
Streptavidin	-	-	APC, APC-Cy7, BV605, FITC, PE-Cy7, PerCP-Cy5.5	BioLegend
TCRβ	H57-597	Armenian Hamster IgG	APC-Cy7, FITC, PE, PE-Cy5	BioLegend
TCR$\gamma\delta$	GL-3	Armenian Hamster IgG	Biotin	eBioscience
Ter-119	TER-119	Rat IgG2b, κ	Biotin	BioLegend
TNFα	MP6-XT22	Rat IgG1, κ	Alexa Fluor 647	BioLegend

Lectin	**Conjugate**	**Source**
UEA-1 (Ulex europaeus agglutinin I)	Cy5, Biotin (labelled in house)	Vector Laboratories

Table 2.4: Antibodies and lectin for flow cytometry.

2.4.3 TNFα production assay

To assess TNFα cytokine licensing, five million thymocytes were cultured for 5 h with anti-CD28 (20 µg/ml, 37.51, Biolegend) and Brefeldin-A (1:1000, Invitrogen) in a 12-well plate coated with anti-CD3 (10 µg/ml, 145-2C11, Biolegend) [111]. Thymocytes were then assessed by flow cytometry using the cell surface staining and intracellular TNFα staining described above.

2.5 Immunofluorescence microscopy

Whole thymic tissues were frozen in OCT (Tissue-Tek) and sectioned into 6 µm thick sections using a cryostat (Cryostar Nx70). The sections were dried and stored at -20 °C. For staining, the sections were fixed with 1.6 % paraformaldehyde (Sigma) in PBS for 30 min and permeabilised with 0.2 % Triton-X100 (Sigma) in PBS for 15 min. Primary antibodies (anti-AIRE (H512, Biolegend) and anti-Cytokeratin 5 (ab52635, Abcam), both 1:400) were added in PBS containing 1 % BSA (Sigma) and 5 % goat serum (Sigma) for 45 min at 37 °C. After washing thrice, secondary antibodies (goat anti-rat conjugated to AF488 and goat anti-rabbit conjugated to AF647 (Thermo Fisher), both 1:800) were added for 30 min at 37 °C. Slides were counterstained with DAPI (Thermo Fisher) for 15 min and then mounted with ProLong Gold Antifade Reagent (Thermo Fisher). Stainings were visualised by confocal microscopy on a Zeiss 880 inverted confocal microscope and image analysis was performed with Fiji.

2.6 RNA methods

2.6.1 RNA extraction and cDNA conversion

Cells for RNA extraction were sorted directly into RLT lysis buffer (Qiagen) and processed with the RNeasy Micro Kit (Qiagen) according to the manufacturer's instructions, with final elution in 14 µl nuclease free water. For reverse transcription to cDNA the Sensifast cDNA Synthesis kit (Bioline) was used following the manufacturer's protocol.

2.6.2 Real time quantitative PCR (qPCR) analysis

RNA samples were analysed by qPCR with relevant primers (see Table 2.5) at 0.25 µM concentration using SensiMix SYBR Hi-ROX kit (Bioline) according to the manufacturer's instructions. The samples were run on a StepOnePlus thermal cycler (Applied Biosystems) using StepOne Software v2.1 with the following conditions: 1x 10 min at 95 °C; 40-50x 15 s at 95 °C, 15 s at 60 °C, 15 s at 72 °C. Melt curve analysis was done according to

the instrument's settings. Analysis of qPCR data was done with the $2^{-\Delta Ct}$ or $2^{-\Delta\Delta Ct}$ method with normalisation to *Gapdh* as a reference gene.

2.6.3 Reverse transcription PCR (RT-PCR) analysis

Alternatively, RNA samples were used for RT-PCR using Phusion High-Fidelity DNA Polymerase (NEB) according to the manufacturers instruction and amplified on a thermocycler (Applied Biosystems) with the following conditions: 1x 30 s at 98 °C; 35x 10 s at 98 °C, 15 s at 60 °C, 15 s at 72 °C; 1x 10 min at 72 °C. Primers are listed in Table 2.5. Products were run on agarose gel as described above.

UTX JMJD3 project (Chapter 3-4)	
Aire for	TGTGCCACGACGGAGGTGAG
Aire rev	GGTTCTGTTGGACTCTGCCCTG
Ccl20 for	CTTGCTTTGGCATGGGTACT
Ccl20 rev	CGTCTGTATGTACGAGAGGCA
Ceacam15 for	GACACCAGAACGGCACACA
Ceacam15 rev	ACCAGTTCCAGCAGATTAAAAGTG
Cxcl13 for	GGATTCAAGTTACGCCCCCT
Cxcl13 rev	TGTAACCATTTGGCACGAGGA
Ebi3 for	CTCTTCCTGTCACTTGCCCTCT
Ebi3 rev	AGAAGCATGGCATTGCACTCTG
Gapdh for	GGTGAAGGTCGGTGTGAACG
Gapdh rev	ACCATGTAGTTGAGGTCAATGAAGG
Gast for	ACAACAGCCAACTATTCCCCA
Gast rev	TCCGAGAAGGTAGCTAGAGCC
Gnb3 for	AGCAGATTGCTGATGCCAGG
Gnb3 rev	TAATGTCCTCCGTGTCCGCA
Jmjd3 for	TGTGTCCTGGAACGTCGCT
Jmjd3 rev	ACCTGACAGTGCTTCATTGACT
Krt10 for	ACGAGAAGCATGGCAACTCA
Krt10 rev	TTGTCAGGGTGAGGATCTGC
Mymk for	ATACTCCGGTCCCATAGGCA
Mymk rev	ATGCTCTTGTCGGGGTACAG
Ngfr for	CAGACCGTGTGTGAACCCTG
Ngfr rev	GGACATACTCTGCAGGCCC
Orm2 for	AGGAATCCAGAGAGAGAATGGGA
Orm2 rev	AAGGCCCCATGCATCTTCAA
Slc13a2 for	CGCTCCTACCTGATTGTGCT
Slc13a2 rev	CGCCATGAGGATGATGGAGTA
Soat2 for	CTCTGCTGCTCTCCATCTTGCAT
Soat2 rev	TCTCGGCGAAGGCGTTG
Utx for	GCTGGCACTGTTCATTGGGTTC
Utx rev	CCACTGCTAACTTATACTGACAGGC
Uty for	GCTCCTTCCAGGAATCATTGAGA
Uty rev	TGCTTTCTGTCTCCTTCCAGA

JARID2 project (Chapter 5)	
TEC (qPCR)	
Jarid2 exon 3 for	GGGAGCCTGAAGGCGGTAAA
Jarid2 exon 4 rev	GGCATCATCCTTCTCGTTCTCT
Jarid2 exon 6 for	ACAATGCTTCATCTTCGTGCC
Jarid2 exon 7 rev	GCTCTTTCTCCCGTGCTGAC
Splice variants (RT-PCR)	
Jarid2 exon 6 rev	ACCATACTGTTGGGCAGCG
Jarid2 exon 5 for	CCCCCGCCAGCTACTCAAAT
Jarid2 exon 5 rev	GCAAACTTCCTTTGTGCTTGC
Jarid2 exon 4 for	GATGCCTCCCAAGTGTCCTC
Jarid2 alt exon 3 for	GCTTATCTTGAGGAACCTGGGA
Jarid2 exon3 rev	TTTCGTACAACTCTCTCTTCTGACC
Jarid2 exon 4 rev2	GCCTTAGCCTGGGCATTACC
Jarid2 exon 2 for	GAGCAAGGAAAGACCCAAGAGG
Thymocytes (qPCR)	
cFlip for	GAAGCCAACATCATTGCTGA
cFlip rev	ACAAAGCCGTTGTTGAGTGG
Foxo1 for	TGCTGTGAAGGGACAGATTG
Foxo1 rev	GAGTGGATGGTGAAGAGCGT
Klf2 for	GTTGCACTACGGGCCTCC
Klf2 rev	GTGGCAGGTGGAGCCAAG
Nemo for	GAAAGGAGTGGTGAGCTGGA
Nemo rev	AAAGTTGGCTGCCATGAGTC
Pak2 for	GCGGAGACCTTTCCTCTCTG
Pak2 rev	TACTGCTCATCCGAACTGGA
Relb for	GTCTTTCCCCACGAGGCTAT
Relb rev	ATCGAGCTTCGAGACTGTGG
S1pr1 for	TATGGAGCTTTTCCTTGGCT
S1pr1 rev	CGGTGTAGACCCAGAGTCCT
Tak1 for	CAAAAGCTCCTCTTCCGACA
Tak1 rev	TTCTGCCAGTGAGATGATCG

Table 2.5: List of primers for qPCR and RT-PCR. All primers were synthesized by Sigma.

2.6.4 Bulk and single cell RNA sequencing (RNA-Seq)

RNA extracted from bulk mTEC^{hi} samples (biological triplicates with 40000-50000 cells) was processed using the SMART-Seq2 method and 75 bp paired-end RNA-Seq was performed on the Illumina HiSeq4000 platform (Wellcome Trust Centre for Human Genetics, University of Oxford). For single cell RNA-Seq, mTEC^{hi} were sorted into SMART-Seq2 lysis buffer containing RNase inhibitors [112], libraries were generated following the SMART-Seq2 protocol and were sequenced on a HiSeq2500 (Wellcome Trust Sanger Institute, Cambridge).

2.7 ChIP-qPCR for histone marks

For ChIP analysis, mTEC^{hi} were sorted in 10000 cell batches and processed according to the Diagenode True Micro ChIP protocol. Fixation was done for 10 min and chromatin was sheared for 5 cycles (30 sec ON, 30 sec OFF) on a Bioruptor pico (Diagenode). S2R+ *Drosophila* cells were a gift from Markus Tegel, University of Oxford. *Drosophila* cells were fixed in batches of 1 million cells and sheared in batches of 500 000 cells using the same conditions as for the TEC samples above. Chromatin equivalent of 10 000 cells was added to the mTEC^{hi} samples immediately before the immunoprecipitation step. Antibodies (1 µg per sample) used were anti-H3K27me3 (07-449, Millipore), anti-H3K4me3 (pAb-003-050, Diagenode) and IgG (kch-504-250, Diagenode). DNA fragment sizes were analysed by agarose gel electrophoresis (as described above) or Tape Station using High-Sensitivity D1000 screen tapes (Agilent) according to the manufacturer's instructions.

ChIP-qPCR was performed with SensiMix SYBR Hi-ROX kit (Bioline) as described above using the primers listed in Table 2.6. Analysis was done with either Percent Input or Fold Enrichment method, the latter using *Drosophila* E4456 signal as a reference.

ChIP Primers		**Species**
Gapdh ChIP for	GCGCGAAAGTAAAGAAAGAAGCCC	Mouse
Gapdh ChIP rev	AGCGGCCCGGAGTCTTAAGTATTAG	Mouse
Gast ChIP for	GGGCAGAGTGACAGGTTGAA	Mouse
Gast ChIP rev	CTCGAGGTTCCTCCCAAACC	Mouse
Hoxd9 ChIP for	CGAGTTCGCCTCGTGTAGTT	Mouse
Hoxd9 ChIP rev	ACACGTACGGGTGGTACAGG	Mouse
Slc13a2 ChIP +4kb for	CGGAACTGTAGTCGAGCAGG	Mouse
Slc13a2 ChIP +4kb rev	GTAGGTGCAAAGTGCCAACG	Mouse
Depleted 4580 for	AGGCAGCGAGATATAGACCGA	*Drosophila*
Depleted 4580 rev	AGCAAAAATGTGCCCGCTATG	*Drosophila*
Enriched 4465 for	TCATAACTCGTTGCTCGCAGA	*Drosophila*
Enriched 4465 rev	TCGGACCGTGACTAACGAAG	*Drosophila*

Table 2.6: Primers used for ChIP qPCR. All primers were synthesized by Sigma.

2.8 T cell receptor excision circles (TREC) assay

TREC analysis was performed on sorted naïve CD4 and CD8 populations following the protocol by Lynch and Sempowski [113]. To this end, 22 µl of TREC lysis buffer (see Table 2.1) was added to each pellet of 110000 sorted cells. The samples were subsequently incubated on a thermomixer (Eppendorf) at 56 °C 1200 rpm for 1 h, followed by an inactivation step at 95 °C for 10 min.

The resulting cell lysates were used to quantify TREC by qPCR. Reactions were set up containing 1 µl 12.5 µM forward and reverse primers (Sigma, see Table 2.7), 1.75 µl 50 mM $MgCl_2$, 1 µl FAM probe (see Table 2.7, IDT), 0.5 µl 10 mM dNTP mix (Sigma), 0.125 µl Platinum Taq enzyme (Thermo Fisher) and 2.5 µl Platinum Taq buffer (Thermo Fisher) and 12.125 µl water. 5 µl of cell lysate (equivalent to 25000 cells) were added to each reaction. Standards containing 10^2, 10^3, 10^4, ... and 10^7 copies of sjTREC plasmids (kind gift from Gregory Sempowski, Duke University) were used to determine a standard curve to calculate the number of TREC per 25000 cells. The samples were run on a StepOnePlus thermal cycler (Applied Biosystems) using StepOne Software v2.1 with the following conditions: 1x 10 min at 95 °C; 45x 15 s at 95 °C, 1 min at 60 °C; 4 °C hold.

sjTREC for	CAT TGC CTT TGA ACC AAG CTG
sjTREC rev	TTA TGC ACA GGG TGC AGG TG
FAM probe	5'-/56-FAM/CA GGG CAG G/ZEN/T TTT TGT AAA GGT GCT CAC TT/3IABkFQ/-3'

Table 2.7: Reagents for TREC assay.

2.9 Statistical analysis

Statistical analysis was done using Excel (Microsoft) or Prism (Graph Pad). Experimental data is depicted as mean ± standard deviation. Statistical significance was determined using two-tailed, unpaired Student's t-tests. Correction for multiple comparisons with the Holm-Sidak method was applied when necessary. When more than two groups were

compared, a one-way or two-way ANOVA with a Turkey post-test was used to determine statistical significance. P values of <0.05 were considered significant.

2.10 Analysis of sequencing data

2.10.1 Bulk RNA-Seq analysis

The analysis of bulk mTEC^{hi} libraries was performed in collaboration with Michael Morgan, Wellcome Trust Sanger Institute, Cambridge. In brief, FASTQ files were adaptor trimmed using Trimmomatic [114], prior to alignment to the mm10 genome using STAR v2.4 [115], filtering reads for known splice junctions constructed from mm10 Ensembl build 86. This includes all known coding and non-coding regions of the mouse genome, and only removes spurious splicing events that might occur due to indel mutations in non-coding regions. Alignments were de-duplicated to remove PCR duplicates using *PicardTools* (http://broadinstitute.github.io/picard), prior to expression quantification using featureCounts [116]. Protein-coding Ensembl86 genes were used to generate gene counts for each of the 6 samples. Non-expressed genes with < 1 count on average across all samples were removed and counts normalised by library depth before further analysis.

The analysis comparing *Utx* and *Jmjd3* RNA expression in different mTEC subpopulations (immature, mature, AIRE^{+} and AIRE KO mTEC) and across different peripheral tissues was done in collaboration with Kathrin Jansen, University of Oxford. For this analysis, libraries from different mTEC subpopulations (sorted according to [50]) that have been previously generated in our lab by Poly(A)+ RNA-sequencing of two biologically replicates were used (4-week old mice, 101 bp paired-end stranded RNA-sequencing, Illumina HiSeq). RNA-sequencing data for 22 mouse tissues were obtained from the mouse ENCODE project (GSE36025; 8-week old mice). The reads of the population RNA-sequencing data were trimmed to 76 bp (fastx trimmer v0.0.14). All samples were downsampled to a common read depth of 60 M reads. Subsequently, transcripts-per-million (TPM) were obtained using Salmon (v0.9.1, Ensembl annotation mm10, v91). These TPM values

were upper-quartile normalised and $\log_2$(n+1)-transformed. Heatmaps were generated in R (v3.4) using the package Heatmap3 (v1.1.1).

2.10.2 Tissue specificity

The tissue specificity was estimated by calculating the tissue specificity index (τ) value of genes [117] using Cap Analysis of Gene Expression with sequencing (CAGE-seq) on all mouse tissues from the FANTOM5 project [118]. Samples were assigned to tissue groups, which were then used to calculate the τ value for each gene. Genes were assigned to one of 3 categories: Constitutive ($\tau \leq 0.4$), TRA ($\tau \geq 0.8$) or Other ($0.4 < \tau < 0.8$).

2.10.3 Histone ChIP-Seq analysis

The ChIP-Seq analysis was performed by Michael Morgan. For this analysis, anti-H3K27me3, anti-H3K4me1 and anti-H3K4me3 ChIP-Seq datasets that have been previously generated in our lab were used (GSE114713). Promoter regions were defined centred on the TSS of Ensembl build 86 genes as -1Kb and +500bp. The aligned reads to these 1500nt intervals on mouse genome mm10 were quantified. Reads were trimmed by Trimmomatic [114] and aligned using BWA [119], then Stampy [120], and filtered for mapping quality (MAPQ > 10) and deduplicated to remove PCR duplicates using PicardTools. Subsequently, ChIP and input signals were quantified over the defined promoter intervals using featureCounts [116].

2.10.4 Single cell RNA-Seq analysis

The single cell RNA-Seq analysis was performed by Michael Morgan. In brief, mTEC^{hi} single cell transcriptomic data sets were generated using the SMART-Seq2 platform. Contaminating adaptors and PCR primers were removed from FASTQ files (one per cell) using Trimmomatic [114], prior to alignment to the mm10 genome using STAR v2.4 [115]. Gene expression was quantified for each cell by counting reads that overlap mouse Ensembl v86 coding and non-coding annotations using featureCounts. High quality cells were

retained based on sequencing coverage (> 5 % genes observed), before normalisation for sequencing depth using estimated size factors [121]. In total, 276 high quality single mTECs were retained for analysis. These were combined with additional available datasets from Sansom et al. [50] (n=174), Brennecke et al. [51] (n=358), and Meredith et al. [52] (n=189), resulting in 997 single cells and 14273 detected genes. Batch effects between data sets were removed for each gene by fitting a blocking factor across all cells relating to the data set. The corrected gene expression values were the residuals from this linear model. All analyses were performed using R.

3

The role of the H3K27me3 demethylases UTX and JMJD3 in TEC biology

Contents

3.1 Introduction **33**
3.2 *Utx*, *Jmjd3* and *Uty* mRNA expression in TEC **35**
3.3 Mouse model with a TEC-specific KO of UTX and JMJD3 . **37**
3.4 TEC with targeted UTX and JMJD3 deficiency **38**
3.5 Transcriptional changes in mTEC^{hi} lacking UTX and JMJD3 **47**
3.6 H3K27me3 landscape in TEC with a loss of JMJD3 and UTX **59**
3.7 Thymocyte development in $Utx^{TEC-/-}$ $Jmjd3^{TEC-/-}$ mice **66**
3.8 Peripheral T cell compartment in $Utx^{TEC-/-}$ $Jmjd3^{TEC-/-}$ mice **89**
3.9 Summary of the $Utx^{TEC-/-}$ $Jmjd3^{TEC-/-}$ mouse model **98**
3.10 Discussion **99**

3.1 Introduction

By expressing almost all protein coding genes, TEC are able to recreate a molecular mirror of what T cells might encounter in the periphery once they have left the thymus. This is essential for their function of creating a tolerant T cell repertoire. The broad expression programme of TEC, called PGE, includes the expression of genes that are usually only expressed in specific tissues (see Chapter 1 for a more detailed overview).

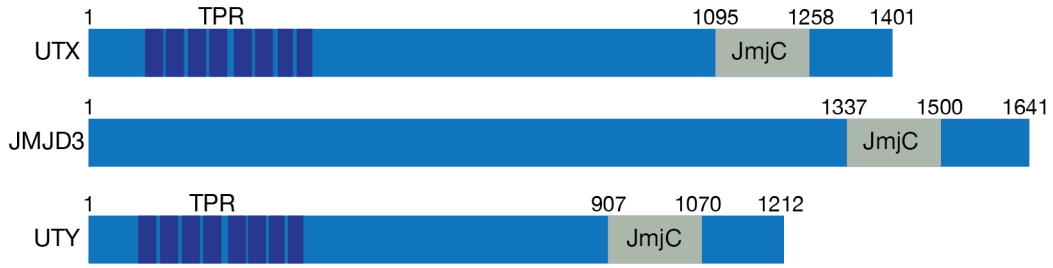

Figure 3.1: Schematic representation of UTX, JMJD3 and UTY. The JmjC domain is the catalytically active domain, which demethylates H3K27me3. It also mediates interaction with H3K27me3 and with chromatin remodelers [94, 124, 126]. Tetratricopeptide repeats (TPR) are present in UTX and UTY [95]. Apart from the JmjC domain, JMJD3 does not contain any other characterised functional domains [127].

It has been shown that the promoters of genes encoding TRA and specifically AIRE-regulated genes are characterised by repressive histone marks. One of these repressive histone marks is H3K27me3 [50, 103].

H3K27me3 is associated with promoters of silenced genes [86, 97]. The long-held belief that gene silencing by H3K27me3 cannot be actively removed was challenged by the recent identification of the H3K27me3 demethylases UTX and JMJD3 [94–96, 122]. UTX and JMJD3 are members of a protein family characterized by the presence of the Jumonji C (JmjC) catalytic domain [123] and their histone demethylase activity is highly specific for H3K27me3 and H3K27me2 as substrates [124]. Males additionally express UTY, a UTX homologue encoded on the Y chromosome [94], which has two mutations in the catalytic JmjC domain that greatly reduce its demethylase activity [125]. UTX and JMJD3 are encoded by *Kdm6a* and *Kdm6b* respectively, which will be referred to as *Utx* and *Jmjd3* hereafter. UTY is encoded by *Kdm6c* and will be referred to as *Uty*.

UTX and JMJD3 are important during development and differentiation and their deletion results in a severe impairment of embryonic development [128–130]. The enzymes' catalytic capacity is responsible for actively removing H3K27me3 from promoters of specific genes that need to be turned on for differentiation [95, 108, 129, 131, 132]. However, UTX and JMJD3 also have demethylase-independent functions [130, 133], as these enzymes have been shown to act as chromatin remodelers by interacting with BRG1 and members of the T-box family [126].

The role of H3K27me3 in the context of PGE is to date unclear. We know that AIRE-regulated PGE is correlated with the presence of the H3K27me3 marks at the TSS of its targets, and that genes are transcribed seemingly regardless of repressive histone modification [50], however it is unclear if the presence of H3K27me3 has a functional role in PGE. TEC with a deficiency in the H3K27me3 demethylases UTX and JMJD3 are unable to actively demethylate H3K27me3. To establish a mechanistic link between H3K27me3 and PGE, it is of great interest to determine whether H3K27me3 marks increase in mutant TEC as a consequence of a targeted loss of both UTX and JMJD3 and whether these deletions translate into an altered representation of "Self" in TEC engaging in PGE.

I hypothesise that the repressive histone mark H3K27me3 is important for PGE as it serves as a landmark to recruit the AIRE-associated transcriptional machinery. To address this hypothesis directly, mice with a TEC-targeted loss of both enzymes have been created and investigated (Chapter 3). My aim is to assess the consequences of UTX and JMJD3 deficiency on TEC maturation and function. Of particular interest are changes in PGE, which would provide a first mechanistic link between H3K27me3 and the expression of AIRE-regulated transcription.

Chapter 4 will investigate in more detail the roles UTX and JMJD3 play individually in TEC. The findings will further be compared to those of male mice with a TEC-specific loss of UTX and JMJD3 expression, as they remain to have a functional *Uty* gene on their Y chromosome.

3.2 *Utx*, *Jmjd3* and *Uty* mRNA expression in TEC

In a first step, I assessed the mRNA expression levels of *Utx*, *Jmjd3* and *Uty* in TEC. For this purpose, I isolated cTEC, mTEC^{lo} and mTEC^{hi} from female and male WT mice and analysed them by qPCR. *Utx* and *Jmjd3* were detected in all TEC subpopulations independent of the gender of the donor animal (Fig. 3.2A).

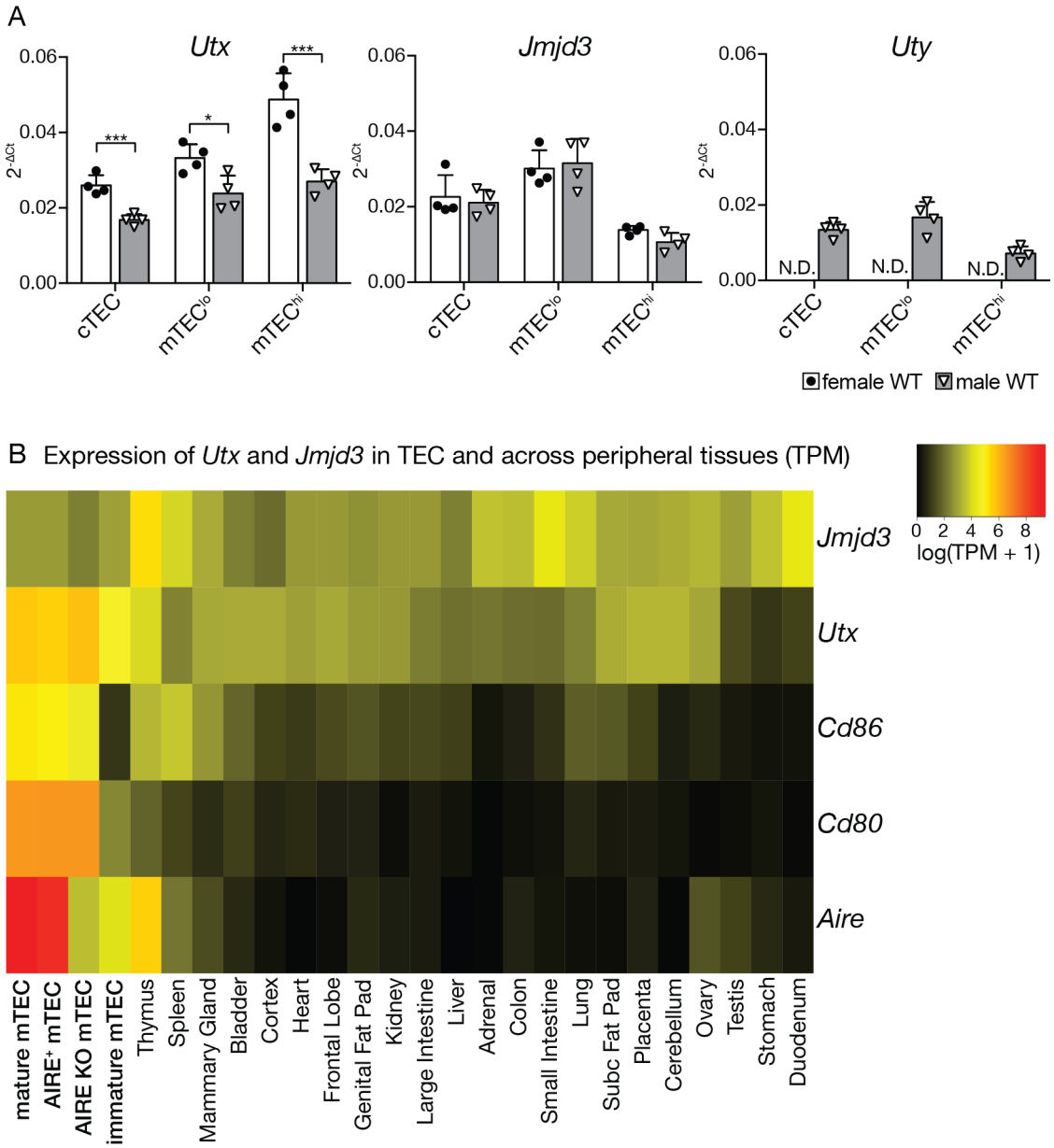

Figure 3.2: *Utx*, *Jmjd3* and *Uty* mRNA expression in TEC subpopulations and in peripheral tissues. (A) Extracted RNA from sorted cTEC, mTEC^{lo} and mTEC^{hi} was used for qPCR, employing primers for the detection of *Utx*, *Jmjd3* and *Uty* mRNA. Data was normalised to *Gapdh* using the $2^{-\Delta Ct}$ method. The bar graphs are pooled from two independent experiments with mice at 4-5 weeks of age (WT female: n=4; WT male: n=4). Statistical analysis was done with a two-tailed unpaired t-test. *p<0.05; **p<0.01, ***p<0.005. **(B)** Expression heatmap of *Utx*, *Jmjd3*, *Cd80*, *Cd86*, and *Aire* in mTEC populations (as sorted by Sansom et al. [50]) and peripheral tissues (GSE36025). The transcripts per million (TPM) values were generated using Salmon and subsequently upper-quartile normalised.

As expected, *Uty* expression was not detectable in female TEC. When comparing expression levels, *Utx* was more highly expressed in female than in male TEC, while *Jmjd3* expression was the same in TEC isolated from either gender (Fig. 3.2A). This finding is compatible with the fact that *Utx* escapes X inactivation and thus could cause a gene dose effect that differs between male and female mice [134].

By using RNA-Seq data from WT immature and mature mTEC and from 22 peripheral tissues (GSE36025), the mRNA expression of *Utx* and *Jmjd3* in TEC was compared to that of peripheral tissues with the expression of *Aire*, *Cd80* and *Cd86* used as a reference (Fig. 3.2b). *Utx* was more highly expressed in TEC than in peripheral tissues. In comparison, *Jmjd3* was expressed at a lower level in both immature and mature mTEC and no differences were observed between mTEC and peripheral tissues. Taken together, these findings suggest that UTX may play a more important role in TEC biology than its counterpart JMJD3. This notion will be further investigated in Chapter 4.

3.3 Mouse model with a TEC-specific KO of UTX and JMJD3

To investigate the molecular and cellular changes in the H3K27me3 landscape in TEC consequent to the loss of UTX and JMJD3, I analysed mice with a TEC-targeted loss of UTX and JMJD3. Designated $Utx^{TEC-/-}$ $Jmjd3^{TEC-/-}$, these mice have LoxP sites flanking the exons encoding the catalytic JmjC domain. Upon Cre-mediated recombination the expression of catalytically active enzymes is lost. TEC specificity of the recombination was achieved using the *Foxn1* promoter for Cre expression (Fig. 3.3). The JmjC domain is responsible for the demethylase activity, for the interaction with H3K27me2/me3 marks and for demethylase-independent functions [94, 124, 126]. Single-gene-deficient mice will be referred to as $Utx^{TEC-/-}$ and $Jmjd3^{TEC-/-}$ respectively. This conditional knockout strategy has previously been successfully used [108].

The deletion of the floxed exons in TEC from $Utx^{TEC-/-}$ $Jmjd3^{TEC-/-}$ mice was verified by PCR in cTEC, $mTEC^{lo}$ and $mTEC^{hi}$, where smaller fragments were amplified accounting

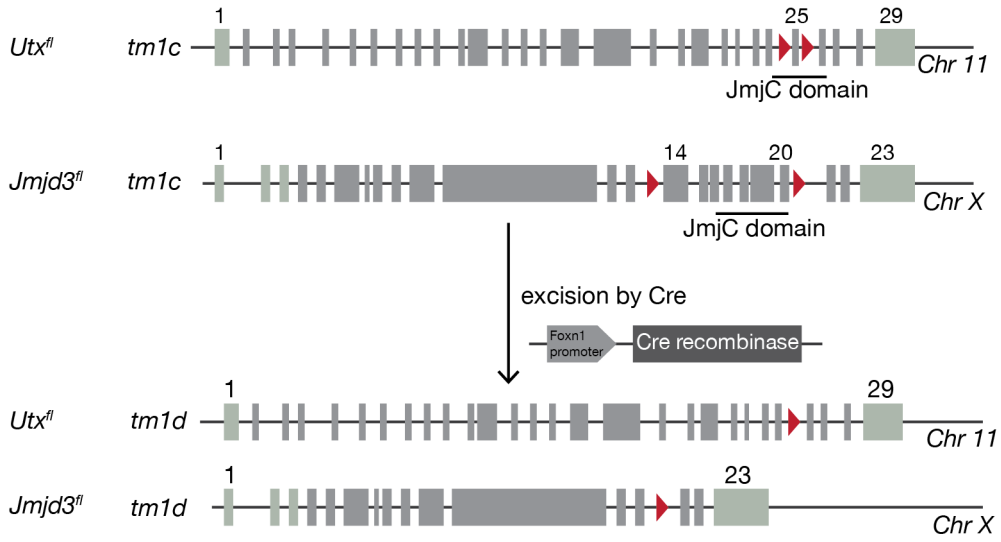

Figure 3.3: Schematic representation of genomic targeting to generate TEC-specific deletions of UTX and JMJD3. LoxP sites (red) flank exon 25 in *Utx* and exon 14-20 in *Jmjd3*. The presence of Cre recombinase under the *Foxn1* promoter results in an excision of exon 25 in *Utx* and exon 14-20 in *Jmjd3* in all *Foxn1* expressing cells.

for the excision of exon 25 in *Utx* and exon 14 to 20 in *Jmjd3* (Fig. 3.4B). $CD45^+$ $EpCAM^-$ cells served as a negative control as these cells do not express *Foxn1*. Notably, only the intact allele could be detected using DNA from total thymus lysate, which is reflective of the fact that the overwhelming majority of cells in the thymus are not TEC and thus do not express *Foxn1*.

3.4 TEC with targeted UTX and JMJD3 deficiency

3.4.1 Loss of UTX and JMJD3 does not affect thymus cellularity or architecture

During embryonic development, expression of *Foxn1* is initiated on E10.5-11.25 shortly after patterning of the thymus anlage [17]. Thus, recombination mediated by Cre expressed under the transcriptional control of the *Foxn1* locus occurs early in TEC development [110]. Given that UTX and JMJD3 have been determined to be important for enabling tissue-specific transcriptional programmes through demethylation of H3K27me3 [135], I probed whether TEC development and the formation of a thymus with normal cellularity and architecture continues despite the absence of UTX and JMJD3. To test the impact of a

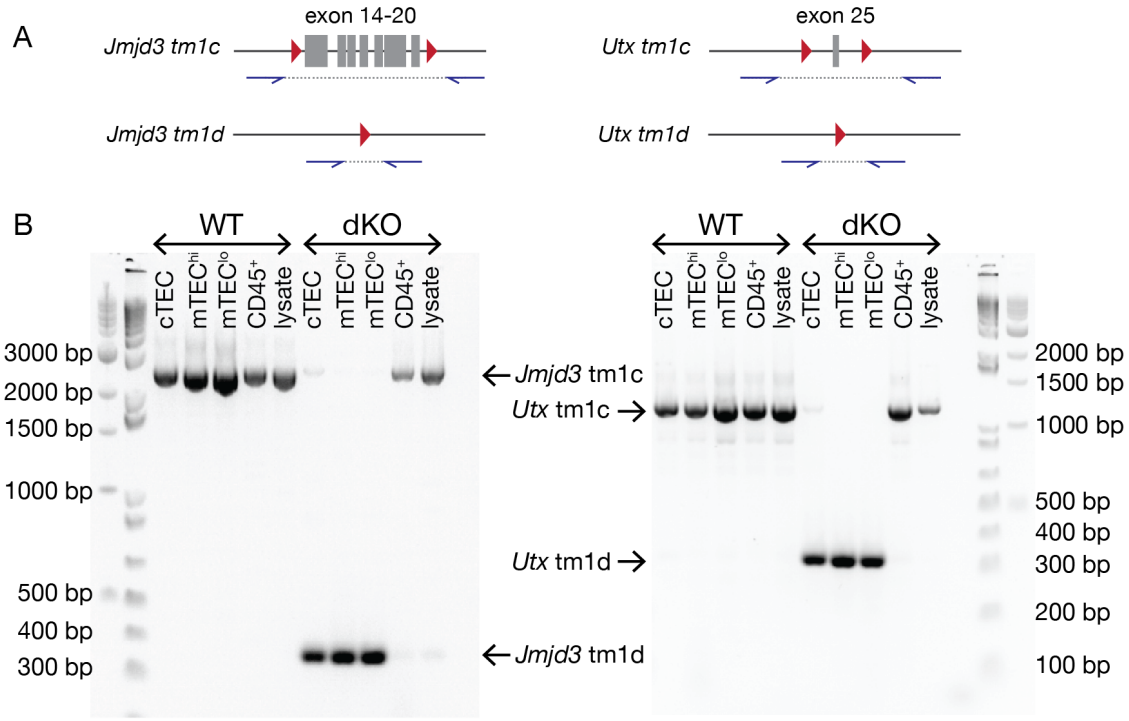

Figure 3.4: Efficient Foxn1-Cre driven genomic excision of floxed exons in TEC of *Utx*$^{TEC-/-}$ *Jmjd3*$^{TEC-/-}$ mice. (A) Schematic of primers around exon 25 (*Utx*) and exon 14-20 (Jmjd3) that were used to detect genomic excision. **(B)** Sorted cTEC, mTEC^{hi}, mTEC^{lo} and CD45+ EpCAM- cells and samples from whole thymus lysate were used for PCR with primers illustrated in (A). Cells were sorted from female mice 4-5 weeks of age (WT: *Utx*$^{fl/fl}$ *Jmjd3*$^{fl/fl}$; dKO: *Utx*$^{TEC-/-}$ *Jmjd3*$^{TEC-/-}$). PCR products were run on a 1.5 % agarose gel. NEB 1kb and 1kb+ ladders were run as reference. Gel is representative of two independent experiments.

loss of both enzymes on thymus organogenesis, total thymus cellularity was determined and thymic architecture was assessed by immunohistochemistry.

At 4-5 weeks of age, thymic cellularity was unchanged in *Utx*$^{TEC-/-}$ *Jmjd3*$^{TEC-/-}$ mice as compared to WT animals (Fig. 3.6A). Thymi from both WT and *Utx*$^{TEC-/-}$ *Jmjd3*$^{TEC-/-}$ animals showed the characteristic staining patterns of cytokeratin 5 (K5) and AIRE expression in mTEC, the latter revealing nuclear speckles (Fig. 3.5B). This finding demonstrated that *Utx*$^{TEC-/-}$ *Jmjd3*$^{TEC-/-}$ mice have a normally sized and structured thymus at 4-5 weeks of age.

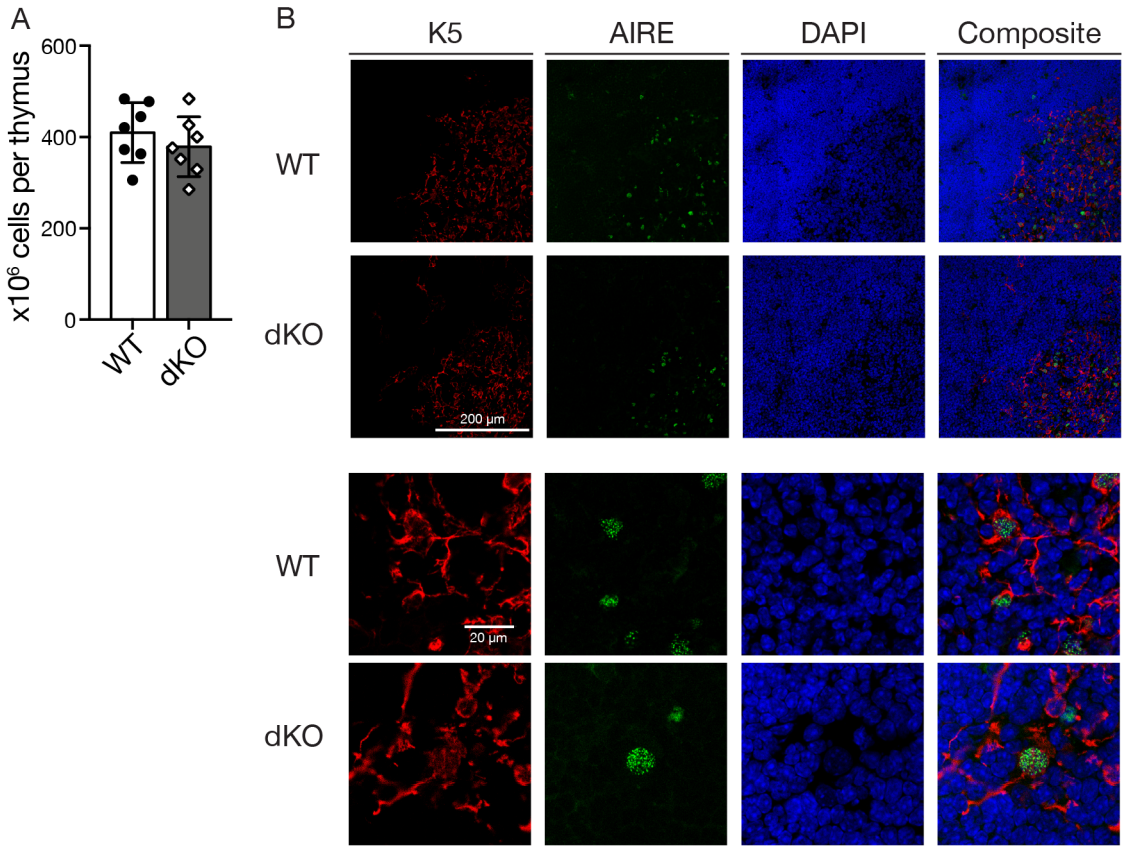

Figure 3.5: Cellularity and architecture of $Utx^{TEC-/-}$ $Jmjd3^{TEC-/-}$ thymi is normal. **(A)** Absolute cell count after enzymatic digestion of two thymic lobes. Data shown in bar graph are pooled from 3 independent experiments using female mice at 4-5 weeks of age. WT ($Utx^{fl/fl}$ $Jmjd3^{fl/fl}$) n=7; dKO ($Utx^{TEC-/-}$ $Jmjd3^{TEC-/-}$) n=7. Statistical analysis was done with a two-tailed unpaired t-test. **(B)** Representative immunofluorescence microscopy images of thymus tissue sections stained with K5 (red), AIRE (green) and DAPI (blue). WT ($Utx^{fl/fl}$ $Jmjd3^{fl/fl}$); dKO ($Utx^{TEC-/-}$ $Jmjd3^{TEC-/-}$).

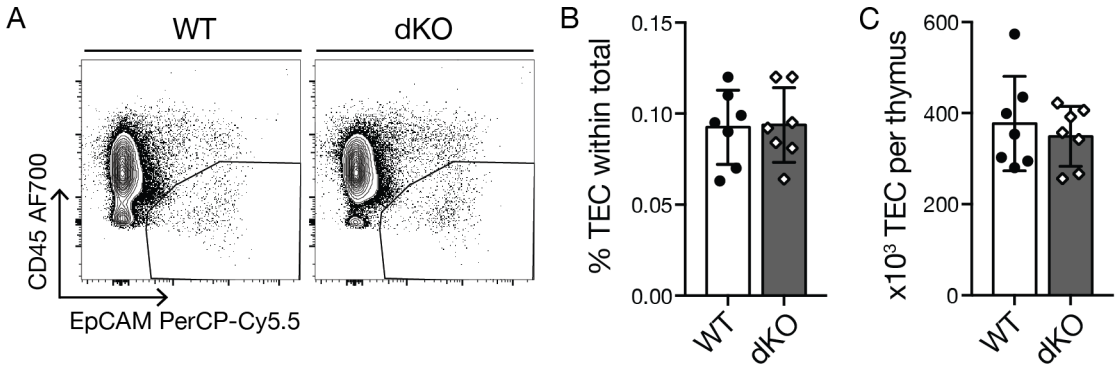

Figure 3.6: Unchanged TEC cellularity in $Utx^{TEC-/-}$ $Jmjd3^{TEC-/-}$ thymi. **(A)** Representative FACS plots of TEC ($EpCAM^{+}$ $CD45^{-}$) within live cells. **(B)** Bar graph showing percentage of TEC within total cells. **(C)** Bar graph showing absolute TEC numbers. Data shown in bar graphs are pooled from three independent experiments using female mice at 4-5 weeks of age. WT ($Utx^{fl/fl}$ $Jmjd3^{fl/fl}$) n=7; dKO ($Utx^{TEC-/-}$ $Jmjd3^{TEC-/-}$) n=7. Statistical analysis was done with a two-tailed unpaired t-test.

3.4.2 Loss of UTX and JMJD3 affects cTEC to mTEC ratio, mTEC maturation and AIRE expression levels

To assess TEC development in the absence of UTX and JMJD3 qualitatively and quantitatively, I used extensive phenotyping by flow cytometry. The gating strategy to identify TEC is detailed in the Supplementary Figure A.1A-B.

At 4 weeks of age, TEC cellularity was comparable for $Utx^{TEC-/-}$ $Jmjd3^{TEC-/-}$ and WT mice (Fig. 3.6). The lack of UTX and JMJD3 did, however, affect the cTEC to mTEC ratio: There was a small, but consistent, decrease in the frequency of cTEC (6.97 % ± 1.64 vs 9.55 % ± 1.92) with a corresponding increase in mTEC (90.13 % ± 2.42 vs 88.18 % ± 2.27) (Fig. 3.8A).

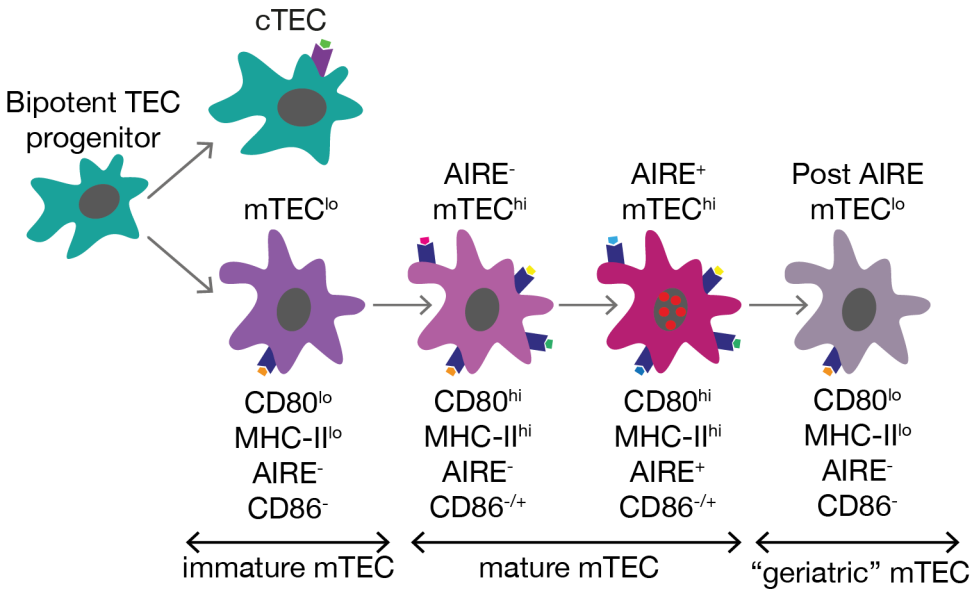

Figure 3.7: Scheme of TEC maturation [71]. mTEC and cTEC originate from a common progenitor. mTEC maturate by upregulating MHC-II, CD80, CD86 and AIRE with some of these cells continuing to a post-AIRE stage where MHC-II and CD80 are downregulated.

The maturational status of mTEC is assessed using the expression of MHC-II, CD80, CD86 and AIRE (see Figure 3.7). Immature mTEC (defined as mTEC^{lo}) are characterised by low cell surface levels of CD80 and MHC-II. Mature mTEC are designated mTEC^{hi}, as they express high levels of MHC-II and CD80. A subpopulation of mTEC^{hi} is AIRE positive [71] though upon further differentiation will lose its AIRE expression and downregulate MHC-II and CD80 to progress to a developmental stage known as post-AIRE mTEC^{lo} [136,

137]. It has to be noted that this population of terminally differentiated cells making up approximately 10 % of mTEC was not considered in my TEC analysis.

The maturation of mTEC in four-week-old, double mutant mice was characterised by a lower frequency of mTEC^{lo} and a higher frequency of AIRE^{+} mTEC^{hi} in the *Utx*$^{TEC-/-}$ *Jmjd3*$^{TEC-/-}$ mice in comparison to WT animals (mTEC^{lo}: 37.26 % ± 2.82 vs 47.36 % ± 5.17; AIRE^{+} mTEC^{hi}: 43.72 % ± 2.19 vs 32.70 % ± 3.65) (Fig. 3.8C). AIRE^{-} mTEC^{hi} were unchanged in frequency. Within the population of mTEC^{hi} the frequency of cells expressing the co-stimulatory molecule CD86^{+} was also increased (29.71 % ± 3.57 vs 20.48 % ± 3.3) (Fig. 3.8D).

To assess AIRE protein levels, the geometric mean fluorescent intensity (gMFI) of AIRE expression in AIRE^{+} cells was determined. The amount of AIRE in individual mutant mTEC^{hi} was lower in comparison to WT mTEC^{hi} (by 10.9 % ± 3.32 for CD86^{-} AIRE^{+} mTEC^{hi} and 15.3 % ± 3.4 for CD86^{+} AIRE^{+} cells) (Fig. 3.8E). Despite the higher frequency of AIRE^{+} mTEC^{hi} in *Utx*$^{TEC-/-}$ *Jmjd3*$^{TEC-/-}$ mice, AIRE expression levels were slightly reduced.

TEC present self-antigens to developing thymocytes using presentation by both MHC-II and MHC-I molecules [138] which is essential for positive selection, CD4/CD8-lineage choices and negative selection [139, 140]. I thus probed for average expression levels of MHC-II and MHC-I on the different TEC subpopulations, which revealed that UTX- and JMJD3-deficient mTEC^{lo} expressed MHC-II levels on their surface that were increased by 42 % compared to WT mice (normalised gMFI: 0.637 ± 0.09 vs 0.447 ± 0.05) (Fig. 3.8F). So, additionally to having an increased frequency of mTEC^{hi}, the mTEC^{lo} already expressed higher levels of MHC-II on their surface than the WT counterpart. While cTEC did not show any differences in MHC-II expression when deficient in UTX and JMJD3, their expression of MHC-I was increased (normalised gMFI: 1.57 ± 0.20 vs 1.19 ± 0.12) (Fig. 3.9). In mTEC, the expression level of MHC-I was not changed significantly.

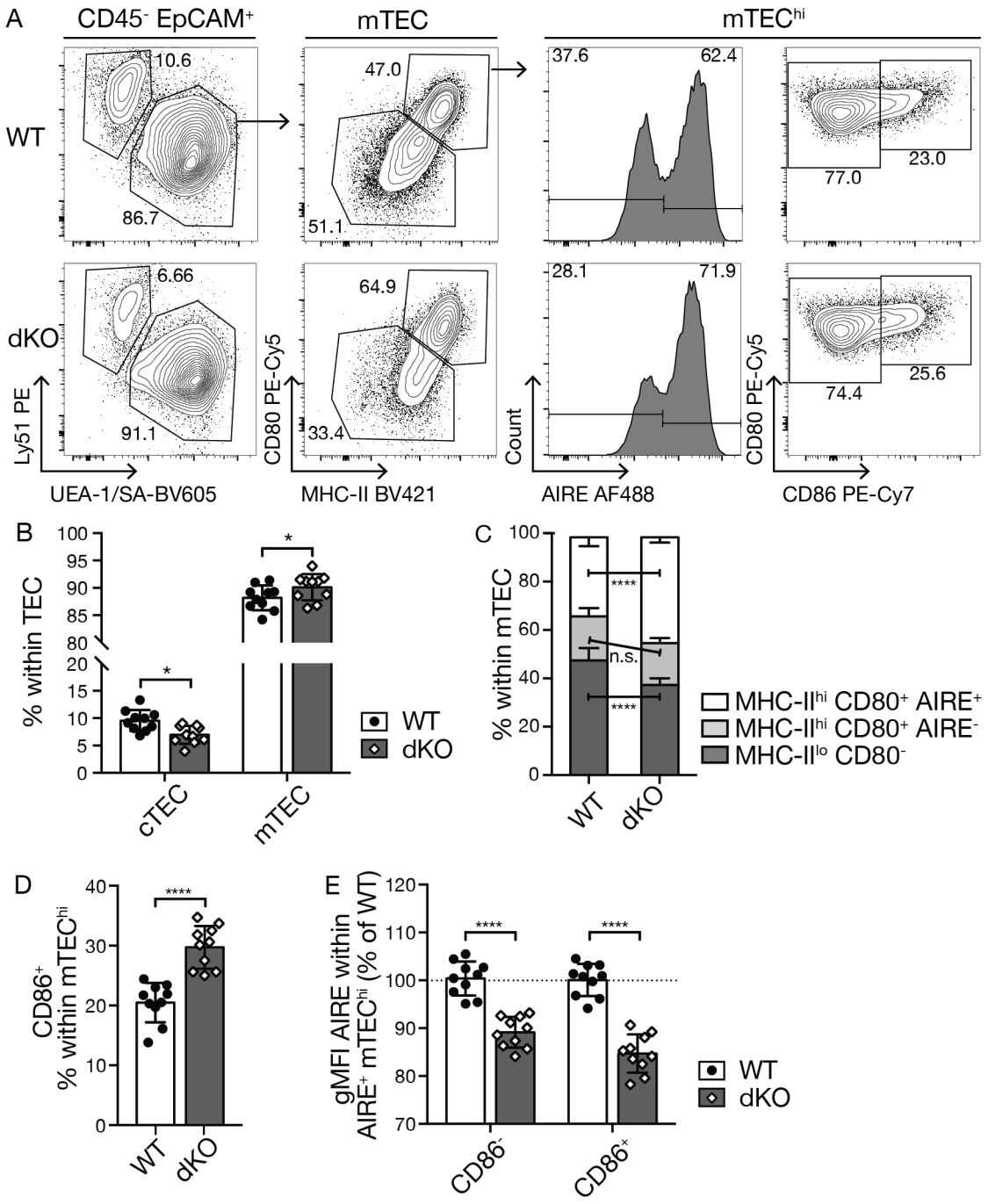
A
CD45- EpCAM+
mTEC
mTEChi
WT
dKO
10.6
86.7
47.0
51.1
37.6
62.4
77.0
23.0
6.66
91.1
64.9
33.4
28.1
71.9
74.4
25.6
Ly51 PE
UEA-1/SA-BV605
CD80 PE-Cy5
MHC-II BV421
Count
AIRE AF488
CD80 PE-Cy5
CD86 PE-Cy7
B
% within TEC
cTEC
mTEC
WT
dKO
C
% within mTEC
MHC-IIhi CD80+ AIRE+
MHC-IIhi CD80+ AIRE-
MHC-IIlo CD80-
n.s.
D
CD86+ % within mTEChi
E
gMFI AIRE within AIRE+ mTEChi (% of WT)
CD86-
CD86x

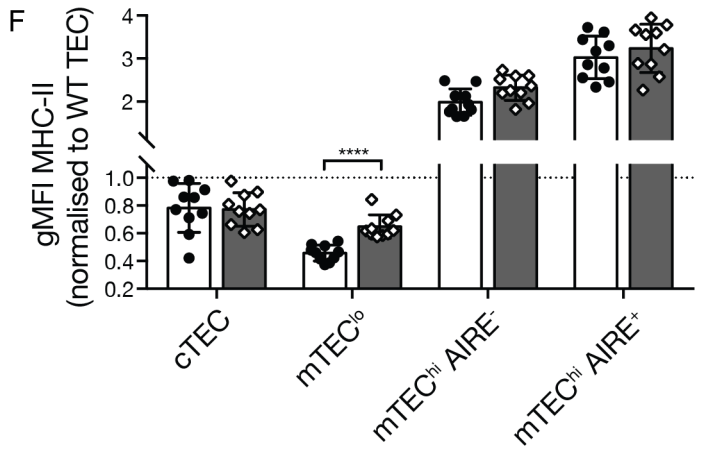

Figure 3.8: Frequency of mature mTEC is increased in mice with TEC-targeted loss of UTX/JMJD3 expression. **(A)** Representative FACS plots show the gating strategy for TEC identification and assessment. **(B)** Bar graph depicts relative frequencies of cTEC and mTEC. **(C)** Bar graph shows mTEC maturation according to MHC-II, CD80 and AIRE expression. **(D)** Bar graph shows relative frequency of $CD86^+$ cells within $mTEC^{hi}$. **(E)** Bar graph shows expression level of AIRE within $AIRE^+$ $CD86^-$ $mTEC^{hi}$ and $AIRE^+$ $CD86^+$ $mTEC^{hi}$ as measused by gMFI normalised to the respective WT population. **(F)** Bar graph shows gMFI of MHC-II in different TEC subpopulations normalised to gMFI of MHC-II in WT total TEC, arbitrarily defined as a value of "1" for these cells. Data shown in graphs are pooled from four independent experiments using female mice at 4-5 weeks of age (WT ($Utx^{fl/fl}$ $Jmjd3^{fl/fl}$) n=10; dKO ($Utx^{TEC\text{-}/\text{-}}$ $Jmjd3^{TEC\text{-}/\text{-}}$) n=10). Statistical analysis was done with two-tailed unpaired t-tests.

3.4.3 UTX- and JMJD3-deficient cTEC and $mTEC^{hi}$ proliferate less

A reduced frequency of cTEC and $mTEC^{lo}$ was observed in $Utx^{TEC\text{-}/\text{-}}$ $Jmjd3^{TEC\text{-}/\text{-}}$ mice whereas the frequency of $AIRE^+$ $mTEC^{hi}$ was increased. I wanted to investigate whether the differences in the frequency of TEC subpopulations were due to changes in proliferation, which I sought to assess by staining the nuclei of these cells for Ki67 expression. Ki67 can be detected in the active phases, but is absent in the quiescent phases of the cell cycle [141].

The deficiency in UTX and JMJD3 resulted in a reduced proliferation in cTEC (7.10 % ± 1.60 vs 10.58 % ± 3.09), explaining the reduction in cTEC frequency in these mice (Fig. 3.10). In contrast, $mTEC^{lo}$ displayed a slightly increased proliferation rate (6.22% ± 1.55 vs 4.44 % ± 0.86), while $AIRE^+$ $mTEC^{hi}$ were less proliferative (9.71% ± 1.45 vs 13.51% ± 1.06). Since the relative cellularity of $mTEC^{lo}$ was decreased, while that of $AIRE^+$ $mTEC^{hi}$ was increased, other factors must have played a role to explain the changes in the population frequencies. The increased frequency of $AIRE^+$ $mTEC^{hi}$ in the $Utx^{TEC\text{-}/\text{-}}$ $Jmjd3^{TEC\text{-}/\text{-}}$ mice could for example be a consequence of a decrease in cell death

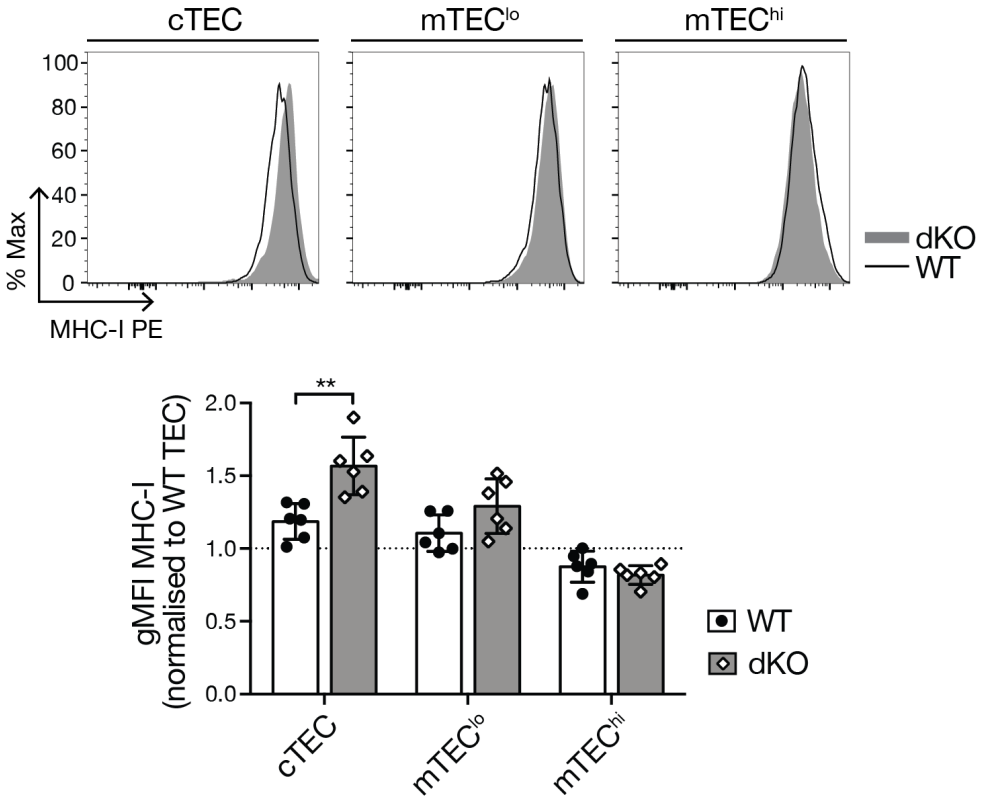

Figure 3.9: Increased MHC-I expression in UTX/JMJD3-deficient cTEC. Representative histograms of MHC-I expression and bar graphs showing the gMFI of MHC-I normalised to gMFI in WT total TEC, providing an arbitrary value of "1" for these cells. Data shown in graphs are pooled from two independent experiments with female mice 4-5 weeks of age (WT (*Utx*$^{fl/fl}$ *Jmjd3*$^{fl/fl}$): n=6; dKO (*Utx*$^{TEC\text{-}/\text{-}}$ *Jmjd3*$^{TEC\text{-}/\text{-}}$): n=6). Two-tailed unpaired t-test with correction for multiple comparisons was used for statistical comparison. *p<0.05; **p<0.01.

or an accelerated maturation from respective precursors. Alternatively, the progression to the post-AIRE stage may be delayed, resulting in an accumulation of AIRE^{+} mTEC^{hi}.

3.4.4 Brief summary of UTX- and JMJD3-deficient TEC

Mice with a TEC-specific deficiency of UTX and JMJD3 have a thymus of normal size and TEC cellularity. I observed a small reduction in the cTEC/mTEC ratio, which is compatible with the reduced proliferation rate of cTEC in these animals. On the other hand, the frequency of AIRE^{+} mTEC^{hi} is increased in the *Utx*$^{TEC\text{-}/\text{-}}$ *Jmjd3*$^{TEC\text{-}/\text{-}}$ mice, despite the fact that they are less proliferative. A potential explanation of why there are more mTEC^{hi} in the gene-targeted mice despite their reduced cell proliferation may be the higher proliferation rate in the mTEC^{lo} and their faster transition to a mature

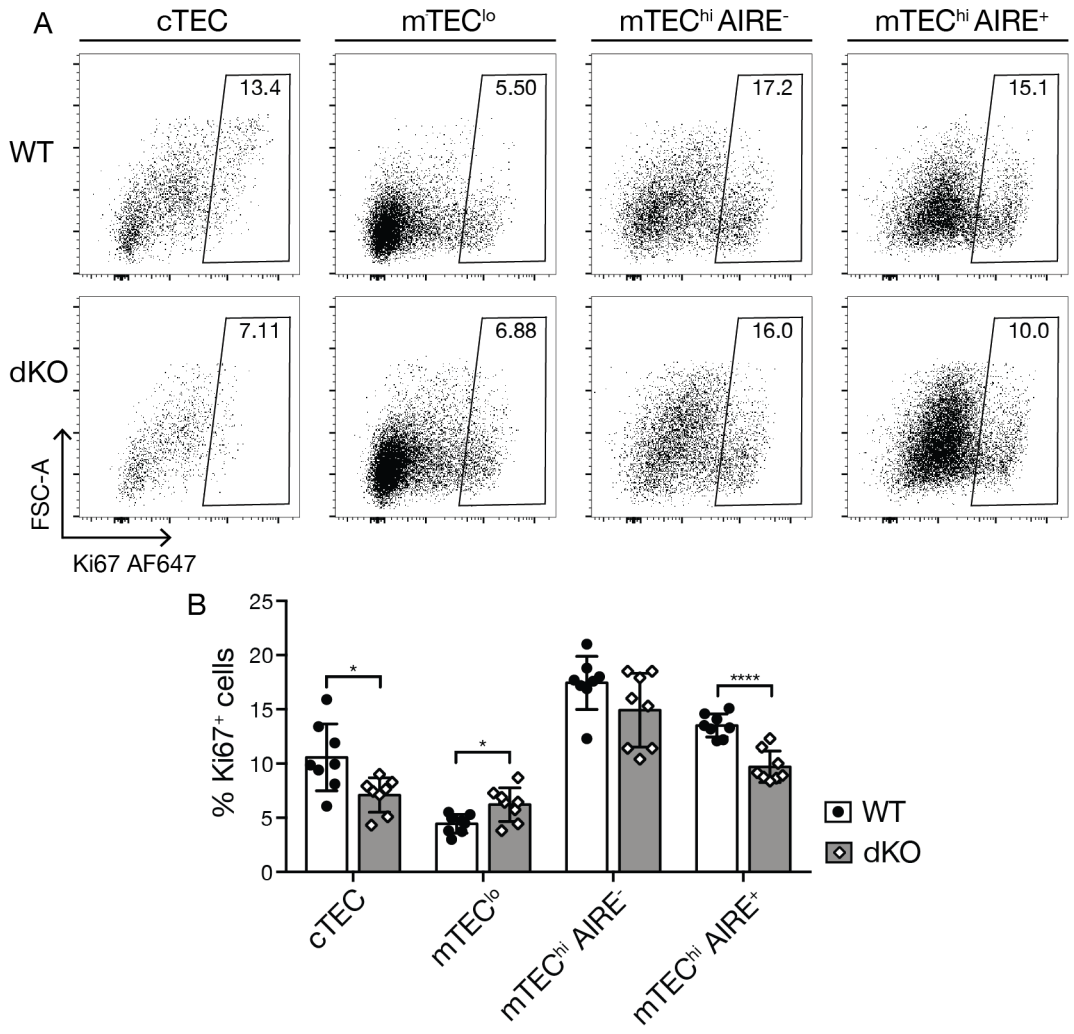

Figure 3.10: UTX- and JMJD3-deficient cTEC and AIRE$^+$ mTEC^{hi} proliferate less. **(A)** Representative FACS plots showing Ki67 expression. **(B)** Bar graph showing relative frequencies of Ki67$^+$ cells. Data in graphs are pooled from three independent experiments. Female mice 4-5 weeks of age; WT (*Utx$^{fl/fl}$ Jmjd3$^{fl/fl}$*): n=8; dKO (*Utx$^{TEC-/-}$ Jmjd3$^{TEC-/-}$*): n=8. Two-tailed unpaired t-test with correction for multiple comparisons. *p<0.05; **p<0.01; ***p<0.005, ****p<0.001.

phenotype. Alternatively, mTEC^{hi} with a UTX/JMJD3 deficiency might have a longer half-life and thus lower turnover, resulting in an accumulation of this cell population.

While the frequency of AIRE$^+$ mTEC^{hi} is increased in *Utx$^{TEC-/-}$ Jmjd3$^{TEC-/-}$* mice, AIRE protein expression levels per cell are reduced by approximately 10 % in comparison to WT animals. Although the differentiation to an AIRE$^+$ mTEC^{hi} phenotype is undiminished, these cells have reduced AIRE expression.

Taken together, the TEC phenotypic changes observed in *Utx$^{TEC-/-}$ Jmjd3$^{TEC-/-}$* mice

are rather subtle, suggesting that their absence hardly disrupts the normal differentiation from TEC progenitors to either cTEC or mTEC and their general maturation.

3.5 Transcriptional changes in mTEC^{hi} lacking UTX and JMJD3

The capacity for PGE is essential to providing a comprehensive repertoire of self-antigens able to efficiently select maturing T cells for the presence of a high-affinity TCR with specificity to these antigens [33]. The genes encoding TRA have chromatin that is preferentially enriched for specific histone marks, most notably H3K27me3, creating a repressive histone landscape especially in the vicinity of the transcriptional start sites of genes that are responsive to AIRE-mediated transcription [50, 103]. Therefore, I assessed changes in the transcriptional programmes due to the UTX/JMJD3 deficiency in mTEC^{hi} as these cells constitute a mature population competent to express a broad range of TRA with some of them under the direct control of AIRE [33].

My proposed hypothesis is that H3K27me3 marks play an important role for AIRE-regulated gene expression programmes. Should this be correct, increased H3K27me3 marks due to the deficiency in UTX/JMJD3 would consequently be expected to enhance the expression of AIRE-regulated loci. Alternatively, UTX and JMJD3 may be important in the local process of demethylating H3K27me3 and thus alleviating transcriptional repression to effect PGE and possibly other gene expression programmes in mTEC^{hi}. Hence, the loss of UTX's and JMJD3's catalytic activity in these cells could result in reduced gene expression.

3.5.1 952 genes are differentially expressed in mTEC^{hi} in the absence of UTX and JMJD3

The impact of an absence of UTX and JMJD3 on gene transcription in mTEC^{hi} was analysed using RNA-Seq. To this end, mTEC^{hi} were sorted, RNA isolated and libraries generated using the SmartSeq2 amplification method. The following bioinformatics

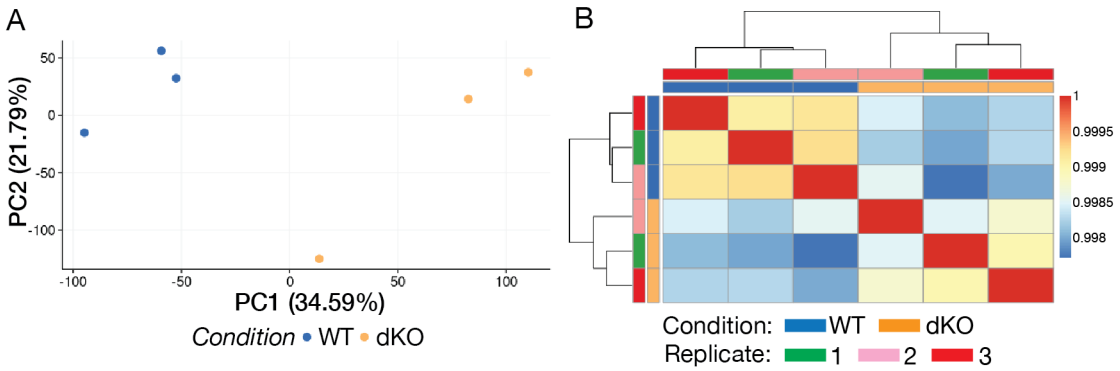

Figure 3.11: Clustering of *Utx*$^{TEC-/-}$ *Jmjd3*$^{TEC-/-}$ and WT mTEC^{hi}. **(A)** Principal component analysis (PCA) of the filtered and normalised samples. **(B)** Unsupervised hierarchical clustering of samples.

analyses were done in collaboration with Michael Morgan from the Wellcome Trust Sanger Institute in Cambridge.

To establish the relatedness between the individual libraries generated from mTEC^{hi} of WT and *Utx*$^{TEC-/-}$ *Jmjd3*$^{TEC-/-}$ mice, the samples were initially subjected to a principal component analysis (PCA) and unsupervised clustering. WT and mutant mTEC^{hi} clustered according to their genotype, albeit more variation was observed in the gene-targeted samples (Fig. 3.11). However, the overall variance was small, and the two conditions were highly similar across their entire transcriptome (Fig. 3.11B), suggesting that the differences only affect a specific set of genes between the samples. This would be compatible with previously published data from T cells that a UTX/JMJD3 deficiency only affects the expression of a small number of genes [108].

The $\log_2$ fold gene expression changes were calculated between WT and mutant mTEC^{hi} and identified 952 significantly changed genes, of which 463 were upregulated and 489 downregulated in the UTX/JMJD3-double-deficient mTEC^{hi}. Of note, the gene expression changes were small with almost all changes lying within $\log_2$ fold change < 2 (Fig. 3.12).

Confirmation of these gene expression changes for the top differential expression hits (according to their adjusted p-value) by qPCR can be found in Chapter 4.4 where the expression of these genes was further tested in mTEC^{hi} isolated from mice with a TEC-specific single deficiency for either UTX or JMJD3 and in double-deficient mTEC^{hi}

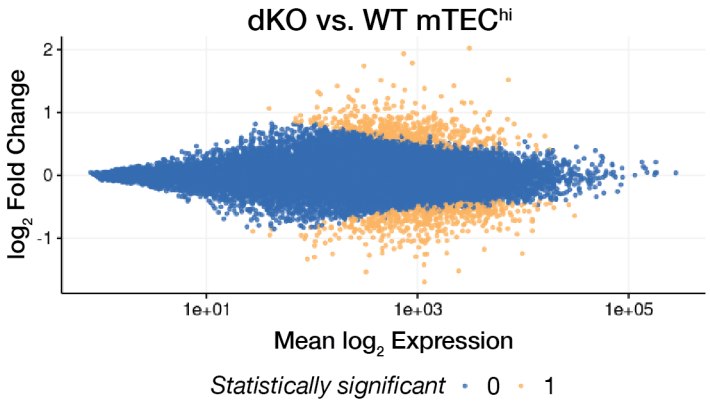

Figure 3.12: UTX/JMJD3 double deficiency causes gene expression changes of small amplitude in mTEC^{hi}. Log_2 fold expression change plotted against mean log_2 expression. Significantly changed genes are coloured orange (adjusted p-value < 0.01).

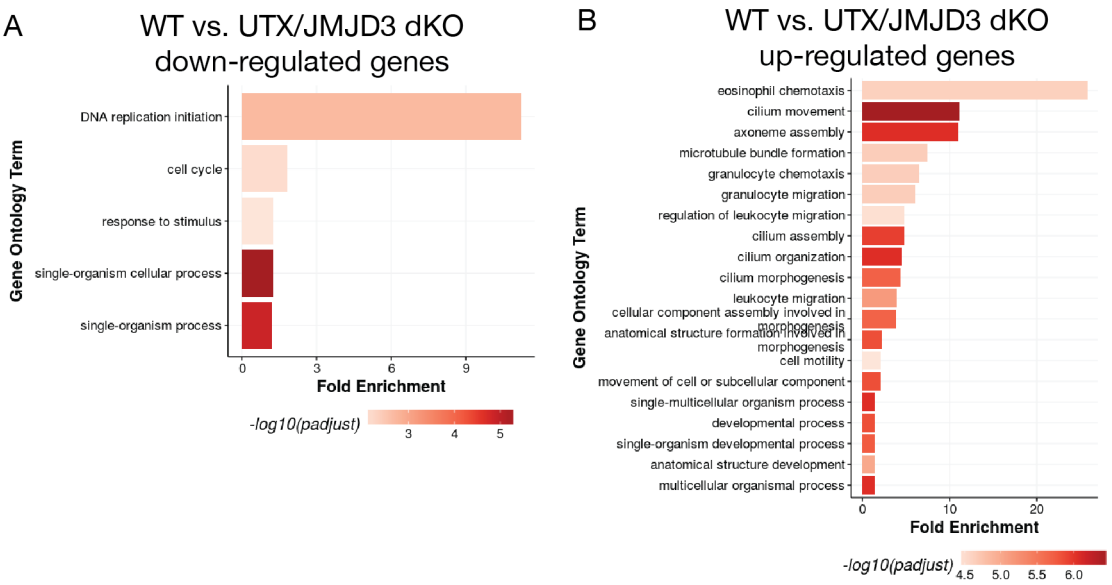

Figure 3.13: Gene ontology analysis of downregulated (A) and upregulated genes (B).

isolated from male mice (which express UTY).

Gene ontology analysis of downregulated genes in the UTX/JMJD3-double-deficient mTEC^{hi} revealed an enrichment in genes associated with the DNA replication mechanism and cell cycle (Fig. 3.13A). This finding agrees with the result that there were fewer Ki67^{+} cells within UTX/JMJD3-double-deficient mTEC^{hi} as assessed by flow cytometry (see Fig. 3.9). Upregulated genes were enriched for genes involved in granulocyte migration and eosinophil chemotaxis (Fig. 3.13B), most likely ascribed to PGE.

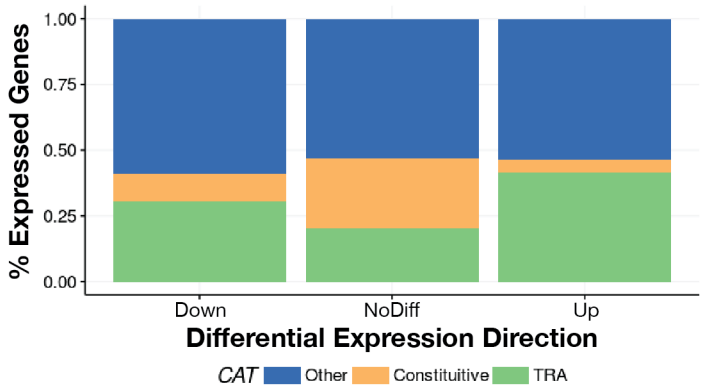

Figure 3.14: Enrichment of TRA in differentially expressed genes. Graph depicts percentage of TRA, constitutive genes and other (defined according to the tissue specificity of their expression) within downregulated, unchanged and upregulated genes in the UTX- and JMJD3-deficient mTEC^{hi}.

3.5.2 Genes upregulated in UTX/JMJD3-deficient mTEC^{hi} are enriched for genes enhanced in their expression in the presence of AIRE

To gain an understanding of how an absence of both UTX and JMJD3 impacts on PGE, genes were first divided into different categories according to their tissue specificity as estimated by their tau (τ) value [50, 117]: (i) genes with a tissue-restricted expression (i.e. genes that encode tissue-restricted antigens, "TRA", $\tau \geq 0.8$), (ii) genes that are constitutively expressed across tissues ("Constitutive", $\tau \leq 0.4$) and (iii) genes that lie in between these two categories ("Other", $0.4 < \tau < 0.8$).

The differentially expressed genes were strongly enriched for TRA (Fig. 3.14). Among the differentially expressed genes there were slightly more TRA that were upregulated, although the difference was subtle (191 TRA upregulated, 149 TRA downregulated). The higher tissue specificity of the upregulated genes was further confirmed by having a significantly higher average τ value in the upregulated genes than in the downregulated genes as determined by a Welch Two Sample t-test.

As some TRA might fall below the threshold of statistical significance, a more liberal cut-off was applied to include more genes in the differential expression analysis. To this end, a mean $\log_2$ expression change threshold of ≥ 0.28 was used, which identified

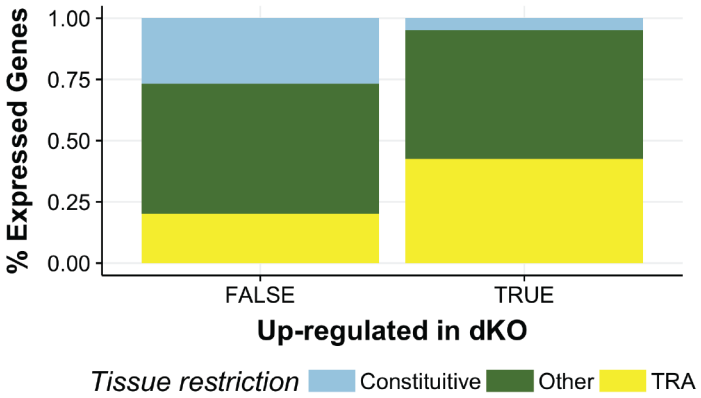

Figure 3.15: Enrichment of TRA in differentially expressed genes. Graph depicts percentage of TRA, constitutive genes and other (defined according to the tissue specificity of their expression) within upregulated and not upregulated genes in the UTX- and JMJD3-deficient mTEC^{hi}. Upregulation was defined as ≥ 0.28 $\log_2$ expression change regardless of statistical significance.

660 genes as upregulated. These upregulated genes showed the same enrichment for TRA genes (Fig. 3.15).

Next, the differentially expressed genes were analysed for their dependency on the transcriptional facilitator AIRE and thus divided into the three following categories: AIRE-dependent genes, which are characterised not to be expressed in the absence of AIRE, AIRE-enhanced genes, which are reduced more than two-fold in the absence of AIRE, and AIRE independent genes, which are not affected by the presence or absence of AIRE.

There was a strong enrichment of AIRE-enhanced genes specific to the upregulated genes in the UTX/JMJD3-deficient mTEC^{hi} (Fig. 3.16). An enrichment of AIRE-dependent genes could not be detected among the upregulated genes, however, since AIRE-dependent genes represent a comparatively small number of genes, changes are not expected to be easily detected. The strong enrichment of AIRE-enhanced genes among the upregulated transcripts in mTEC^{hi} deficient in UTX and JMJD3 highlights the importance of these epigenetic enzymes for PGE. The proposed increase of H3K27me3 marks in the gene-targeted cells thus correlates with an increased expression of AIRE-regulated PGE, thus supporting my initial hypothesis.

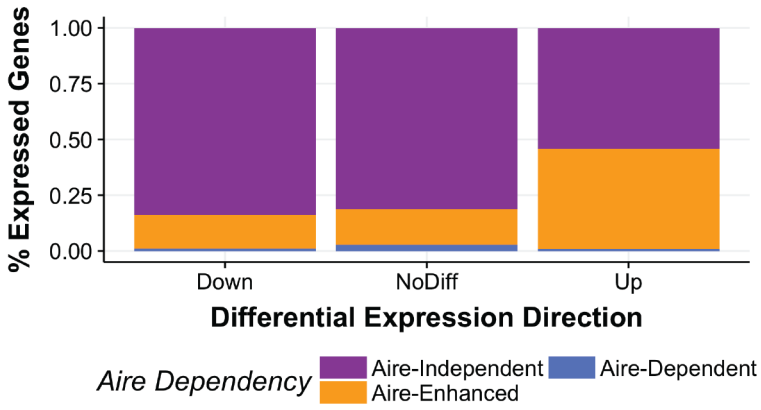

Figure 3.16: Enrichment of AIRE-enhanced genes is specific to upregulated genes. Graph shows percentage of AIRE-independent, -enhanced and -dependent genes within downregulated, unchanged and upregulated genes in the UTX- and JMJD3-deficient mTEC^{hi}. Upregulation was defined as ≥ 0.28 $\log_2$ expression change regardless of statistical significance.

3.5.3 The expression of mTEC-specific NFκB signaling genes are unchanged in UTX/JMJD3-deficient mTEC^{hi}

A deficiency of UTX and JMJD3 expression in mTEC^{hi} combined with an inability to demethylate promoter sequences could also affect gene expression independent of PGE. In the context of T cell development, H3K27me3 demethylation of the promoter of *S1pr1* requires UTX or JMJD3 and a concurrent loss of both enzymes results in a decreased expression of the *S1pr1* locus, causing a delayed egress of thymocytes to the periphery [108]. I thus probed whether genes that are known to be essential for mTEC maturation and function depend for their expression on H3K27me3 demethylation in the vicinity of their promoters in order to be expressed. Members of the NFκB signalling pathway, which play a major role in mTEC differentiation, as well as other genes that have been identified to be important for mTEC function, were unchanged in their expression between WT and UTX/JMJD3-deficient mTEC^{hi} (Table 3.1A-B) [20, 142]. Handel et al. have identified candidate transcription factors that are differentially expressed between mTEC^{lo} and mTEC^{hi} [103]. However, none of these factors (*Cdx1, Runx3, Tbx21, Tcf7*) shows significant differential expression between WT and UTX/JMJD3-deficient mTEC^{hi} (Table 3.1C). Thus, these factors do not rely on UTX/JMJD3-mediated H3K27me3 demethylation to be correctly expressed in mTEC^{hi}.

	Gene	baseMean	log2 Fold Change	Adjusted p-value	Significant
A	*Akt1*	1720.2	-0.203	0.439	No
	Chuk	2158.9	0.150	0.606	No
	Nfkb1	4272.4	0.119	0.612	No
	Nfkb2	18117.2	-0.212	0.316	No
	Rel	1984.7	-0.084	0.820	No
	Rela	3865.5	-0.069	0.809	No
	Relb	14585.2	-0.352	0.093	No
B	*Ifnb1*	104.4	0.301	0.498	No
	Igf1	5944.4	0.179	0.405	No
	Irf4	2901.0	-0.312	0.138	No
	Irf7	3762.8	0.051	0.874	No
	Ltbr	1514.1	-0.197	0.491	No
	Spib	24081.8	-0.286	0.288	No
	Tgfbr2	328.3	0.007	0.994	No
	Tnfrsf11a	4816.1	-0.004	0.994	No
	Tnfrsf11b	15828.3	-0.017	0.965	No
	Trp53	10184.3	-0.371	0.023	No
C	*Cdx1*	13695.8	-0.268	0.120	No
	Runx3	2951.4	-0.323	0.090	No
	Tbx21	2236.7	-0.195	0.502	No
	Tcf7	1609.0	-0.208	0.365	No

Table 3.1: Gene expression in WT and UTX/JMJD3-deficient mTEC^{hi}. (A) Genes of NFκB signaling. (B) Genes that have been identified to play a role in mTEC differentiation [142]. (C) Candidate transcription factors for mTEC^{lo} to mTEC^{hi} development [103].

3.5.4 Histone landscape of differentially expressed genes

Genes expressed differentially in the absence of UTX and JMJD3 in the mTEC^{hi} RNA-Seq dataset were next investigated for their histone landscape, as established in WT mTEC^{hi} using ChIP Seq previously generated in our lab [50, 103].

Promoters were defined by the -1kb to +500bp region around the transcriptional start site (TSS). As previously published, TRA – in particular AIRE-regulated TRA – had a more repressive promoter landscape with higher levels of H3K27me3 and at these sites a relative depletion of the active histone mark H3K4me3 (Fig. 3.17A, B).

Genes upregulated in the UTX/JMJD3-deficient mTEC^{hi} displayed a higher H3K27me3 signal in their promoter regions when compared to the corresponding sequence of downregulated genes (Fig. 3.17C). H3K4me1 levels were unchanged when comparing

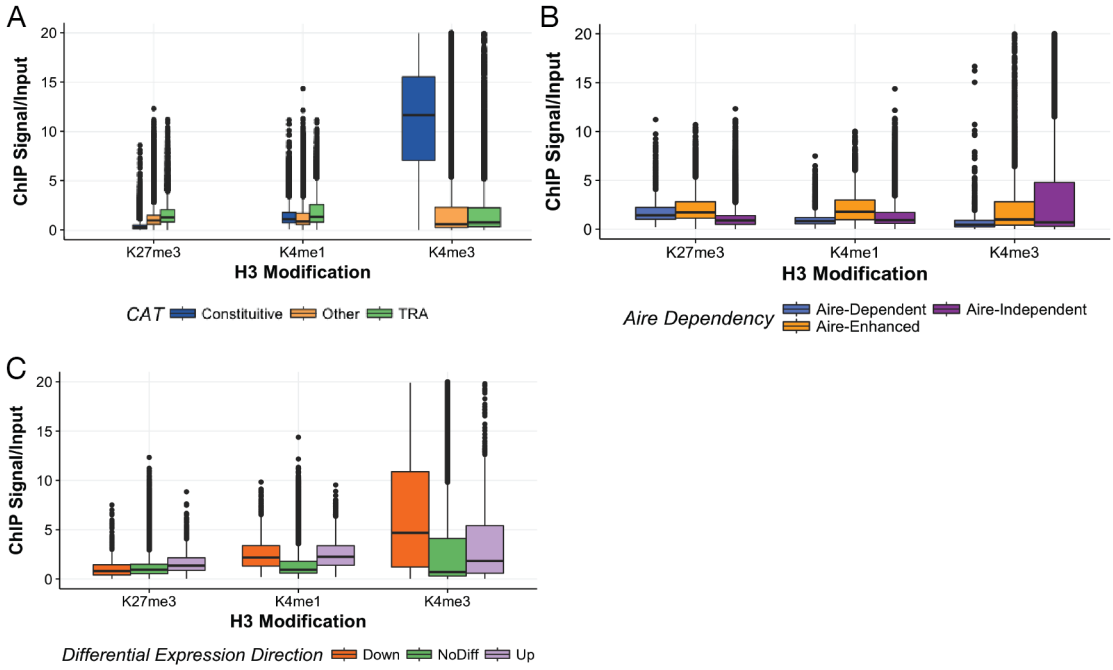

Figure 3.17: Genes upregulated in UTX/JMJD3-deficient mTEC^{hi} are marked with higher levels of H3K27me3. Graphs show ChIP Signal over Input for H3K27me3, H3K4me1 and H3K4me3 in the promoters of different gene groups: **(A)** defined according to the tissue specificity of their expression, **(B)** depending on their AIRE dependency, **(C)** depending on gene direction change in UTX/JMJD3-deficient mTEC^{hi} RNA-Seq dataset.

up- and downregulated genes. The permissive H3K4me3 mark was higher among genes that were downregulated as a consequence of the loss of UTX/JMJD3. This behavior would be in line with the notion that these genes may require H3K27me3 demethylation for their expression.

3.5.5 Relationship of H3K27me3 marks in promoter with expression frequency and average expression levels in mTEC^{hi}

Expressing genes despite – or even due to – repressive histone marks (e.g. H3K27me3) placed at their promoter regions seems paradoxical. To obtain a more detailed picture of the relationship between gene expression and H3K27me3 enrichment, single cell RNA-Seq data from WT mTEC^{hi} (combining datasets that have been generated in our lab and publicly available ones [51, 52], totalling to 997 single cells) were used to determine gene expression frequency and levels. In this way, 14273 genes were detected, which were then correlated to H3K27me3 enrichment in promoters.

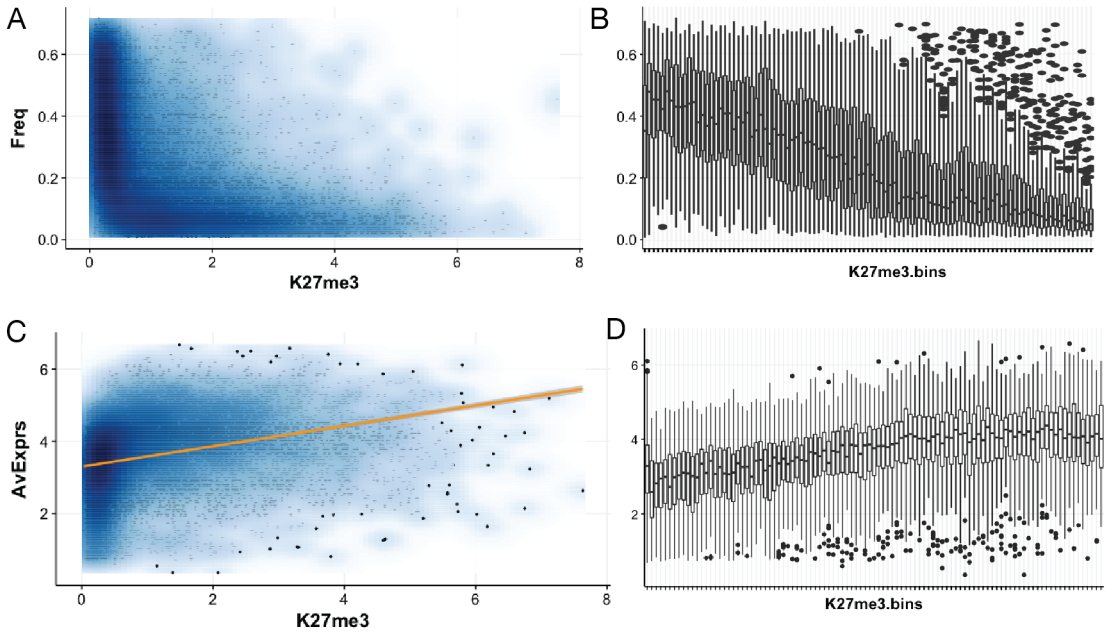

Figure 3.18: H3K27me3 levels are negatively correlated with expression frequency, but positively correlated with average expression. (A-B) Graphs show ChIP Signal over Input for H3K27me3 on the x-axis and expression frequency on the y-axis. **(C-D)** Graphs show ChIP Signal over Input for H3K27me3 on the x-axis and average expression (in cells that express the gene) on the y-axis. In (B) and (D) H3K27me3 levels were split into 100 bins with an equal number of genes in each category to flatten out the non-linear relationship.

This analysis revealed that a higher H3K27me3 promoter signal was correlated with a lower gene expression frequency (Fig. 3.18A). The relationship was however not linear in that the expression frequency dropped drastically above a certain H3K27me3 signal. This relationship was not surprising given that H3K27me3 in the promoter is involved in gene repression. In contrast, a higher H3K27me3 signal in a gene's promoter was correlated with a higher average expression in cells that do express the gene (Fig. 3.18C). This analysis demonstrated that despite having a lower expression frequency, genes with high H3K27me3 in their promoter were more highly expressed than genes marked by lower H3K27me3 levels.

These relationships held up when dividing the genes according to their AIRE dependency (Fig. 3.19A-B). AIRE-dependent and AIRE-enhanced genes were expressed at lower frequency, but at higher average expression under condition where these were characterized by more H3K27me3 marks (Fig. 3.19C-D). This finding is also in line with previously reported findings from single cell analyses, that AIRE-enhanced and AIRE dependent genes are expressed at low frequency, but of higher average expression level [50–52, 143].

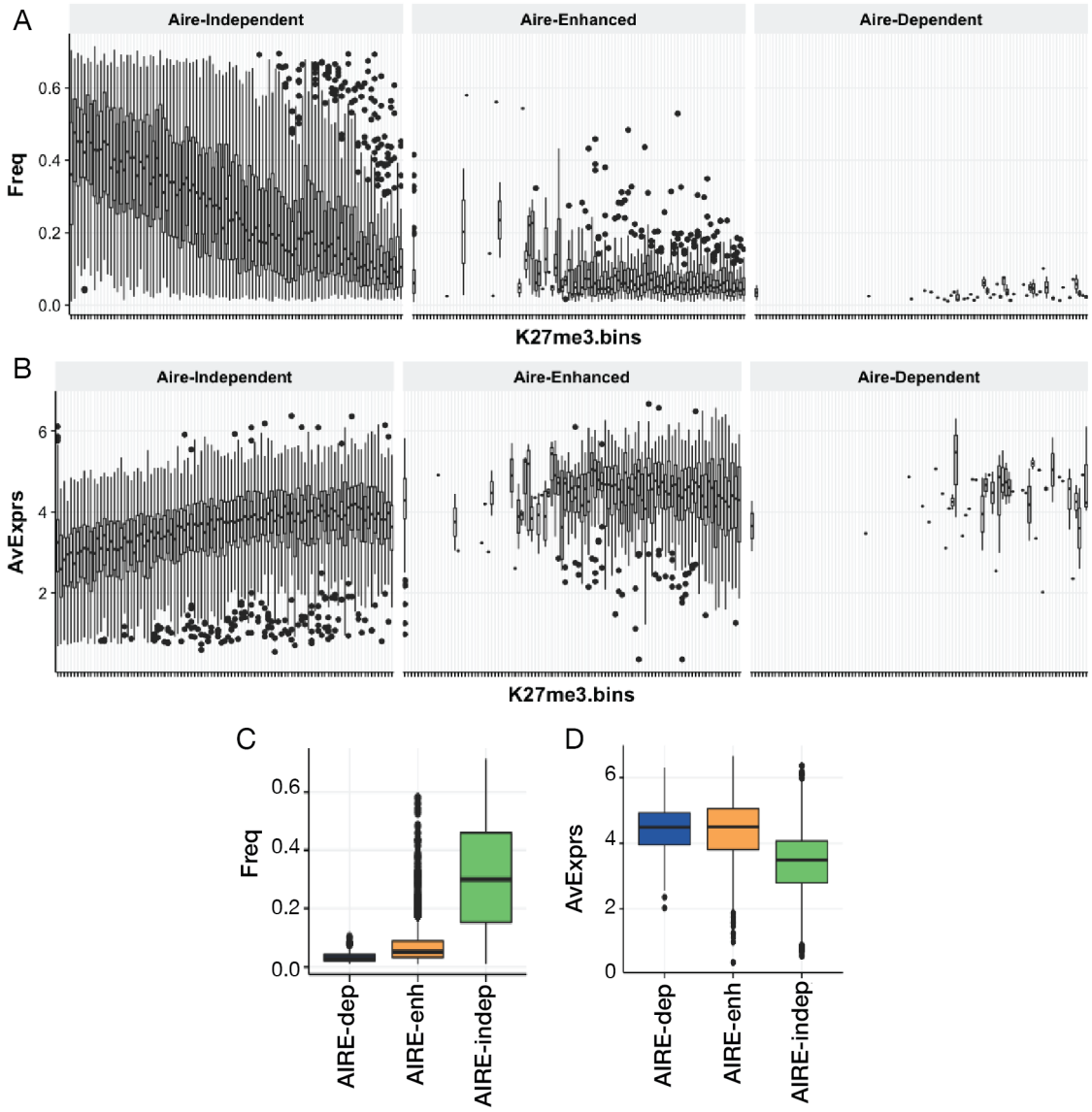

Figure 3.19: Relationship of H3K27me3 levels with expression frequency and average expression of AIRE-dependent, -enhanced and -independent genes. **(A-B)** Graphs showing ChIP Signal over Input for H3K27me3 divided into 100 equally sized bins on the x-axis and expression frequency **(A)** or average expression **(B)** on the y-axis. **(C)** Graph showing expression frequency of AIRE-dependent, -enhanced and -independent genes. **(D)** Graph showing average expression in AIRE-dependent, -enhanced and -independent genes.

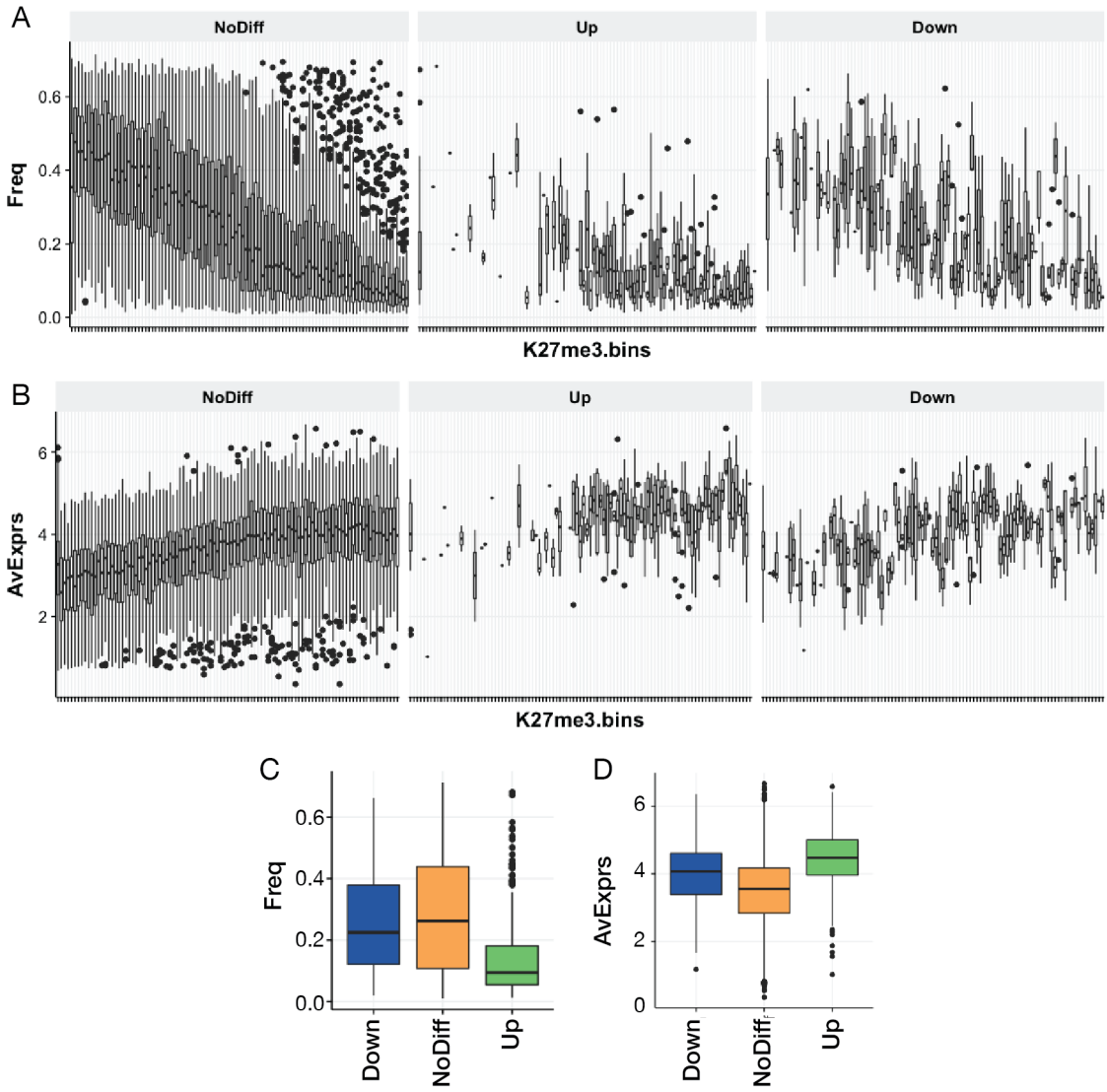

Figure 3.20: Relationship of H3K27me3 levels with expression frequency and average expression of genes up- or downregulated in UTX/JMJD3-deficient mTEC^{hi}. (A-B) Graphs show ChIP Signal over Input for H3K27me3 divided into 100 bins containing equal gene numbers on the x-axis and expression frequency **(A)** or average expression **(B)** on the y-axis. **(C)** Graph shows expression frequency of genes upregulated, downregulated or unchanged in UTX/JMJD3-deficient mTEC^{hi}. **(D)** Graph shows average expression in genes upregulated, downregulated or unchanged in UTX/JMJD3-deficient mTEC^{hi}.

Finally, the same analysis was performed for genes identified as differentially expressed in the RNA-Seq analysis comparing WT to UTX/JMJD3-deficient mTEC^{hi}. Genes that were upregulated in the mutant mTEC^{hi} were expressed at a lower frequency but higher average expression than downregulated and unchanged loci (Fig. 3.20).

3.5.6 Brief summary of the RNA-Seq analysis of mTEC^{hi} from *Utx$^{TEC-/-}$ Jmjd3$^{TEC-/-}$* mice

The deficiency in UTX and JMJD3 in mTEC^{hi} leads to gene expression changes of small amplitude in around 900 genes differentially expressed, of which half were upregulated and the other half downregulated. Most importantly, there was a strong enrichment for AIRE-enhanced genes in the genes that were upregulated in UTX/JMJD3-deficient mTEC^{hi}. This is in line with the initial hypothesis that H3K27me3 has a functional importance for AIRE-regulated PGE. AIRE-dependent genes are not affected by the UTX/JMJD3 deficiency, however it is not clear if this is just a sensitivity issue since these genes are fewer in number, or if they are less affected by the UTX and JMJD3 deficiency than the AIRE-enhanced genes which might be due to different regulation mechanisms between AIRE-enhanced and AIRE-dependent genes. The genes that are upregulated in the UTX/JMJD3-deficient mTEC^{hi} have a higher signal for H3K27me3 marks in their promoters than downregulated and not differentially expressed genes when analysing the promoters of these genes in available H3K27me3 ChIP Seq data from WT mTEC^{hi}.

Additionally, this subchapter has also looked at the relationship of H3K27me3 signal and expression frequency and average expression levels using available mTEC^{hi} single cell data. This revealed that while H3K27me3 levels in the promoter were correlated negatively with the expression frequency of a gene, they were positively correlated with the average expression level per cell. So while genes with high H3K27me3 decoration were expressed at low frequency within mTEC^{hi} population, the genes were more highly expressed the higher their H3K27me3 levels were. The genes that were upregulated in the UTX/JMJD3-deficient mTEC^{hi} also follow this pattern and were expressed at low frequency, but if they were expressed, they were expressed at high average expression levels.

3.6 H3K27me3 landscape in TEC with a loss of JMJD3 and UTX

After identifying gene expression changes in the UTX/JMJD3-deficient mTEC^{hi}, I wanted to determine whether the observed transcriptomic changes were linked to altered levels of H3K27me3 marks at the promoters of differentially expressed genes. Thus, I planned to analyse the H3K27me3 signal in UTX/JMJD3-deficient mTEC^{hi} and correlate this result to the transcriptomic profile of these cells. Combining ChIP-Seq data and RNA-Seq data would give strength to the argument that the demethylase function of UTX and JMJD3 acting at the specific loci is responsible for the detected changes in AIRE-enhanced PGE. This subchapter summarises my pilot experiments to establish an anti-H3K27me3 ChIP-Seq to address this question.

3.6.1 Absence of global changes in H3K27me3 marks in UTX- and JMJD3-deficient TEC

Before analysing the loci-specific distribution of H3K27me3, I first probed whether global H3K27me3 changes could be detected in UTX/JMJD3-deficient TEC. I therefore used a flow cytometric approach to quantify H3K27me3 in these cells normalising the gMFI of H3K27me3 to that of H3. This analysis did not reveal any significant changes between WT and UTX/JMJD3-deficient TEC (Fig. 3.21) and is in keeping with previously published results that demonstrated UTX and JMJD3 to be responsible for the demethylation of only a small number of genes when tested by ChIP-Seq [108].

3.6.2 Feasibility of H3K27me3 ChIP on 10 000 mTEC^{hi}

To establish a causal relationship between the detected changes in gene expression and H3K27me3 marks, H3K27me3 ChIP experiments with WT and UTX/JMJD3-deficient mTEC^{hi} was required. However, there are several difficulties to be taken into account for such an approach. First and foremost, there is only a limited number of mTEC^{hi} that can be isolated from a single mouse. In recent years, there has been significant progress

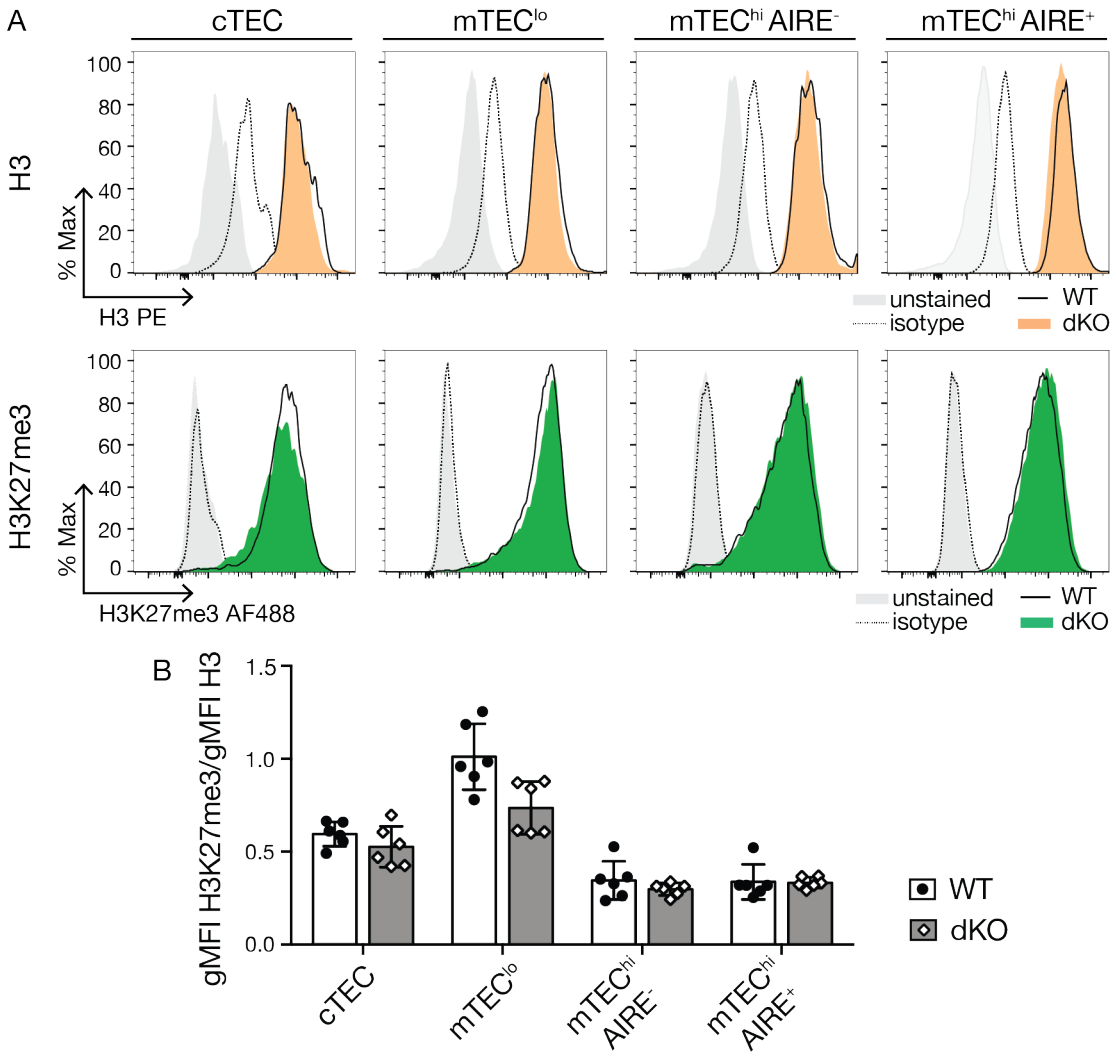

Figure 3.21: Unchanged H3K27me3 levels in UTX/JMJD3-deficient TEC. (A) Representative histograms of H3 and H3K27me3 expression. **(B)** Bar graphs showing gMFI of H3K27me3 normalised to H3. Graphs are pooled from two independent experiments with female mice 4-5 weeks of age; WT ($Utx^{fl/fl}$ $Jmjd3^{fl/fl}$): n=6; dKO ($Utx^{TEC\text{-}/\text{-}}$ $Jmjd3^{TEC\text{-}/\text{-}}$): n=6. Statistical comparison was done with two-tailed unpaired t-tests with correction for multiple comparisons.

to reduce cell numbers required for ChIP, however the data generated from low input ChIP generally has higher variability than data generated from millions of cells [144]. This limitation poses another difficulty for using this method with UTX/JMJD3-deficient TEC, as the expected differences in H3K27me3 marks are likely to be subtle [108]. Given that the anti-H3K27me3 ChIP with WT mTEC^{hi} samples demonstrated that the promoter of genes upregulated in mTEC^{hi} in the absence of UTX/JMJD3 have higher local H3K27me3 levels marking their promoter, it was conceivable that this specific

signal would be even more prominent in the mutant UTX/JMJD3 mTEC^{hi}. Hence, this assumption implies the need for a quantitative analysis, where it is crucial to normalise the data. For this reason, I adopted a strategy to use *Drosophila* chromatin added to the mouse sample, a method designated ChIP-Rx [145]. This method uses the addition of a defined amount of *Drosophila* reference chromatin to each ChIP reaction, which in addition works as a carrier under conditions of low sample input [146]. An overview of the workflow I used is shown in Figure 3.22.

As chromatin fragment sizes determine the positional resolution of the data, sonication conditions were optimised, since they may vary with cell type studied, cell number used and fixation method applied [147]. Therefore, I tested different sonication times (3, 5, 6 and 8 cycles, each consisting of 30 sec ON and 30 sec OFF) using the Bioruptor pico (Diagenode). Five cycles of sonication resulted in the correct fragment size, i.e. a range of 100-600 bp (Fig. 3.23A-B).

This protocol was then tested for anti-H3K27me3 and -H3K4me3 ChIP on mTEC^{hi} samples sorted isolated from female WT mice. As a read-out, ChIP-qPCR was done and compared to results from previously established ChIP-Seq datasets obtained in the lab [50, 103]. The regions around the TSS of *Gast*, *Slc13a2* and *Hoxd9* were specifically enriched for H3K27me3 marks, with the latter also enriched for H3K4me3 marks. In contrast, the TSS regions of *Gast* and *Slc13a2* were depleted of this active histone mark. The region around the TSS of *Gapdh* TSS was depleted of H3K27me3 but enriched for H3K4me3 marks (Fig. 3.23C). These ChIP-qPCR results obtained from 10 000 sorted mTEC^{hi} match with the chromatin patterns predicted from the established ChIP-Seq data.

For the normalisation strategy, publicly available anti-H3K27me3 ChIP-Chip data from the *Drosophila* cell line S2-DRSC (GSE20781) were used to identify genomic regions that are enriched for H3K27me3 and primers were designed to bind within an enriched region (annotated as enriched region 4465). As expected, these primers identified an enrichment for H3K27me3, but not for H3K4me3 marks (Fig. 3.23C).

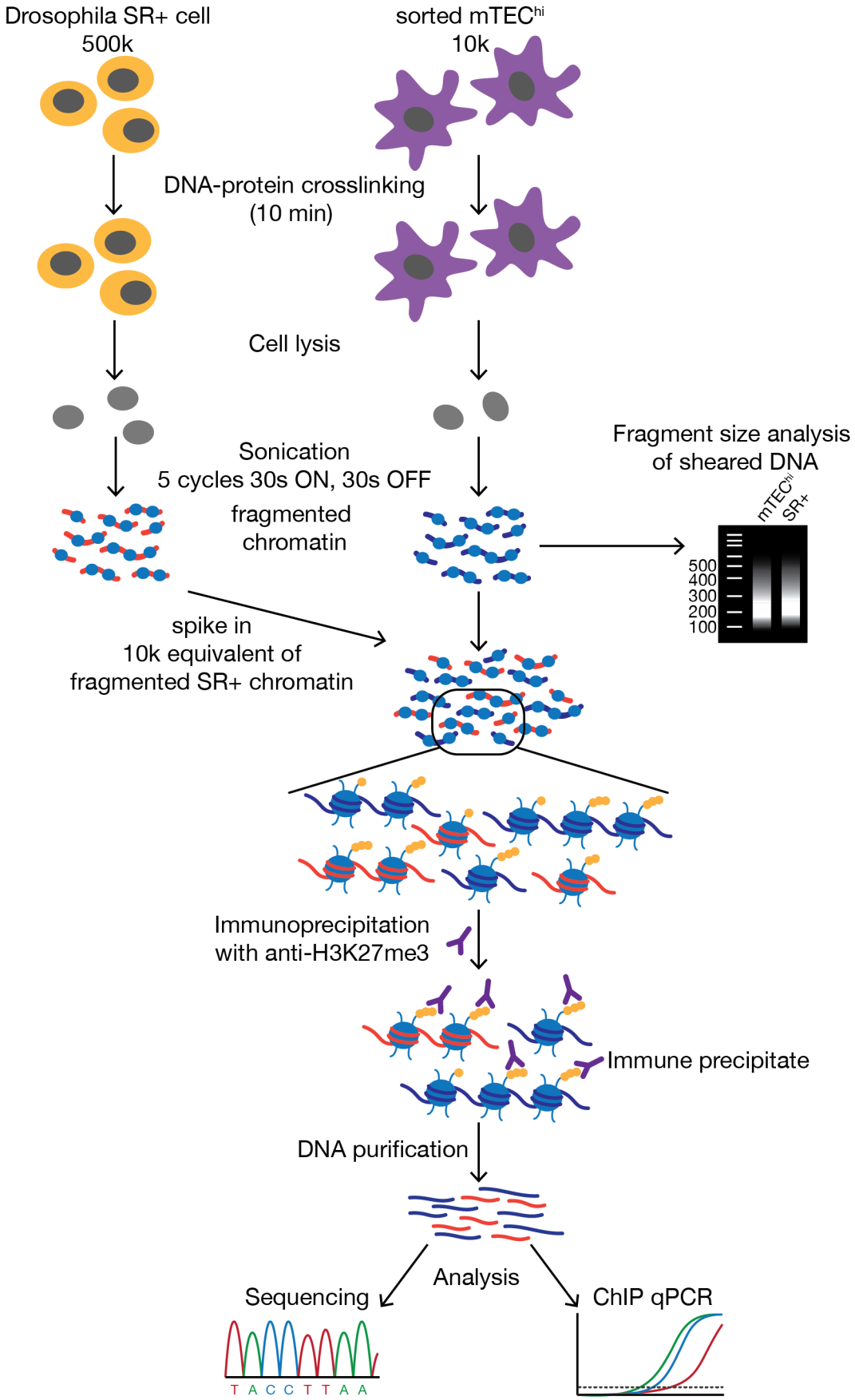

Figure 3.22: H3K27me3 ChIP on low input mTEC^{hi} samples. The schematic shows the workflow for crosslinking, lysing, shearing and immunoprecipitating H3K27me3 in sorted mTEC^{hi} samples with *Drosophila* SR+ chromatin as spike-ins.

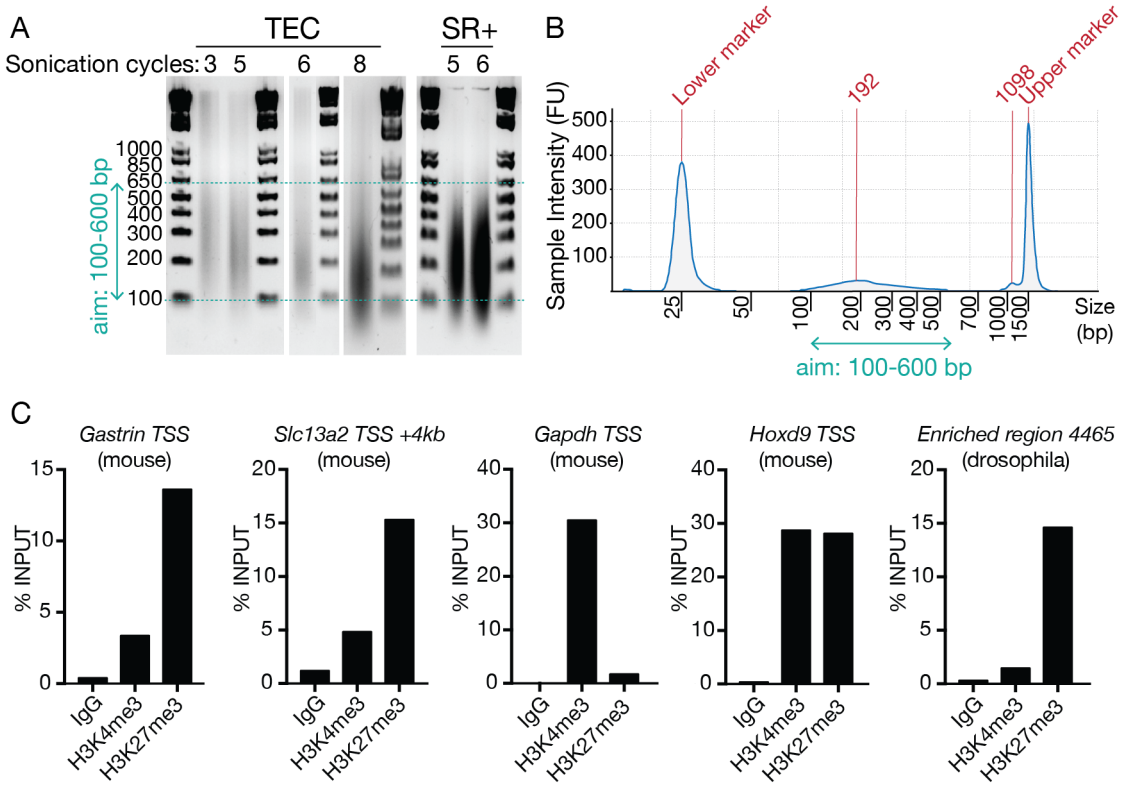

Figure 3.23: Chromatin shearing optimisation and ChIP-PCR on 10k mTEC^{hi}. (A) Analysis of fragment size resulting from chromatin shearing on 1.5 % agarose gel. Shearing was done on a Bioruptor pico (Diagenode) for 3, 5, 6 and 8 cycles (30 sec ON/30 sec OFF) for the TEC samples and for 5 and 6 cycles for the SR+ *Drosophila* cell line samples. To visualise fragment sizes on a gel, the chromatin of several 10k TEC pellets was combined (3x 10k for 3, 5, 6 cycles and 6x 10k for 8 cycles). SR+ *Drosophila* chromatin was sheared and analysed in 500k batches. 1kb+ ladder was run as a reference. **(B)** Analysis of fragment size resulting from chromatin shearing by tape station. ChIP Input sample from 10k mTEC^{hi} with SR+ *Drosophila* cell spike-ins (1:1) sheared for 5 cycles (30 sec ON/30 sec OFF) on a Bioruptor pico. **(C)** ChIP-qPCR on 10k mTEC^{hi} with SR+ *Drosophila* cell spike-ins. ChIP was done with IgG (negative control), H3K4me3 and H3K27me3. 10k mTEC^{hi} were sorted from female WT mouse, n=1. Percent input method was used to determine signal over background.

Consequently, the data from this experiment demonstrated that 10 000 mTEC^{hi} could be used to establish reliable ChIP data. Both H3K27me3 and H3K4me3 patterns established by ChIP-qPCR were in accordance with that of previously generated ChIP-Seq experiments also using WT mTEC^{hi}.

3.6.3 ChIP-qPCR reveals increase in H3K27me3 levels at one gene upregulated in UTX/JMJD3-deficient mTEC^{hi}

Next, I established the H3K27me3 marks in mTEC^{hi} of WT and UTX/JMJD3-double-deficient mTEC^{hi} using the established ChIP conditions and focused on promoter regions of genes that were identified to be differentially expressed in my corresponding RNA-Seq dataset (from Chapter 3.5). For this purpose, a pilot experiment was first carried out using primers binding in the proximity of the TSS of two genes (*Slc13a2* and *Gast*) that were more highly expressed in the UTX/JMJD3-deficient mTEC^{hi} in comparison to WT. Primers binding in the promoter region of *Hoxd9* were used as a control, because the expression of this gene remained unchanged despite an absence of UTX and JMJD3. In this experiment, a strongly increased H3K27me3 signal was detected at the *Slc13a2* gene in the UTX/JMJD3-deficient samples as compared to WT. In contrast, such differences were not detectable using primers recognising sequences around the TSS of *Gast* and *Hoxd9* (Fig. 3.24B).

As ChIP-qPCR feasibly only enables the analysis of a limited number of loci, the ChIP-Seq approach was chosen to obtain a genome-wide, comprehensive analysis of the H3K27me3 changes related to the detected transcriptional alterations. Therefore, mTEC^{hi} from WT and $Utx^{TEC-/-}$ $Jmjd3^{TEC-/-}$ mice were sorted to perform anti-H3K27me3 ChIP-Seq. The results of this analysis are not yet ready for inclusion in this thesis, as the libraries have only just been sequenced. Hence, I have included here the ChIP-qPCR data which was obtained to determine the ChIP quality before sequencing (Fig. 3.24C). Primers directed to the H3K27me3-enriched region 4465 and to the H3K27me3-depleted region 4580 were used as controls and the expected H3K27me3 signal patterns could be detected (Fig. 3.24C left). Notably, this experiment also clearly demonstrated that the normalisation using *Drosophila* chromatin H3K27me3 signals greatly reduced the variability in the data (please compare Fig. 3.24C middle and right panel). The difference between WT and UTX/JMJD3-deficient mTEC^{hi} becomes clear and statistically significant (2-fold change between WT and $Utx^{TEC-/-}$ $Jmjd3^{TEC-/-}$: 0.38 ± 0.09 vs 0.80 ± 0.02), only when calculating the fold enrichment relative to enriched region E4465.

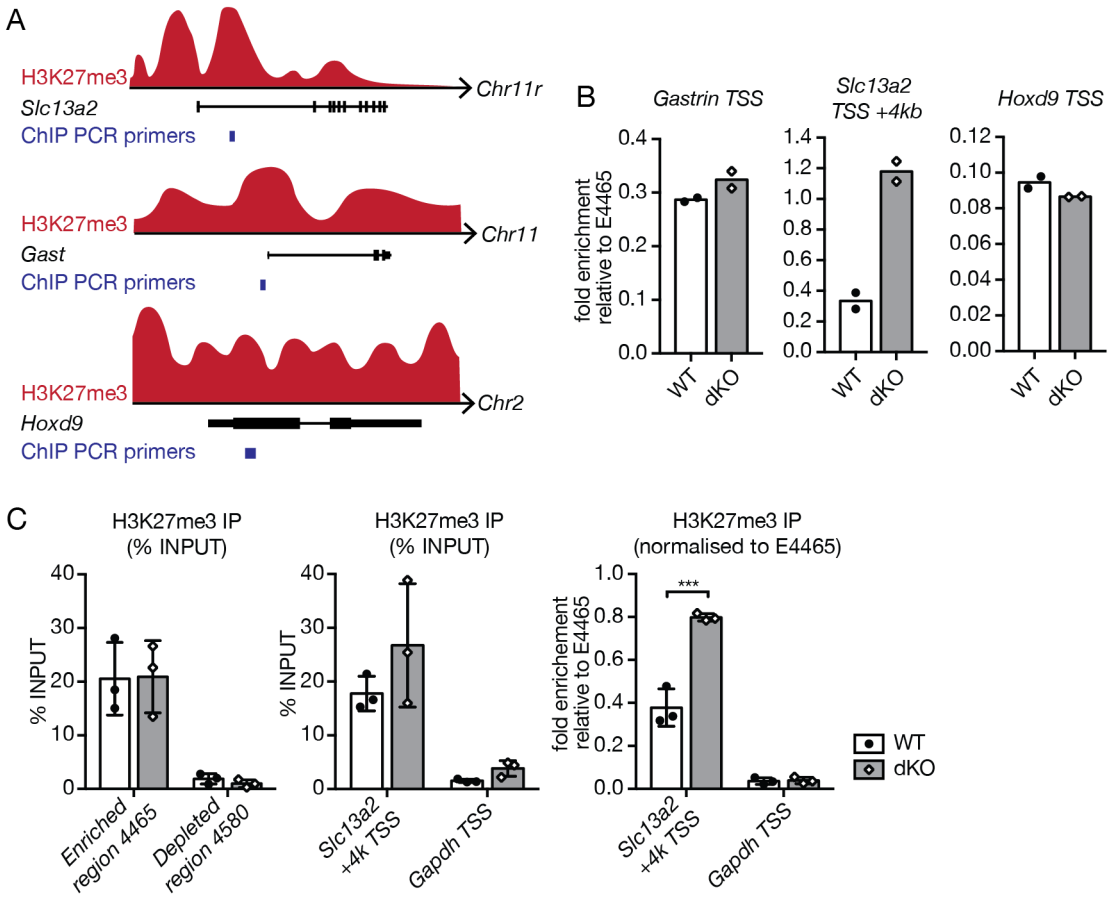

Figure 3.24: H3K27me3 ChIP-qPCR on UTX/JMJD3-deficient mTEC^{hi}. **(A)** Schematic of the H3K27me3 landscape in WT mTEC^{hi} at the genes encoding *Slc13a2*, *Gastrin* and *Hoxd9* indicating the position of the ChIP-qPCR primers. **(B)** H3K27me3 ChIP-qPCR on 10k sorted mTEC^{hi}. Data was normalised to *Drosophila* chromatin as fold enrichment over signal from enriched region 4465. Experiment was done with 4-5 week old female mice: WT ($Utx^{fl/fl}$ $Jmjd3^{fl/fl}$): n=1; dKO ($Utx^{TEC-/-}$ $Jmjd3^{TEC-/-}$) n=1. Data points are two technical ChIP replicates. **(C)** H3K27me3 ChIP-qPCR on 10k sorted mTEC^{hi}. Experiment with 4-5 week old female mice: WT ($Utx^{fl/fl}$ $Jmjd3^{fl/fl}$): n=3; dKO ($Utx^{TEC-/-}$ $Jmjd3^{TEC-/-}$) n=3. Data points are three biological replicates. Left and middle bar graph: Percent input method was used to determine signal over background. Right bar graph: Data was normalised to *Drosophila* chromatin as fold enrichment over signal from enriched region 4465. Two-tailed unpaired t-test with correction for multiple comparisons was used for statistical comparison. *p<0.05; **p<0.01; ***p<0.005.

3.6.4 Brief summary of H3K27me3 ChIP in *Utx*$^{TEC-/-}$ *Jmjd3*$^{TEC-/-}$ mTEC^{hi}

Results obtained with a ChIP method adapted to as few as 10 000 mTEC^{hi} and complemented with *Drosophila* chromatin spike-ins were in accordance with published mTEC^{hi} ChIP-Seq data [50, 103]. It is therefore anticipated that the experimental design chosen will be informative in assessing differences in H3K27me3 marks between UTX/JMJD3-deficient and WT mTEC^{hi}. My data using ChIP-qPCR has so far shown that H3K27me3 marks are increased in UTX/JMJD3-deficient mTEC^{hi} at regions adjacent to the TSS of *Slc13a2*. *Slc13a2* encodes a solute carrier that is expressed in the intestine and kidneys, and was one of the genes that was more highly expressed in the UTX/JMJD3-deficient mTEC^{hi}.

3.7 Thymocyte development in *Utx*$^{TEC-/-}$ *Jmjd3*$^{TEC-/-}$ mice

Next, I assessed if the deficiency of UTX and JMJD3 in TEC results in an altered capacity to support thymocyte development and to establish a functional and self-tolerant peripheral T cell compartment. As discussed in the introduction, TEC are crucial for all stages in thymopoiesis: from attracting thymocyte precursors to the thymus, to positive and negative selection events, up to the maturational changes before thymic egress [71]. Disturbances in the cellularity, composition of subpopulations and/or the function of TEC may impact any of these steps. Thymocyte development was therefore comparatively assessed analysing in detail distinct developmental stages in WT and *Utx*$^{TEC-/-}$ *Jmjd3*$^{TEC-/-}$ mice.

3.7.1 Early thymocyte development and positive selection are unchanged in *Utx*$^{TEC-/-}$ *Jmjd3*$^{TEC-/-}$ mice

Precursors seeding to the thymus and their immediate progeny are negative for the expression of both co-receptors CD8 and CD4 and therefore conveniently designated double negative (DN). DN thymocytes progress through different sequential maturational

stages defined by the surface expression of CD25 and CD44: DN1 ($CD44^{hi}$ $CD25^{-}$) → DN2 ($CD44^{hi}$ $CD25^{+}$) → DN3 ($CD44^{lo}$ $CD25^{+}$) → DN4 ($CD44^{lo}$ $CD25^{-}$) [148].

When analysing DN thymocytes by flow cytometry it is important to exclude cells from other lineages that might also be $CD4^{-}CD8^{-}$. For this reason cells were stained to exclude B cells (CD19), γδ T cells (GL3), dendritic cells (CD11b, CD11c), red blood cells (TER119), NK cells (NK1.1 CD49b), NK T cells (CD49b) and myeloid cells (F4/80, Gr-1) using antibodies with a single fluorochrome. $CD8^{-}CD4^{-}$ thymocytes were further gated for their expression of CD24 and TCRβ, and cells highly positive for CD24 but completely negative for TCRβ were designated "True DN". The gating strategy is displayed in Figure 3.25A. A detailed analysis of the first maturation steps of DN thymocytes was identical for WT and $Utx^{TEC-/-}$ $Jmjd3^{TEC-/-}$ mice (Fig. 3.25B).

Completing DN differentiation successfully, thymocytes adopt a so-called double positive (DP) i.e. $CD4^{+}$ and $CD8^{+}$ phenotype in the cortex and then finally progress to single positive (SP) CD4 and CD8 cells which are subject in the medulla to further functional scrutiny and post-selectional maturation. Cells identified as $CD8^{+}CD4^{-}$ are further characterised as mature SPCD8 (mSPCD8), which – as required for mature thymocytes – are $TCR\beta^{+}$, and iCD8, which are $TCR\beta^{-}$ and represent immature cells that are on the way from DN to become DP thymocytes. The gating strategies for identifying these subpopulations are displayed in Figure 3.25A. This analysis did not reveal any differences in thymocyte maturation between WT and $Utx^{TEC-/-}$ $Jmjd3^{TEC-/-}$ mice (Fig. 3.25C).

During their early maturation stages, thymocytes rearrange the TCR and start to express it on the surface. The specificity of the newly generated TCR has been selected at random and therefore needs to be tested for its affinity to interact with pMHC complexes initially on cTEC. Successful interaction will result in signalling that leads to positive selection. Too little signalling results in programmed cell death called "death by neglect". Positive selection happens at the DP stage and is characterised by the cell surface upregulation of TCR and the activation marker CD69. The precise surface expression levels define the specific maturational stages of their positive selection [149]. Thymocytes with a

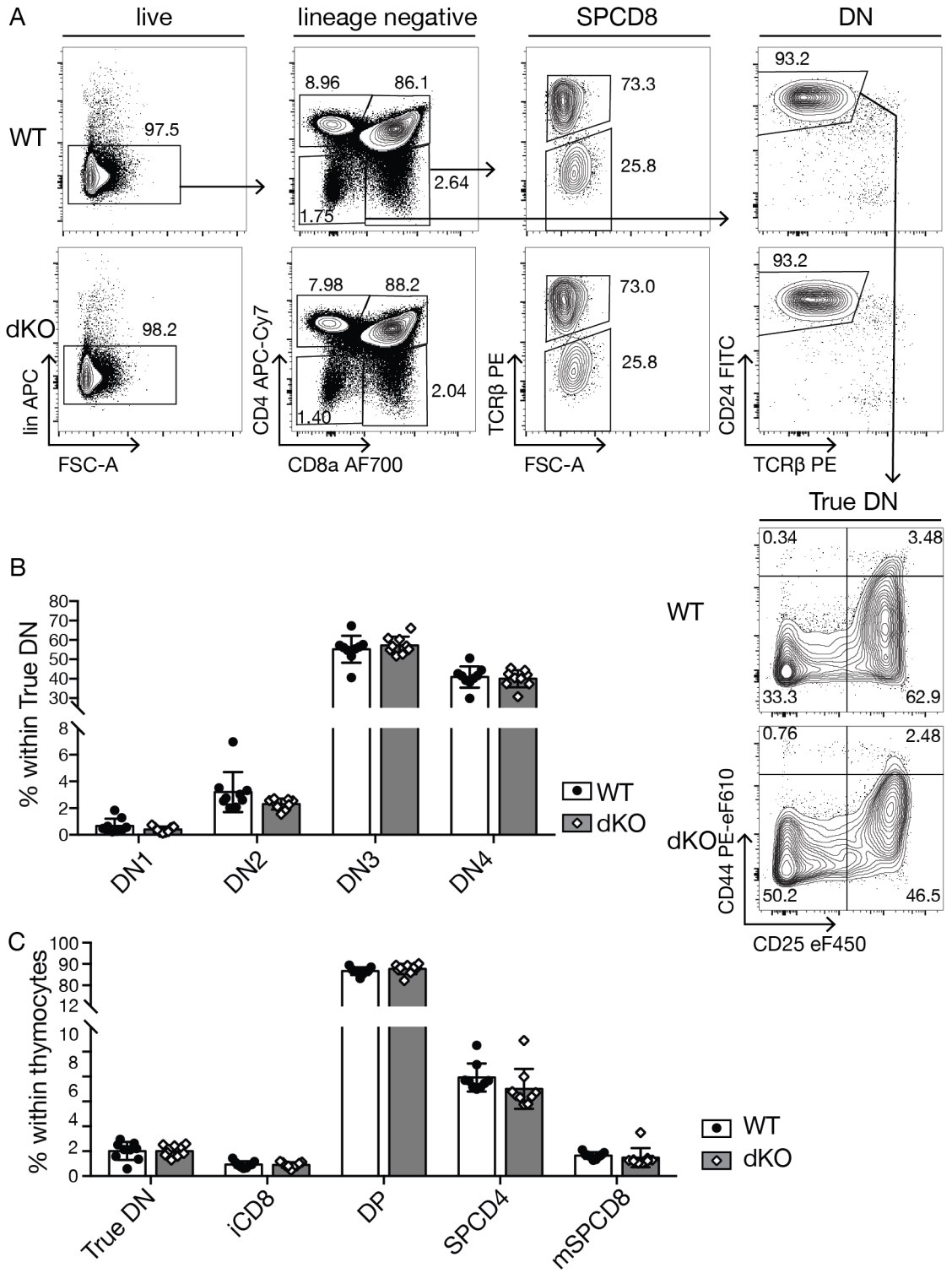

Figure 3.25: *Utx*$^{TEC-/-}$ *Jmjd3*$^{TEC-/-}$ thymi support normal early thymocyte development. **(A)** Representative FACS plots showing gating strategy for defining True DN, iCD8, mSPCD8, DP and SPCD4. True DN are further divided into DN1 (CD44^{hi} CD25^{-}), DN2 (CD44^{hi} CD25^{+}), DN3 (CD44^{hi} CD25^{-}) and DN4 (CD44^{hi} CD25^{+}). Lineage markers include antibodies against CD11b, CD11c, Gr-1, CD19, CD49b, F4/80, NK1.1, GL3 and TER119. **(B)** Bar graph depicts frequencies of DN1-DN4 within True DN (lin^{-} CD4^{-} CD8^{-} TCRβ^{lo}, CD24^{+}). **(C)** Bar graph shows relative frequency of the defined subpopulations within lineage negative thymocytes. Graphs are pooled from 3 independent experiments. Female mice 4-5 weeks of age; WT (*Utx*$^{fl/fl}$ *Jmjd3*$^{fl/fl}$): n=9; dKO (*Utx*$^{TEC-/-}$ *Jmjd3*$^{TEC-/-}$): n=9. Statistical comparison was done with two-tailed unpaired t-tests with correction for multiple comparisons.

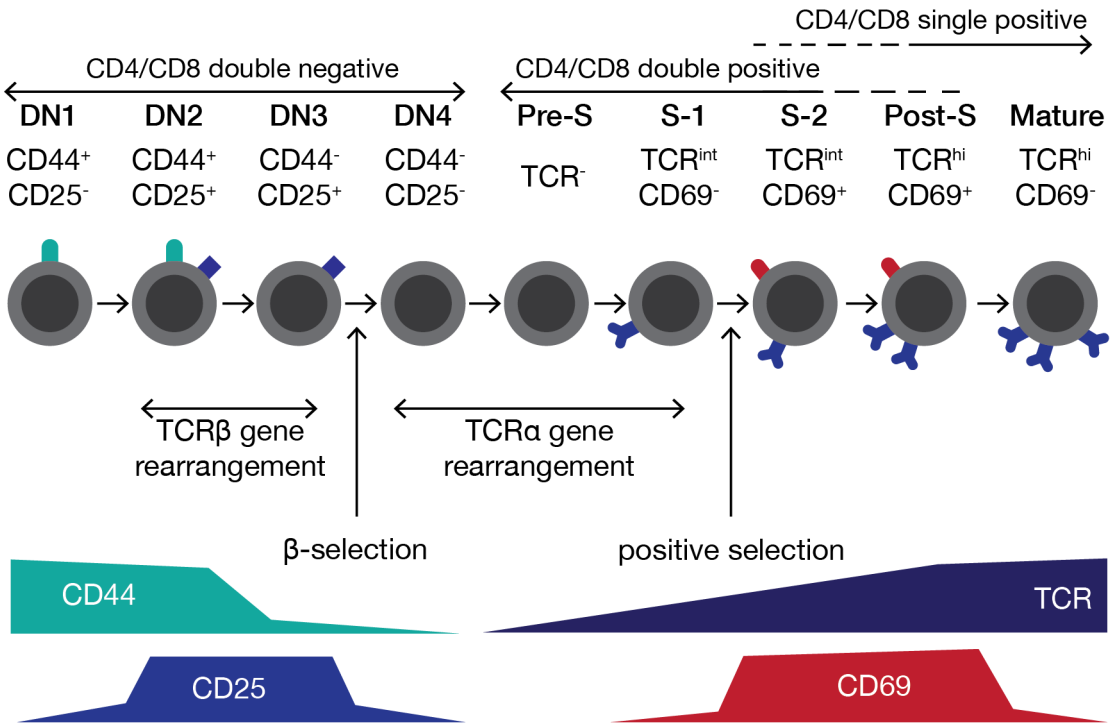

Figure 3.26: Scheme of progression of thymocytes through DN stages and subsequent positive selection [149].

pre-selection phenotype (pre-S) are TCR$^-$ and CD69$^-$ and thus represent the earliest stage of this trajectory. The subsequent stage of positive selection is characterised by a TCR^{int} CD69$^-$ phenotype referred to as Selection Stage 1 (S1), followed by a TCR^{int} CD69$^+$ Selection Stage 2 (S2). Post-selection thymocytes are characterised by TCR^{hi} CD69$^+$, which then changes due to the downregulation of CD69 to what is considered to be a mature phenotype. An overview of thymocyte progression along these maturational stages is depicted in Figure 3.26 whereas the corresponding FACS gating strategy is shown in Figure 3.27A.

The progression through the pre-selection to mature stages was identical for thymocytes isolated from WT and *Utx*$^{TEC-/-}$ *Jmjd3*$^{TEC-/-}$ animals (Fig. 3.27B-C) and a more detailed analysis assessing CD8 and CD4 expression within Pre-S, S1, S2, Post-S and M stages also reveals identical results and the lineage fate decisions were comparable between both mouse strains (Fig. 3.27D-E).

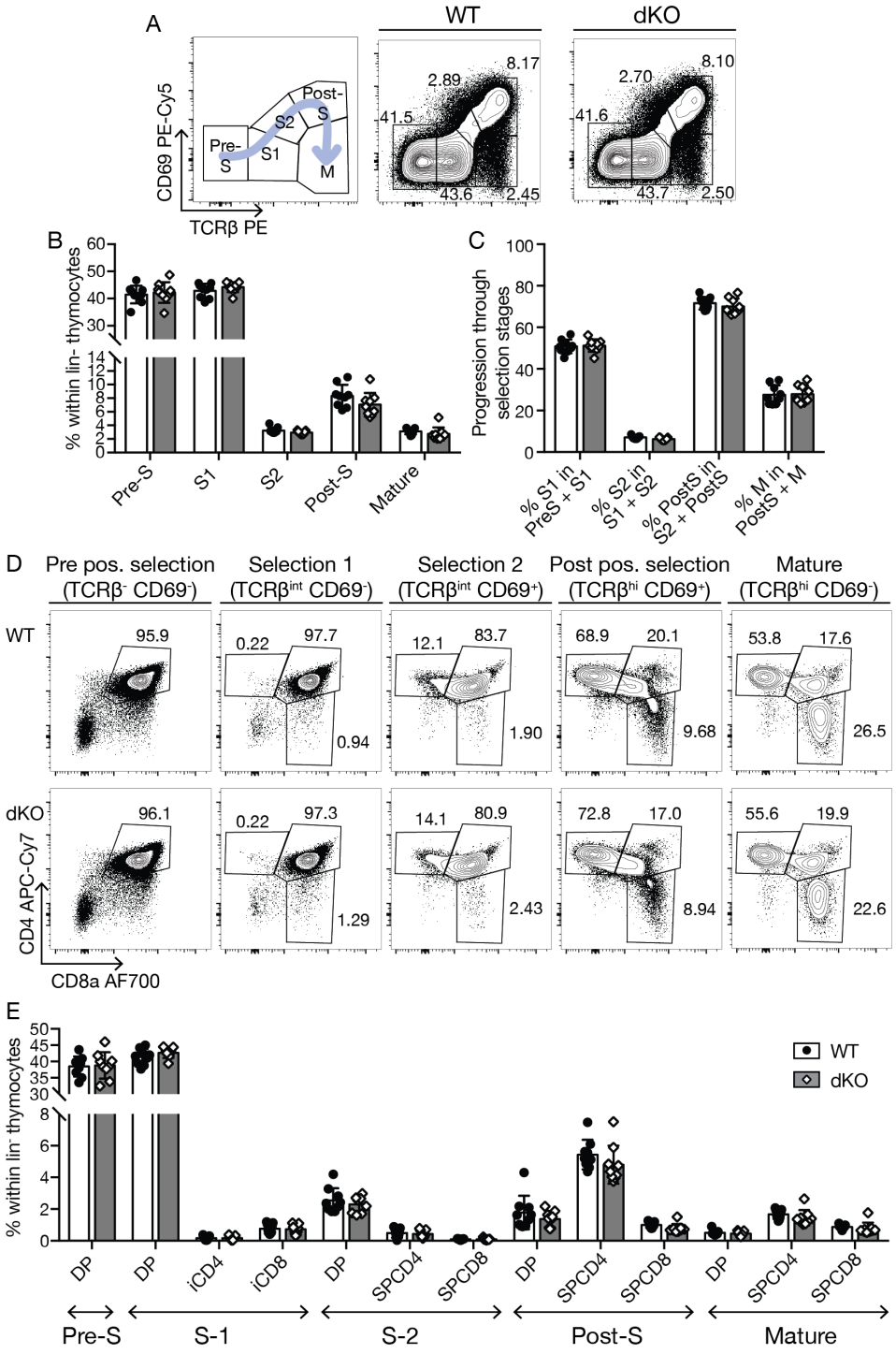

Figure 3.27: Unchanged positive selection in *Utx*$^{TEC-/-}$ *Jmjd3*$^{TEC-/-}$ mice. **(A)** Representative FACS plots for defining the different stages in regard to positive selection: Pre-S (TCRβ^{-} CD69^{-}), S1 (TCRβ^{int} CD69^{-}), S2 (TCRβ^{int} CD69^{+}), Post-S (TCRβ^{hi} CD69^{+}) and M (TCRβ^{hi} CD69^{-}). **(B)** Bar graph showing relative frequencies of positive selection stages. **(C)** Bar graph showing progression through sequential positive selection stages. Calculation: (Stage B)/(Stage A+B)x100 where A is the maturation stage immediately before B. **(D)** Representative FACS plots showing CD8a and CD4 expression in the different maturational stages defined in (A). **(E)** Bar graph showing the percentage of DP, SPCD4, SPCD8 within PreS to M stages within total thymocytes. Bar graphs are pooled from 3 independent experiments with female mice 4-5 weeks of age; WT (*Utx*$^{fl/fl}$ *Jmjd3*$^{fl/fl}$): n=9; dKO (*Utx*$^{TEC-/-}$ *Jmjd3*$^{TEC-/-}$): n=9. Statistical comparison was done with two-tailed unpaired t-tests with correction for multiple comparisons.

3.7.2 TCRβ^{hi} thymocytes are reduced in *Utx$^{TEC-/-}$ Jmjd3$^{TEC-/-}$* thymi

The further development of the positively selected TCRβ^{hi} thymocytes was next compared between WT and *Utx$^{TEC-/-}$ Jmjd3$^{TEC-/-}$* mice. This analysis focused on TCRβ^{hi} thymocytes that have upregulated the activation marker CD5 (Fig. 3.28A). Thymocytes with this specific phenotype were consistently, albeit mildly reduced in *Utx$^{TEC-/-}$ Jmjd3$^{TEC-/-}$* mice when compared to WT animals (9.96 % ± 0.53 vs 11.52 % ± 0.73) (Fig. 3.28B). This difference was specific for TCRβ^{hi} CD5^{+} thymocytes, as the corresponding analysis of TCRβ^{hi} CD69$^{+/-}$ (see 3.7.1) did not reveal any difference in frequency. This discrepancy may be due to differential use of activation markers used to identify the subpopulations within TCRβ^{hi} thymocytes. Notably, the reduction observed (13.5 %) is relatively small and was therefore likely masked, not least because CD5 and CD69 identify different aspects of thymocyte activation.

I next investigated whether the reduction in TCRβ^{hi} thymocytes occurred in a specific thymocyte subpopulation, i.e. SPCD8, SPCD4 and/or DP cells (Fig. 3.28C). Thus, the frequencies of each of these subpopulations were determined as fraction of all thymocytes analysed, which revealed that all subpopulations contributed to the reduction: DP (2.36 % ± 0.23 vs 2.11 % ± 0.22), SPCD8 (1.51 % ± 0.2 vs 1.14 % ± 0.1), SPCD4 (7.00 % ± 0.43 vs 6.10 % ± 0.41). The biggest reduction was observed in the SPCD8 population (Fig. 3.28D).

3.7.3 Semimature and mature SPCD8 are reduced in *Utx$^{TEC-/-}$ Jmjd3$^{TEC-/-}$* thymi

The maturation of TCRβ^{hi} SPCD8 and SPCD4 thymocytes was analysed next. These cells go through several well-characterised maturational stages before they reach a state at which they are able to leave the thymus. The expression of the differentiation markers CCR7, CD69, CD24 and CD69 are typically used to define the sequential stages that reach from DP^{dull}, immature, semimature finally to mature thymocytes. These individual maturational stages are depicted in Figure 3.29.

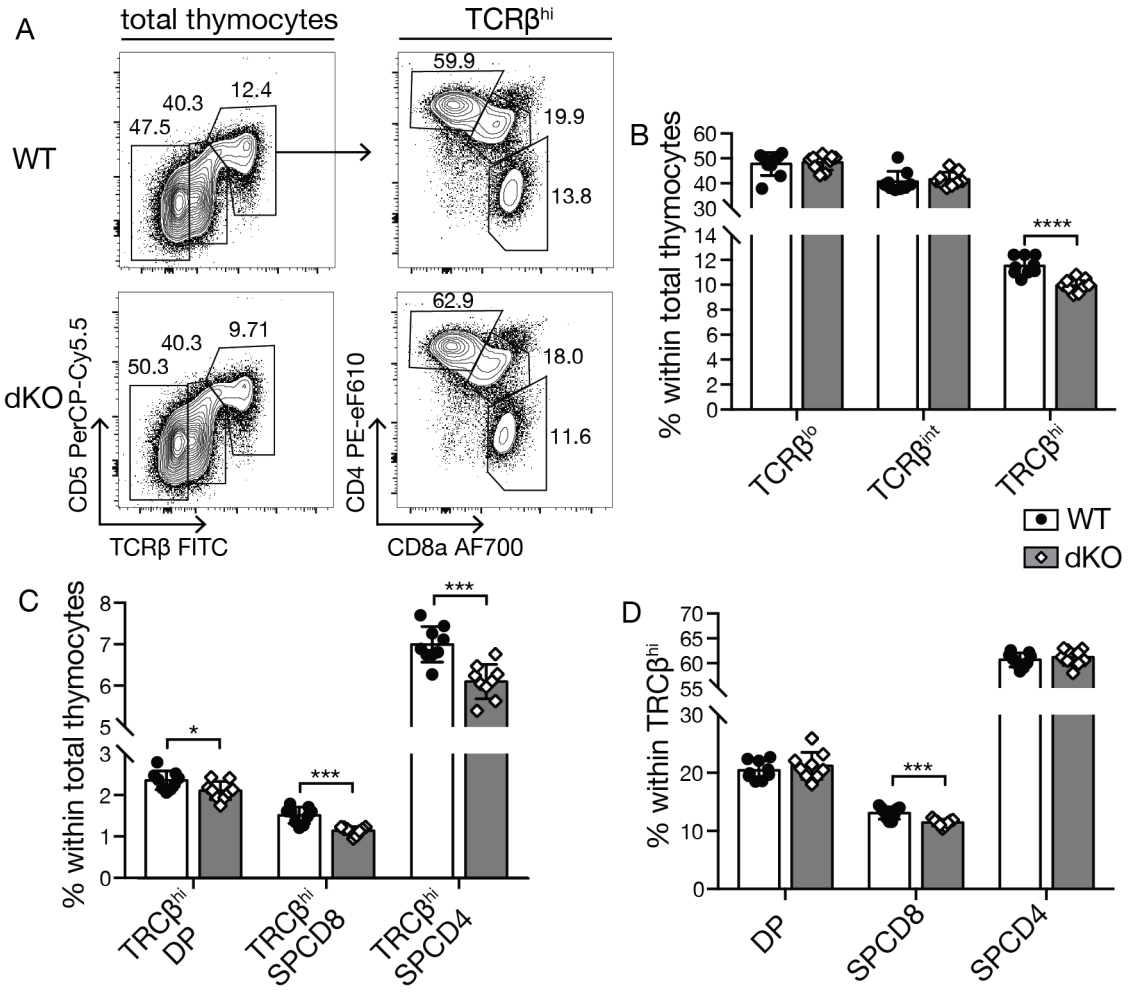

Figure 3.28: Lower frequency of TCRβ^{hi} thymocytes in *Utx$^{TEC-/-}$ Jmjd3$^{TEC-/-}$* mice. **(A)** Representative FACS plots for defining TCRβ^{lo}, TCRβ^{int} and TCRβ^{hi} according to TCRβ and CD5 expression and SPCD4, SPCD8 and DP within TCRβ^{hi}. **(B)** Bar graph shows the relative frequencies of the indicated phenotypes within the pool of total thymocytes. **(C)** Bar graph shows the relative frequencies of the indicated phenotypes within the pool of total thymocytes. **(D)** Bar graph shows the relative frequencies of the indicated phenotypes within TCRβ^{hi}. Bar graphs are pooled from 3 independent experiments with female mice 4-5 weeks of age; WT (*Utx$^{fl/fl}$ Jmjd3$^{fl/fl}$*): n=9; dKO (*Utx$^{TEC-/-}$ Jmjd3$^{TEC-/-}$*): n=9. Statistical comparison was done with two-tailed unpaired t-tests with correction for multiple comparisons. *p<0.05; **p<0.01; ***p<0.005, ****p<0.001.

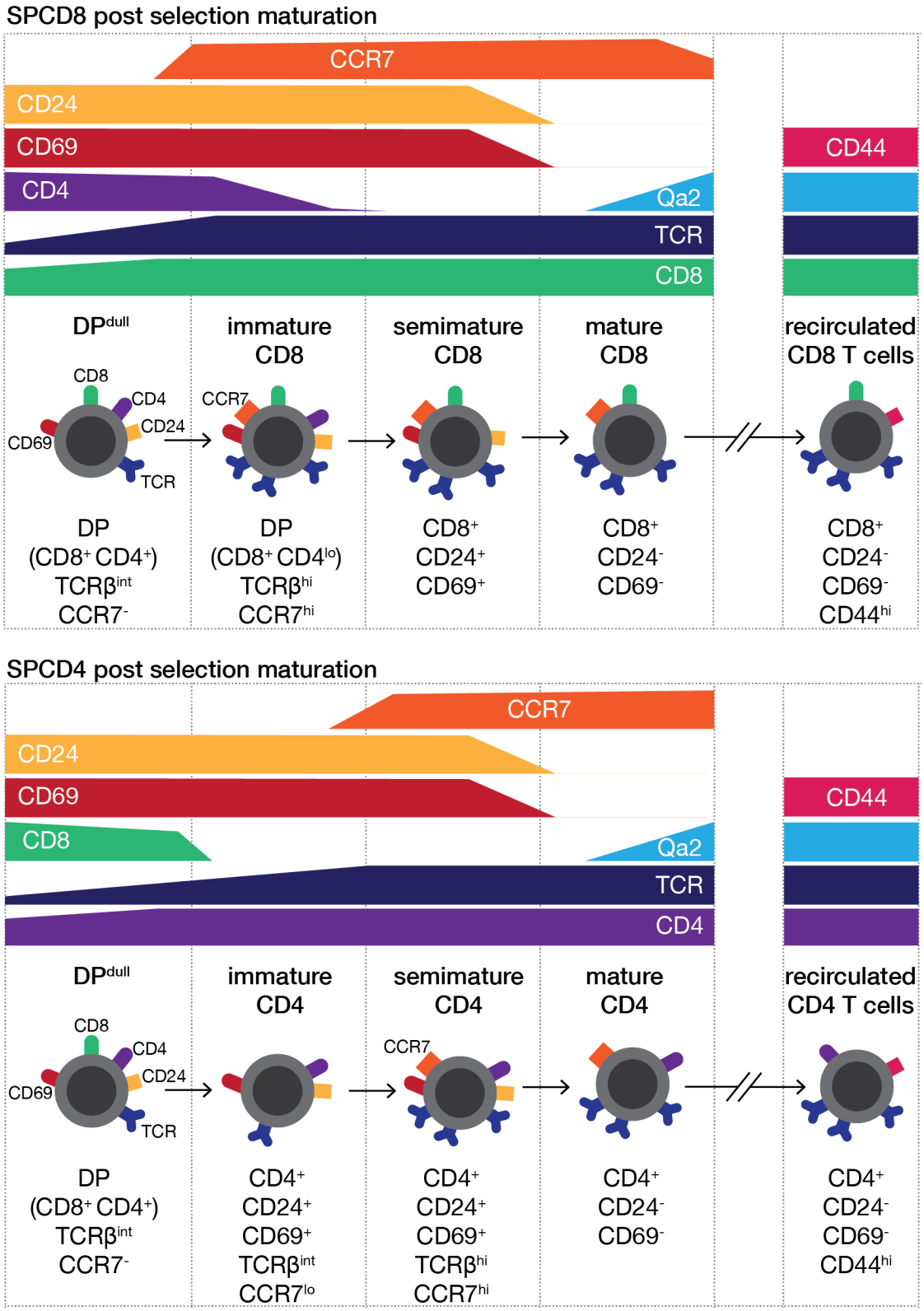

Figure 3.29: Post selection maturation of the SPCD8 and SPCD4 lineage according to the expression of TCRβ, CCR7, CD24 and CD69. After positive selection, DP downregulate the expression of CD4 and CD8 and adopt a DP^{dull} phenotype. Subsequently, thymocytes become SP for either CD8 or CD4 depending on the MHC class restriction of their TCR. Additionally, thymocytes start expressing CCR7, which enables them to move to the medulla. During their final maturational step thymocytes downregulate CD24 and CD69. Recirculating mature T cells can be excluded by identifying thymocytes with a $CD44^{hi}$ $CD24^{-}$ phenotype.

A small reduction in the semimature and mature SPCD8 was observed (semimature: 5.0 % ± 0.65 (WT) vs 4.28 % ± 0.31 (KO); mature: 7.66 % ± 0.68 (WT) vs 6.42 % ± 0.43 (KO)), when comparing the post selection maturation of SPCD8 between WT and $Utx^{TEC-/-}$ $Jmjd3^{TEC-/-}$ mice, (Fig. 3.30B). These changes are significant, albeit small. There was a subtle partial block in the progression from DP^{dull} to immature CD8 (Fig. 3.30C). The difference was statistically significant (22.6 % ± 2.7 vs 25.5 % ± 1.8), but the biological significance of this difference remains undefined. The analysis of the post selectional maturation within the SPCD4 lineage was unaffected by the loss of UTX and JMJD3 expression in TEC (Fig. 3.30B-D).

Within mature SP thymocytes, the high surface expression of CD44 and concomitant absence of CD24 identify T cells that have recirculated from the periphery to the thymus. There were significantly more of these recirculating $CD8^+$ T cells in the thymus of $Utx^{TEC-/-}$ $Jmjd3^{TEC-/-}$ mice when compared to WT animals (0.055 % ± 0.035 vs 0.024 % ± 0.01). Notably, the frequency of recirculating $CD4^+$ T cells was similar in mutant and WT mice. Different reasons have been considered for explaining the presence of recirculating mature T cells in the thymus, ranging from a role in antigen presentation to the concept that the pool of these intrathymic T cells represent a repository for memory T cells [150]. Mature T cell recirculation increases with age and has also been shown to be associated with pathological conditions such as lymphopenia or thymic atrophy [150–152]. The reason why $Utx^{TEC-/-}$ $Jmjd3^{TEC-/-}$ mice have more recirculating $CD8^+$ T cells in their thymi remains unclear as neither of these conditions are observed in these animals. The identification of the cause for this observation is however the focus of future studies beyond the scope of this thesis.

Different methods have been established to assess the maturation of thymocytes that eventually will be competent to egress from the thymus. Complementary to the strategy to detail SP thymocyte maturation described above, Hogquist et al. proposed to quantify MHC-I and CD69 cell surface expression as a means to identify the three sequential stages of SP thymocyte maturation depicted in Figure 3.32: SM (MHC-I^{lo} $CD69^+$) → M1 (MHC-I^{hi} $CD69^+$) → M2 (MHC-I^{hi} $CD69^-$) [153].

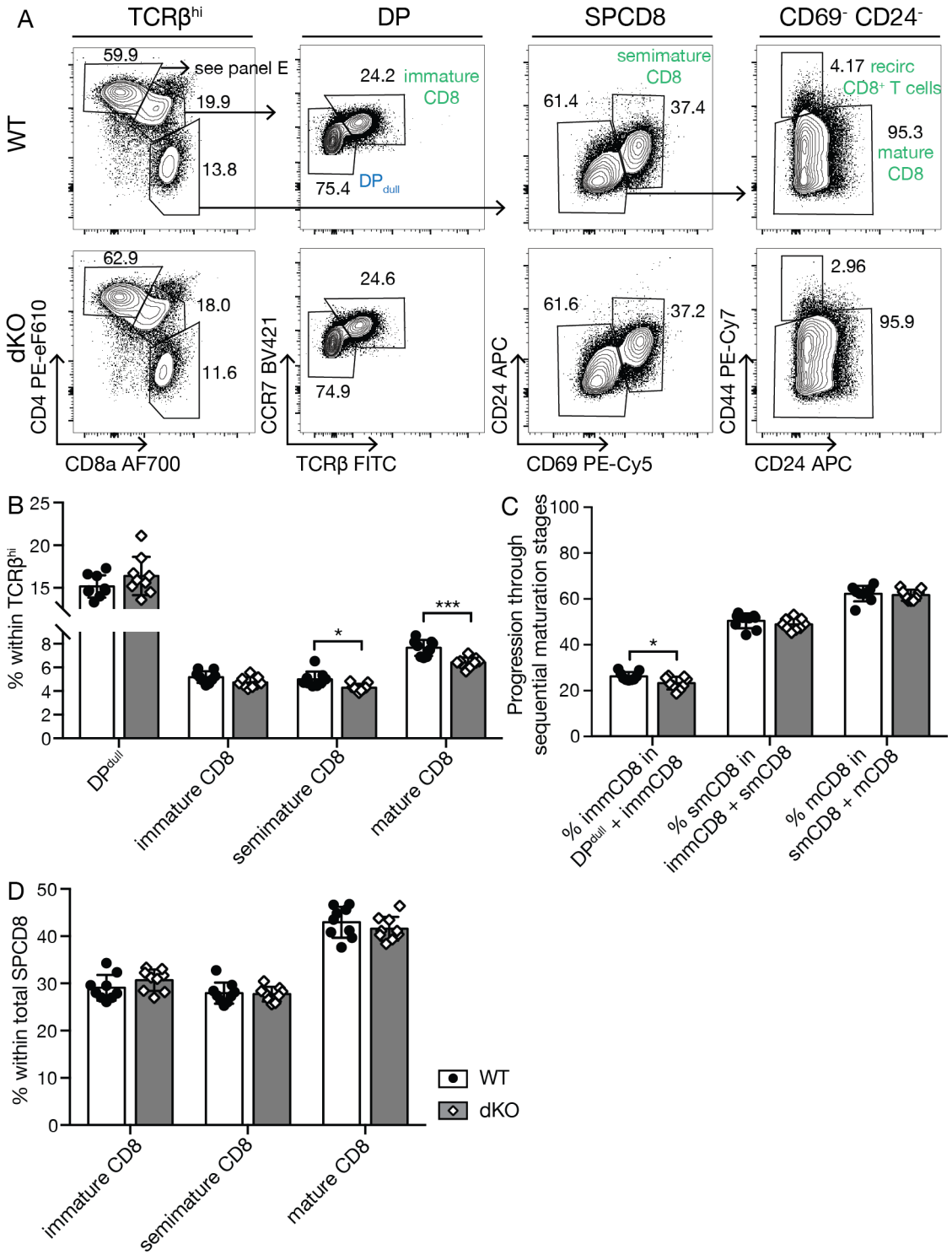

Figure 3.30: Lower frequency of semimature and mature SPCD8 in *Utx*$^{TEC-/-}$ *Jmjd3*$^{TEC-/-}$ mice. **(A)** Representative FACS analysis for defining SPCD8 post selection maturation. This is done according to the scheme in Figure 3.29. **(B)** Bar graph depicts relative frequencies of the defined SPCD8 maturational stages within TCRβ^{hi} thymocytes. **(C)** Bar graph shows progression through sequential maturational stages. Calculation: (Stage B)/(Stage A+B)x100 where A is the maturation stage immediately before B. **(D)** Bar graph depicts relative frequencies of the defined maturational stages within total SPCD8 thymocytes. Bar graphs are pooled from 3 independent experiments with female mice 4-5 weeks of age; WT (*Utx*$^{fl/fl}$ *Jmjd3*$^{fl/fl}$): n=9; dKO (*Utx*$^{TEC-/-}$ *Jmjd3*$^{TEC-/-}$): n=9. Statistical comparison was done with two-tailed unpaired t-tests with correction for multiple comparisons. *p<0.05; **p<0.01; ***p<0.005, ****p<0.001.

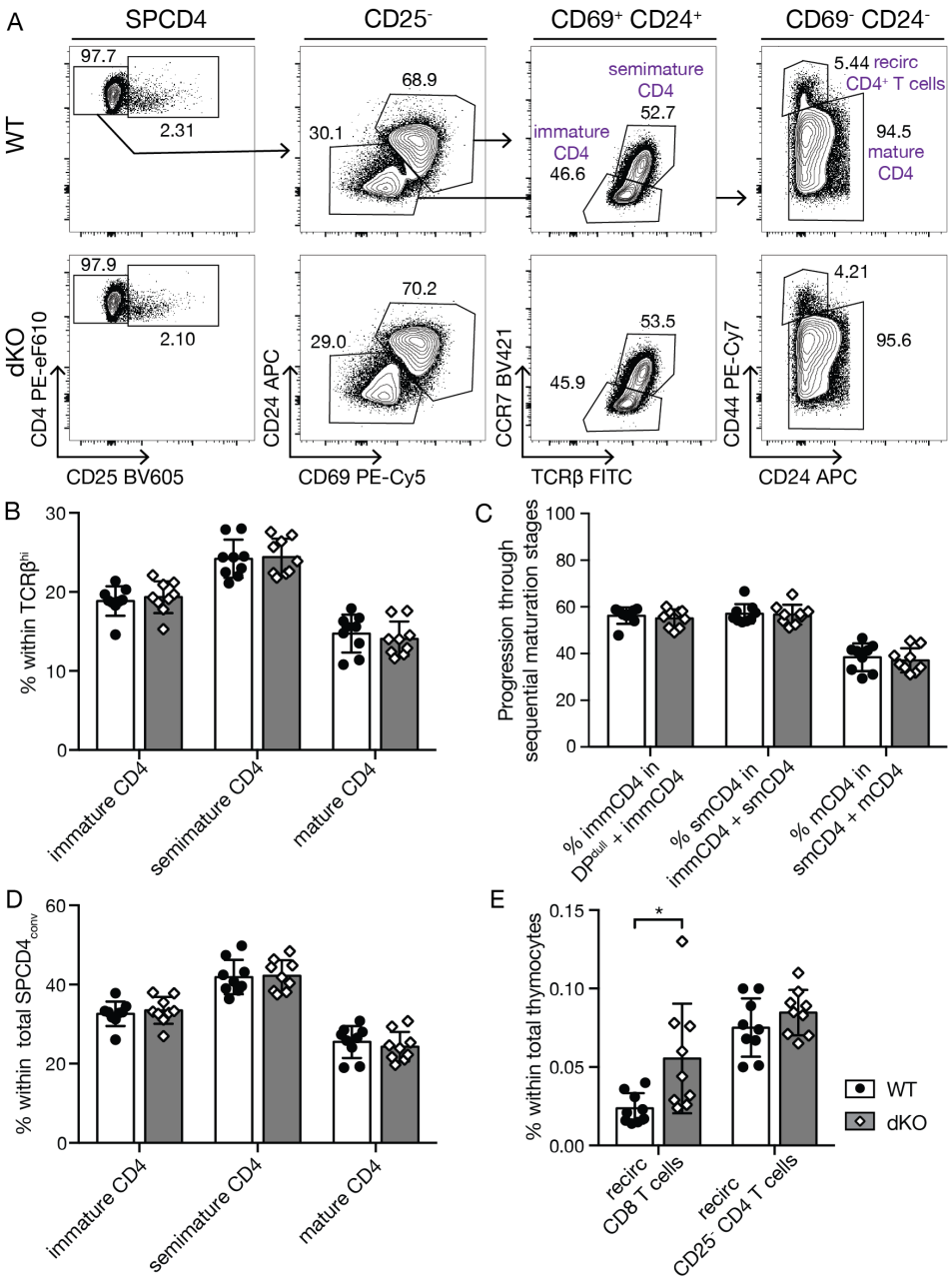

Figure 3.31: Unchanged maturation of SPCD4 in $Utx^{TEC-/-}$ $Jmjd3^{TEC-/-}$ mice. (A) Representative FACS analysis depicts the gating strategy for defining conventional SPCD4 post selection maturation. This is done according to the scheme in Figure 3.29. **(B)** Bar graph depicts relative frequencies of the defined SPCD4 maturational stages within TCRβ^{hi} thymocytes. **(C)** Bar graph shows progression through sequential maturational stages. Calculation: (Stage B)/(Stage A+B)x100 where A is the maturation stage immediately before B. **(D)** Bar graph depicts relative frequencies of the defined maturational stages within total CD25$^-$ SPCD4 thymocytes. Bar graphs are pooled from 3 independent experiments with female mice 4-5 weeks of age; WT ($Utx^{fl/fl}$ $Jmjd3^{fl/fl}$): n=9; dKO ($Utx^{TEC-/-}$ $Jmjd3^{TEC-/-}$): n=9. Statistical comparison was done with two-tailed unpaired t-tests with correction for multiple comparisons. *p<0.05; **p<0.01.

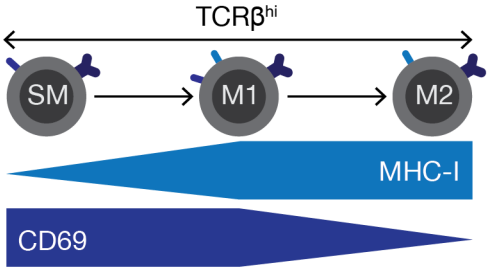

Figure 3.32: Post selectional maturation defined by cell surface expression of MHC-I and CD69.

The gating strategy is displayed in Figure 3.33A and F. This complementary gating strategy confirmed the limited reduction of TCRβ^{hi} CD4^{lo}CD8^{+}, SPCD8 and SPCD4 thymocytes (Fig. 3.33B-C). Furthermore, a comparable reduction during the late maturational stages within the SPCD8 lineage of *Utx*$^{TEC-/-}$ *Jmjd3*$^{TEC-/-}$ mice was observed, with a marginal, yet statistically significant reduction in the M2 stage compared to WT (8.99 % ± 0.83 vs 10.13 % ± 0.87) (Fig. 3.33D).

In contrast to the previous gating strategy, this complementary strategy to identify SM, M1, M2 stages did reveal changes concerning the post selection maturation of SPCD4 cells in *Utx*$^{TEC-/-}$ *Jmjd3*$^{TEC-/-}$ mice (Fig. 3.33G), as SM cells in this lineage were decreased in comparison to WT animals (37.33 % ± 2.88 vs 41.2 % ± 1.66), with a corresponding increase in cells in the M1 stage (33.43 % ± 2.88 vs 28.43 % ± 1.90). The frequency of M2 cells remained, however, unchanged between WT and *Utx*$^{TEC-/-}$ *Jmjd3*$^{TEC-/-}$ mice (28.06 % ± 2.04 vs 28.88 % ± 2.3). Accordingly, SPCD4 progression from SM to M1 was increased while progression to M2 was decreased (Fig. 3.33H).

Taken together, the lack of UTX/JMJD3 expression in TEC impacts the maturation of SP thymocytes. *Utx*$^{TEC-/-}$ *Jmjd3*$^{TEC-/-}$ mice had changes in the post selectional maturation of TCRβ^{hi} thymocytes that affected both the SPCD8 and SPCD4 lineages. However, these differences were relatively small and their biological significance will need to be determined. While the later maturational stages within the SPCD8 lineage were mildly reduced, comparable changes were not observed for the mature stages of SPCD4, i.e. M2, but could be appreciated for the SM and M1 stages. Since the antibody-based phenotyping and their analysis by flow cytometry provide only limited information

regarding the dynamics of cell maturation, Bromodeoxyurine (BrdU) DNA labelling and cell tracing appears to be a more suitable method to determine the exact dynamics of the maturational perturbations observed here.

3.7.4 Negative selection is impaired in $Utx^{TEC-/-}$ $Jmjd3^{TEC-/-}$ thymi

The random rearrangement of the TCR locus generates an enormously diverse TCR repertoire that by chance also includes TCR with autoreactive specificities. Developing thymocytes therefore have to be submitted to a stringent quality control mechanism that efficiently eliminates thymocytes with an autoreactive TCR. Otherwise these cells have the potential to elicit autoimmune diseases once they have seeded in the periphery. TCR specificity is probed by pMHC complexes on TEC and other stromal cells able to process and present self-antigens. Under conditions that the TCR interacts with their cognate pMHC with an avidity above a certain threshold, signals are transduced that trigger programmed cell death and thus lead to the depletion of these cells.

The transcriptional analysis of UTX/JMJD3-deficient mTEC^{hi} demonstrated that these cells express at a population level increased transcript numbers of AIRE-enhanced genes. Moreover, the frequency of mTEC^{hi} was increased in the thymi of these mice. The question that follows from these observations is whether these changes influence thymocyte negative selection. It is conceivable that an increased availability of some TRA and a higher frequency of mature mTEC may tip the delicate balance that determines negative selection in favour of a higher efficiency of this process in $Utx^{TEC-/-}$ $Jmjd3^{TEC-/-}$ mice.

Negative selection is effected at separate stages during thymocyte maturation [154]. A so called first wave (wave 1) is observed in the cortex and is differentiated into two separate phases: Wave 1a selects autoreactive thymocytes at a DP stage, while wave 1b affects cortical cells with a SP phenotype. Thymocytes subject to wave 1 negative selection coexpress HELIOS and PD-1 at high levels. Wave 2 negative selection, which takes place in the medulla, can also be subdivided into two consecutive stages: wave 2a affects immature SP thymocytes as characterised by a CD69^{+}CD24^{+} phenotype, whereas wave 2b selects

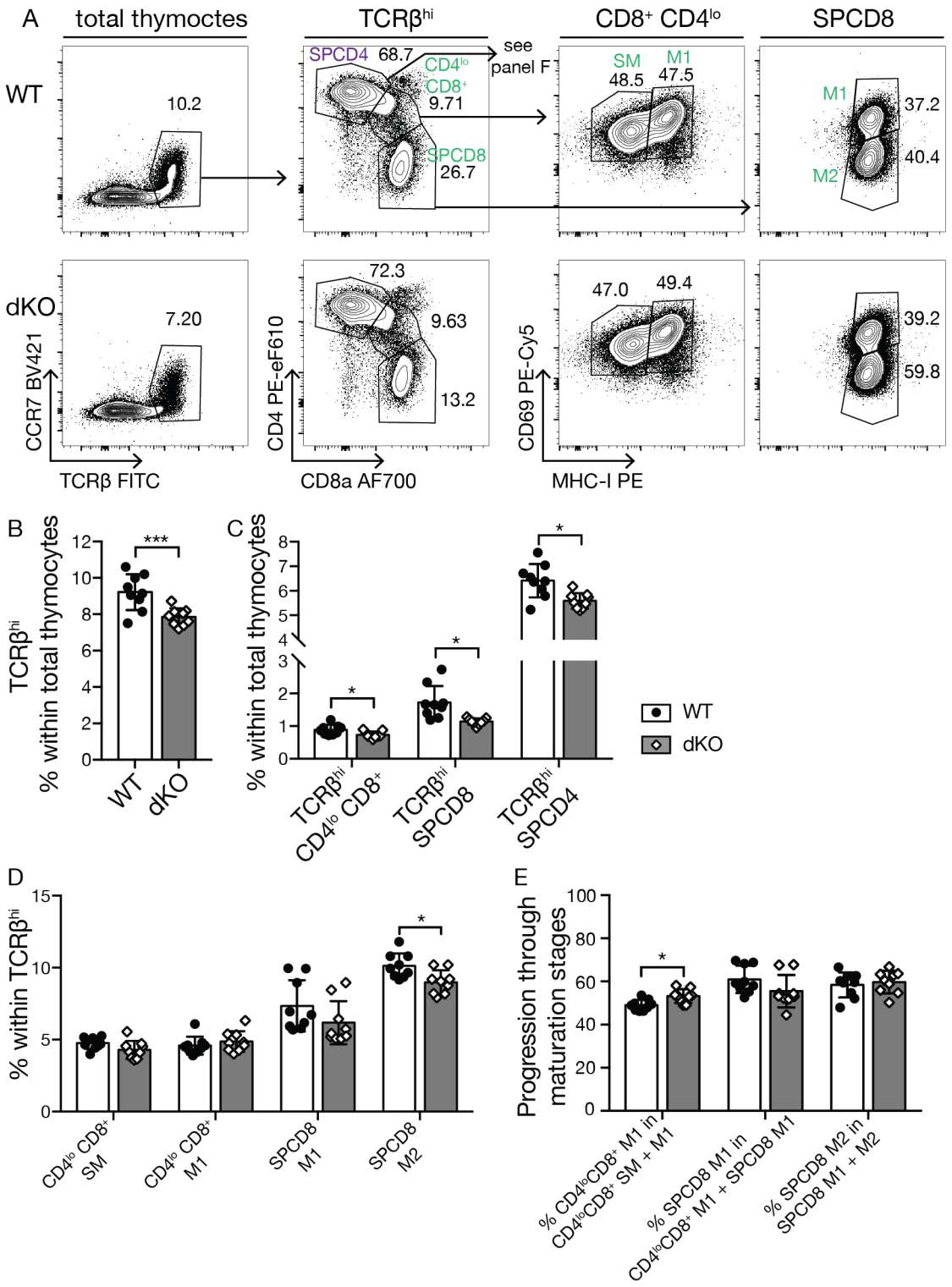
A
total thymoctes
TCRβhi
CD8+ CD4lo
SPCD8
WT
10.2
SPCD4 68.7
CD4lo
CD8+
9.71
SPCD8
26.7
see
panel F
SM
M1
48.5
47.5
M1
37.2
40.4
M2
dKO
7.20
72.3
9.63
13.2
47.0
49.4
39.2
59.8
CCR7 BV421
TCRβ FITC
CD4 PE-eF610
CD8a AF700
CD69 PE-Cy5
MHC-I PE
B
% within total thymocytes
TCRβhi
***
WT
dKO
C
% within total thymocytes
TCRβhi
CD4lo CD8+
TCRβhi
SPCD8
TCRβhi
SPCD4
WT
dKO
D
% within TCRβhi
CD4lo CD8+
SM
CD4lo CD8+
M1
SPCD8
M1
SPCD8
M2
E
Progression through
maturation stages
% CD4loCD8+ M1 in
CD4loCD8+ SM + M1
% SPCD8 M1 in
CD4loCD8+ M1 + SPCD8 M1
% SPCD8 M2 in
SPCD8 M1 + M2

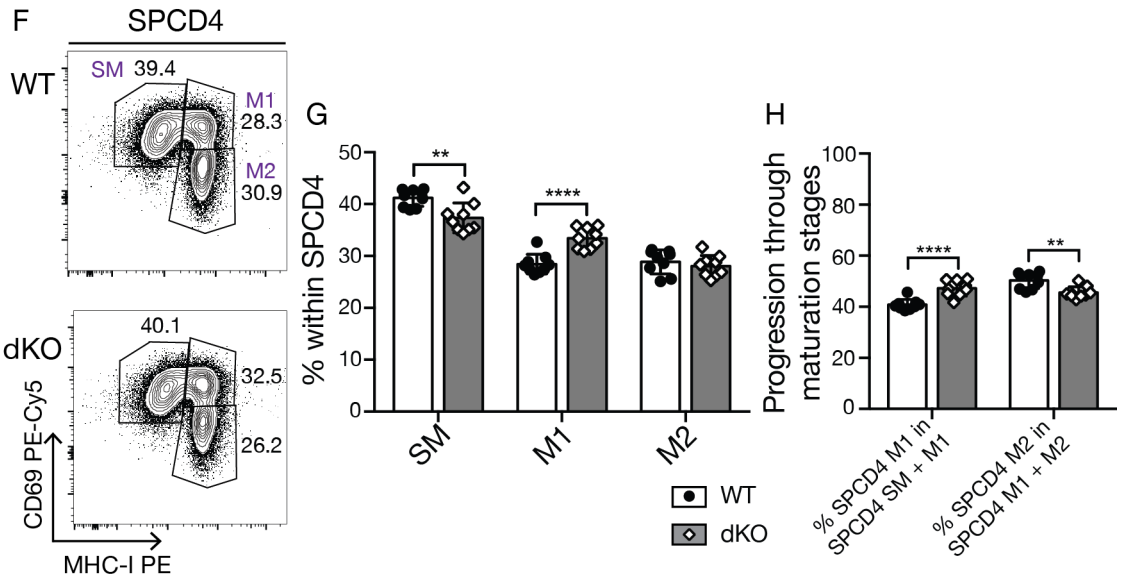

Figure 3.33: Lower frequency of SM and higher frequency of M1 in SPCD4 maturation in *Utx*$^{TEC-/-}$ *Jmjd3*$^{TEC-/-}$ mice. **(A)** Representative FACS plots showing the gating strategy to identify the post selection maturation of SPCD8 within TCRβ^{hi} according to the scheme depicted in Figure 3.32. **(B)** Bar graph displays the relative frequency of TCRβ^{hi} thymocytes within the population of total thymocytes. **(C)** Bar graph shows the relative frequencies of TCRβ^{hi} CD4^{lo}CD8^{+}, SPCD8 and SPCD4 within the population of total thymocytes. **(D)** Bar graph shows the relative frequencies of SPCD8 maturation within TCRβ^{hi} according to (A). **(E)** Bar graph shows progression through sequential maturational SPCD8 stages. Calculation: (Stage B)/(Stage A+B)x100 where A is the maturation stage immediately before B. **(F)** Representative FACS plots showing the gating strategy to identify the post selection maturation of SPCD4 according to the scheme depicted in Figure 3.32. **(G)** Bar graph shows the relative frequencies of SM, M1, M2 maturation within SPCD4 according to (F). **(H)** Bar graph shows progression through sequential maturational SPCD4 stages. Calculation: (Stage B)/(Stage A+B)x100 where A is the maturation stage immediately before B. Bar graphs are pooled from 3 independent experiments with female mice 4-5 weeks of age; WT (*Utx*$^{fl/fl}$ *Jmjd3*$^{fl/fl}$): n=9; dKO (*Utx*$^{TEC-/-}$ *Jmjd3*$^{TEC-/-}$): n=9. Statistical comparison was done with two-tailed unpaired t-tests with correction for multiple comparisons.

mature SP thymocytes with a CD69^{-}CD24^{-} phenotype. Negatively selected thymocytes in wave 2 express high levels of HELIOS. A schematic of the different waves of negative selection is shown in Figure 3.34. The gating strategy is displayed in Figure 3.35A and B.

This analysis revealed that negative selection in the *Utx*$^{TEC-/-}$ *Jmjd3*$^{TEC-/-}$ mice was impaired. In the cortex both wave 1a- and 1b-mediated negative selection were decreased in comparison to WT mice (wave 1a: 0.26 % ± 0.05 vs 0.34 % ± 0.05; SPCD4 wave 1b: 0.4 % ± 0.06 vs 0.49 % ± 0.1) (Fig. 3.35C-D). The early medullary wave 2a of negative selection spared SPCD4 thymocytes to a larger degree with fewer cells being selected for cell death (7.11 % ± 0.65 vs 8.15 % ± 0.62) (Fig. 3.35E), in contrast, more SPCD4 cells

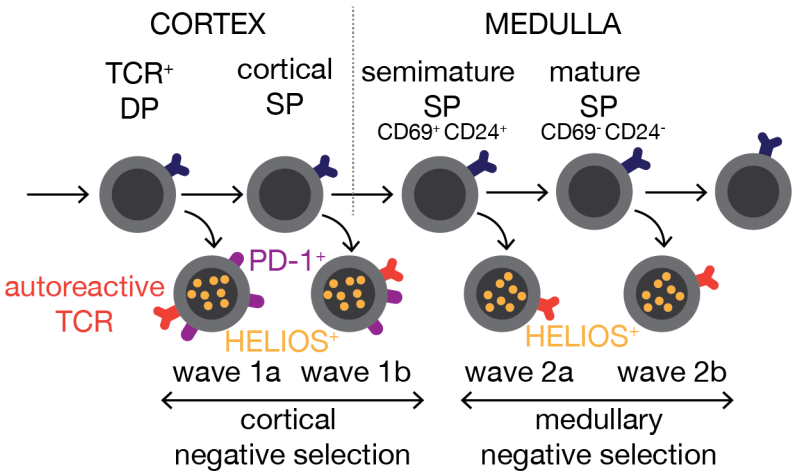

Figure 3.34: Schematic of thymocyte negative selection.

were negatively selected by wave 2b (11.2 % ± 1.05 vs 8.82 % ± 0.79) (Fig. 3.35F).

The negative selection of thymocytes of the CD8 lineage (i.e. wave 1b, wave 2a-b) was undisturbed in the $Utx^{TEC-/-}$ $Jmjd3^{TEC-/-}$ mice (Fig. 3.35G-I). It is however of note that the identification of negatively selected cells measuring nuclear HELIOS expression has not been verified and reported for SPCD8 cells [154]. A possible reason for this may indeed be that the threshold for HELIOS positivity is less obvious in flow cytometric analysis of wave 2 negative selection.

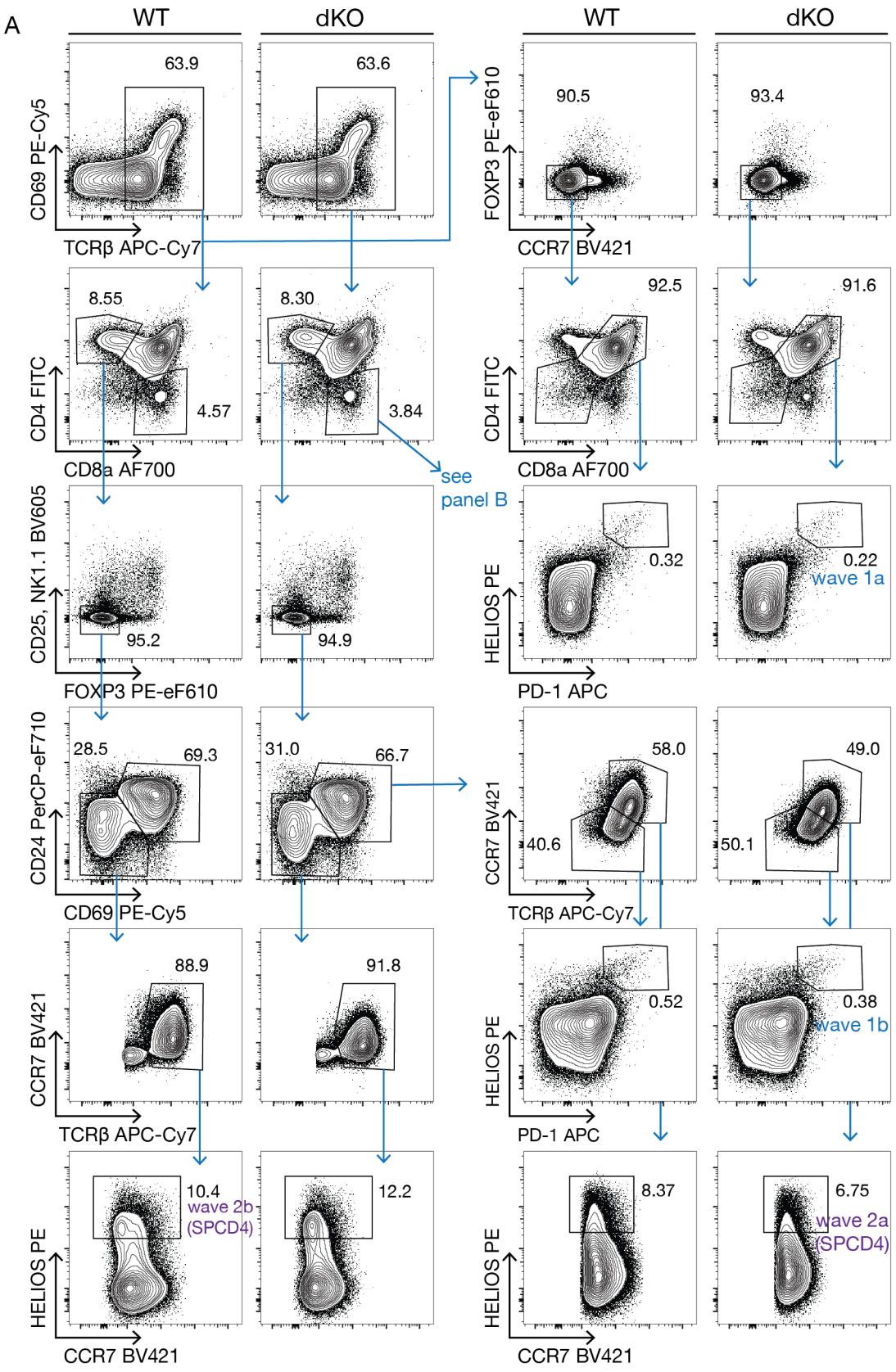
A
WT
dKO
WT
dKO
63.9
63.6
90.5
93.4
CD69 PE-Cy5
TCRβ APC-Cy7
FOXP3 PE-eF610
CCR7 BV421
8.55
4.57
8.30
3.84
92.5
91.6
CD4 FITC
CD8a AF700
see panel B
95.2
94.9
0.32
0.22
wave 1a
CD25, NK1.1 BV605
FOXP3 PE-eF610
HELIOS PE
PD-1 APC
28.5
69.3
31.0
66.7
58.0
40.6
49.0
50.1
CD24 PerCP-eF710
CD69 PE-Cy5
CCR7 BV421
TCRβ APC-Cy7
88.9
91.8
0.52
0.38
wave 1b
CCR7 BV421
TCRβ APC-Cy7
HELIOS PE
PD-1 APC
10.4
wave 2b
(SPCD4)
12.2
8.37
6.75
wave 2a
(SPCD4)
HELIOS PE
CCR7 BV421
HELIOS PE
CCR7 BV421

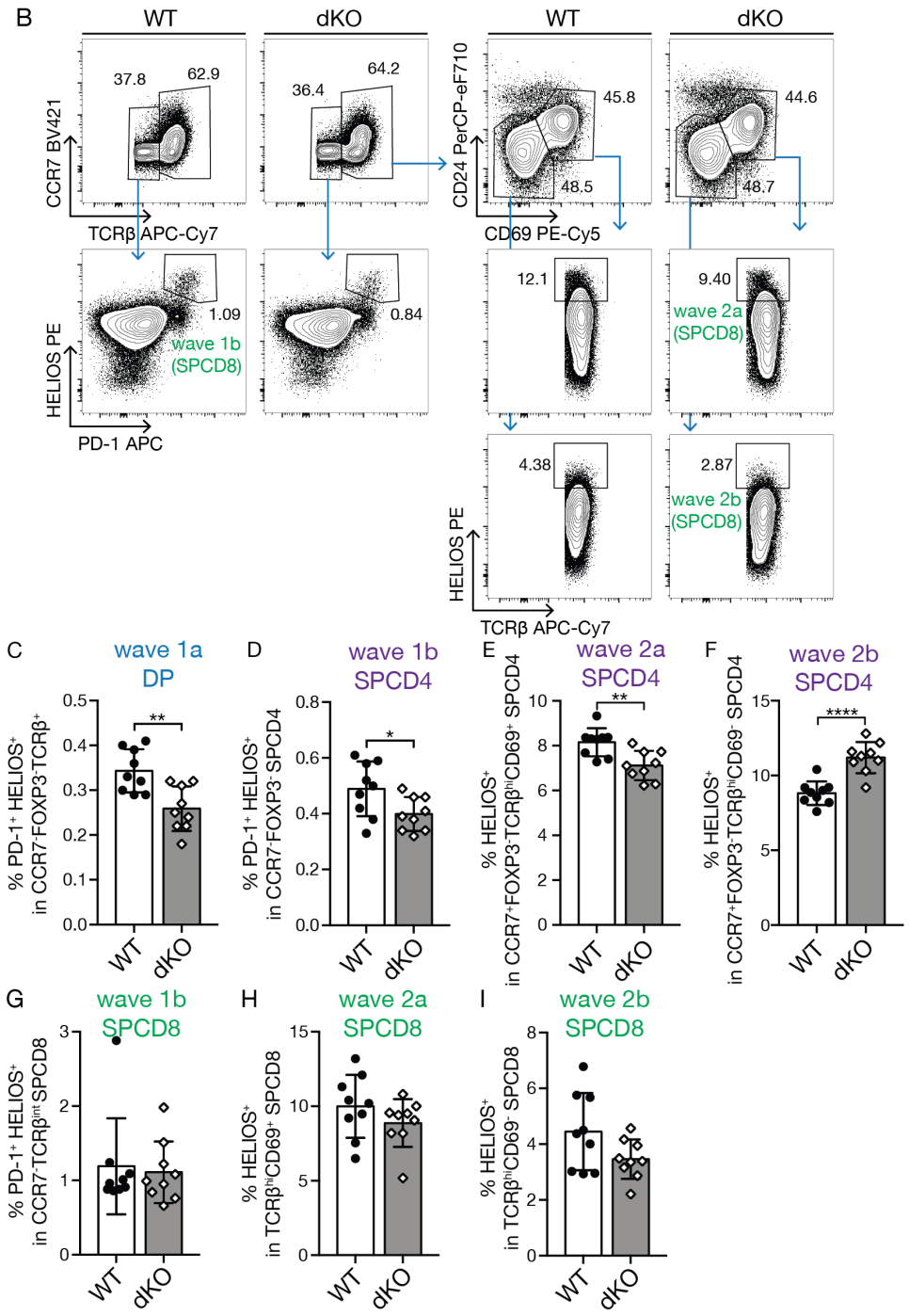

Figure 3.35: Decreased cortical negative selection and early medullary negative selection, increased late negative selection in *Utx*$^{TEC-/-}$ *Jmjd3*$^{TEC-/-}$ mice. (A-B) Representative FACS plots show the gating strategy for defining the different waves of negative selection in the thymus. **(C)** Bar graph shows frequency of wave 1a (PD-1$^+$ HELIOS$^+$) within CCR7$^-$FOXP3$^-$TCRβ$^-$ thymocytes. **(D)** Bar graph shows frequency of SPCD4 wave 1b (PD-1$^+$ HELIOS$^+$) within CCR7$^-$FOXP3$^-$ SPCD4. **(E)** Bar graph shows frequency of SPCD4 wave 2a (HELIOS$^+$) within CCR7$^+$FOXP3$^-$TCRβ^{hi}CD69$^+$ SPCD4. **(F)** Bar graph shows frequency of SPCD4 wave 2a (HELIOS$^+$) within CCR7$^+$FOXP3$^-$TCRβ^{hi}CD69$^-$ SPCD4. **(G)** Bar graph shows frequency of SPCD8 wave 1b (PD-1$^+$ HELIOS$^+$) within CCR7$^-$TCRβ^{int} SPCD8. **(H)** Bar graph shows frequency of SPCD8 wave 2a (HELIOS$^+$) within CCR7$^+$ TCRβ^{hi}CD69$^+$ SPCD8. **(I)** Bar graph shows frequency of SPCD8 wave 2a (HELIOS$^+$) within CCR7$^+$ TCRβ^{hi}CD69$^-$ SPCD8. Bar graphs are pooled from 3 independent experiments with female mice 4-5 weeks of age; WT (*Utx*$^{fl/fl}$ *Jmjd3*$^{fl/fl}$): n=9; dKO (*Utx*$^{TEC-/-}$ *Jmjd3*$^{TEC-/-}$): n=9. Statistical comparison was done with two-tailed unpaired t-tests with correction for multiple comparisons. *p<0.05; **p<0.01; ***p<0.005, ****p<0.001.

Fewer thymocytes were negatively selected in the cortex of $Utx^{TEC-/-}$ $Jmjd3^{TEC-/-}$ mice. cTEC that lack UTX and JMJD3 may be incapable of effecting negative selection in an efficient way. Their reduced frequency and proliferation could indeed reflect essential changes in cTEC functionality. In the medulla, the picture appears to be more complex: While negative selection of SPCD8 remained unchanged, the absence of UTX and JMJD3 expression in TEC correlated with a reduced negative selection of SPCD4 thymocytes subject to wave 2a, but not wave 2b, where a higher frequency of thymocytes were destined for cell death.

There are various reasons why negative selection might be differently affected at specific developmental stages. One of the limitations of assessing negative selection using the markers for HELIOS and PD-1 concerns the rate by which apoptotic cells are scavenged by thymus-resident phagocytic cells, as their position and cellularity may vary between these mouse strains. In the absence of data showing the presence of dendritic cells and macrophages in $Utx^{TEC-/-}$ $Jmjd3^{TEC-/-}$ mice, it remains unknown whether the subtle but specific changes in negative selection (especially the difference between wave 2a and wave 2b negative selection of SPCD4 thymocytes) are caused by differences in efficiently removing apoptotic cells. Indeed, this staining for HELIOS and PD-1 will only identify a small fraction of negatively selected cells as the clearing of apoptotic cells is incredibly efficient in the thymus. It is therefore conceivable that the assessment of negative selection in its full scope can only be done in apoptosis-deficient mice [154].

3.7.5 The generation of thymic T_{reg} cells is unaffected in the $Utx^{TEC-/-}$ $Jmjd3^{TEC-/-}$ mice

Positively selected SPCD4 thymocytes with a high-affinity TCR for self-peptide MHC complexes can - alternatively to being negatively selected - be diverted towards a T_{reg} cell fate [155]. Precursor T_{reg} cells start by expressing either CD25 or FOXP3 before becoming T_{reg} cells that are double positive for both of these markers [156]. Once they leave the thymus T_{reg} cells are essential for suppressing the proliferation of autoreactive T

cells [157]. Given that negative selection was altered in the *Utx*$^{TEC-/-}$ *Jmjd3*$^{TEC-/-}$ mice, I next probed whether the generation of T_{reg} cells was also affected.

The thymic frequencies of the direct precursor populations (CD25^{-}FOXP3^{+} and CD25^{+} FOXP3^{-}) and of CD25^{+}FOXP3^{+} T_{reg} cells themselves were comparable for WT and *Utx*$^{TEC-/-}$ *Jmjd3*$^{TEC-/-}$ mice (Fig. 3.36B). To identify recirculating T_{reg} cells, thymic T_{reg} cells were also stained for ICOS and CD103, markers whose expression is initiated in lymph nodes. ICOS^{+} CD103^{+} T_{reg} cells, which characteristically have a high suppressive potency [158], were increased in the thymi of *Utx*$^{TEC-/-}$ *Jmjd3*$^{TEC-/-}$ mice (10.16 % ± 3.28 vs 5.66 % ± 2.23) (Fig. 3.36C).

ICOS and CD103 only mark a subset of recirculating T_{reg} cells and thus this phenotype cannot distinguish between newly generated and recirculating T_{reg} cells [158]. The chemokine receptor CCR6 has recently been proposed as a marker to distinguish between *in situ* generated and recirculating T_{reg} cells [159] (Fig. 3.37). Staining for CCR6 was therefore used to identify all recirculating T_{reg} cells in the thymus of WT and mutant mice in this study. A more detailed assessment of this gating strategy using CCR6 can be found in Chapter 5.4.7.

The frequency of recirculating CCR6^{+} T_{reg} cells was unchanged comparing *Utx*$^{TEC-/-}$ *Jmjd3*$^{TEC-/-}$ to WT mice (Fig. 3.38B). Hence, the higher frequency of the "activated" ICOS^{+} CD103^{+} T_{reg} in the thymus was reflective of an overall increase in T_{reg} cells recirculating to the thymus, but seemingly concerned only this subpopulation of recirculating T_{reg} cells. Notably, the frequency of ICOS^{+} CD103^{+} CCR6^{-} cells (i.e. *in situ* T_{reg} cells) was also increased (3.63 % ± 0.54 vs 1.83 % ± 0.95) (Fig. 3.38C), suggesting that the altered microenvironment of *Utx*$^{TEC-/-}$ *Jmjd3*$^{TEC-/-}$ mice may impose ICOS and CD103 expression on newly generated T_{reg} cells.

The role of recirculating T_{reg} cells is not completely elucidated. So far, it has been shown that these cells appear to negatively regulate thymic T_{reg} cell development by competing for IL-2 [160], however other studies could not confirm this claim as differences in thymic T_{reg} cell development were not observed under conditions of fewer recirculating T_{reg}

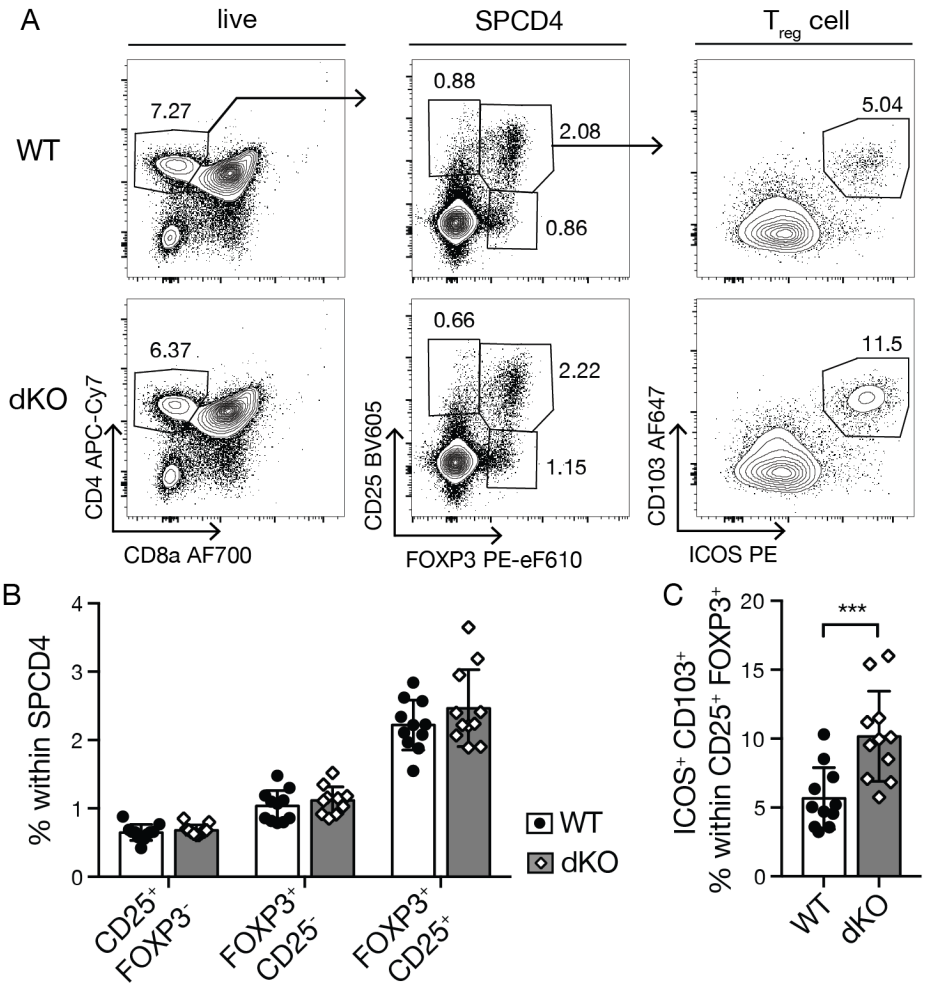

Figure 3.36: Increased frequency of ICOS$^+$CD103$^+$ T$_{reg}$ cells in the thymus. (A) Representative FACS plots show the gating of thymic T$_{reg}$ cells using CD25 and FOXP3. Thymic T$_{reg}$ cells were identified as CD25$^+$FOXP3$^+$ while T$_{reg}$ cell precursors were either CD25$^-$FOXP3$^+$ or CD25$^+$FOXP3$^-$. CD25$^+$FOXP3$^+$ T$_{reg}$ cells were further gated for ICOS and CD103 expression. **(B)** Bar graph shows frequency of CD25$^+$FOXP3$^-$, CD25$^-$FOXP3$^+$ and CD25$^+$FOXP3$^+$ T$_{reg}$ cells within SPCD4. **(C)** Bar graph shows frequency ICOS$^+$CD103$^+$ cells within CD25$^+$FOXP3$^+$ T$_{reg}$ cells. Bar graphs are pooled from 3 independent experiments with female mice 4-5 weeks of age; WT (*Utx$^{fl/fl}$ Jmjd3$^{fl/fl}$*): n=11; dKO (*Utx$^{TEC-/-}$ Jmjd3$^{TEC-/-}$*): n=11. Statistical comparison was done with two-tailed unpaired t-tests with correction for multiple comparisons. *p<0.05; **p<0.01; ***p<0.005, ****p<0.001.

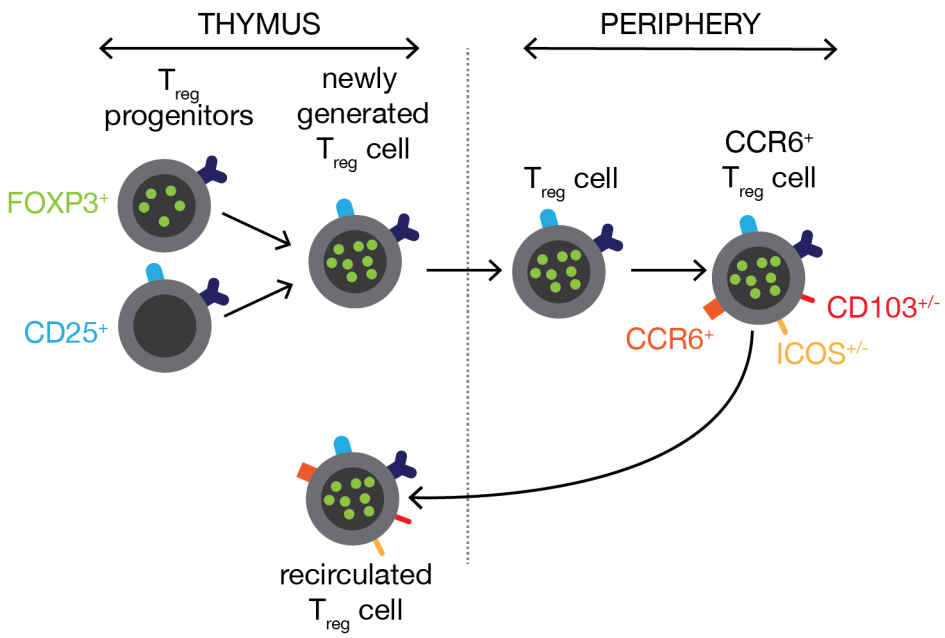

Figure 3.37: Scheme of intrathymic T_{reg} cell generation and recirculation of peripheral T_{reg} cells.

cells [161]. Nonetheless, it is conceivable that $ICOS^+CD103^+$ T_{reg} cells could have a specific biological role in thymopoiesis given their high suppressive potency, which would be in keeping with the notion that $mTEC^{hi}$ control the recirculation of T_{reg} cells via their production of CCL20 [162]. It is of note, however, that *Ccl20* expression in the UTX/JMJD3-deficient $mTEC^{hi}$ was decreased (fold change: 0.35 ± 0.12) (Fig. 3.38D). The increased number of $mTEC^{hi}$ in these mice may, however, compensate for the lower expression levels, explaining the normal frequency of $CCR6^+$ T_{reg} cells within the thymi of $Utx^{TEC-/-}$ $Jmjd3^{TEC-/-}$ mice.

3.7.6 Brief summary of thymocyte development in $Utx^{TEC-/-}$ $Jmjd3^{TEC-/-}$ mice

Thymocyte development in $Utx^{TEC-/-}$ $Jmjd3^{TEC-/-}$ mice was largely comparable to that of WT mice, including an unchanged DN thymocyte development and an unchanged positive selection. However, the loss of UTX and JMJD3 in the TEC did have a mild but consistent impact on thymopoiesis, and thymi from $Utx^{TEC-/-}$ $Jmjd3^{TEC-/-}$ mice contained fewer SPCD8 and SPCD4 $TCR\beta^{hi}$ thymocytes. The SPCD8 lineage was mildly

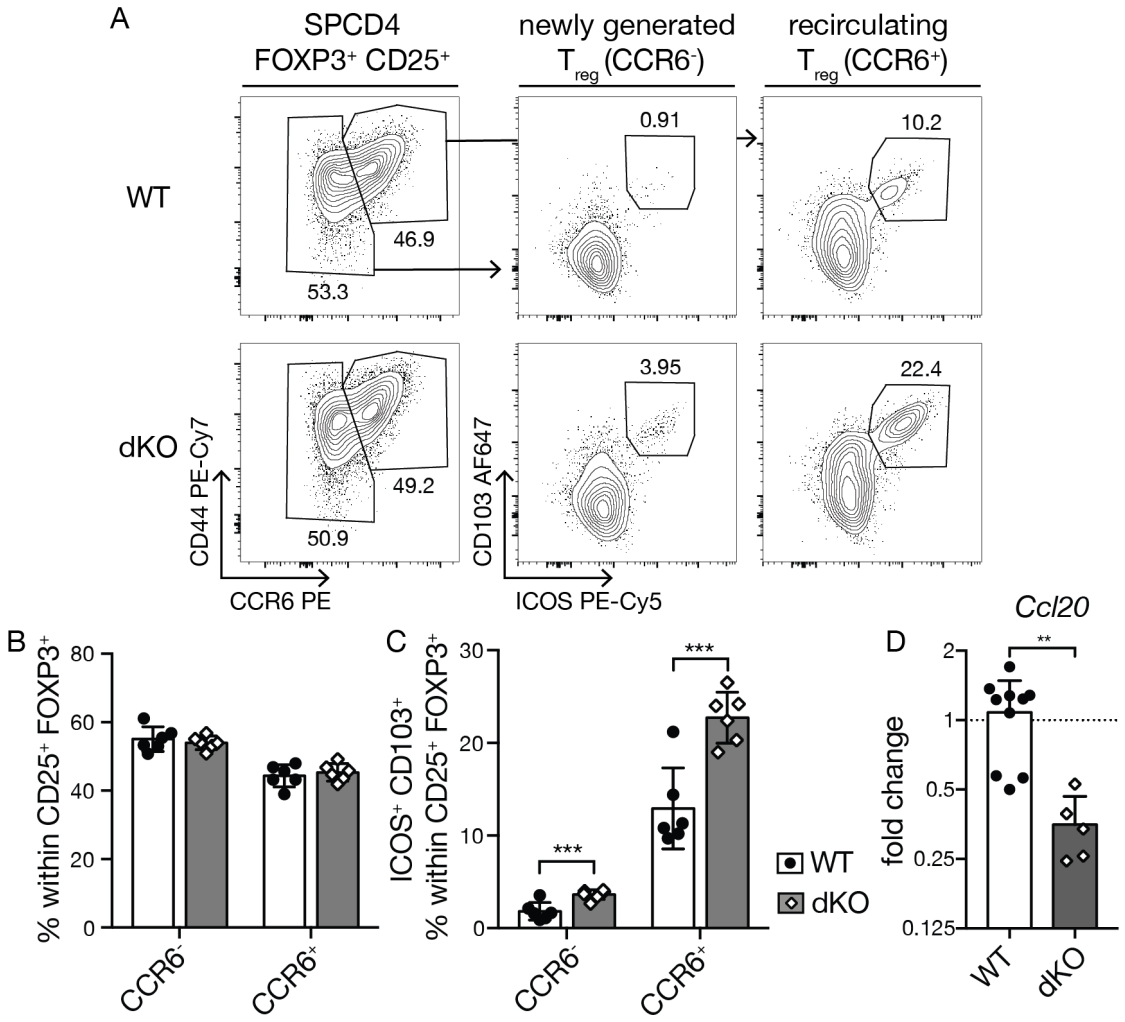

Figure 3.38: Frequency of recirculating T_{reg} cells is unchanged, however there are more ICOS$^+$ CD103$^+$ cells within recirculating T_{reg} cells. (A) Representative FACS plots show the gating of newly generated (CCR6$^-$) and recirculating (CCR6$^+$) T_{reg} cells. CCR6$^-$ and CCR6$^+$ T_{reg} cells were further gated for ICOS and CD103 expression. **(B)** Bar graph shows frequency of CCR6$^-$ and CCR6$^+$ cells within T_{reg} cells (SPCD4 CD25$^+$FOXP3$^+$). **(C)** Bar graph shows frequency of ICOS$^+$CD103$^+$ cells within newly generated (CCR6$^-$) and recirculating (CCR6$^+$) T_{reg} cells. Bar graphs are pooled from 2 independent experiments with female mice 4-5 weeks of age; WT (*Utx*$^{fl/fl}$ *Jmjd3*$^{fl/fl}$): n=6; dKO (*Utx*$^{TEC-/-}$ *Jmjd3*$^{TEC-/-}$): n=6. **(D)** Extracted RNA from sorted mTEC^{hi} was used for qPCR for detecting the expression of *Ccl20*. Data was analysed using the $2^{-\Delta\Delta Ct}$ method with normalising to *Gapdh* expression and setting expression in WT to 1. The experiment was done with female mice at 4-5 weeks of age. WT (*Utx*$^{fl/fl}$ *Jmjd3*$^{fl/fl}$): n=10; dKO (*Utx*$^{TEC-/-}$ *Jmjd3*$^{TEC-/-}$): n=5. Statistical comparison was done with two-tailed unpaired t-tests with correction for multiple comparisons. *p<0.05; **p<0.01; ***p<0.005, ****p<0.001.

reduced in frequency at the last maturational steps before thymic egress. *Utx*$^{TEC-/-}$ *Jmjd3*$^{TEC-/-}$ mice had a reduced negative selection in the cortex, as well as in the early stages in the medulla, in contrast late medullary negative selection was increased. T_{reg} cell development in *Utx*$^{TEC-/-}$ *Jmjd3*$^{TEC-/-}$ mice was comparable to WT mice, however there were more CD103$^+$ ICOS$^+$ T_{reg} cells recirculating to the thymus. Additionally, more CD8$^+$ T cells recirculated to *Utx*$^{TEC-/-}$ *Jmjd3*$^{TEC-/-}$ thymi.

3.8 Peripheral T cell compartment in *Utx*$^{TEC-/-}$ *Jmjd3*$^{TEC-/-}$ mice

Newly generated (i.e. naïve) T cells egress from the thymus to the periphery where they recirculate between secondary and tertiary lymphoid tissues via the blood, and are ready to execute their defence functions upon recognition of their cognate antigen presented together on MHC molecules.

In this subchapter, the peripheral T cells educated in TEC microenvironment lacking UTX and JMJD3 were assessed. Changes in thymic T cell output were first sought and related to peripheral T cell frequencies and variations in the composition of different CD4$^+$ and CD8$^+$ T cell subsets. Specifically, I noted an increase in the frequency of recirculating ICOS$^+$CD103$^+$ T_{reg} and CD8$^+$ T cells in the thymus of *Utx*$^{TEC-/-}$ *Jmjd3*$^{TEC-/-}$ mice and therefore wanted to probe whether there was a corresponding change in the periphery.

In the periphery, T cells constantly scan pMHC with their TCR, which results in low-affinity interactions that are crucial for the survival of naïve T cells [163]. Once they encounter their cognate antigen in the form of a foreign peptide with sufficient affinity in the presence of co-stimulating signals (e.g. CD28 receptor engagement and cytokine signals), they become activated and start proliferating [164]. The activated cells will adapt an effector memory phenotype by upregulating CD44 expression and downregulating the lymph node homing receptor CD62L. Once the pathogen is cleared, the effector memory T cells are no longer needed and the majority of them undergo apoptosis, as they lack activation signals though the TCR. However, a small fraction of the T cells

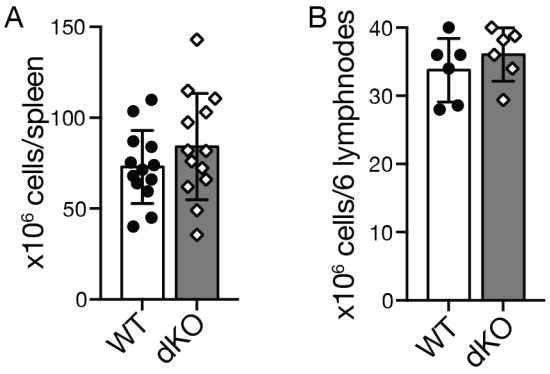

Figure 3.39: Cellularity of spleen and lymph nodes is unchanged in *Utx$^{TEC-/-}$ Jmjd3$^{TEC-/-}$* mice. (A) Bar graph depicts total splenic cellularity after red blood cell lysis and represent 4 independent experiments with female mice 4-5 weeks of age; WT (*Utx$^{fl/fl}$ Jmjd3$^{fl/fl}$*): n=13; dKO (*Utx$^{TEC-/-}$ Jmjd3$^{TEC-/-}$*): n=13. **(B)** Bar graph depicts the overall cellularity of 6 lymph nodes and represents 2 independent experiments with female mice 4-5 weeks of age; WT (*Utx$^{fl/fl}$ Jmjd3$^{fl/fl}$*): n=6; dKO (*Utx$^{TEC-/-}$ Jmjd3$^{TEC-/-}$*): n=6. Statistical comparison was done with two-tailed unpaired t-tests.

having responded to antigen will become long-lived central memory T cells, which are characterised by high level of CD62L and CD44 surface expression [163].

3.8.1 CD8$^+$ T cells are skewed towards memory phenotype in *Utx$^{TEC-/-}$ Jmjd3$^{TEC-/-}$* mice

The total cellularity of spleen and lymph nodes in *Utx$^{TEC-/-}$ Jmjd3$^{TEC-/-}$* mice was comparable to WT animals (Fig. 3.39A-B). The frequencies of splenic B cells and naïve as well as memory CD4$^+$ T cells was also similar in *Utx$^{TEC-/-}$ Jmjd3$^{TEC-/-}$* mice and WT mice (Fig. 3.40B-C). In contrast, the frequency of peripheral CD8$^+$ T cells with a central memory phenotype was increased (40.74 % ± 5.51 vs 29.3 % ± 2.67) (Fig. 3.40E). An expansion of memory T cells can be observed in response to infections or with age [165, 166]. As both mechanisms do not account for the shift of peripheral CD8$^+$ T cells to a memory phenotype in young, non-infected mice, the propensity of CD8$^+$ T cells to adopt a central memory phenotype in *Utx$^{TEC-/-}$ Jmjd3$^{TEC-/-}$* thymi could be accounted for by a decreased thymic output of this lineage with a subsequent compensating homeostatic expansion of these cells in the periphery. I therefore quantified recent thymic emigrants (RTE) as a surrogate for recent thymic output.

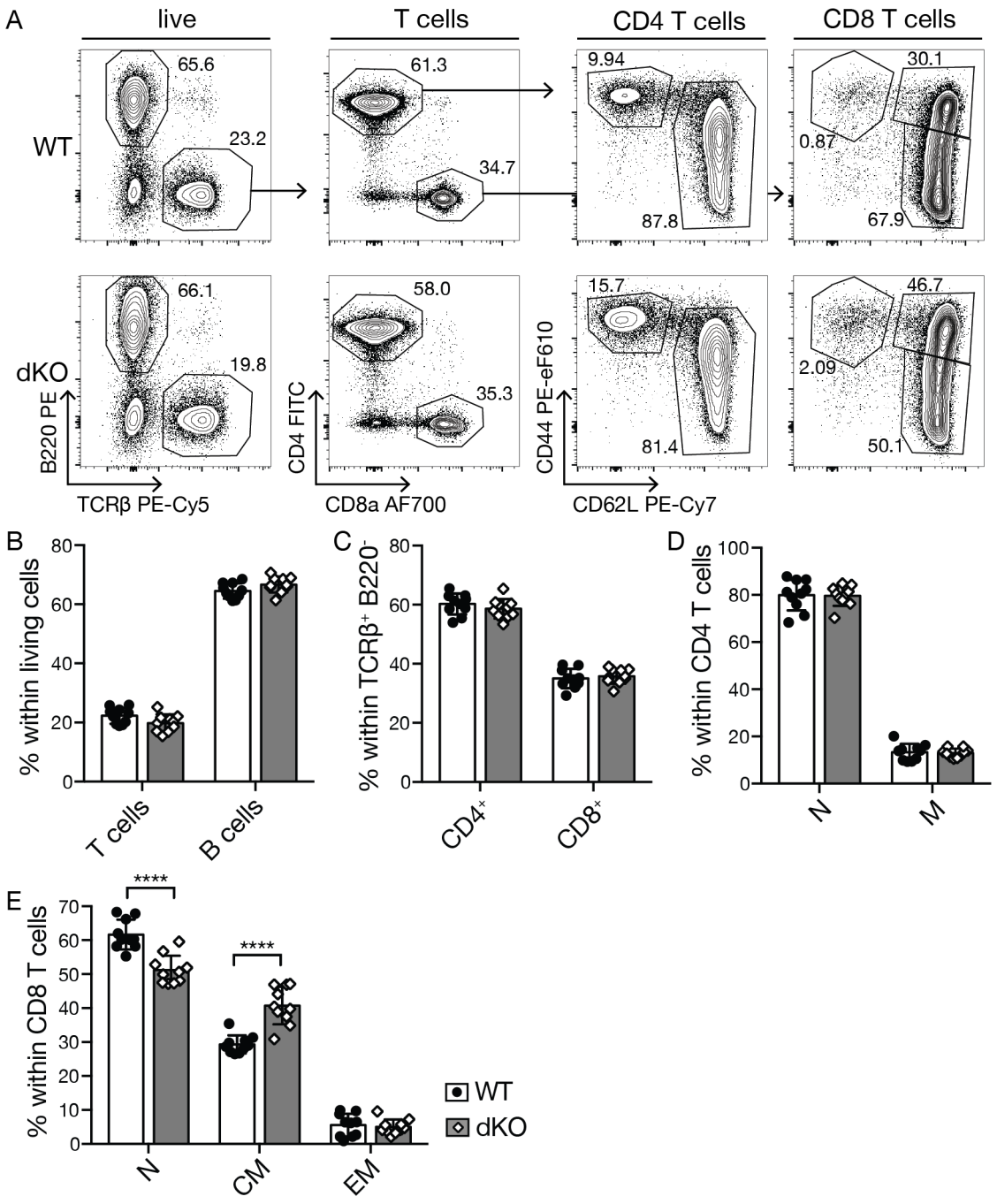

Figure 3.40: Splenic CD8$^+$ T cells are skewed towards a memory phenotype in *Utx$^{TEC-/-}$ Jmjd3$^{TEC-/-}$*. **(A)** Representative FACS plots show the gating strategy to assess T cells (B220$^-$ TCRβ$^+$) and B cells (B220$^+$ TCRβ$^-$) in the spleen. T cells are further split into CD4$^+$ and CD8$^+$ T cell subsets. CD4$^+$ are divided into naïve (CD62L$^+$ CD44^{lo}) and memory (CD62L$^-$ CD44^{hi}) and CD8$^+$ T cells are divided into naïve (CD62L$^+$ CD44^{lo}), central memory (CD62L$^+$ CD44^{hi}) and effector memory (CD62L$^-$ CD44^{hi}) cells. **(B)** Bar graph shows frequencies of B and T cells within total splenocytes. **(C)** Bar graph shows frequencies of CD4$^+$ and CD8$^+$ T cells within total T cells. **(D)** Bar graph shows frequencies of naïve (N) and memory (M) cells within CD4$^+$ T cells. **(E)** Bar graph shows frequencies of naïve (N), central memory (CM) and effector memory (EM) cells within CD8$^+$ T cells. Bar graphs are pooled from 3 independent experiments with female mice 4-5 weeks of age; WT (*Utx$^{fl/fl}$ Jmjd3$^{fl/fl}$*): n=10; dKO (*Utx$^{TEC-/-}$ Jmjd3$^{TEC-/-}$*): n=10. Statistical comparison was done with two-tailed unpaired t-tests with correction for multiple comparisons. *p<0.05; **p<0.01; ***p<0.005, ****p<0.001.

3.8.2 Recent thymic emigrants in *Utx$^{TEC-/-}$ Jmjd3$^{TEC-/-}$* mice

T cells that have recently left the thymus are referred to as RTE and are functionally different from mature naïve (non-RTE) T cells. RTE are characterised by decreased proliferative response and lower cytokine production upon stimulation and will require further maturation to achieve functional competence [167, 168].

Quantifying RTE frequency was used to assess thymic output in the *Utx$^{TEC-/-}$ Jmjd3$^{TEC-/-}$* mice [151]. Especially, the output of CD8$^+$ T cells was measured to strengthen or refute the argument that the observed increase in CD8$^+$ T cells with a memory phenotype was caused by a diminished thymic output and the consequent need for peripheral homeostatic proliferation. Although different surface markers have been proposed to identify RTE, a consensus exists that these cells can be identified by their expression of CD24^{hi}, Qa2^{lo}, CD45RB^{lo} and CD55^{lo} which contrast with the phenotype of mature naïve T cells (CD24^{lo}, Qa2^{hi}, CD24RB^{hi} and CD55^{hi}) [151, 169]. It is, however, of note that the anticipated differences in marker expression between RTE and mature naïve T cells are small. Optimal gating would require the use of Rag2-GFP T cells as RTE can be identified by the presence of green fluorescence [170].

Staining CD4$^+$ T cells for the expression of CD55 and CD45RB and CD8$^+$ T cells for CD55 and Qa2 appeared to be the best strategy to identify CD4$^+$ (CD55^{lo} CD45RB^{lo}) and CD8$^+$ (CD55^{lo} Qa2^{lo}) RTE (Fig. 3.41A). Using this specific approach, the frequencies of RTE within the population of naïve T cells of lymph nodes were comparable for WT and *Utx$^{TEC-/-}$ Jmjd3$^{TEC-/-}$* mice (Fig. 3.41D-E).

An alternative method to assess thymic output is the quantitation of T cell receptor excision circles (TREC). The detection of these by-products of TCR rearrangement relies on the measurement of circular DNA encoding intervening sequences of the TCRβ locus. These TREC are non-replicable and are therefore diluted with every cell division [113]. Thus, assessing TREC within naïve T cells can be used as a measure of thymic output. The frequency of TREC I detected in sorted CD4$^+$ RTE and mature naïve CD4$^+$ T cells was comparable when determined in WT and *Utx$^{TEC-/-}$ Jmjd3$^{TEC-/-}$* mice (Fig. 3.42A).

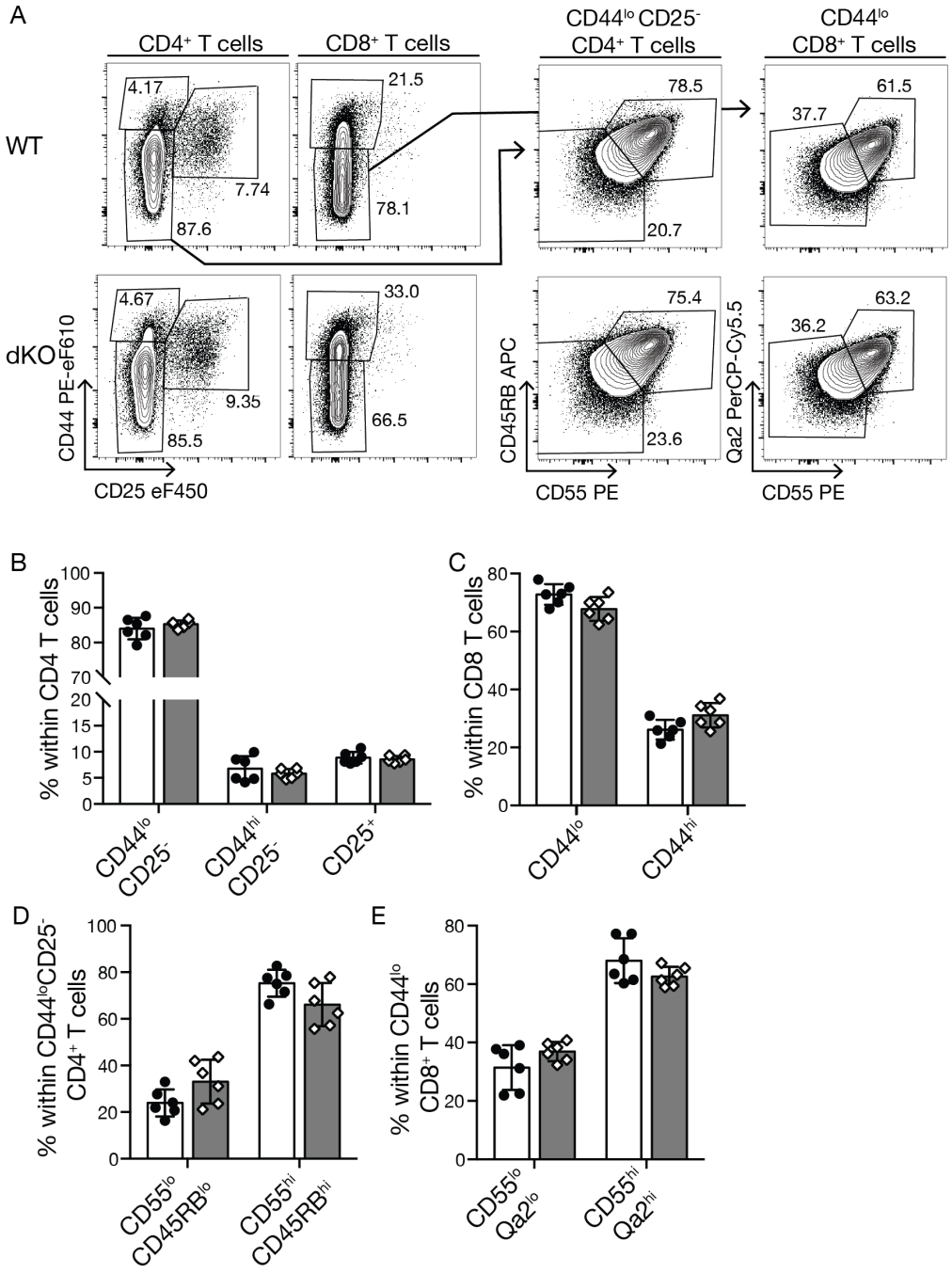

Figure 3.41: The frequency of RTE is comparable for WT and *Utx$^{TEC-/-}$ Jmjd3$^{TEC-/-}$* mice. (A) Representative FACS plots show the gating strategy to assess RTE cells in the lymph nodes. Conventional naïve (CD25^{-} CD44^{lo}) CD4^{+} T cells are divided into RTE (CD55^{lo} CD45RB^{lo}) and mature naïve cells (CD55^{hi} CD45RB^{hi}). Naïve (CD44^{lo}) CD8^{+} T cells are divided into RTE (CD55^{lo} Qa2^{lo}) and mature naïve cells (CD55^{hi} Qa2^{hi}). **(B)** Bar graph shows frequencies of conventional naïve (CD25^{-} CD44^{lo}), conventional memory (CD25^{-} CD44^{hi}) and CD25^{+} within total CD4^{+} T cells. **(C)** Bar graph shows frequencies of naïve (CD44^{lo}) and memory (CD44^{hi}) within total CD8^{+} T cells. **(D)** Bar graph shows frequencies of RTE (CD55^{lo} CD45RB^{lo}) and mature naïve cells (CD55^{hi} CD45RB^{hi}) within conventional naïve (CD25^{-} CD44^{lo}) CD4^{+} T cells. **(E)** Bar graph shows frequencies of RTE (CD55^{lo} Qa2^{lo}) and mature naïve cells (CD55^{hi} Qa2^{hi}) within naïve (CD44^{lo}) CD8^{+} T cells. Bar graphs represent 2 independent experiments with female mice 4-5 weeks of age; WT (*Utx$^{fl/fl}$ Jmjd3$^{fl/fl}$*): n=6; dKO (*Utx$^{TEC-/-}$ Jmjd3$^{TEC-/-}$*): n=6. Statistical comparison was done with two-tailed unpaired t-tests with correction for multiple comparisons. *p<0.05; **p<0.01; ***p<0.005, ****p<0.001.

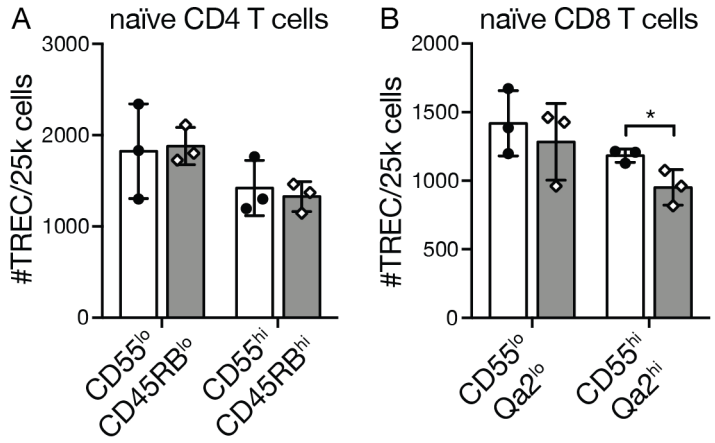

Figure 3.42: TREC in naïve CD4 and CD8 T cells from *Utx$^{TEC-/-}$ Jmjd3$^{TEC-/-}$* mice. **(A)** Bar graph shows number of TREC per 25000 sorted RTE (CD55^{lo} CD45RB^{lo}) and mature naïve (CD55^{hi} CD45RB^{hi}) CD4^{+} T cells. **(B)** Bar graph shows number of TREC per 25000 sorted RTE (CD55^{lo} CD45RB^{lo}) and mature naïve (CD55^{hi} CD45RB^{hi}) CD8^{+} T cells. Cells were sorted from lymph nodes. Bar graphs represent one experiment with female mice 4-5 weeks of age; WT (*Utx$^{fl/fl}$ Jmjd3$^{fl/fl}$*): n=3; dKO (*Utx$^{TEC-/-}$ Jmjd3$^{TEC-/-}$*): n=3. Statistical comparison was done with two-tailed unpaired t-tests with correction for multiple comparisons. *p<0.05; **p<0.01; ***p<0.005, ****p<0.001.

In contrast, fewer TREC were detected in CD8^{+} mature naïve T (951 ± 129 vs 1183 ± 48) (Fig. 3.42B). Given the variability of the TREC detected in independent biological samples the significance of the observed difference is unclear. Additionally, it is of note that altered T cell proliferation will affect TREC concentration independent of thymic output [171, 172]. In aggregate, the frequency of lower TREC number in mature naïve CD8^{+} T cells is compatible with, but not a proof of, these cells' homeostatic proliferation.

Despite the methodological limitation of the essays used, the analysis of RTE in the *Utx$^{TEC-/-}$ Jmjd3$^{TEC-/-}$* mice suggests that the thymic output of CD4^{+} or CD8^{+} T cells in *Utx$^{TEC-/-}$ Jmjd3$^{TEC-/-}$* mice is comparable to that of WT mice and thus probably cannot account for the observed higher frequency of CD8 T cells with a central memory phenotype in double mutant animals.

3.8.3 Peripheral T$_{reg}$ cells are unchanged in *Utx$^{TEC-/-}$ Jmjd3$^{TEC-/-}$* mice

T$_{reg}$ cells limit the proliferative response of conventional T cells activated by their cognate antigen and thus prevent the expansion of autoreactive cells in the periphery [173].

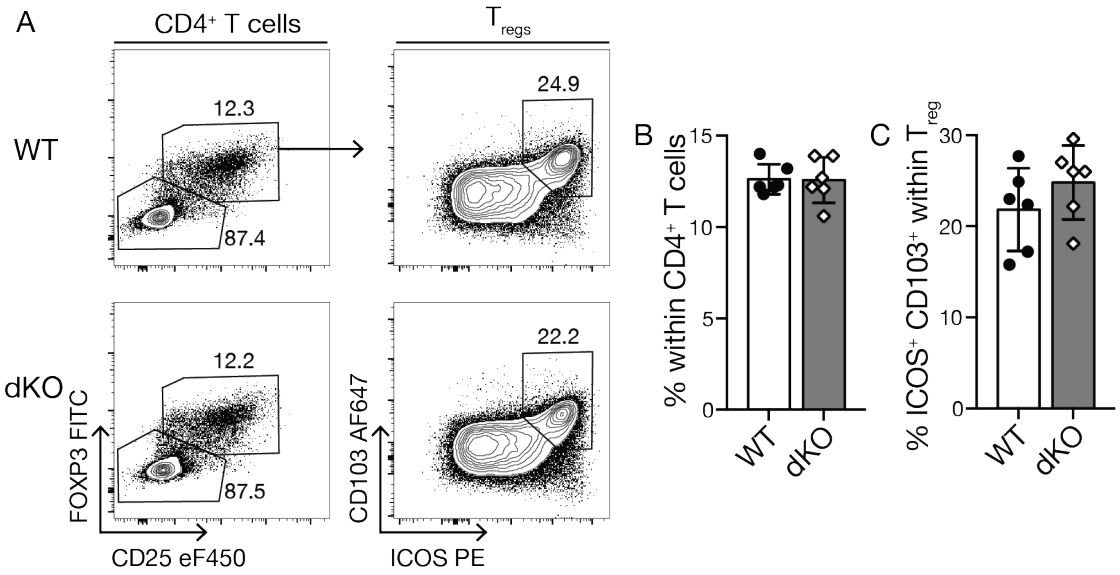

Figure 3.43: Normal frequency and phenotype of T_{reg} cells in lymph nodes of *Utx*$^{TEC-/-}$ *Jmjd3*$^{TEC-/-}$ mice. **(A)** Representative FACS plots show the gating strategy to analyse T_{reg} cells ($CD25^+$ $FOXP3^+$) within $CD4^+$ T cells in lymph nodes. T_{reg} cells are further assessed for ICOS and CD103 expression. **(B)** Bar graph shows frequencies of T_{reg} cells within total $CD4^+$ T cells. **(C)** Bar graph shows frequencies of $ICOS^+$ $CD103^+$ cells within total T_{reg} cells. Bar graphs represent 2 independent experiments with female mice 4-5 weeks of age; WT (*Utx*$^{fl/fl}$ *Jmjd3*$^{fl/fl}$): n=6; dKO (*Utx*$^{TEC-/-}$ *Jmjd3*$^{TEC-/-}$): n=6. Statistical comparison was done with two-tailed unpaired t-tests with correction for multiple comparisons.

Different markers can be used to identify T_{reg} cells with different functions. One of these subsets is characterised by the expression of ICOS and CD103, which have high suppressive potency [158]. In the thymus of *Utx*$^{TEC-/-}$ *Jmjd3*$^{TEC-/-}$ mice, there was an increase in recirculating $ICOS^+$ $CD103^+$ T_{reg} cells, which may reflect the cells' preferential homing to the thymic microenvironment of *Utx*$^{TEC-/-}$ *Jmjd3*$^{TEC-/-}$ mice (see Chapter 3.7.5). Whether the $ICOS^+$ $CD103^+$ T_{reg} cells are expanded in lymph nodes and spleen was next determined using flow cytometry. The frequency of T_{reg} cells and that of their $ICOS^+$ $CD103^+$ subpopulation was comparable for WT and *Utx*$^{TEC-/-}$ *Jmjd3*$^{TEC-/-}$ mice (Fig. 3.43- 3.44), suggesting that the observed increase of thymic $ICOS^+$ $CD103^+$ T_{reg} cells reflects a mechanism intrinsic to the thymus and does not represent a "spill over" of these cells from the periphery. One explanation for this result may therefore be that $ICOS^+$ $CD103^+$ T_{reg} cells are preferentially attracted to recirculate to the thymus or, alternatively, expand locally within the thymic microenvironment of *Utx*$^{TEC-/-}$ *Jmjd3*$^{TEC-/-}$ mice.

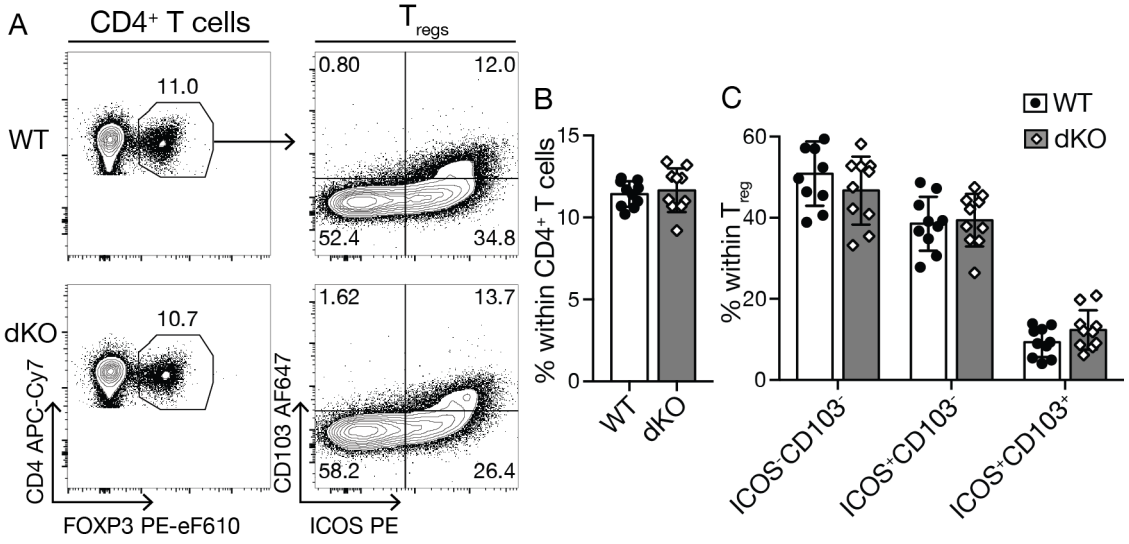

Figure 3.44: Normal frequency and phenotype of T_{reg} cells in the spleen of *Utx*$^{TEC-/-}$ *Jmjd3*$^{TEC-/-}$ mice. (A) Representative FACS plots show the gating strategy to analyse T_{reg} cells (FOXP3$^+$) within CD4$^+$ T cells in the spleen. T_{reg} cells are further assessed for ICOS and CD103 expression. **(B)** Bar graph shows frequencies of T_{reg} cells within total CD4$^+$ T cells. **(C)** Bar graph shows frequencies of ICOS$^-$CD103$^-$, ICOS$^+$CD103$^-$ and ICOS$^+$CD103$^+$ T_{reg} subsets within total T_{reg} cells. Bar graphs represent 3 independent experiments with female mice 4-5 weeks of age; WT (*Utx*$^{fl/fl}$ *Jmjd3*$^{fl/fl}$): n=10; dKO (*Utx*$^{TEC-/-}$ *Jmjd3*$^{TEC-/-}$): n=10. Statistical comparison was done with two-tailed unpaired t-tests with correction for multiple comparisons.

3.8.4 Unchanged frequency of anergic CD4$^+$ T cells in *Utx*$^{TEC-/-}$ *Jmjd3*$^{TEC-/-}$

Several mechanisms operative in the periphery assure that the escape of autoreactive T cells from the thymus does not cause autoimmunity. One of these mechanisms concerns the induction of a state of non-responsiveness of T cells which has been designated anergy [174]. Anergy is established upon TCR-mediated cell activation in the absence of co-stimulatory signals. Anergic CD4$^+$ T cells can be identified by their expression of folate receptor 4 (FR4) and the co-stimulatory molecule CD73 on the cells' surface [175]. A small number of anergic CD4$^+$ T cells can be detected in healthy individuals [176]. An increased escape of autoreactive T cells from the thymus due to changed negative selection may thus be mirrored by a change in the frequency of anergic T cells. A change in the frequency of anergic cells could be anticipated for *Utx*$^{TEC-/-}$ *Jmjd3*$^{TEC-/-}$ mice, as the expression of a number of TRA was increased in mTEC^{hi}, possibly contributing to a better efficiency in negative selection. However, it remained to be tested whether under these circumstances a decrease in the frequency of anergic cells could be detected. Conventional

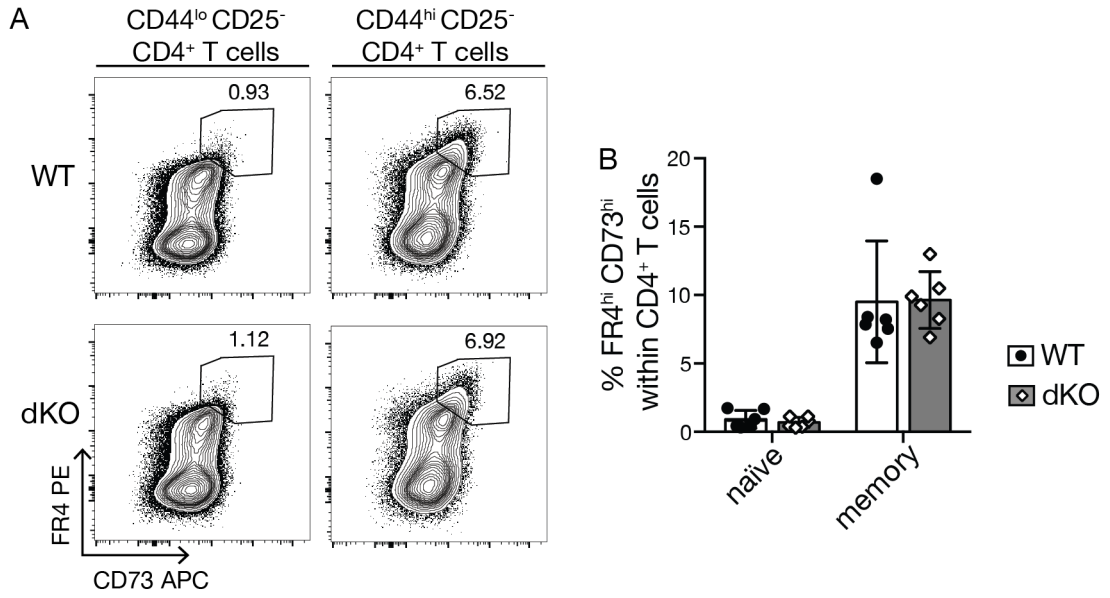

Figure 3.45: The frequency of anergic CD4$^+$ T cells are unchanged in lymph nodes in *Utx$^{TEC-/-}$ Jmjd3$^{TEC-/-}$* mice. (A) Representative FACS plots show the gating strategy to assess anergic cells (FR4$^+$ CD73$^+$) in lymph nodes. Anergic cells were determined in conventional naïve (CD25$^-$ CD44^{lo}) and memory (CD25$^-$ CD44^{hi}) CD4$^+$ T cells. **(B)** Bar graph shows frequencies of anergic cells within naïve and memory CD4$^+$ T cells. Bar graphs represent 2 independent experiments with female mice 4-5 weeks of age; WT (*Utx$^{fl/fl}$ Jmjd3$^{fl/fl}$*): n=6; dKO (*Utx$^{TEC-/-}$ Jmjd3$^{TEC-/-}$*): n=6. Statistical comparison was done with two-tailed unpaired t-tests with correction for multiple comparisons.

memory CD4$^+$ T cells (CD25$^-$ CD44^{hi}) isolated from lymph nodes were analysed for their CD73 and FR4 expression, using conventional naïve CD4$^+$ T cells (CD25$^-$ CD44^{lo}) as a negative control (Fig. 3.45A). The frequency of anergic CD4$^+$ T cells was unchanged in the *Utx$^{TEC-/-}$ Jmjd3$^{TEC-/-}$* mice when compared to WT mice (Fig. 3.45B), suggesting negative selection not to be compromised in *Utx$^{TEC-/-}$ Jmjd3$^{TEC-/-}$* mice in a way that requires input from peripheral tolerance mechanisms.

3.8.5 Brief summary of peripheral T cells in *Utx$^{TEC-/-}$ Jmjd3$^{TEC-/-}$* mice

The size and phenotypic composition of the peripheral T cell compartment was largely identical for WT and *Utx$^{TEC-/-}$ Jmjd3$^{TEC-/-}$* mice. A notable exception was the increased frequency of CD8$^+$ T cells with a central memory phenotype in *Utx$^{TEC-/-}$ Jmjd3$^{TEC-/-}$* mice. A possible explanation for this finding could be a reduction in CD8$^+$ T cell output followed by homeostatic proliferation and an accumulation of CD8$^+$ central memory

T cells and would correlate with a reduction in the frequency of SPCD8 thymocytes. Experimental evidence using several methodological approaches including the assessment of $CD8^+$ RTE and TREC measurement could not support this hypothesis. It remains unknown why there is an expansion of $CD8^+$ central memory T cells. Moreover, the frequency of peripheral anergic $CD4^+$ T cells and T_{reg} cells remained unchanged in $Utx^{TEC-/-}$ $Jmjd3^{TEC-/-}$ mice despite the observed changes in thymocyte negative selection in these animals. Finally, the peripheral frequency of $ICOS^+$ $CD103^+$ T_{reg} cells was undisturbed in $Utx^{TEC-/-}$ $Jmjd3^{TEC-/-}$ mice, indicating that the increased frequency of this cell type is a local phenomenon in the thymus.

3.9 Summary of the $Utx^{TEC-/-}$ $Jmjd3^{TEC-/-}$ mouse model

The results detailed in this chapter demonstrated subtle changes in cTEC and mTEC differentiation and maturation in $Utx^{TEC-/-}$ $Jmjd3^{TEC-/-}$ mice, suggesting a definitive role of these histone demethylases in TEC biology. The increased frequency of $AIRE^+$ $mTEC^{hi}$ might either be due to decreased cell death in this population, or a consequence of the higher proliferation in $mTEC^{lo}$ combined with an accelerated maturation from $mTEC^{lo}$ to $mTEC^{hi}$. A third option might be a block in $AIRE^+$ $mTEC^{hi}$ progressing to the post AIRE $mTEC^{lo}$ stage, which results in an accumulation at the $mTEC^{hi}$ stage. While gene expression changes between WT and UTX/JMJD3-deficient $mTEC^{hi}$ were of small amplitude and affected a limited number of genes, there was a large skew towards AIRE-enhanced genes in the upregulated genes in UTX and JMJD3 deficiency.

Anti-H3K27me3 ChIP-Seq data from WT $mTEC^{hi}$ show that the upregulated genes distinguish themselves from other genes – namely downregulated genes and genes that are not differentially expressed – by higher levels of H3K27me3 in their promoters. The combination of the anti-H3K27me3 ChIP-Seq dataset with $mTEC^{hi}$ single cell RNA-Seq data further revealed a positive correlation of H3K27me3 signal in the promoter with higher expression levels of the gene within a single cell albeit at a lower expression frequency.

I have further demonstrated the feasibility of H3K27me3 ChIP on 10 000 mTEC^{hi} using *Drosophila* chromatin to normalise the data. While the ChIP-Seq results are still pending, this method is able to pick up an H3K27me3 increase at the *Slc13a2* gene with ChIP-qPCR in the UTX- and JMJD3-deficient mTEC^{hi}, demonstrating an increase in H3K27me3 that is correlated with an increase in gene transcription as a consequence of UTX and JMJD3 deficiency.

cTEC lacking UTX and JMJD3 are able to instruct normal thymocyte progression through the early DN stages and mediate a normal positive selection. However, *Utx$^{TEC-/-}$ Jmjd3$^{TEC-/-}$* mice have a mild reduction in TCRβ^{hi} cells in the thymus, affecting both the CD8 and the CD4 lineage, with the former being affected in their late maturation stages before thymic egress. The ability of the UTX- and JMJD3-deficient TEC to impose negative selection is altered: Cortical negative and early medullary selection is decreased, while late medullary negative selection is increased.

In the periphery, CD8$^+$ T cells are skewed towards a central memory phenotype. A possible explanation is that the reduced frequency in the late maturation stages of SPCD8 thymocytes leads to a lower thymic output of CD8$^+$ T cells, which needs to be compensated with homeostatic proliferation in the periphery. However, I was unable to detect any differences in thymic output by measuring RTE and TREC.

3.10 Discussion

Several epigenetic mechanisms including specific histone modifications have been linked to the phenomenon of PGE [50, 69, 177] and their relevance is further reflected in the observation that AIRE directly recognizes unmethylated H3K4, a repressive histone mark typically found in the promoter region of silenced gene loci [68]. Moreover, ChIP analyses of mTEC^{hi} reveal a reduction of active histone marks and an increase of repressive marks such as H3K27me3 and H3K9me3 in the promoter region of AIRE-dependent genes [50]. Irrespective of the correlative association of AIRE-regulated PGE and H3K27me3 marks at the genes' promoter, it has remained untested whether

this post-translational modification is of functional importance for PGE in general and AIRE-mediated transcription in particular.

The molecular mechanism by which H3K27me3 mediates gene silencing is still poorly understood, but is most likely mediated by regulatory molecules that interact with H3K27me3 and by sterically preventing other molecules to bind to the chromatin [97]. However, H3K27me3-mediated gene repression can be alleviated by the ubiquitously expressed H3K27me3 demethylases UTX and JMJD3 and the Y-chromosome encoded UTY.

To date, the role of UTX and JMJD3 in TEC biology has not been explored, whereas their role in thymocytes has been studied, where UTX and JMJD3 are important for initiating part of the gene transcription programme necessary for terminal thymocyte differentiation by demethylating H3K27me3 in gene promoters relevant for thymic egress [108]. A similar role of UTX and JMJD3 in cell differentiation has also been claimed for other cell types of the immune system including type 2 macrophages and iNKT cells [131, 178]. A constitutive absence of UTX leads to severe defects in the development of the mesoderm germ layer resulting in the death of embryos at E10-11 [130, 133]. While most tissues and organs develop normally in mice with a constitutive loss of JMJD3, the mice die at birth due to respiratory failure secondary to a deficient development of the respiratory centre [129].

Generating a mouse model with a TEC-specific loss of UTX and JMJD3 expression created a unique tool to study the functional importance of these enzymes in creating a differential H3K27me3 landscape in TEC that might impact on PGE. This chapter reports on the results of phenotypic and functional analysis obtained from mice that have a TEC-specific deficiency of both enzymes. Manna et al. demonstrated that there is a partial redundancy of UTX and JMJD3's catalytic activity in H3K27me3 demethylation [108]. Chapter 4 will complement these studies, as experiments are presented that focus on the TEC-targeted deficiency of each enzyme alone.

3.10.1 The role of UTX and JMJD3 in TEC development and maturation

The combined deficiency in UTX and JMJD3 expression in TEC does not affect the cellularity or the architectural organisation of the thymus. This finding is surprising as the loss of the enzymes' catalytic function was engineered to take place early in the thymus organogenesis coincident with the initiation of *Foxn1* expression at E11.25 [14, 17]. A lineage differentiation into cTEC and mTEC is possible and the maturational programme from mTEC^{lo} to AIRE expressing mTEC^{hi} can progress as expected despite an absence in UTX and JMJD3 expression. Nevertheless, closer examination revealed that the frequency of individual TEC subpopulations and the kinetics of the mTEC maturation appears to be altered with a lower frequency of mTEC^{lo} and a higher relative representation of mTEC^{hi}, a result possibly explained by an accelerated maturational progression to the mature phenotype. This obvious lack of striking changes in TEC cellularity, differentiation and special organisation argues against a central role of UTX and JMJD3 demethylating H3K27me3 marks in promoters of genes relevant for these aspects of TEC biology. This contention is mirrored in the gene expression profile of the double mutant mTEC^{hi}. For example, the expression of genes relevant for NFκB signalling which are essential for mTEC^{hi} differentiation is normal. Not all developmentally induced promoters are dependent on the catalytic activity of UTX or JMJD3. Alternative mechanisms that remove H3K27me3 marks have been proposed and include the dilution of H3K27me3 through cell division, nucleosome repositioning and potentially other enzymes with H3K27me3 demethylase activity [108, 179, 180].

The frequency of cTEC on the other hand is mildly reduced in the $Utx^{TEC-/-}$ $Jmjd3^{TEC-/-}$ mice, possibly identifying genes relevant for normal cTEC cellularity that depend on the ability to demethylate H3K27me3 in specific promoters. Future experiments will therefore need to probe the differential expression of genes relevant for cTEC lineage proliferation and for survival.

Another observation to be followed up with future experiments is that the expression of *Cytokeratin10* (*Krt10*) and *Involucrin*, two markers of post-AIRE mTEC, are reduced

in UTX/JMJD3-deficient mTEC^{hi}. As the population of so-called post-AIRE mTEC represent a post-mitotic group of cells, it is conceivable that adopting this differentiation stage may require active H3K27me3 demethylation [136].

3.10.2 The role of UTX and JMJD3 for AIRE-regulated PGE

Initially, I had put forward three hypotheses regarding the roles of UTX and JMJD3 in PGE: A) The expression of promiscuously expressed genes requires reprogramming of the chromatin state in the promoter regions changing from a repressive to a permissive landscape in order to initiate gene transcription. In this scenario, UTX and JMJD3 are essential for the demethylation of H3K27me3. B) H3K27me3 marks are directly recognised by the molecular machinery that initiates PGE. Consequently, demethylation of H3K27me3 by UTX and JMJD3 will prevent PGE with the enzymes acting as negative regulators. C) Neither H3K27me3 marks in promoter regions nor UTX and JMJD3 are of essential importance for PGE. Alternatively and/or additionally to these different options, UTX and JMJD3 may impact on gene expression via demethylase-independent functions that can, but need not necessarily, influence the expression of genes involved in PGE.

The differential gene expression analysis using RNA-Seq data from mTEC^{hi} revealed that genes that are upregulated in UTX/JMJD3-deficient samples have a strong enrichment of genes that fall within the AIRE-enhanced category. This result gives particular weight to the notion that H3K27me3 is important for AIRE-regulated TRA expression, and UTX and JMJD3 are negatively regulating this form of PGE.

The promoters of genes identified to be upregulated in the UTX- and JMJD3-deficient mTEC^{hi} are typically marked by high levels of H3K27me3 modifications. In the event that the role of UTX and JMJD3 is indeed related to their demethylase function, I expect to detect even higher levels of H3K27me3 at the corresponding promoter sites in double mutant mTEC^{hi}. In other words, both demethylases may, under wild type conditions, demethylate the promoters of these genes and thus participate in fine tuning and limiting AIRE-regulated gene expression. Limiting PGE is thought to be important, as high levels

of tissue-specific genes could have adverse effects on the cellular integrity of TEC themselves or possibly the entire organism in the context of secreted factors, such as insulin [67, 181].

However, without genome-wide anti-H3K27me3 ChIP-Seq datasets comparing WT and JMJD3/UTX-deficient mTEC^{hi}, a firm conclusion cannot be drawn regarding the demethylase-dependent roles of UTX and JMJD3.

The changes in gene expression uncovered by the RNA-Seq analysis of mTEC^{hi} lacking UTX and JMJD3 expression were confined to a limited number of genes, which is in keeping with previously published studies that demonstrated UTX- and JMJD3-mediated H3K27me3 demethylation only affects a small number of promoters in the order of <1 % [108]. A key difference regarding the impact of a loss of UTX and JMJD3 catalytic activity in thymocytes is that the majority of differentially expressed genes were downregulated in these cells [108]. In contrast the number of upregulated and downregulated genes in UTX- and JMJD3-deficient mTEC^{hi} was approximately 4.5 % of protein coding genes and was balanced. This can be understood to reflect the fundamentally different nature of PGE and its transcriptional regulation where a replacement of a repressive mark is correlated to this unique transcriptional mechanism.

3.10.3 H3K27me3 and PGE

The causal relationship that can be drawn between H3K27me3 changes and PGE are at present limited, as ChIP-Seq data from the *Utx*$^{TEC-/-}$ *Jmjd3*$^{TEC-/-}$ mTEC^{hi} are not available. However, in support of a causative link, one of the TRA (*Slc13a2*) with increased expression in the UTX/JMJD3-deficient mTEC^{hi} displayed increased H3K27me3 marks in the promoter region. Further strength is added to the argument by the finding that the promoter regions of genes upregulated in the double mutant mTEC^{hi} have increased H3K27me3 marks, which sets them apart from loci whose transcription is either unchanged or downregulated.

Handel et al. have recently demonstrated that the chromatin landscape is similar for immature and mature mTEC. This includes the chromatin landscape of AIRE-regulated

genes and suggests that the chromatin landscape of mTEC^{hi} is established early in TEC differentiation. However, some differences in the H3K27me3 landscape were detected between mTEC^{hi} and mTEC^{lo}, as H3K27me3 peaks in mTEC^{lo} have an enrichment in known PRC2 targets, which is not present in mTEC^{hi}. This argues H3K27me3 remodelling occurs during mTEC maturation.

It remains unanswered whether bulk H3K27me3 ChIP-Seq analysis is informative here for gaining a better understanding of the process controlling PGE. Genes encoding TRA are characteristically expressed at very low frequencies, which may preclude the detection of those chromatin landscapes in mTEC^{hi} that actually do express the specific gene of interest, given the dilution at a population level analysis. There have been major advances in reducing the cell number required for ChIP-Seq experiments, with experiments successfully performed even at single cell resolution [182]. However, ChIP-Seq methods that require only low to single cell input are not firmly established and will provide only very low sequence coverage per cell. For the analysis of TEC in the context of deciphering the mechanism controlling PGE, it will likely be more informative to correlate chromatin landscape to specific TRA expression using limited cell numbers as input. This can be achieved by employing tissue-restricted genes whose product is expressed on the cell surface, thus allowing their identification by flow cytometry. Sorting these TEC for ChIP analysis will be a sensible approach to obtain a relatively uniform cell population. A comparable approach has been successfully used for ATAC-Seq analyses, revealing higher chromatin accessibility for genes within the same co-expression pattern as the TRA chosen for cell sorting [51].

3.10.4 Demethylase-independent functions of UTX and JMJD3 in the context of PGE

The function of UTX and JMJD3 does not exclusively rely on the enzymes' demethylase activity, but appears to also involve their role in chromatin remodelling complexes displacing nucleosomes and initiating gene transcription [126, 183, 184]. Both UTX and JMJD3 interact with BRG1, which has recently been found to have a crucial role in

initiating AIRE-regulated PGE [107]. However, since the absence of UTX and JMJD3 increase AIRE-enhanced gene expression, while the absence of BRG1 abrogates AIRE-regulated transcription, a synergistic role of UTX/JMJD3 and BRG1 in TEC is unlikely.

3.10.5 Conclusion

This chapter demonstrated that the absence of UTX and JMJD3 expression in TEC is compatible with the formation of a largely normal thymus able to support normal thymopoiesis. However, my data showed that these two enzymes influence PGE as negative regulators of the expression of AIRE-enhanced genes. Specifically, UTX and JMJD3 appear to play an important role in fine-tuning TRA expression. Hence the presented results add weight to the hypothesis that AIRE-regulated gene expression is controlled by epigenetic regulation. The exact mechanism by which UTX and JMJD3 act on PGE remains to be elucidated.

4

The individual roles of UTX, JMJD3 and UTY in TEC biology

Contents

4.1 Introduction . . . 106
4.2 *Utx*$^{TEC-/-}$, *Jmjd3*$^{TEC-/-}$ and male *Utx*$^{TEC-/Y}$ *Jmjd3*$^{TEC-/-}$ mice 107
4.3 UTX- or JMJD3-single-deficient and male double-deficient TEC . . . 109
4.4 Transcriptional changes in mTEC^{hi} from *Utx*$^{TEC-/-}$, *Jmjd3*$^{TEC-/-}$ and male *Utx*$^{TEC-/Y}$ *Jmjd3*$^{TEC-/-}$ mice . . . 113
4.5 Thymocytes in *Utx*$^{TEC-/-}$, *Jmjd3*$^{TEC-/-}$ and male *Utx*$^{TEC-/Y}$ *Jmjd3*$^{TEC-/-}$ mice . . . 116
4.6 Peripheral T cells in *Utx*$^{TEC-/-}$, *Jmjd3*$^{TEC-/-}$ and male *Utx*$^{TEC-/Y}$ *Jmjd3*$^{TEC-/-}$ mice . . . 120
4.7 Summary . . . 120
4.8 Discussion . . . 122

4.1 Introduction

The H3K27me3 demethylases UTX and JMJD3 play a crucial role in development and differentiation with some studies demonstrating overlapping [108, 178], but most reports highlighting distinct roles [129–131]. Under certain conditions, such as cell reprogramming and cancer, UTX and JMJD3 have even been reported to effect opposite roles [132, 185,

186]. As mentioned in the last chapter, UTX has a paralog, UTY, encoded on the Y chromosome, which has two point substitutions within the JmjC catalytic domain at position 947 and 955 [133], that greatly diminish, but do not completely abrogate, its demethylase activity when compared to UTX and JMJD3 [125]. Nonetheless UTY is able to attenuate some of the consequences of a UTX deficiency [108, 132, 133].

This chapter investigates the individual roles of UTX and JMJD3 in TEC development and function. Specifically, the question addressed was whether the findings in mice with a UTX/JMJD3 double deficiency in TEC could be attributed to a single loss of these enzymes. To this end, mice that have a TEC-specific single deficiency of either UTX or JMJD3 were generated. In addition, I tested whether the presence of UTY in male mice would compensate for a UTX and JMJD3 deficiency in TEC.

4.2 $Utx^{TEC-/-}$, $Jmjd3^{TEC-/-}$ and male $Utx^{TEC-/Y}$ $Jmjd3^{TEC-/-}$ mice

It is possible that common mechanisms regulate the expression of UTX and JMJD3 [187]. It would therefore be conceivable that in the absence of one of these demethylases, the expression of the other could be upregulated as compensation. To test this contention, cTEC, $mTEC^{lo}$ and $mTEC^{hi}$ were isolated from $Utx^{TEC-/-}$ and $Jmjd3^{TEC-/-}$ mice to quantify the expression of *Utx* and *Jmjd3* using qPCR. In the JMJD3-deficient TEC, the *Utx* expression level remained comparable to that of WT TEC (Fig. 4.1A). Conversely, the *Jmjd3* expression level was unchanged in UTX-deficient TEC (Fig. 4.1B). As expected, there was a loss of *Utx* expression in the TEC isolated from the $Utx^{TEC-/-}$ mice and a loss of *Jmjd3* expression in the $Jmjd3^{TEC-/-}$ TEC.

Previously published studies have found a downregulation of *Uty* as a consequence of a loss of UTX expression in ES cells [130, 188]. Thus, I assessed *Uty* expression in cTEC, $mTEC^{lo}$ and $mTEC^{hi}$ isolated from male $Utx^{TEC-/Y}$ $Jmjd3^{TEC-/-}$ mice. Although *Utx* and *Jmjd3* expression was lost in these animals, *Uty* expression remained unaffected.

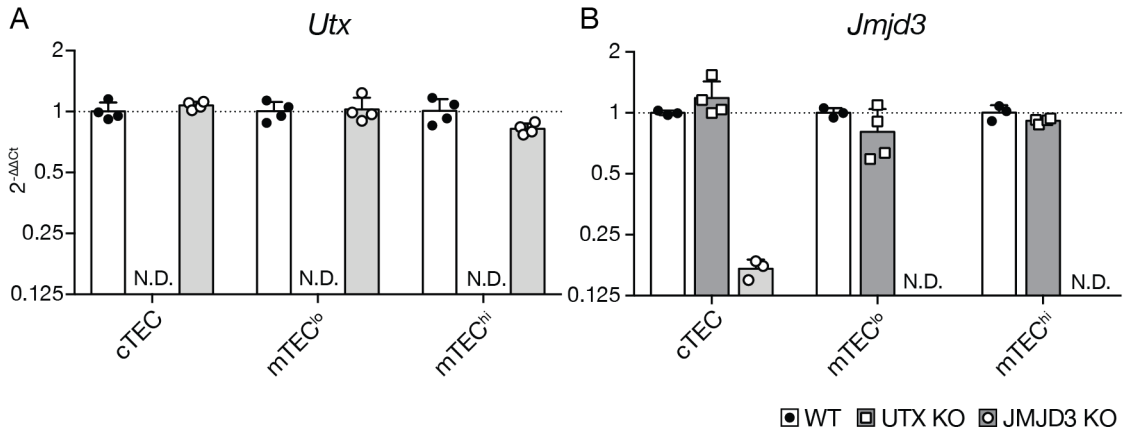

Figure 4.1: Single deficiency in UTX and JMJD3 does not lead to a change in the expression levels of the other demethylase. Extracted RNA from sorted TEC subpopulations (cTEC, mTEC^{lo} and mTEC^{hi}) was used for qPCR for detecting the expression of *Utx* **(A)** and *Jmjd3* **(B)**. Data was analysed using the $2^{-\Delta\Delta Ct}$ method with normalising to *Gapdh* expression and setting expression in WT to 1. The experiment was done with female mice at 4-5 weeks of age. Each data point represents an individual mouse. WT: $Utx^{wt/wt}$ $Jmjd3^{fl/fl}$ or $Utx^{fl/fl}$ $Jmjd3^{wt/wt}$; UTX KO: $Utx^{TEC-/-}$; JMJD3 KO: $Jmjd3^{TEC-/-}$. Statistical analysis was done with multiple t-tests with correction for multiple comparisons.

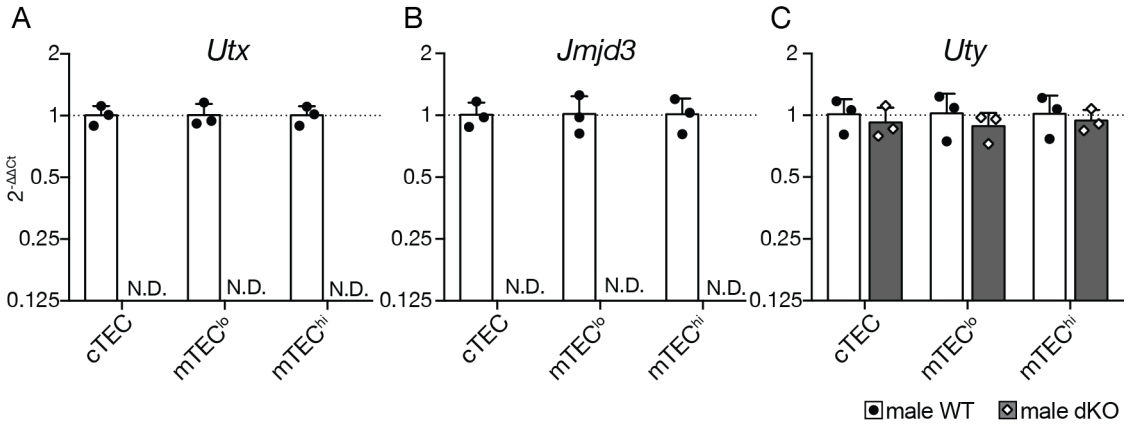

Figure 4.2: *Uty* expression was unchanged in male TEC with a double deficiency in UTX and JMJD3. Extracted RNA from sorted TEC subpopulations (cTEC, mTEC^{lo} and mTEC^{hi}) was used for qPCR for detecting the expression of *Utx* **(A)**, *Jmjd3* **(B)** and *Uty* **(C)**. Data was analysed using the $2^{-\Delta\Delta Ct}$ method with normalising to *Gapdh* expression and setting expression in WT to 1. The experiment was done with male mice at 4-5 weeks of age. Each data point represents an individual mouse. WT: $Utx^{fl/Y}$ $Jmjd3^{fl/fl}$; male dKO: $Utx^{TEC-/Y}$ $Jmjd3^{TEC-/-}$. Statistical analysis was done with multiple t-tests with correction for multiple comparisons.

In conclusion, the single deficiency of either UTX or JMJD3 did not affect the expression of the other demethylase. Moreover, *Uty* expression was also unchanged in the absence of UTX and JMJD3 in male $Utx^{TEC-/Y}$ $Jmjd3^{TEC-/-}$ mice. Hence, there are no compensatory mechanisms in place in TEC to correct for a loss of either or both of the enzymes. It is of note that this analysis did not assess compensation mechanisms that might be in place at a protein level, such as increased translation or reduced degradation, and do not affect mRNA abundance.

4.3 UTX- or JMJD3-single-deficient and male double-deficient TEC

Female $Utx^{TEC-/-}$ $Jmjd3^{TEC-/-}$ mice demonstrated a reduction in cTEC frequency and an increase in $AIRE^{+}$ $mTEC^{hi}$. To attribute these findings to the catalytic function of one or both of these enzymes, female mice with a single deficiency of the demethylases or male animals deficient in both were further investigated for their TEC compartment.

Female $Utx^{TEC-/-}$ mice had a reduced frequency of cTEC (8.90 % ± 2.00 vs 11.98 % ± 1.64) and a corresponding increase in mTEC, similar to the changes seen in $Utx^{TEC-/-}$ $Jmjd3^{TEC-/-}$ animals (see Chapter 3.4). In contrast, $Jmjd3^{TEC-/-}$ mice had an unimpaired TEC differentiation into cortical and medullary cells (Fig. 4.3B). However, individual stages of mTEC maturation were affected in both single mutant strains (Fig. 4.3C). The mice with a single UTX deficiency in TEC displayed – similar to the double-deficient animals – a reduced $mTEC^{lo}$ frequency but an increased relative cellularity of $AIRE^{+}$ $mTEC^{hi}$. The frequency of $AIRE^{-}$ $mTEC^{hi}$ remained unchanged compared to WT mice. Mice with a single JMJD3 deficiency in TEC displayed an increase in both $AIRE^{-}$ and $AIRE^{+}$ $mTEC^{hi}$ and an even larger reduction in the frequency of $mTEC^{lo}$.

An increase in $mTEC^{hi}$ expressing CD86 was observed in the $Utx^{TEC-/-}$, but not in the $Jmjd3^{TEC-/-}$ mice (22.68 % ± 1.67 (WT) vs 31.73 % ± 2.18 (UTX KO) vs 21.24 % ± 2.67 (JMJD3 KO)) (Fig. 4.3D). Comparing this result with the female double-deficient

TEC (see Fig. 3.8D and Table 4.1) identifies the phenotypic change in these mice as entirely caused by the lack of UTX.

The mean AIRE expression per cell was assessed by measuring the gMFI of AIRE protein by FACS in the AIRE^{+} CD86^{-} and CD86^{+} mTEC^{hi} subpopulations. *Utx$^{TEC-/-}$ Jmjd3$^{TEC-/-}$* mice had a reduced mean AIRE expression of 15 % and 11 % respectively in these two populations (compare Fig. 3.8E, Table 4.1). In the TEC from *Utx$^{TEC-/-}$* mice, reduction of AIRE expression levels was statistically significant albeit mild (-7.0 % ± 4.0) in CD86^{-} AIRE^{+} mTEC^{hi}, whereas its expression remained unchanged in CD86^{+} AIRE^{+} mTEC^{hi} (Fig. 4.3E). In contrast, a single JMJD3 deficiency in these cells did not change AIRE protein levels (Fig. 4.3E). Taken together this identifies that both UTX and JMJD3 have to be absent for the full phenotype of the double deficiency to manifest.

TEC isolated from male *Utx$^{TEC-/Y}$ Jmjd3$^{TEC-/-}$* mice had normal cTEC and mTEC frequencies when compared to male WT animals (Fig. 4.4B), demonstrating that the presence of UTY can rescue the phenotype in the female double mutant mice. Additional phenotypic differences between male and female double mutant mice included the frequency of CD86^{+} cells (Fig. 4.4D) and AIRE protein expression levels (Fig. 4.4E), which were unchanged in male *Utx$^{TEC-/Y}$ Jmjd3$^{TEC-/-}$* mice. This corroborated a compensatory role of UTY in TEC differentiation.

Nevertheless, mTEC maturation was affected in male *Utx$^{TEC-/Y}$ Jmjd3$^{TEC-/-}$* compared to WT mice, in that the frequency of mTEC^{lo} was reduced (42.28 % ± 3.80 vs 49.7 % ± 3.53), and that of AIRE^{+} mTEC^{hi} increased (35.96 % ± 3.23 vs 29.50 % ± 1.7) (Fig. 4.4C). As this phenotype is comparable to that of female double mutant animals, this suggests that not all phenotypic changes can be rescued by the presence of UTY.

Taken together, the comparative analysis of this extensive TEC phenotyping revealed a complex pattern of how the single or combined absence of UTX and JMJD3 expression in female and male (i.e. UTY positive) TEC affected their differentiation. Table 4.1 provides an overview of these results.

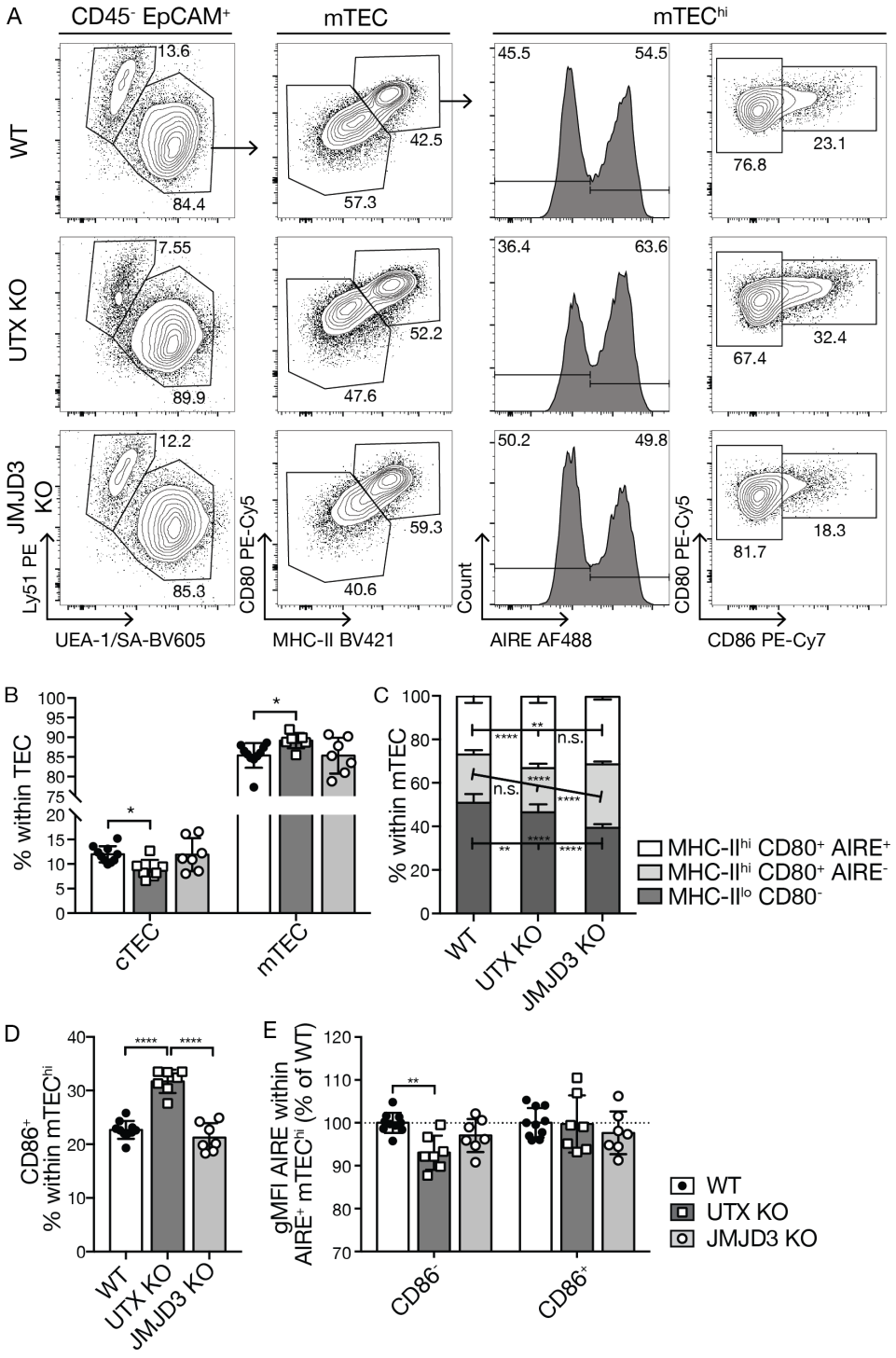

Figure 4.3: TEC differentiation and maturation are altered in mice with a TEC-targeted single deficiency of UTX and JMJD3 expression. **(A)** Representative FACS plots show the gating strategy for TEC assessment. **(B)** Bar graph depicts relative frequencies of cTEC and mTEC. **(C)** Bar graph shows mTEC maturation according to MHC-II, CD80 and AIRE expression. **(D)** Bar graph shows relative frequency of $CD86^+$ cells within $mTEC^{hi}$. **(E)** Bar graph shows expression level of AIRE within $AIRE^+$ $CD86^-$ $mTEC^{hi}$ and $AIRE^+$ $CD86^+$ $mTEC^{hi}$ as measured by gMFI normalised to the respective WT population. Data shown in graphs are pooled from four independent experiments using female mice at 4-5 weeks of age. WT ($Utx^{wt/wt}$ $Jmjd3^{fl/fl}$, $Utx^{fl/fl}$ $Jmjd3^{wt/wt}$): n=10; UTX KO ($Utx^{TEC\text{-}/\text{-}}$): n=7; JMJD3 KO ($Jmjd3^{TEC\text{-}/\text{-}}$): n=7. Statistical comparison was done with one- or two-way ANOVA. *p<0.05, **p<0.01, ***p<0.001, ****p<0.0001.

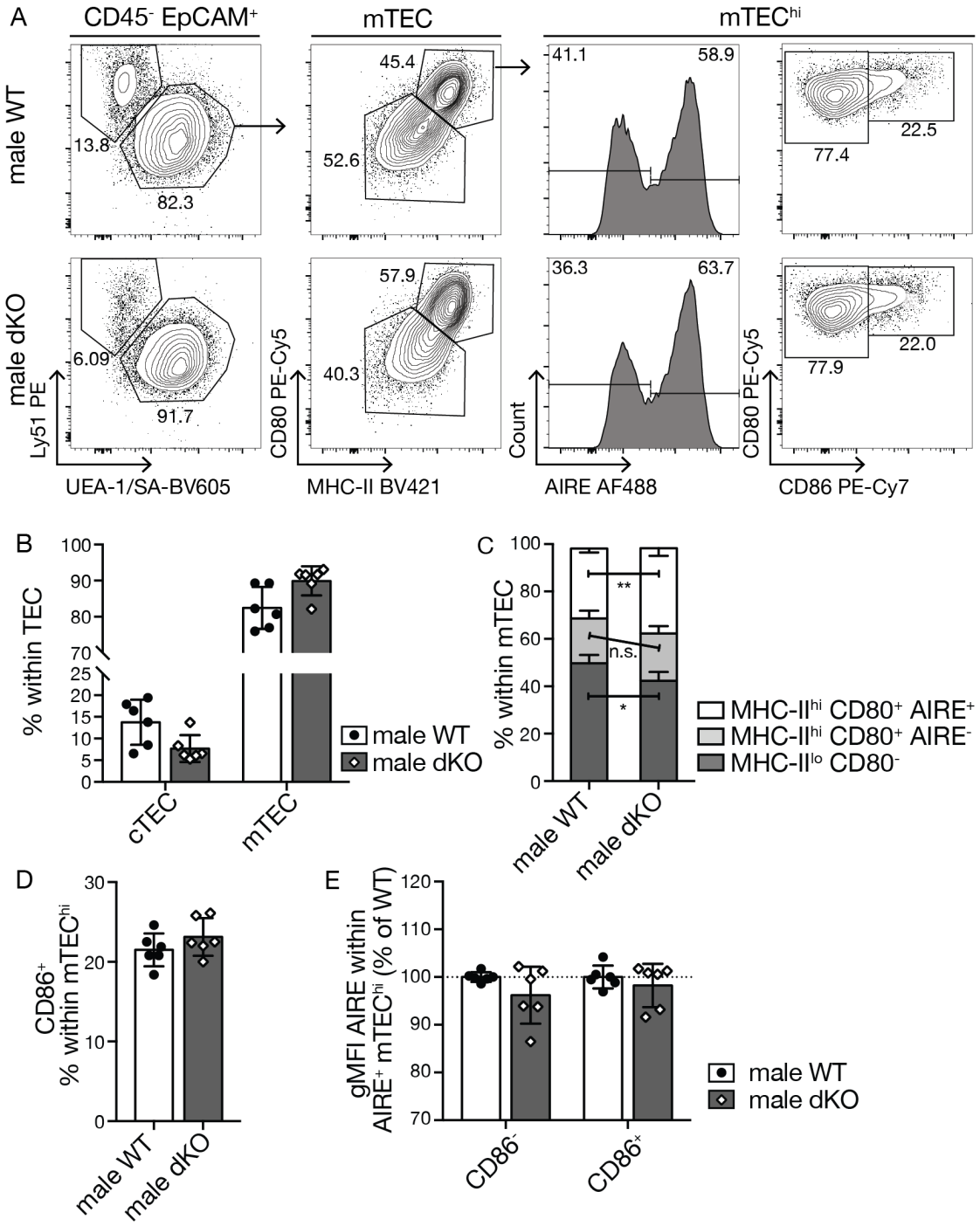

Figure 4.4: TEC differentiation and maturation are altered in male mice with a TEC-targeted deficiency of UTX and JMJD3 expression. (A) Representative FACS plots show the gating strategy for TEC assessment. **(B)** Bar graph depicts relative frequencies of cTEC and mTEC. **(C)** Bar graph shows mTEC maturation according to MHC-II, CD80 and AIRE expression. **(D)** Bar graph shows relative frequency of $CD86^+$ cells within $mTEC^{hi}$. **(E)** Bar graph shows expression level of AIRE within $AIRE^+$ $CD86^-$ $mTEC^{hi}$ and $AIRE^+$ $CD86^+$ $mTEC^{hi}$ as measured by gMFI normalised to the respective WT population. Data shown in graphs are pooled from two independent experiments using male mice at 4-5 weeks of age (WT ($Utx^{fl/Y}$ $Jmjd3^{fl/fl}$) n=6; dKO ($Utx^{TEC\text{-}/Y}$ $Jmjd3^{TEC\text{-}/\text{-}}$) n=6). Statistical analysis was done with two-tailed unpaired t-tests.

This analysis established, for example, that the increased frequency of AIRE^{+} mTEC^{hi} was noted in all mutant mice tested. It is, however, of note that the differences in comparison to WT mice were the most prominent in female double mutant mice suggesting a partial compensation by UTX, JMJD3 and UTY.

		dKO female	**UTX KO**	**JMJD3 KO**	**dKO male**
cTEC	Frequeny within TEC	-27 %	-26 %	-	-
mTEClo	Frequency within mTEC	-21 %	-9 %	-23 %	-15 %
AIRE^{-} mTEC^{hi}	Frequency within mTEC	-	-	+32 %	-
AIRE^{+} mTEC^{hi}	Frequency within mTEC	+34%	+23 %	+16 %	+22 %
CD86^{+}	Frequency within mTEC^{hi}	+45 %	+40 %	-	-
Average AIRE expression	gMFI within AIRE^{+} CD86^{-}	-15 %	-7 %	-	-
	gMFI within AIRE^{+} CD86^{+}	-11 %	-	-	-

Table 4.1: Summary of TEC phenotypic changes as a result of an absence of UTX, JMJD3 and/or UTY expression. Differences were calculated as % change to WT. A dash marks features that were not significantly changed. dKO: *Utx$^{TEC-/-}$ Jmjd3$^{TEC-/-}$*; UTX KO: *Utx$^{TEC-/-}$*; JMJD3 KO: *Jmjd3$^{TEC-/-}$*.

4.4 Transcriptional changes in mTEC^{hi} from *Utx$^{TEC-/-}$*, *Jmjd3$^{TEC-/-}$* and male *Utx$^{TEC-/Y}$ Jmjd3$^{TEC-/-}$* mice

The RNA-Seq analysis of mTEC^{hi} from female WT and *Utx$^{TEC-/-}$ Jmjd3$^{TEC-/-}$* mice revealed an increase in the expression of AIRE-enhanced genes (compare Chapter 3.5). To extend this result to an analysis of which of these two demethylases was responsible for this change in gene expression, mTEC^{hi} from female single mutant mice and male double mutant mice were isolated and analysed by qPCR for a selection of genes which were differentially expressed in the RNA-Seq dataset (genes with the highest p-values were chosen). This included *Slc13a2*, *Cxcl13*, *Orm2*, *Gast*, *Ngfr* and *Mymk* that were upregulated, and *Ebi3*, *Gbn3*, *Soat2* and *Krt10* that were downregulated in the UTX- and JMJD3-deficient mTEC^{hi}. *Aire* expression was also determined as an internal control.

The expression profiles of these selected genes as established by RNA-Seq was confirmed using qPCR in mTEC^{hi} sorted from female WT and *Utx$^{TEC-/-}$ Jmjd3$^{TEC-/-}$* mice. mTEC^{hi} with a single deficiency in UTX expression displayed the same gene expression changes

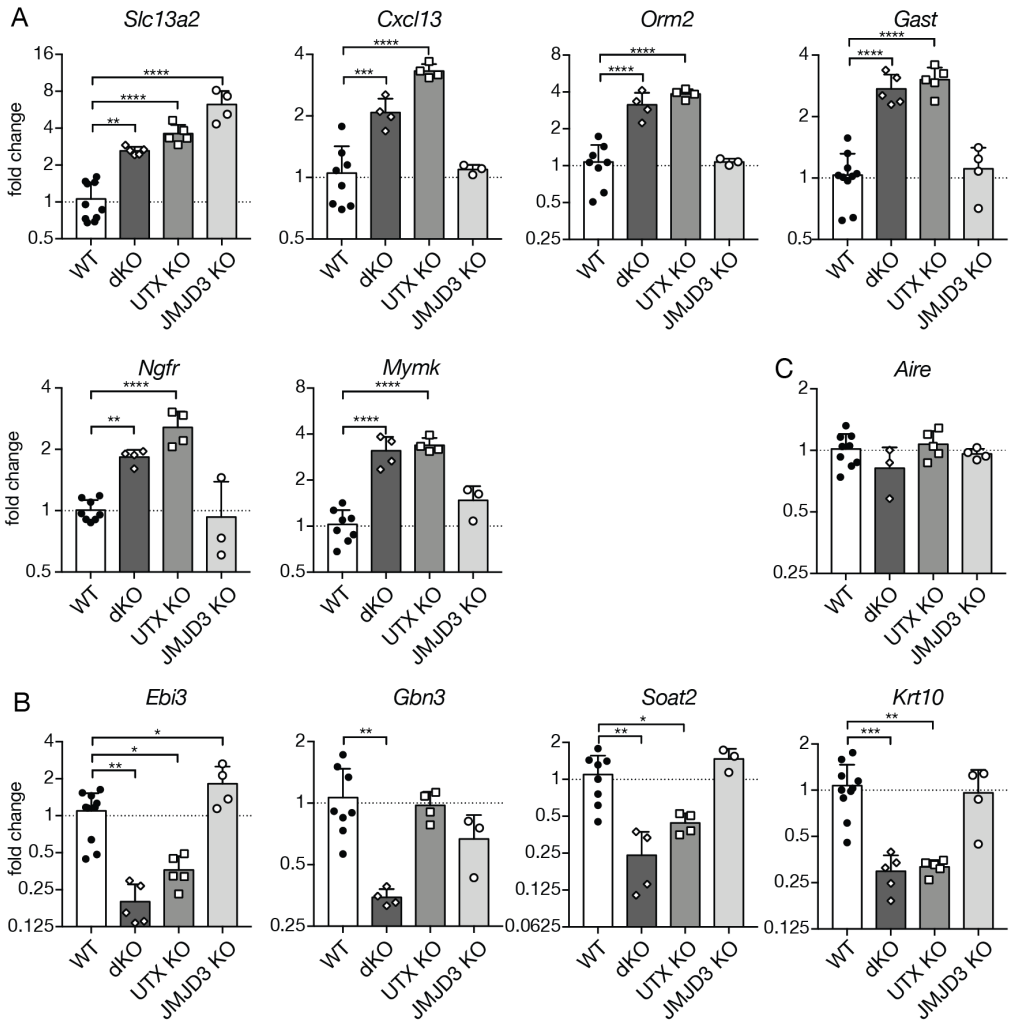

D

	Slc13a2	Cxcl13	Orm2	Gast	Ngfr	Mymk	Ebi3	Gbn3	Soat2	Krt10	Aire
WT vs. dKO	**	***	****	****	**	****	**	**	**	***	ns
WT vs. UTX KO	****	****	****	****	****	****	*	ns	*	**	ns
WT vs. JMJD3 KO	****	ns	ns	ns	ns	ns	*	ns	ns	ns	ns
dKO vs. UTX KO	ns	***	ns	ns	*	ns	ns	*	ns	ns	ns
dKO vs. JMJD3 KO	****	**	***	****	**	***	****	ns	**	*	ns
UTX KO vs. JMJD3 KO	***	****	****	****	****	***	***	ns	**	*	ns

Figure 4.5: Differential gene expression assessed by qPCR in mTEC^{hi} from female *Utx$^{TEC-/-}$ Jmjd3$^{TEC-/-}$*, *Utx$^{TEC-/-}$* and *Jmjd3$^{TEC-/-}$* mice. Extracted RNA from sorted mTEC^{hi} was used for qPCR. Data was analysed using the $2^{-\Delta\Delta Ct}$ method normalising it to *Gapdh* expression and setting expression in WT mTEC^{hi} to 1. The experiment was done with female mice at 4-5 weeks of age. Each data point represents an individual mouse. WT: *Utx$^{wt/wt}$ Jmjd3$^{fl/fl}$*, *Utx$^{fl/fl}$ Jmjd3$^{wt/wt}$* or *Utx$^{fl/fl}$ Jmjd3$^{fl/fl}$*; dKO: *Utx$^{TEC-/-}$ Jmjd3$^{TEC-/-}$*; UTX KO: *Utx$^{TEC-/-}$*; JMJD3 KO: *Jmjd3$^{TEC-/-}$*. Statistical testing was done with a One-way ANOVA. In the bar graph only statistical differences to the WT sample are depicted. A summary for all the statistical comparisons can be found in (D). **(A)** The expression of six genes (*Slc13a2*, *Cxcl13*, *Orm2*, *Gast*, *Ngfr*, *Mymk*) that were upregulated in dKO RNA-Seq analysis was tested in the sorted mTEC^{hi} samples. **(B)** The expression of four genes (*Ebi3*, *Gbn3*, *Soat2*, *Krt10*) that were downregulated in dKO RNA-Seq analysis was tested in the sorted mTEC^{hi} samples. **(C)** The expression of *Aire* was tested in the sorted mTEC^{hi}. **(D)** Summary of statistical analysis. *p<0.05; **p<0.01, ***p<0.001, ****p<0.0001.

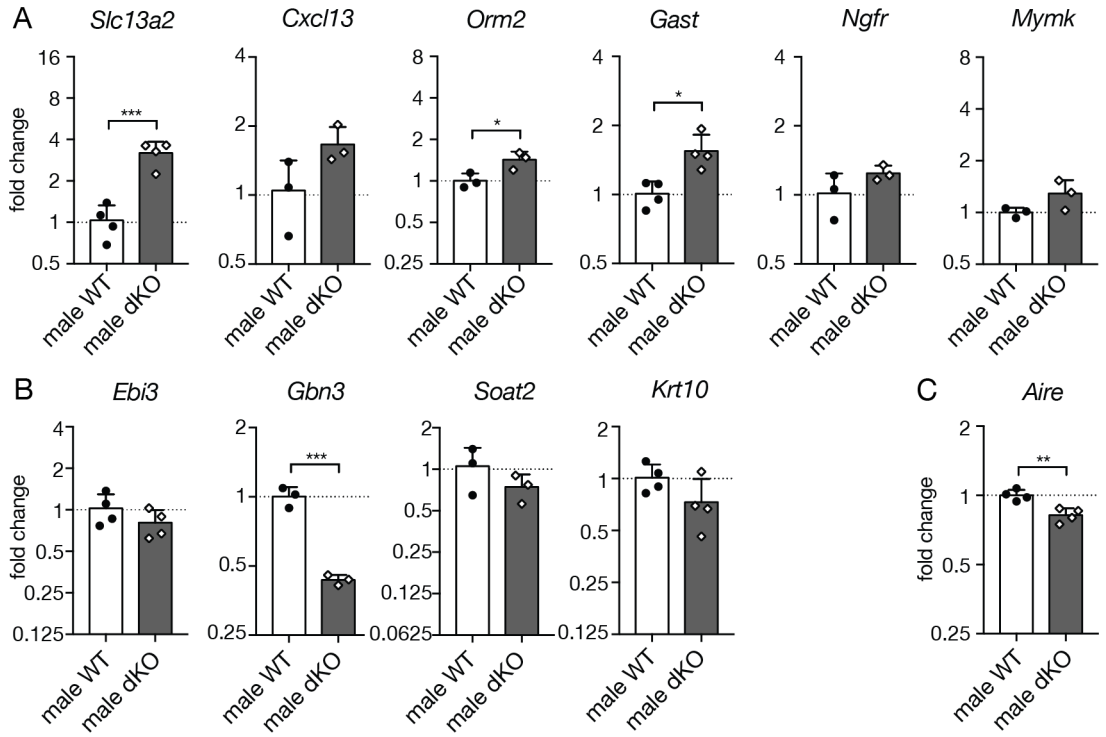

Figure 4.6: Differential gene expression assessed by qPCR in mTEC^{hi} from male *Utx$^{TEC-/Y}$ Jmjd3$^{TEC-/-}$* mice. Extracted RNA from sorted mTEC^{hi} was used for qPCR. Data was analysed using the $2^{-\Delta\Delta Ct}$ method normalising it to *Gapdh* expression and setting expression in WT mTEC^{hi} to 1. The experiment was done with male mice at 4-5 weeks of age. Each data point represents an individual mouse. WT: *Utx$^{fl/Y}$ Jmjd3$^{fl/fl}$*; dKO: *Utx$^{TEC-/Y}$ Jmjd3$^{TEC-/-}$*. Statistical testing was done with an unpaired two-tailed t-test. **(A)** The expression of six genes (*Slc13a2*, *Cxcl13*, *Orm2*, *Gast*, *Ngfr*, *Mymk*) that were upregulated in dKO RNA-Seq analysis was tested in the sorted mTEC^{hi} samples. **(B)** The expression of four genes (*Ebi3*, *Gbn3*, *Soat2*, *Krt10*) that were downregulated in dKO RNA-Seq analysis was tested in the sorted mTEC^{hi} samples. **(C)** The expression of *Aire* was tested in the sorted mTEC^{hi}. *p<0.05; **p<0.01, ***p<0.005.

with the exception of *Gbn3* (Fig. 4.5A-B). Of note, *Cxcl13* and *Ngfr* were expressed at a higher level in mTEC^{hi} from *Utx$^{TEC-/-}$* mice when compared to corresponding cells from double mutant mice (*Cxcl13* fold change to WT: 2.07 (dKO) vs 3.31 (UTX KO); *Ngfr*: 1.83 (dKO) vs 2.56 (UTX KO)). In contrast, mTEC^{hi} sorted from *Jmjd3$^{TEC-/-}$* mice only had significant gene expression changes for *Slc13a2* and *Ebi3* (Fig. 4.5A-B), the latter showing paradoxically an increase in expression when compared to the pattern observed in *Utx$^{TEC-/-}$ Jmjd3$^{TEC-/-}$* animals.

To test the ability of UTY to compensate for the loss of UTX and JMJD3 expression in TEC, the expression of the same genes was assessed in mTEC^{hi} from male *Utx$^{TEC-/Y}$ Jmjd3$^{TEC-/-}$* mice. Significant gene expression changes were only observed in four out

of the ten genes tested in the male double KO mTEC^{hi}. Changes in *Slc13a2* and *Gnb3* transcript were comparable in fold change with that of female double mutant mTEC^{hi}. In contrast, the changes in transcripts of *Orm2* and *Gast* were more moderate (Fig. 4.6A-B).

In summary, the UTX deficiency was largely responsible for the gene expression changes observed in the female double-deficient mTEC^{hi}. Given the compromised catalytic activity, it was surprising to note that UTY expression in male mice rescued most of the gene expression changes detected in a female double-deficient mTEC^{hi}. The results of this set of gene expression analyses are summarised in Table 4.2.

Gene	Mean expression	log2 Fold Change	Tissue specificity	AIRE Dependency	dKO female	UTX KO	JMJD3 KO	dKO male
Slc13a2	3103.58	1.89	TRA	Independent	Up	Up	Up	Up
Cxcl13	7242.44	1.43	Other	Enhanced	Up	Up	-	-
Orm2	738.72	1.69	TRA	Enhanced	Up	Up	-	Up
Gast	1164.25	1.27	TRA	Enhanced	Up	Up	-	Up
Ngfr	3233.82	1.09	Other	Independent	Up	Up	-	-
Mymk	1679.25	1.15	TRA	Enhanced	Up	Up	-	-
Ebi3	1162.96	-1.57	Other	Independent	Down	Down	Up	-
Gnb3	1890.36	-1.14	TRA	Independent	Down	-	-	Down
Soat2	1225.81	-1.14	TRA	Independent	Down	Down	-	-
Krt10	1152.46	-1.42	TRA	Enhanced	Down	Down	-	-

Table 4.2: Summary of gene expression changes. Mean expression and log2 fold change are from the mTEC^{hi} RNA-Seq dataset comparing female WT and dKO. A dash marks genes that were not significantly changed. dKO: $Utx^{TEC-/-}$ $Jmjd3^{TEC-/-}$; UTX KO: $Utx^{TEC-/-}$; JMJD3 KO: $Jmjd3^{TEC-/-}$.

4.5 Thymocytes in $Utx^{TEC-/-}$, $Jmjd3^{TEC-/-}$ and male $Utx^{TEC-/Y}$ $Jmjd3^{TEC-/-}$ mice

Thymocyte development was affected in female $Utx^{TEC-/-}$ $Jmjd3^{TEC-/-}$ mice (see Chapter 3.7). The frequencies of TCRβ^{hi} thymocytes and cortical and early medullary negative selection were reduced in these mice, whereas late medullary negative selection of SPCD4 thymocytes was increased. Because the TEC compartment of female $Utx^{TEC-/-}$ and $Jmjd3^{TEC-/-}$ mice was differently composed when compared to double-deficient mice, thymocyte development and selection were analysed in the single mutant animals. These

studies were extended to the analysis of $Utx^{TEC-/Y}$ $Jmjd3^{TEC-/-}$ male mice, as these mice displayed an attenuated TEC phenotype due to the presence of UTY.

4.5.1 Changes in negative selection are mainly caused by UTX deficiency

An assessment of negative selection revealed that cortical negative selection of DP thymocytes (wave 1a) was decreased in $Utx^{TEC-/-}$ mice to the same extent as in double mutant mice (0.36 % ± 0.04 (WT) vs 0.26 % ± 0.05 (dKO) vs 0.28 % ± 0.03 (UTX KO)). In contrast, the TEC-specific absence of JMJD3 expression did not affect this stage of thymocyte negative selection (Fig. 4.7C). Wave 1a negative selection was reduced in male $Utx^{TEC-/Y}$ $Jmjd3^{TEC-/-}$ mice (0.40 % ± 0.03 vs 0.34% ± 0.05) (Fig. 4.7C), whereas the subsequent two selection waves, i.e. wave 1b and wave 2a, were unaffected in both female single and male double mutant mice (Figs. 4.7F and 4.8C). However, wave 2b, was increased in $Utx^{TEC-/-}$ mice, comparable to female $Utx^{TEC-/-}$ $Jmjd3^{TEC-/-}$ mice (WT: 9.15 % ± 0.86; dKO: 11.2 % ± 1.05; UTX KO: 12.18 % ± 1.79), but remained unaffected in $Jmjd3^{TEC-/-}$ and male $Utx^{TEC-/Y}$ $Jmjd3^{TEC-/-}$ animals (Fig. 4.8F).

Taken together, UTX-single-deficient TEC had the same impact on wave 1a and wave 2b as the double-deficient TEC. However, the loss of this demethylase did not impact wave 1b and 2a thymocyte negative selection. In other words, only in instances where both enzymes were missing in TEC were wave 1b and wave 2a of negative selection affected. Of note, TEC with a single JMJD3 deficiency had a normal capacity to effect thymocyte negative selection. The expression of UTY in $Utx^{TEC-/Y}$ $Jmjd3^{TEC-/-}$ mice could not rescue the compromised wave 1a selection, but compensated the combined loss of UTX and JMJD3 of all other negative selection check points during thymocyte maturation.

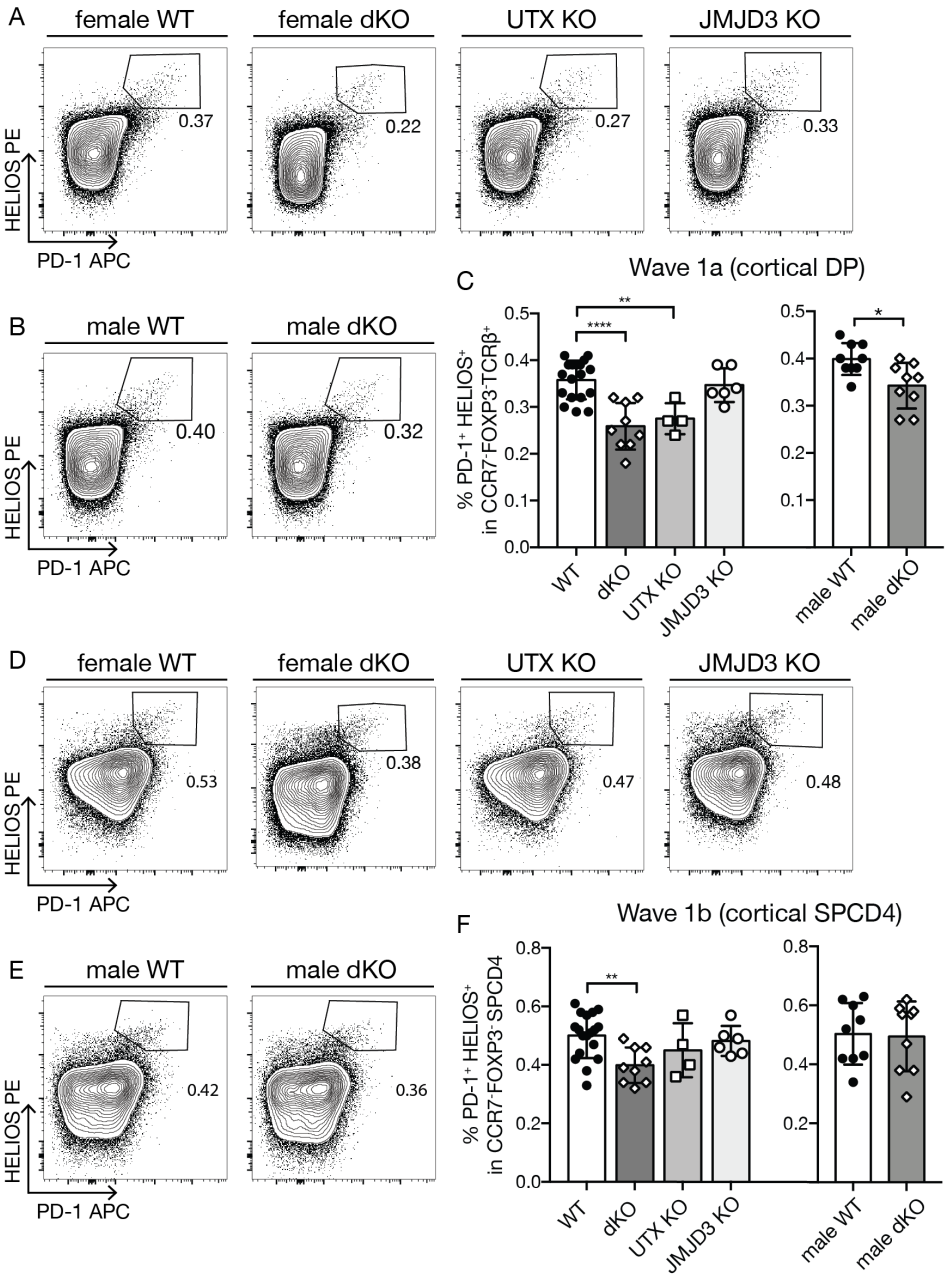

Figure 4.7: Cortical negative selection in $Utx^{TEC-/-}$, $Jmjd3^{TEC-/-}$ and male $Utx^{TEC-/Y}$ $Jmjd3^{TEC-/-}$ mice. (A-B) Representative FACS plots show the gating of wave 1a (PD-1$^+$ HELIOS$^+$) within CCR7$^-$FOXP3$^-$TCRβ$^-$ thymocytes in female WT, dKO, UTX KO, JMJD3 KO (A) and male WT and dKO (B). **(C)** Bar graph shows frequency of wave 1a (PD-1$^+$ HELIOS$^+$) within CCR7$^-$FOXP3$^-$TCRβ$^-$ thymocytes. **(D-E)** Representative FACS plots show the gating of wave 1b (PD-1$^+$ HELIOS$^+$) within CCR7$^-$FOXP3$^-$ SPCD4 thymocytes in female WT, dKO, UTX KO, JMJD3 KO (D) and male WT and dKO (E). **(F)** Bar graph shows frequency of SPCD4 wave 1b (PD-1$^+$ HELIOS$^+$) within CCR7$^-$FOXP3$^-$ SPCD4. The bar graphs of female WT, dKO, UTX KO and JMJD3 KO are pooled from six independent experiments with female mice 4-5 weeks of age; WT ($Utx^{wt/wt}$ $Jmjd3^{fl/fl}$, $Utx^{fl/fl}$ $Jmjd3^{wt/wt}$ or $Utx^{fl/fl}$ $Jmjd3^{fl/fl}$): n=19; dKO ($Utx^{TEC-/-}$ $Jmjd3^{TEC-/-}$): n=10; UTX KO ($Utx^{TEC-/-}$): n=4; JMJD3 KO ($Jmjd3^{TEC-/-}$): n=6. Statistical comparison was done with a one-way ANOVA, only comparisons to WT are depicted. **p<0.01, ***p<0.001, ****p<0.0001. The bar graphs of male WT and dKO are pooled from three independent experiments with male mice 4-5 weeks of age; male WT ($Utx^{fl/Y}$ $Jmjd3^{fl/fl}$): n=10; male dKO ($Utx^{TEC-/Y}$ $Jmjd3^{TEC-/-}$): n=10. Statistical comparison was done with two-tailed unpaired t-tests. *p<0.05.

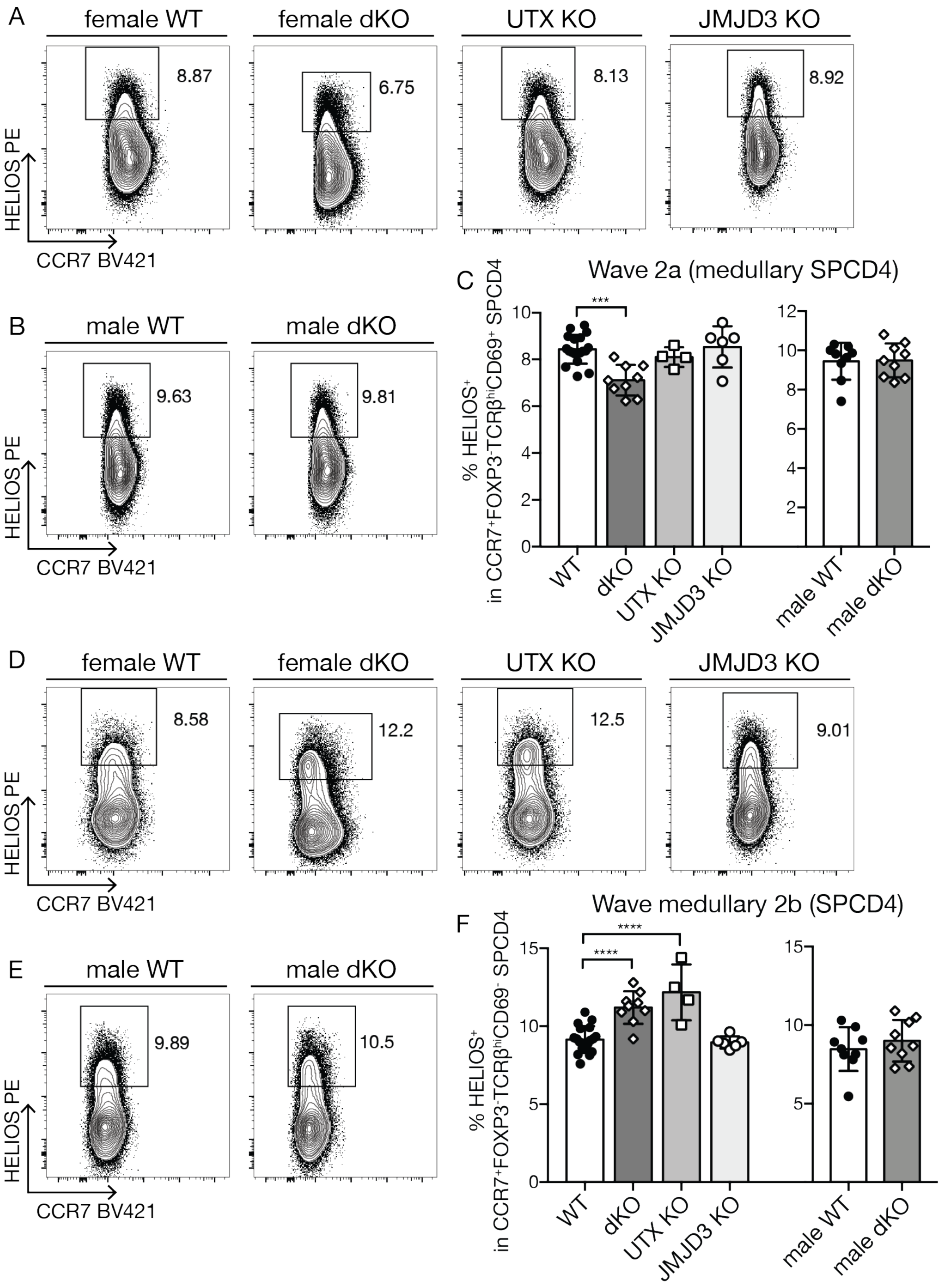

Figure 4.8: Medullary negative selection in *Utx*$^{TEC-/-}$, *Jmjd3*$^{TEC-/-}$ and male *Utx*$^{TEC-/Y}$ *Jmjd3*$^{TEC-/-}$ mice. (A-B) Representative FACS plots show the gating of wave 2a (HELIOS$^+$) within CCR7$^+$FOXP3$^-$TCRβ^{hi}CD69$^+$ SPCD4 thymocytes in female WT, dKO, UTX KO, JMJD3 KO (A) and male WT and dKO (B). **(C)** Bar graph shows frequency of SPCD4 wave 2a (HELIOS$^+$) within CCR7$^+$FOXP3$^-$TCRβ^{hi}CD69$^+$ SPCD4. **(D-E)** Representative FACS plots show the gating of wave 2b (HELIOS$^+$) within CCR7$^+$FOXP3$^-$TCRβ^{hi}CD69$^-$ SPCD4 thymocytes in female WT, dKO, UTX KO, JMJD3 KO (D) and male WT and dKO (E). **(F)** Bar graph shows frequency of SPCD4 wave 2b (HELIOS$^+$) within CCR7$^+$FOXP3$^-$TCRβ^{hi}CD69$^-$ SPCD4. The bar graphs of female WT, dKO, UTX KO and JMJD3 KO are pooled from six independent experiments with female mice 4-5 weeks of age; WT (*Utx*$^{wt/wt}$ *Jmjd3*$^{fl/fl}$, *Utx*$^{fl/fl}$ *Jmjd3*$^{wt/wt}$ or *Utx*$^{fl/fl}$ *Jmjd3*$^{fl/fl}$): n=19; dKO (*Utx*$^{TEC-/-}$ *Jmjd3*$^{TEC-/-}$): n=10; UTX KO (*Utx*$^{TEC-/-}$): n=4; JMJD3 KO (*Jmjd3*$^{TEC-/-}$): n=6. Statistical comparison was done with a one-way ANOVA, only comparisons to WT are depicted. **p<0.01, ***p<0.001, ****p<0.0001. The bar graphs of male WT and dKO are pooled from three independent experiments with male mice 4-5 weeks of age; male WT (*Utx*$^{fl/Y}$ *Jmjd3*$^{fl/fl}$): n=10; male dKO (*Utx*$^{TEC-/Y}$ *Jmjd3*$^{TEC-/-}$): n=10. Statistical comparison was done with two-tailed unpaired t-tests. *p<0.05.

4.6 Peripheral T cells in *Utx$^{TEC-/-}$*, *Jmjd3$^{TEC-/-}$* and male *Utx$^{TEC-/Y}$ Jmjd3$^{TEC-/-}$* mice

The loss of UTX and JMJD3 expression in TEC did not impact on the phenotype of peripheral T cells with the notable exception of a higher frequency of CD8$^+$ T cells with a central memory phenotype (see Chapter 3.8). To ascribe this finding to the function of either UTX or JMJD3 in TEC, peripheral T cells of single KO mice were analysed. A higher increase of CD8$^+$ central memory T cells was also present in the *Utx$^{TEC-/-}$* mice, but could not be identified in the *Jmjd3$^{TEC-/-}$* animals (Fig. 4.9A-B). The increased frequency of CD8$^+$ T central memory was comparable to that of female *Utx$^{TEC-/-}$ Jmjd3$^{TEC-/-}$* mice (WT: 28.68 % ± 3.65; dKO: 40.74 % ± 5.51; UTX KO: 45.42 % ± 0.52). I further studied the peripheral T cells in male *Utx$^{TEC-/Y}$ Jmjd3$^{TEC-/-}$* mice where there were no significant changes in naïve and memory phenotypes in CD8$^+$ T cells in comparison to WT.

The phenotypic changes among peripheral CD8$^+$ T cells in female *Utx$^{TEC-/-}$ Jmjd3$^{TEC-/-}$* mice correlated with a loss of UTX expression in TEC, while the absence of JMJD3 did not have an impact on the representation of different CD8$^+$ T cell states. As male double mutant mice had an unchanged peripheral CD8$^+$ T cell compartment, I conclude that the presence of UTY compensates for the loss of UTX expression in TEC.

4.7 Summary

UTX and JMJD3 are important for TEC maturation and thymocyte development, albeit they play different roles (Table 4.3). A single deficiency in either UTX or JMJD3 expression in TEC was not entirely mimicking the phenotype observed in the double mutant mice. The phenotypic features can be broadly divided into three patterns depending on the findings in the mouse models with a single deficiency in either UTX or JMJD3 in TEC.

Firstly, it is sufficient to have either of the two enzymes present in TEC to prevent a perturbation of AIRE protein expression levels in AIRE$^+$ mTEC^{hi} and *Gbn3* expression in mTEC^{hi}, as observed in the *Utx$^{TEC-/-}$ Jmjd3$^{TEC-/-}$* mice.

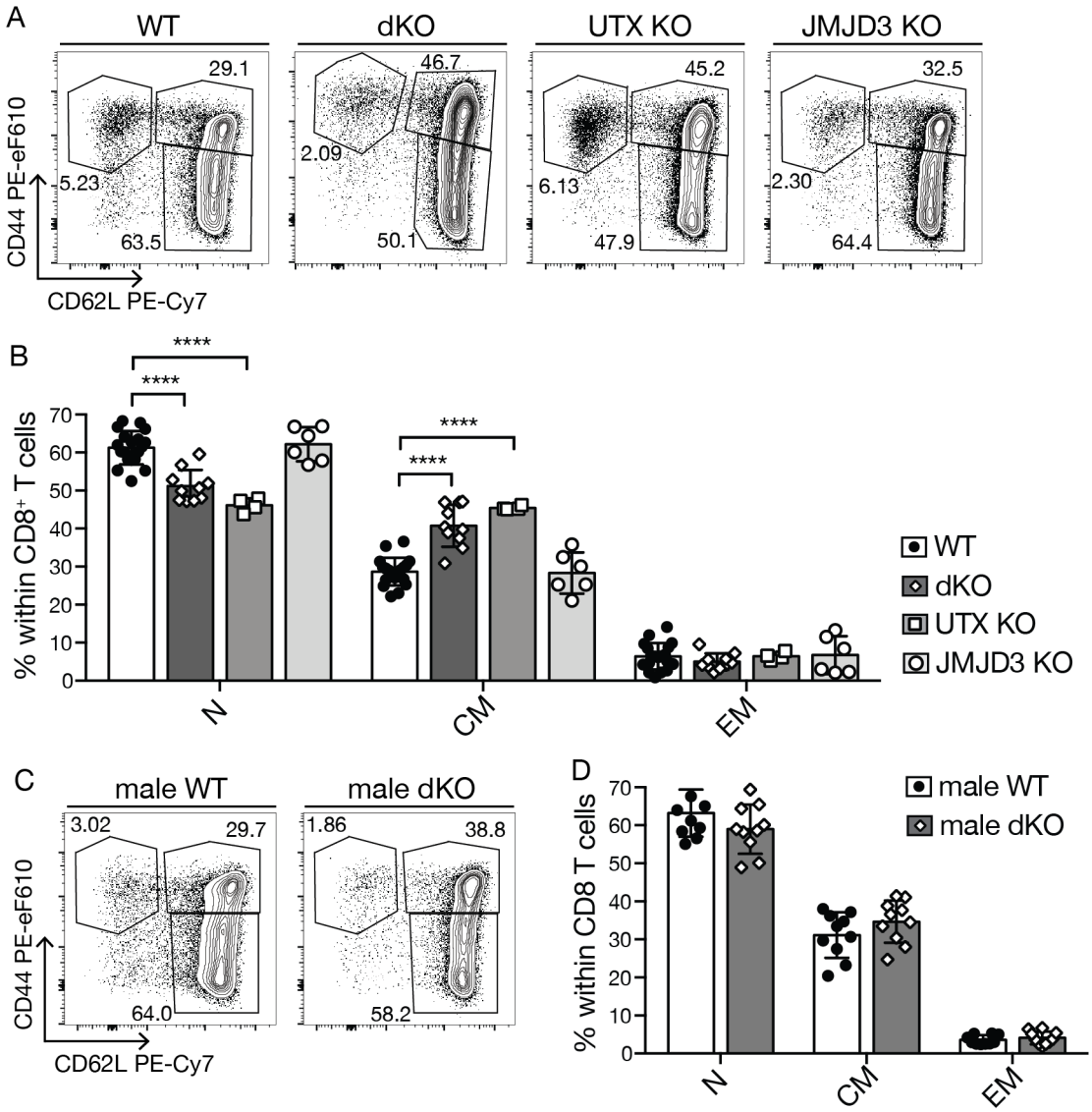

Figure 4.9: CD8$^+$ T cells in the spleen are skewed towards memory phenotype in *Utx$^{TEC-/-}$*, but not in *Jmjd3$^{TEC-/-}$* mice, and can be rescued in male mice. (A) Representative FACS plots show naïve (CD62L$^+$ CD44^{lo}), central memory (CD62L$^+$ CD44^{hi}) and effector memory (CD62L$^-$ CD44^{hi}) cells within splenic CD8$^+$ T cells from female WT, dKO, UTX KO and JMJD3 KO mice. **(B)** Bar graph shows frequencies of naïve (N), central memory (CM) and effector memory (EM) cells within CD8$^+$ T cells. (A-B) Bar graphs are pooled from six independent experiments with female mice 4-5 weeks of age; WT (*Utx$^{wt/wt}$ Jmjd3$^{fl/fl}$*, *Utx$^{fl/fl}$ Jmjd3$^{wt/wt}$* or *Utx$^{fl/fl}$ Jmjd3$^{fl/fl}$*): n=19; dKO (*Utx$^{TEC-/-}$ Jmjd3$^{TEC-/-}$*): n=10; UTX KO (*Utx$^{TEC-/-}$*): n=4; JMJD3 KO (*Jmjd3$^{TEC-/-}$*): n=6. Statistical comparison was done with a two-way ANOVA, only comparisons to WT are depicted. ****p<0.0001. **(C)** Representative FACS plots show naïve (CD62L$^+$ CD44^{lo}), central memory (CD62L$^+$ CD44^{hi}) and effector memory (CD62L$^-$ CD44^{hi}) cells within splenic CD8$^+$ T cells from male WT and dKO mice. **(D)** Bar graph shows frequencies of naïve (N), central memory (CM) and effector memory (EM) cells within CD8$^+$ T cells in male WT and dKO mice. (C-D) Bar graphs are pooled from three independent experiments with male mice 4-5 weeks of age; WT (*Utx$^{fl/Y}$ Jmjd3$^{fl/fl}$*): n=10; dKO (*Utx$^{TEC-/Y}$ Jmjd3$^{TEC-/-}$*): n=10. Statistical comparison was done with two-tailed unpaired t-tests with correction for multiple comparisons.

Secondly, there are phenotypic changes that can only be observed in $Utx^{TEC-/-}$ mice and $Utx^{TEC-/-}$ $Jmjd3^{TEC-/-}$ mice, such as the reduction in cTEC frequency, the increase in $CD86^{+}$ frequency, change in wave 1a and wave 2b of negative selection, the variation in the expression of several selected genes (e.g. *Cxcl13*, *Orm2* and *Soat2*), and the higher frequency of $CD8^{+}$ memory phenotype T cells. None of these findings were observed in the absence of JMJD3, strongly suggesting that these changes are exclusively caused by the loss of UTX.

Thirdly, there were phenotypic changes that manifested themselves in both $Utx^{TEC-/-}$ mice and $Jmjd3^{TEC-/-}$ mice, such as the increased frequency of $AIRE^{+}$ $mTEC^{hi}$ and the increase in expression of *Slc13a2*. Thus, there is no compensation by the other enzyme and both enzymes need to be present in TEC to assure normal function.

Several of the phenotypic changes observed in female $Utx^{TEC-/-}$ $Jmjd3^{TEC-/-}$ mice could be rescued by the presence of UTY in male mice. However, I could not identify an obvious pattern of rescue.

4.8 Discussion

UTX and JMJD3 are essential for development and differentiation of tissues by epigenetically modulating gene expression programmes. In some processes, such as late thymocyte development, the two enzymes have largely overlapping functions and single deficiencies show a milder phenotype than their combined loss [108]. However many studies have also highlighted their individual, tissue-specific roles: During embryogenesis UTX controls mesoderm and ectoderm development and embryos with a loss of UTX die at E10-11 due to heart defects [128, 130]. On the other hand, JMJD3 expression controls the differentiation of neurons and bone formation and JMJD3 KO mice die at birth due to a dysplasia of the neurons controlling respiration [129, 189]. The fact that UTX and JMJD3 control different sets of genes is further underlined by the opposing roles the two enzymes have in cancer, cell reprogramming and the preimplantation embryo [185, 187, 190, 191].

			dKO female	UTX KO	JMJD3 KO	dKO male
TEC	cTEC	Frequency within TEC	Down	Down	-	-
	$mTEC^{lo}$	Frequency within mTEC	Down	Down	Down	Down
	$AIRE^{-}$ $mTEC^{hi}$	Frequency within mTEC	-	-	Up	-
	$AIRE^{+}$ $mTEC^{hi}$	Frequency within mTEC	Up	Up	Up	Up
	$CD86^{+}$	Frequency within $mTEC^{hi}$	Up	Up	-	-
	gMFI AIRE	gMFI within $AIRE^{+}$	Down	-	-	-
	Gene expression $mTEC^{hi}$	*Slc13a2*	Up	Up	Up	Up
		Cxcl13, Ngfr, Mymk	Up	Up	-	-
		Orm2, Gast	Up	Up	-	Up
		Ebi3	Down	Down	Up	-
		Gbn3	Down	-	-	Down
		Soat2, Krt10	Down	Down	-	-
Thymocytes	Negative selection	Wave 1a (DP)	Down	Down	-	Down
		Wave 1b (SPCD4)	Down	-	-	-
		Wave 2a (SPCD4)	Down	-	-	-
		Wave 2b (SPCD4)	Up	Up	-	-
T cells	Central memory cells	Frequency within $CD8^{+}$ T cells	Up	Up	-	-

Table 4.3: Summary of changes caused by a TEC-specific deficiency of UTX and JMJD3. A dash marks features that were not significantly changed. dKO: $Utx^{TEC-/-}$ $Jmjd3^{TEC-/-}$; UTX KO: $Utx^{TEC-/-}$; JMJD3 KO: $Jmjd3^{TEC-/-}$.

This chapter demonstrates that in TEC biology, UTX and JMJD3 have some functional redundancy, however many of the phenotypic and transcriptomic changes observed in the double mutant mouse strain are caused by the deficiency in UTX. This includes the reduced cTEC frequencies and increased CD86 expression in $mTEC^{hi}$ that can be observed in $Utx^{TEC-/-}$ but not in $Jmjd3^{TEC-/-}$ mice. This pattern can also be seen in many of the gene expression changes in $mTEC^{hi}$, which is in keeping with the higher *Utx* than *Jmjd3* expression levels in this cell type. The larger impact of the loss of UTX compared to the loss of JMJD3 in TEC is also reflected in the impact on negative selection and on the increased frequency of memory $CD8^{+}$ T cells in peripheral lymphoid tissues, which cannot be seen in $Jmjd3^{TEC-/-}$ animals.

However, the lack of JMJD3 has an impact on TEC biology. This can be seen best in

the mTEC maturation process from mTEC^{lo} to AIRE^{-} mTEC^{hi} and finally to AIRE^{+} mTEC^{hi}, where different stages are affected by the loss of UTX and JMJD3. While a loss of JMJD3 predominantly causes an increased frequency of AIRE^{-} mTEC^{hi}, a UTX deficiency leads to an increased frequency of AIRE^{+} mTEC^{hi}. The double mutant mice have an altered mTEC maturation that results from a combination of these two phenotypes. Taken together it seems that UTX and JMJD3 are both important for mTEC maturation and each affects different maturational stages.

I was especially interested to see whether there is a relationship between gene expression changes in mTEC^{hi} caused by UTX and/or JMJD3 and their dependency on AIRE. However, the number of genes tested by qPCR is too small to detect a pattern. RNA-Seq of mTEC^{hi} with a single deficiency of UTX and JMJD3 will be needed to establish which gene sets each of these enzymes controls and how they relate to known PGE categories.

In studies of embryonic development, UTX and UTY have been shown to have functional redundancy [130, 133, 192]. Thus, while a homozygous KO of UTX is embryonically lethal for female mice, male animals that have *Uty* on their Y chromosome survive [192]. Nevertheless, male UTX KO mice are born at a reduced frequency and are smaller than their WT counterparts, demonstrating that UTY cannot fully compensate for the lack of UTX. While the contention that UTY can rescue UTX deficiency is also supported by other studies [193, 194], there are biological settings, such as in late thymocyte development, where UTY is not able to compensate for a loss of UTX expression [108].

In this chapter, I compared the phenotypic and transcriptional changes found in female $Utx^{TEC\text{-}/\text{-}}$ $Jmjd3^{TEC\text{-}/\text{-}}$ mice to those in male $Utx^{TEC\text{-}/Y}$ $Jmjd3^{TEC\text{-}/\text{-}}$ mice and demonstrated that UTY is able to rescue some of the changes that were caused by the lack of UTX and JMJD3, while others were unaffected.

Whether or not a perturbation caused by the lack of UTX can be rescued by UTY was frequently used as a proof of concept that UTX's function was demethylase-independent, since UTY was thought to have no demethylase capacity. However, this direct deduction has been questioned by the finding that UTY still has some residual enzymatic

activity [125]. Therefore, while the notion that UTX's function in TEC might be demethylase-independent is supported by the fact that UTY can compensate for many of the consequences of a loss of UTX and JMJD3 in TEC, it nevertheless cannot be concluded with certainty. A definite answer to the question of whether UTX has a demethylase-dependent or -independent role in TEC would be possible by using mice that have a knock-in of an enzyme-dead version of UTX [130]. Moreover, the H3K27me3 landscape comparisons between WT and double mutant TEC, which will be available soon, will be able to provide us with a more accurate answer to this question.

One caveat to keep in mind when attributing any differences between female $Utx^{TEC-/-}$ $Jmjd3^{TEC-/-}$ mice and male $Utx^{TEC-/Y}$ $Jmjd3^{TEC-/-}$ mice to the presence of UTY is that there might also be other gender-specific differences that are responsible for the presumed rescue by UTY. Sex hormones are known to impact thymic biology [195]. Thus, in order to minimize this effect, I did the experiments using sexually immature mice at four to five weeks of age. However, a mouse model with a TEC-specific loss of UTY would be the most reliable control to exclude any gender-specific confounders.

Overall, UTX, JMJD3 and UTY contribute to different aspects of TEC function that cannot be reduced to one single pattern. A deficiency in UTX has a larger impact on TEC biology than a deficiency in JMJD3. However, both enzymes are involved in regulating mTEC maturation. UTY can rescue or attenuate some of the features seen in female double knockout mice, however not all.

5

The role of JARID2 in TEC biology

Contents

5.1 Introduction 126
5.2 Mouse model with a targeted loss of JARID2 expression . . 127
5.3 TEC with a deficiency in JARID2 137
5.4 Thymocyte development in *Jarid2*$^{TEC-/-}$ mice 146
5.5 The peripheral T cell compartment in *Jarid2*$^{TEC-/-}$ mice . . . 164
5.6 Summary 171
5.7 Discussion 174

5.1 Introduction

To elucidate the effect of a reduced and misplaced density of H3K27me3 marks on TEC biology, I opted to further study a TEC-specific perturbation of PRC2 as this complex is crucial for establishing and maintaining H3K27me3 at silenced genes [97]. PRC2 is made up of four core subunits (EZH1/2, EED, SUZ12 and RbAp46/48), and relies on various cofactors such as JARID2, AEBP2 and PCL proteins to perform its function [89]. JARID2 is a cofactor of PRC2 and is thought to play a role in regulating the enzymatic activity of PRC2 and directing the complex to the correct target sites [89, 91]. A loss of JARID2 does not completely abolish H3K27me3 as it is the case in EZH2 and EED

KO, but causes more subtle changes and misplacement of H3K27me3 marks [89]. In addition to its role as a cofactor of PRC2, JARID2 has also been reported to interact with the H3K9me3 methyltransferases GLP/G9a and SETDB1 [196, 197]. H3K9me3 constitutes a further repressive histone mark enriched at transcriptional start sites of genes promiscuously expressed in mTEC [50]. It is therefore interesting to link changes in either histone mark in mTEC to PGE.

Unpublished results from our group demonstrated that a TEC-specific loss of EZH2 and EED protein expression resulted in a perturbation of TEC development and a concurrent drastic reduction of thymus cellularity. Due to this severe defect, it is difficult to study the direct effect of H3K27me3 on PGE. We thus identified JARID2 as a potential candidate to study the correlation of H3K27me3 and TEC function.

5.2 Mouse model with a targeted loss of JARID2 expression

To investigate changes in the H3K27me3 landscape in TEC, I used mice with a TEC-targeted loss of JARID2. To this end, mice with LoxP sites flanking exon 3 were crossed to animals that express Cre recombinase in TEC, i.e. Foxn1-Cre. The Cre-mediated excision of exon 3 results in a frame shift and a premature STOP codon at the beginning of exon 4 giving rise to a truncated protein that lacks the known functional domains of the protein (Fig. 5.1). This conditional knockout strategy has previously been successfully used [196, 198]. This mouse model will be referred to as $Jarid2^{TEC-/-}$.

5.2.1 Genomic excision of exon 3 of *Jarid2*

The efficient excision of exon 3 was tested by PCR on FACS sorted TEC subpopulations (cTEC, $mTEC^{lo}$, $mTEC^{hi}$). $CD45^{+}$ $EpCAM^{-}$ cells and total thymus tissue were used as a negative control. The efficient excision resulting in the desired loss of exon 3 was proven by the detection of a unique amplification product with a specific size (866 bp) in PCR reactions using lysates from $mTEC^{hi}$, $mTEC^{lo}$ and cTECs isolated from

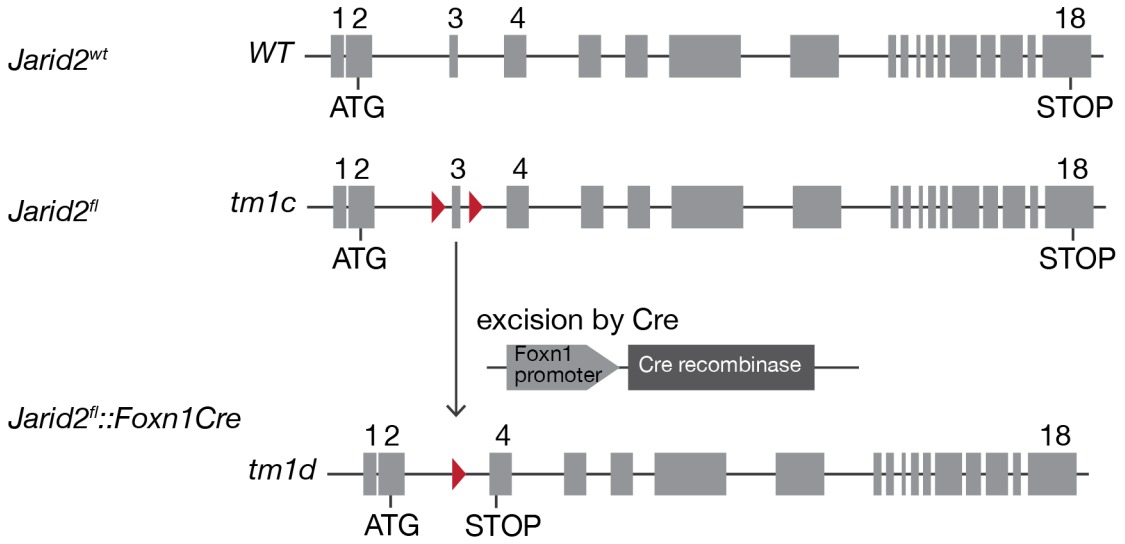

Figure 5.1: Schematic representation of gene construct to generate a TEC-specific JARID2 KO. *LoxP* sites (red) flank exon 3 of *Jarid2*. The presence of the Cre recombinase under the *Foxn1* promoter results in an excision of the third exon of *Jarid2* and a premature STOP codon at the beginning of exon 4 in all *Foxn1* expressing cells.

Jarid2$^{TEC-/-}$ mice. In contrast, the PCR product using lysates from CD45^{+} cells revealed only an unexcised tm1c allele (1762 bp). In total thymus lysates, both bands could be detected which is reflective of the presence of both TEC and thymocytes within the sample (Fig. 5.2). Taken together, these results demonstrate that the excision of exon 3 is efficiently executed in TEC from *Jarid2*$^{TEC-/-}$ mice.

5.2.2 *Jarid2* RNA expression

Jarid2 mRNA expression was assessed in cTEC, mTEC^{lo} and mTEC^{hi} sorted from *Jarid2*$^{TEC-/-}$, *Jarid2*$^{wt/TEC-}$ and *Jarid2*$^{fl/fl}$ mice. Two primer pairs were used to detect *Jarid2* expression: The first one spanning exons 3 and 4 and the second exons 6 and 7. As predicted, the first primer pair did not amplify a product in TEC sorted from *Jarid2*$^{TEC-/-}$ mice proving the absence of mRNA transcripts with the exon 3 of *Jarid2*. In TEC sorted from *Jarid2*$^{wt/TEC-}$ mice, *Jarid2* transcripts containing exon 3 were reduced by half. The second primer pair amplified *Jarid2* at a similar level in TEC isolated from *Jarid2*$^{TEC-/-}$, *Jarid2*$^{wt/TEC-}$ and *Jarid2*$^{fl/fl}$ mice, demonstrating the undisrupted presence of *Jarid2* transcripts without exon 3.

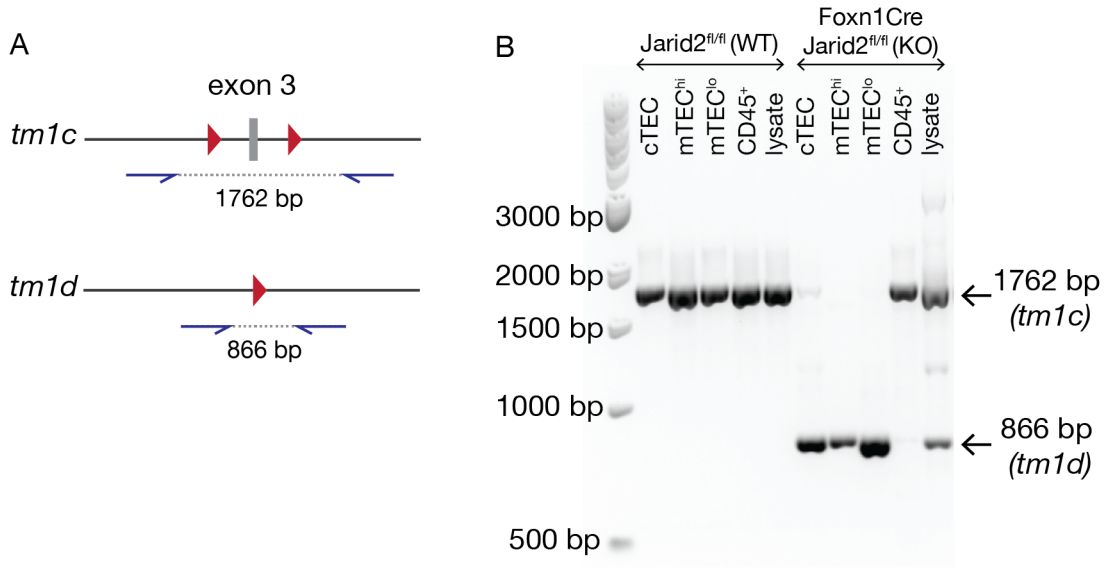

Figure 5.2: Efficient genomic excision in *Jarid2*$^{TEC-/-}$ TEC. (A) Schematic representation of primers around exon 3 used to detect genomic excision. **(B)** Sorted cTEC, mTEC^{hi}, mTEC^{lo} and CD45^{+} EpCAM^{-} cells and samples from whole thymus lysate were used for PCR with the primers illustrated in (A). PCR products were run on a 1.5 % agarose gel. NEB 1kb ladder was run as a reference.

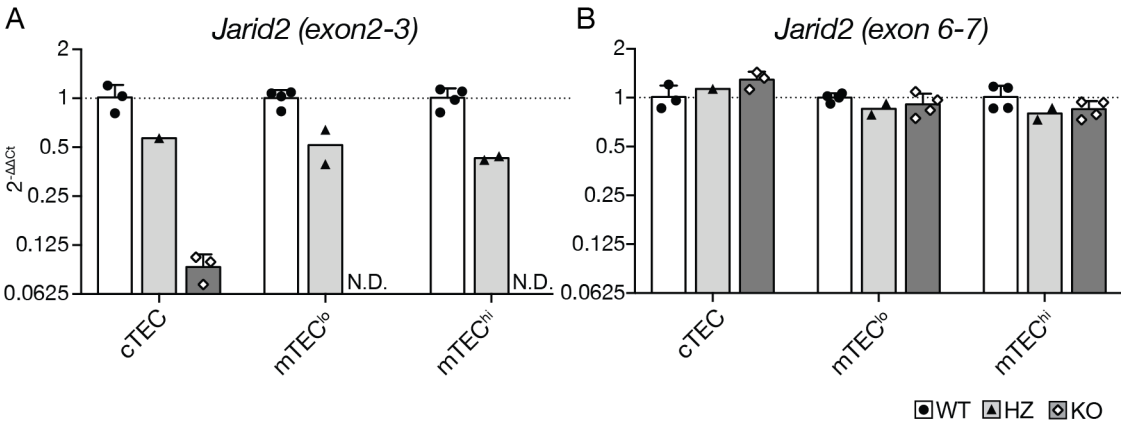

Figure 5.3: *Jarid2* transcripts without exon 3 are expressed in TEC isolated from *Jarid2*$^{TEC-/-}$ mice. (A-B) Extracted RNA from sorted cTEC, mTEC^{lo} and mTEC^{hi} was used for qPCR employing primers for the detection of *Jarid2* mRNA spanning from exon 3 to 4 (A) and from exon 6 to 7 (B). Data was analysed using the $2^{-\Delta\Delta Ct}$ method with normalisation to *Gapdh* expression and setting expression in WT to 1. The experiment was done with mice at 5 weeks of age. Each data point represents an individual mouse. WT: *Jarid2*$^{wt/fl}$ or *Jarid2*$^{fl/fl}$; HZ: *Jarid2*$^{wt/TEC-}$; KO: *Jarid2*$^{TEC-/-}$.

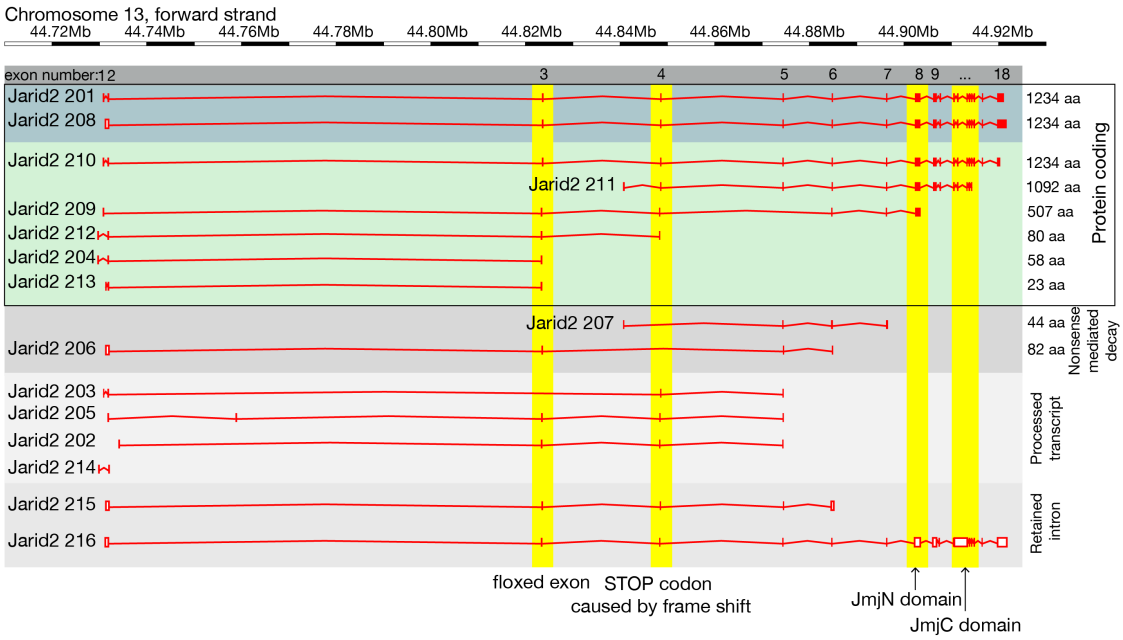

Figure 5.4: Transcript variants of *Jarid2* in TEC. Summary of transcript variants of *Jarid2* based on the Ensembl database.

5.2.3 *Jarid2* transcript variants

In a next step, I wanted to prove the loss of intact JARID2 protein in TEC from *Jarid2*$^{TEC-/-}$ mice caused by the premature STOP codon in exon 4. To this end, I used an immunofluorescence JARID2 staining for microscopy, however a nuclear signal of equal intensity was detected in WT and JARID2-deficient TEC (data not shown). As I suspected cross-reactivity of the antibody to another nuclear protein, I tried Western blotting, however the antibody that showed a band at the expected size for JARID2 in a cell line, did not work in low protein input Western blot done on sorted TEC populations (data not shown).

Due to the inability to show the loss of protein in TEC from *Jarid2*$^{TEC-/-}$ mice, I assessed transcript variants that avoid the frame shift and premature STOP codon by RT-PCR. Figure 5.4A shows a summary of all transcript variants of *Jarid2* found on the Ensembl database. Of particular interest was Jarid 211 that uses an alternative exon skipping the floxed exon 3. To detect the presence of this transcript variant, a PCR primer was designed to bind within the alternative sequence (see “i” and “h” in Figure 5.5B). No product

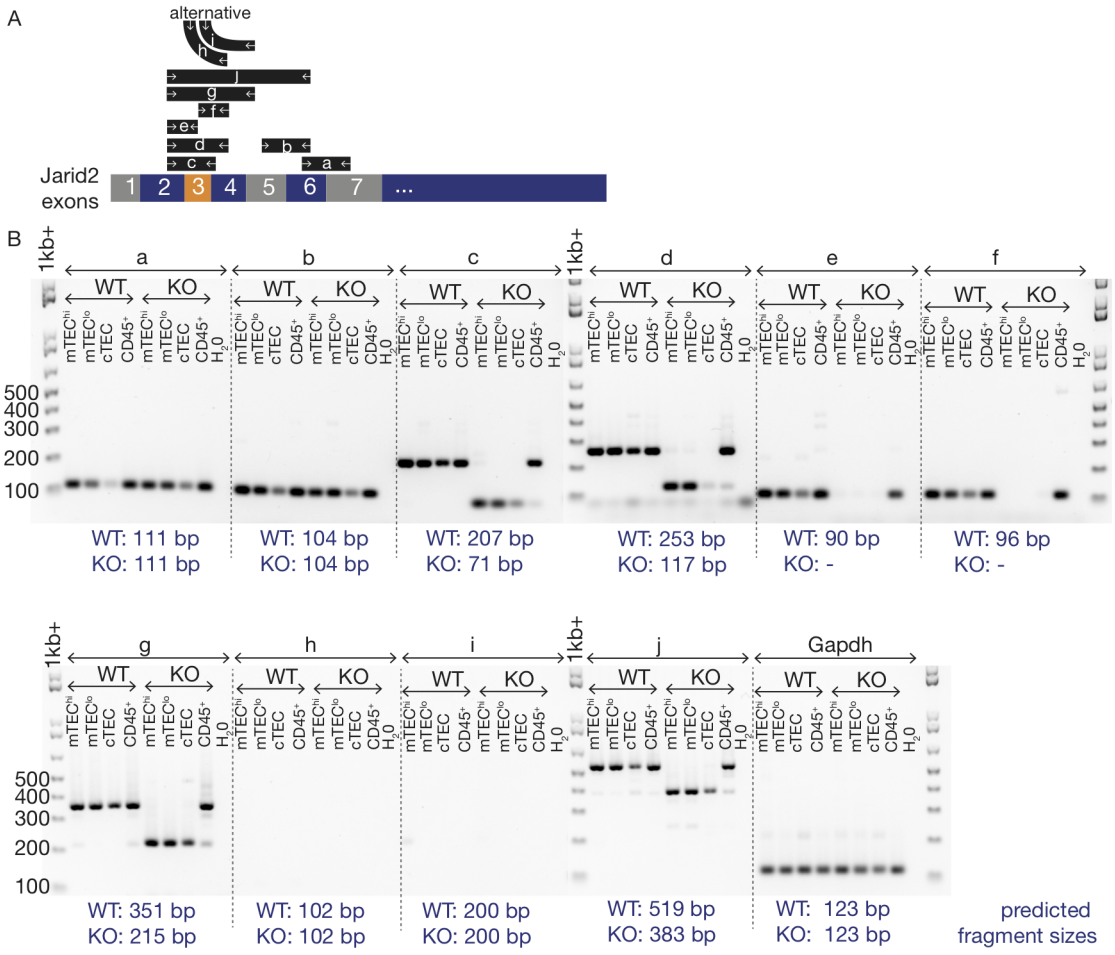

Figure 5.5: No alternative *Jarid2* transcripts were detected in WT and KO TEC. **(A)** Schematic of PCR reactions used in (B). **(B)** Sorted cTEC, mTEC^{hi}, mTEC^{lo} and CD45^{+} EpCAM^{-} cells used for PCR with the primers illustrated in (A). PCR products were run on a 1.5 % agarose gel. 1kb+ ladder was run as a reference. WT: *Jarid2*$^{fl/fl}$; KO: *Jarid2*$^{TEC-/-}$

was detected for reactions using this primer sequence. Further, all other PCR reactions designed around exon 3 did not give any indication for the presence of splice variants in the *Jarid2*-deficient TEC. Although this was not an exhaustive test for all possible ways to avoid an altered *Jarid2* transcript with a STOP codon in exon 4, it suggested that the knockout strategy should be effective in generating a JARID2 deficiency.

5.2.4 The conditional *Jarid2* locus does not affect thymus biology

To assess the effect of the genetic alteration of inserting LoxP sites adjacent to exon 3 of *Jarid2*, *Jarid2*$^{fl/fl}$ mice, which are devoid of Cre, were compared to wild type C57BL/6

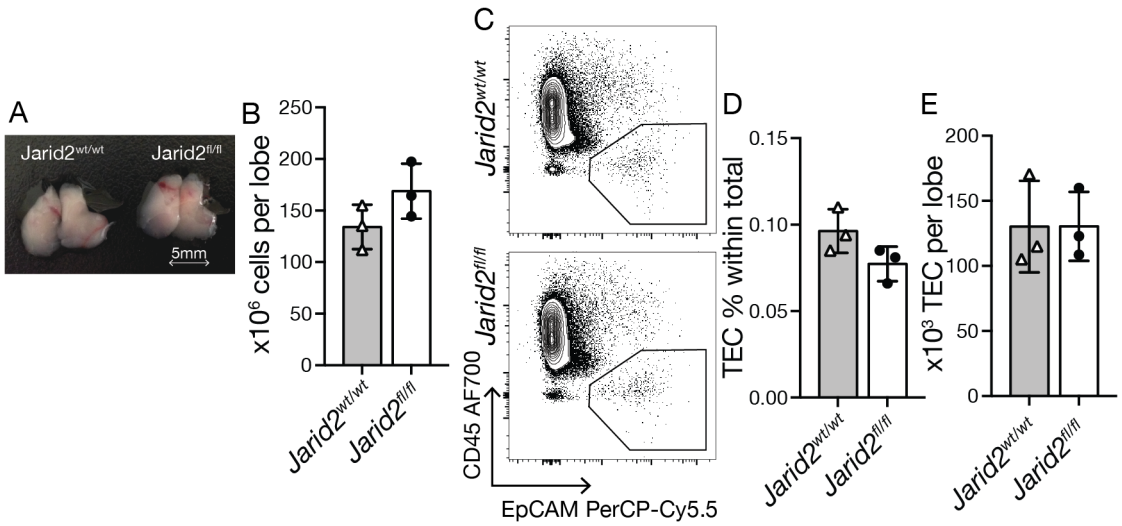

Figure 5.6: Total thymus and TEC cellularity is comparable between *Jarid2$^{wt/wt}$* and *Jarid2$^{fl/fl}$*. **(A)** Representative image of the thymus at 4 weeks of age. **(B)** Bar graph shows absolute cell number after mechanic disruption of one thymic lobe. **(C)** Representative FACS plots of TEC (EpCAM$^+$ CD45$^-$) within live cells. **(D)** Bar graph depicts relative frequencies of TEC (EpCAM$^+$ CD45$^-$) within total. **(E)** Bar graph shows absolute TEC numbers per thymic lobe. Data shown in graphs is from one experiment. *Jarid2$^{wt/wt}$*: n=3; *Jarid2$^{fl/fl}$*: n=3. Statistical analysis was done with two-tailed unpaired t-tests.

animals (designated *Jarid2$^{wt/wt}$*). This demonstrated that overall cellularity, TEC and thymocyte compartment, as well as T cell compartment in the spleen were comparable in *Jarid2$^{fl/fl}$* and *Jarid2$^{wt/wt}$* mice at 4 weeks of age (Figs. 5.6-5.10).

Taken together, this data demonstrated that the flox-targeted allele does not disrupt TEC development or maturation, and that it does not impact on thymocyte development. I therefore concluded that it is valid to use *Jarid2$^{fl/fl}$* mice in my experiments as a WT control.

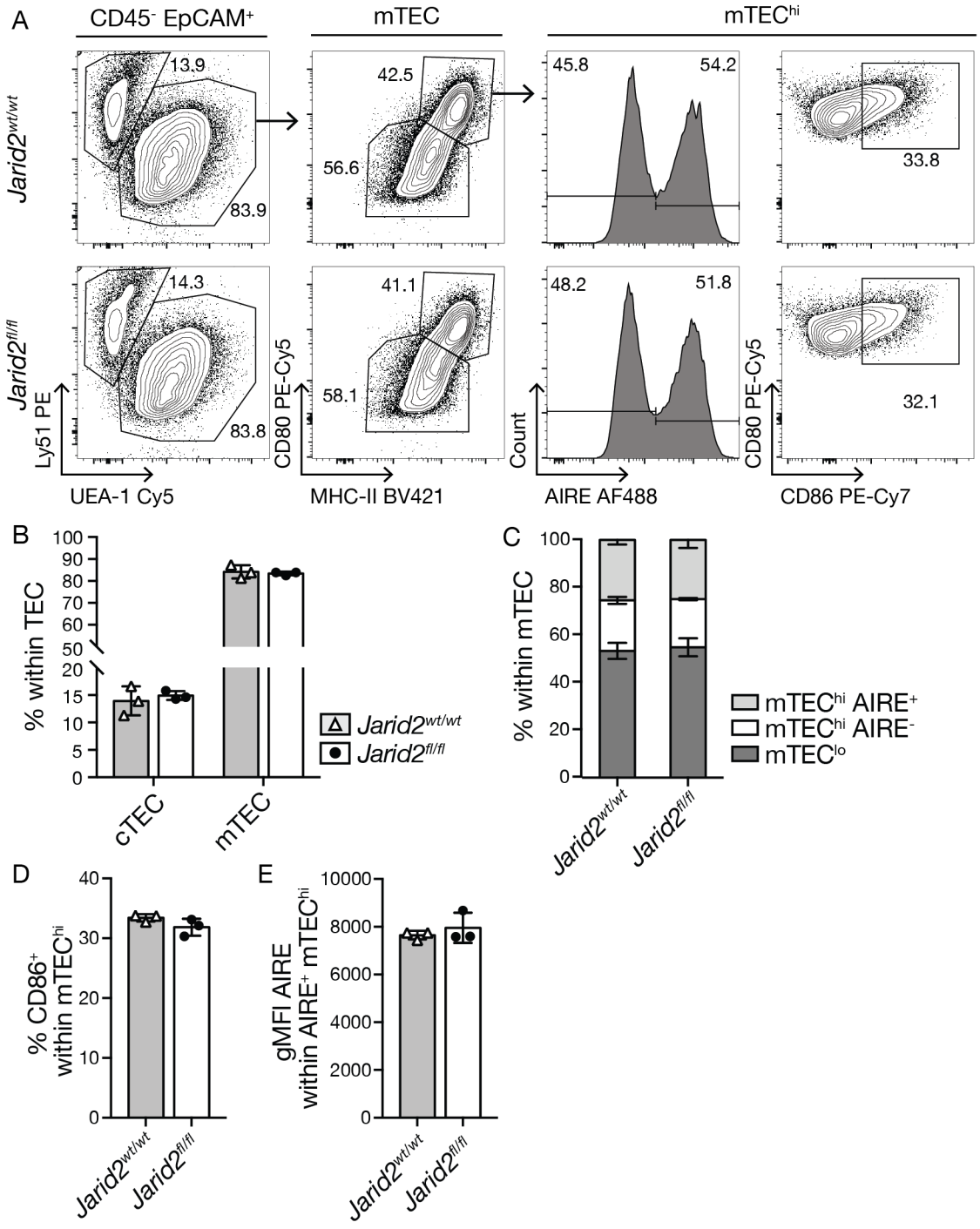

Figure 5.7: mTEC maturation is comparable between *Jarid2*$^{wt/wt}$ and *Jarid2*$^{fl/fl}$. **(A)** Representative FACS plots show gating strategy for TEC assessment. **(B)** Bar graph shows relative frequencies of mTEC and cTEC. **(C)** Bar graph depicts mTEC maturation according to MHC-II, CD80 and AIRE expression. **(D)** Bar graph shows relative frequency of CD86^{+} cells within mTEC^{hi}. **(E)** Bar graph shows expression level of AIRE within AIRE^{+} CD86^{-} mTEC^{hi} and AIRE^{+} CD86^{+} mTEC^{hi} as measured by gMFI normalised to respective WT population. Data shown in graphs is from one experiment. *Jarid2*$^{wt/wt}$: n=3; *Jarid2*$^{fl/fl}$: n=3. Statistical analysis was done with a two-tailed unpaired t-test with correction for multiple comparisons.

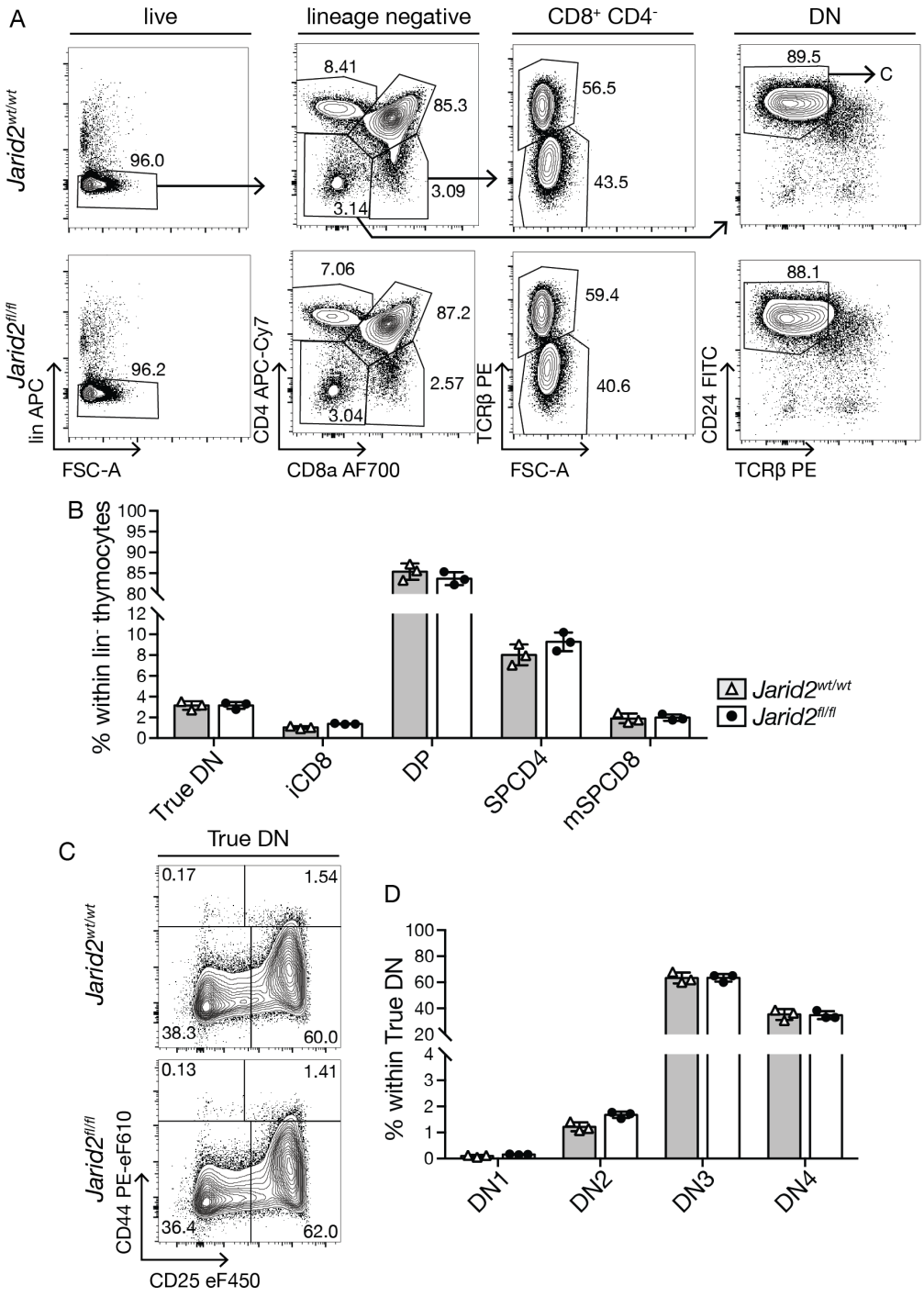

Figure 5.8: Thymocyte maturation is comparable between *Jarid2*$^{wt/wt}$ and *Jarid2*$^{fl/fl}$. **(A)** Representative FACS plots show gating strategy for defining True DN, iCD8, mSPCD8, DP and SPCD4. Lineage markers include antibodies against CD11b, CD11c, Gr-1, CD19, CD49b, F4/80, NK1.1, GL3 and TER119. **(B)** Bar graph shows relative frequencies of the defined subpopulations within lineage negative thymocytes. **(C)** Representative FACS plots show DN1 (CD44^{hi} CD25^{-}), DN2 (CD44^{hi} CD25^{+}), DN3 (CD44^{lo} CD25^{+}) and DN4 (CD44^{lo} CD25^{-}). Bar graph depicts frequencies within True DN (lin^{-} CD4^{-} CD8^{-} TCRβ^{lo} CD24^{+}). Data shown in graphs is from one experiment. *Jarid2*$^{wt/wt}$: n=3; *Jarid2*$^{fl/fl}$: n=3. Statistical analysis was done with two-tailed unpaired t-tests with correction for multiple comparisons.

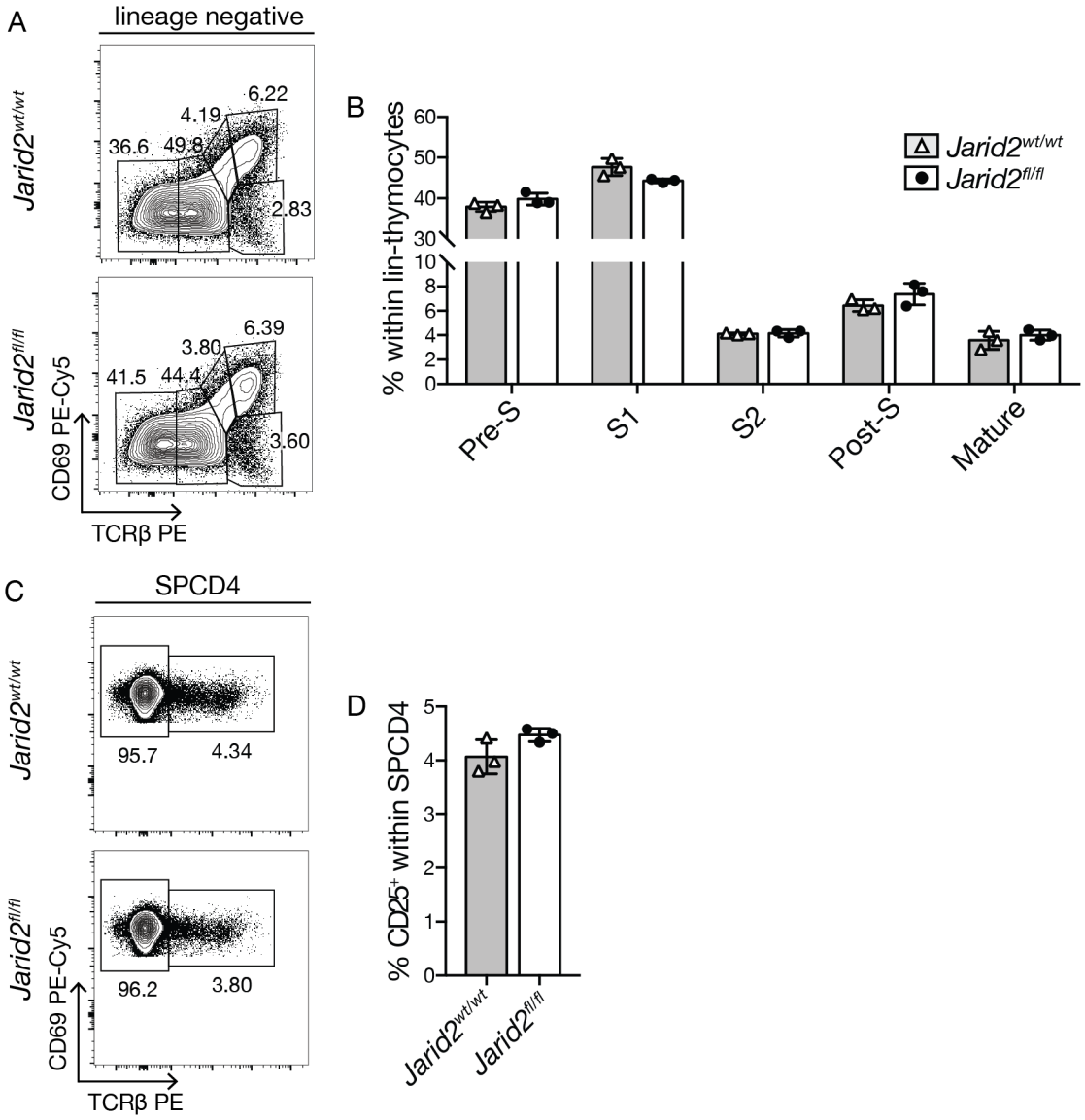

Figure 5.9: Positive selection and the frequency of CD25$^+$ SPCD4 are comparable between *Jarid2$^{wt/wt}$* and *Jarid2$^{fl/fl}$*. **(A)** Representative FACS plots show gating strategy for defining Pre-S (TCRβ$^-$ CD69$^-$), S1 (TCRβ^{int} CD69$^-$), S2 (TCRβ^{int} CD69$^+$), Post-S (TCRβ^{hi} CD69$^+$), M (TCRβ^{hi} CD69$^-$). **(B)** Bar graph shows relative frequencies of the defined subpopulations within lin$^-$ thymocytes. **(C)** Representative FACS plots show the gating CD25$^+$ cells within SPCD4. **(D)** Bar graph shows relative frequencies of CD25$^+$ cells within SPCD4. Data shown in graphs is from one experiment. *Jarid2$^{wt/wt}$*: n=3; *Jarid2$^{fl/fl}$*: n=3. Statistical analysis was done with two-tailed unpaired t-tests with correction for multiple comparisons.

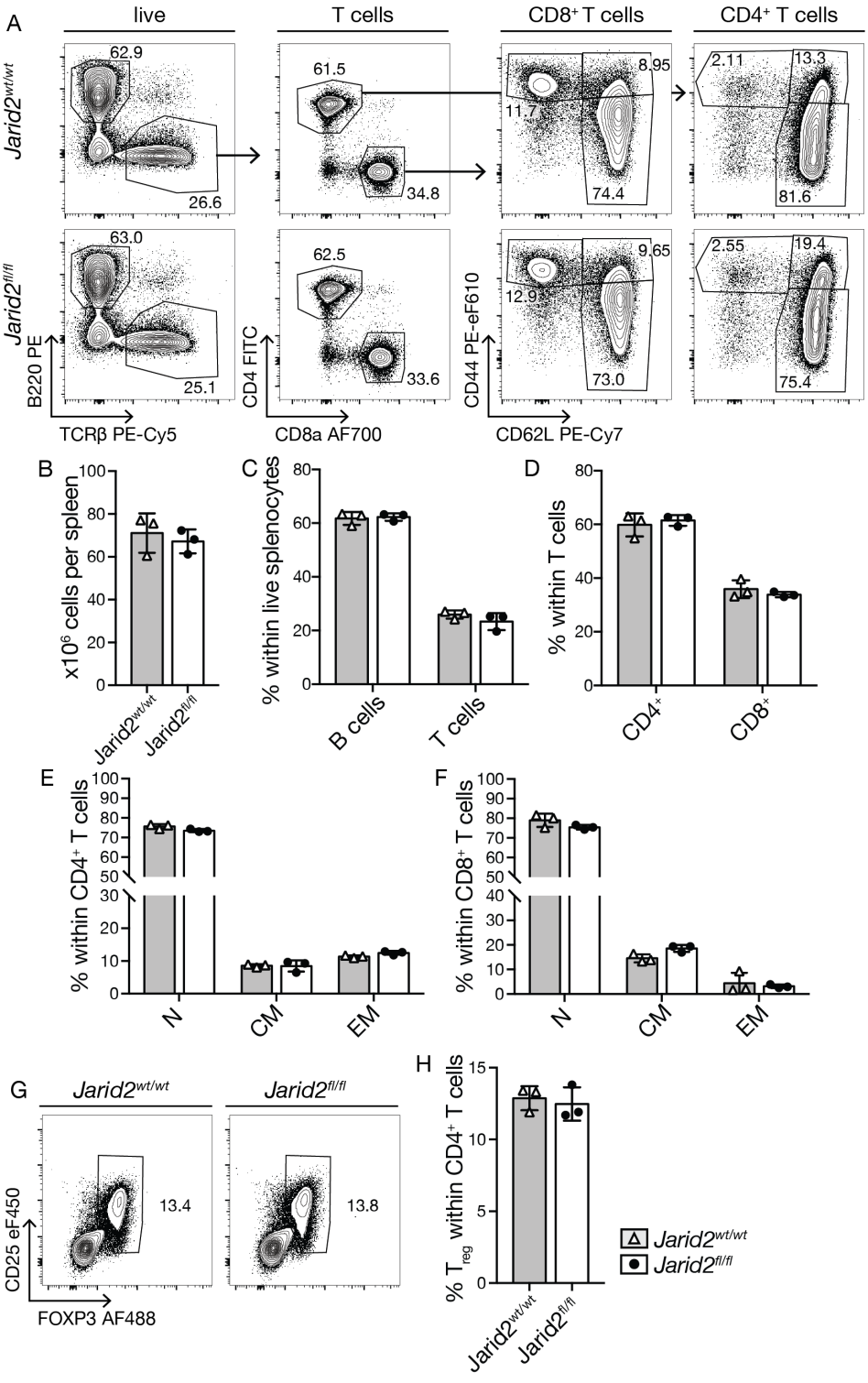

Figure 5.10: Splenic T cells are comparable between *Jarid2*$^{wt/wt}$ and *Jarid2*$^{fl/fl}$. **(A)** Representative FACS plots display the gating strategy to assess T cells in lymph nodes. **(B)** Bar graph shows T and B cell frequencies within total lymph node cells. **(C)** Bar graph displays relative frequencies of CD4$^+$ and CD8$^+$ within T cells. **(D-E)** Bar graphs show CD62L$^+$ CD44^{lo} naïve (N), CD62L$^+$ CD44^{hi} central memory (CM) and CD62L$^-$ CD44^{hi} effector memory (EM) within CD4$^+$ T cells (D) and within CD8$^+$ T cells (E). Data shown in graphs is from one experiment. *Jarid2*$^{wt/wt}$: n=3; *Jarid2*$^{fl/fl}$: n=3. Statistical analysis was done with two-tailed unpaired t-tests with correction for multiple comparisons.

5.3 TEC with a deficiency in JARID2

5.3.1 Loss of JARID2 in TEC does not affect thymus cellularity and architecture at 5 weeks of age

Having established that the *Jarid2*$^{TEC-/-}$ mouse model is valid, the next step was to investigate if TEC phenotype and function were altered due to the loss of JARID2 expression.

At 5 weeks of age, the thymi of mice with a TEC-targeted loss of JARID2 had a normal appearance and cellularity (Fig. 5.11A-B). The morphology was assessed using immunofluorescence microscopy staining for K5 and AIRE. The thymic architecture and distribution of AIRE^{+} cells was comparable between WT and *Jarid2*$^{TEC-/-}$ mice.

5.3.2 Loss of JARID2 affects mTEC maturation and AIRE expression levels

At 5 weeks of age, relative and absolute TEC cellularity was similar when comparing WT, *Jarid2*$^{TEC-/-}$ and *Jarid2*$^{wt/TEC-}$ (Fig. 5.12B-C). These observations suggest that a normal thymus can form even in the absence JARID2.

Moreover, there was a normal frequency of cTEC and mTEC in the mutant mice. However, the frequency of mature mTEC (as defined by MHC-II, CD80, CD86 and AIRE expression) was increased, with an expansion of AIRE^{+} mTEC^{hi} (35.08 % ± 1.61 vs 25.31 % ± 3.28) as compared to WT (Fig. 5.13C). The frequency of CD86^{+} cells within mTEC^{hi} was also increased (25.13 % ± 1.44 vs 22.45 % ± 2.35) (Fig. 5.13D). This phenotype was similar to the one observed in *Utx*$^{TEC-/-}$ *Jmjd3*$^{TEC-/-}$ mice.

The AIRE protein expression levels as assessed with gMFI within AIRE^{+} TEC was increased (Fig. 5.13E). This result was observed in AIRE^{+} cells both within CD86^{-} and CD86^{+} mTEC^{hi} subpopulations, but was more pronounced in the latter subpopulation (113.8 % of WT ± 5.9 %). This finding contrasts with the decrease in AIRE protein expression levels in *Utx*$^{TEC-/-}$ *Jmjd3*$^{TEC-/-}$ mice, which suggests that AIRE

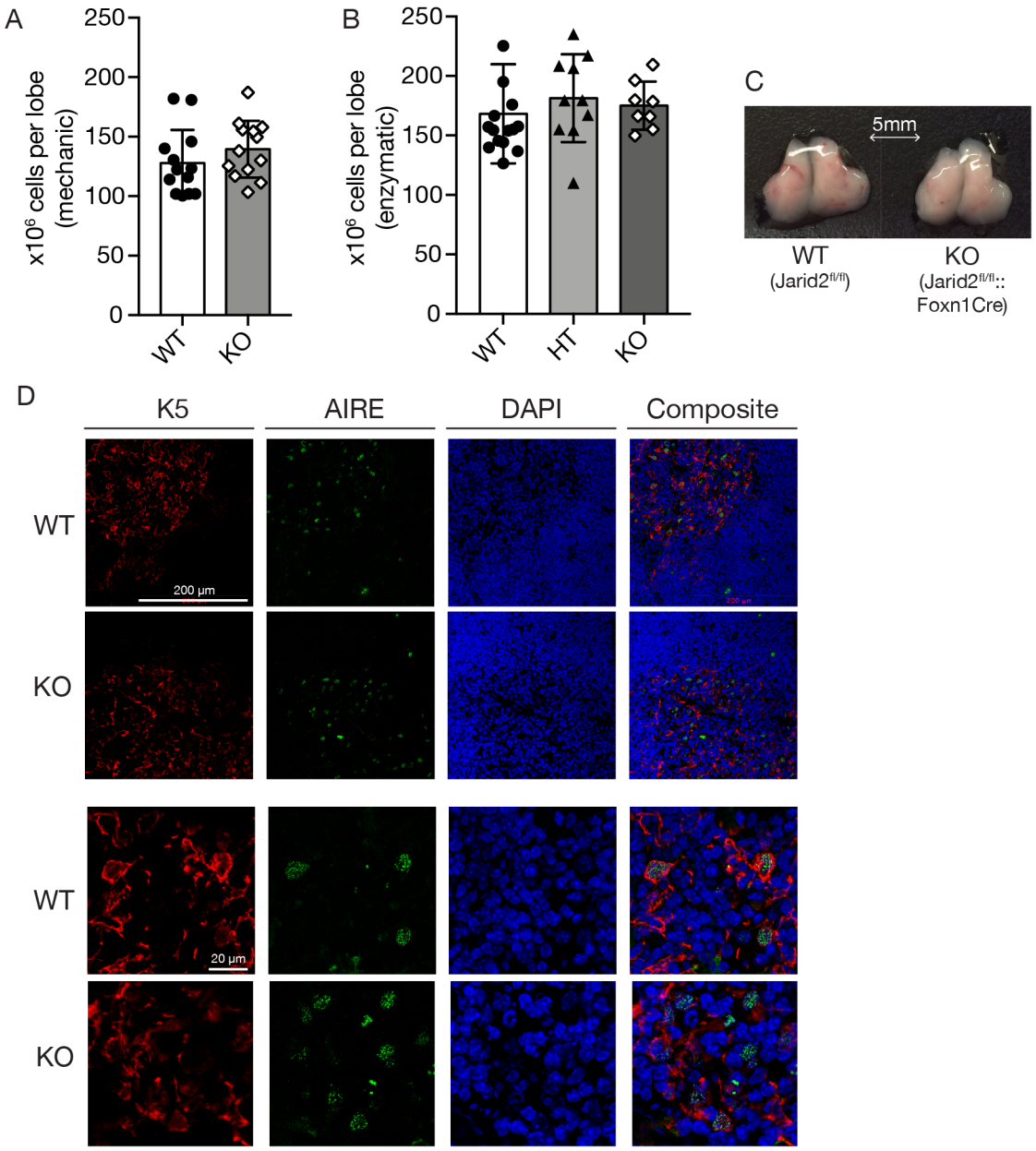

Figure 5.11: Normal total cellularity and architecture of the thymus with a TEC-specific loss of JARID2. (A) Absolute cell count was assessed after mechanical disruption of one thymic lobe. Data shown in bar graph is pooled from 4 independent experiments (WT: n=13; KO: n=13). **(B)** Absolute cell count was assessed after enzymatic digestion of one thymic lobe. Data in bar graph is pooled from 6 independent experiments (WT (*Jarid2*$^{wt/wt}$, *Jarid2*$^{wt/fl}$ or *Jarid2*$^{fl/fl}$): n=15; HZ (*Jarid2*$^{wt/TEC-}$): n=10; KO (*Jarid2*$^{TEC-/-}$): n=8). Statistical comparison was done with two-tailed unpaired t-test (A) and one-way ANOVA (B). **(C)** Representative image of the thymus at 5 weeks of age. **(D)** Representative immunofluorescence microscopy images of thymus sections stained with Cytokeratin 5 (K5, red), AIRE (green) and DAPI (blue). WT: *Jarid2*$^{fl/fl}$; KO: *Jarid2*$^{TEC-/-}$.

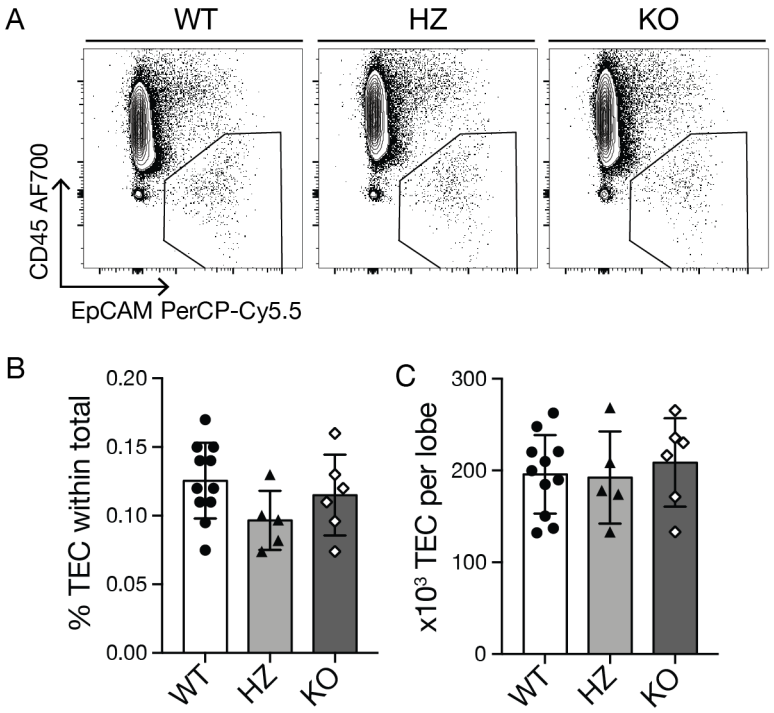

Figure 5.12: TEC cellularity is comparable between WT, *Jarid2*$^{TEC-/-}$ and *Jarid2*$^{wt/TEC-}$ mice. (A) Representative FACS plots show TEC (EpCAM^{+} CD45^{-}) within live cells. **(B)** Bar graph depicts frequency of TEC within total cells. **(C)** Bar graph shows absolute TEC numbers. Data in graphs is pooled from four independent experiments. WT (*Jarid2*$^{wt/wt}$, *Jarid2*$^{wt/fl}$ or *Jarid2*$^{fl/fl}$): n=11; HZ (*Jarid2*$^{wt/TEC-}$): n=5; KO (*Jarid2*$^{TEC-/-}$): n=6. Statistical analysis was done by one-way ANOVA.

or its upstream regulators might be sensitive to changes in H3K27me3 levels. MHC-II surface expression levels in different TEC subpopulations were comparable in WT and *Jarid2*$^{TEC-/-}$ mice (Fig. 5.13F).

The results suggested that, although the impact was relatively mild, JARID2 plays a role in mTEC maturation. In these experiments, TEC with a heterozygous deficiency in JARID2 displayed a phenotype intermediate between the WT and TEC with a homozygous deficiency, implying that only having one intact *Jarid2* allele already has consequences for mTEC biology.

5.3.3 MHC-I expression is increased in JARID2-deficient mTEC

The presentation of antigens on MHC-I and MHC-II molecules is crucial for TEC function, as it mediates positive and negative selection as well as CD4/CD8 lineage commitment of

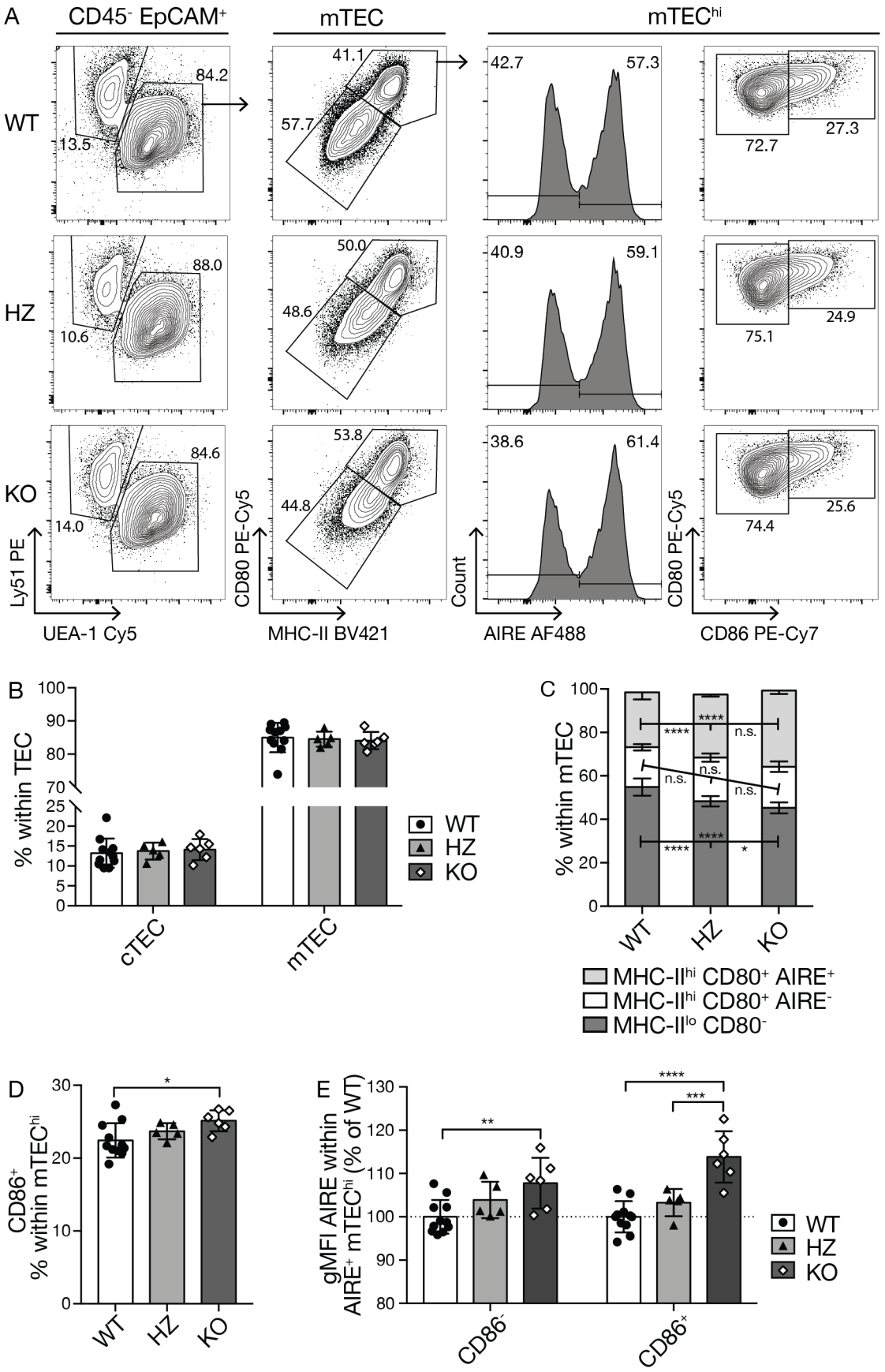
A
CD45- EpCAM+
mTEC
mTEChi
WT
HZ
KO
84.2
13.5
41.1
57.7
42.7
57.3
72.7
27.3
88.0
10.6
50.0
48.6
40.9
59.1
75.1
24.9
84.6
14.0
53.8
44.8
38.6
61.4
74.4
25.6
Ly51 PE
UEA-1 Cy5
CD80 PE-Cy5
MHC-II BV421
Count
AIRE AF488
CD80 PE-Cy5
CD86 PE-Cy7
B
% within TEC
cTEC
mTEC
WT
HZ
KO
C
% within mTEC
WT
HZ
KO
MHC-IIhi CD80+ AIRE+
MHC-IIhi CD80+ AIRE-
MHC-IIlo CD80-
D
CD86+ % within mTEChi
E
gMFI AIRE within AIRE+ mTEChi (% of WT)
CD86-
CD86+

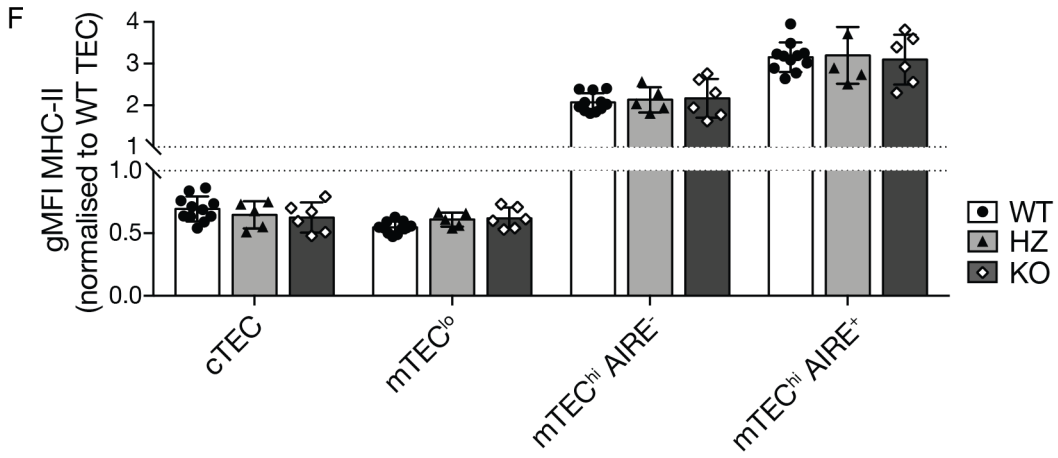

Figure 5.13: mTEC maturation is altered in JARID2-deficient TEC. (A) Representative FACS plots show the gating strategy for TEC identification and characterisation. **(B)** Bar graph depicts relative frequencies of mTEC and cTEC. **(C)** Bar graph shows mTEC maturation according to MHC-II, CD80 and AIRE expression. **(D)** Bar graph shows relative frequency of $CD86^+$ cells within $mTEC^{hi}$. **(E)** Bar graph shows expression level of AIRE within $AIRE^+$ $CD86^-$ $mTEC^{hi}$ and $AIRE^+$ $CD86^+$ $mTEC^{hi}$ as measured by gMFI normalised to respective WT population. **(F)** Bar graph depicts gMFI of MHC-II of different TEC subpopulations normalised to gMFI of MHC-II in total WT TEC, arbitrarily defined as a value of "1". Data shown in graphs is pooled from 4 independent experiments. WT (*Jarid2*$^{wt/wt}$, *Jarid2*$^{wt/fl}$ or *Jarid2*$^{fl/fl}$): n=11; HZ (*Jarid2*$^{wt/TEC-}$): n=5; KO (*Jarid2*$^{TEC-/-}$): n=6. Statistical analysis between the three groups (WT, HZ and KO) was done by one-way ANOVA. *p<0.05, **p<0.01, ***p<0.001, ****p<0.0001.

developing thymocytes. While peptide-MHC-I complexes (i.e. pMHC-I) are recognised by TCR in conjunction with the invariant co-receptor CD8, the interaction of TCR with pMHC-II is assisted by the co-receptor CD4.

As seen in Figure 5.13C and 5.13F, the loss of JARID2 expression in TEC led to an increase in the frequency of $MHC\text{-}II^{hi}$ mTEC, while the mean MHC-II surface expression per cell remained the same. There are two distinct populations of TEC based on their MHC-II expression profile, i.e. $MHC\text{-}II^{lo}$ and $MHC\text{-}II^{hi}$, in mTEC, whereas MHC-I is expressed more uniformly and at relatively high level in all TEC (Fig. 5.14). Notably, MHC-I expression levels were increased in mTEC isolated from *Jarid2*$^{TEC-/-}$ mice. This increase was observed on both $mTEC^{lo}$ and $mTEC^{hi}$ with the former cell type displaying a more pronounced difference (1.069 ±0.08 (WT) vs 1.269 ±0.13 (KO)). This demonstrated that both MHC-II and MHC-I expression were affected in mTEC lacking JARID2. In cTEC, MHC-I expression was unchanged when comparing WT and *Jarid2*$^{TEC-/-}$ mice (Fig. 5.14).

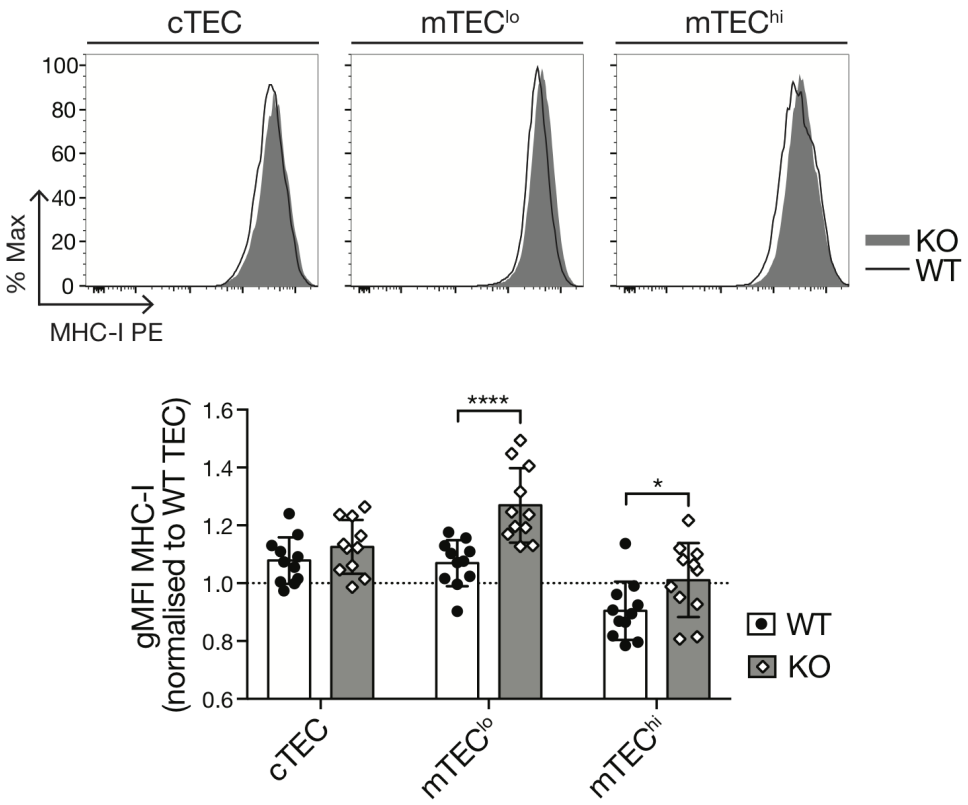

Figure 5.14: Decreased MHC-I expression in JARID2-deficient mTEC. Representative histograms show MHC-I expression and bar graphs depict gMFI of MHC-I normalised to gMFI of MHC-I in WT total TEC, providing an arbitrary value of "1" for these cells. Data shown in graphs is pooled from three independent experiments. WT (*Jarid2*$^{fl/fl}$): n=11; KO (*Jarid2*$^{TEC-/-}$): n=11. Statistical analysis was done with two-tailed unpaired t-tests. *p<0.05, **p<0.01, ***p<0.005, ****p<0.001.

5.3.4 Global H3K27me3 and H3K9me3 levels are unchanged in JARID2-deficient TEC

As JARID2 is involved in methyltransferase complexes that methylate H3K27 and H3K9, global H3K27me3 and H3K9me3 levels in TEC of *Jarid2*$^{TEC-/-}$ mice were assessed by FACS staining. H3K27me3 and H3K9me3 levels were normalised to global H3 levels. No differences in H3K27me3 and H3K9me3 were detected between WT and KO TEC (Fig. 5.15).

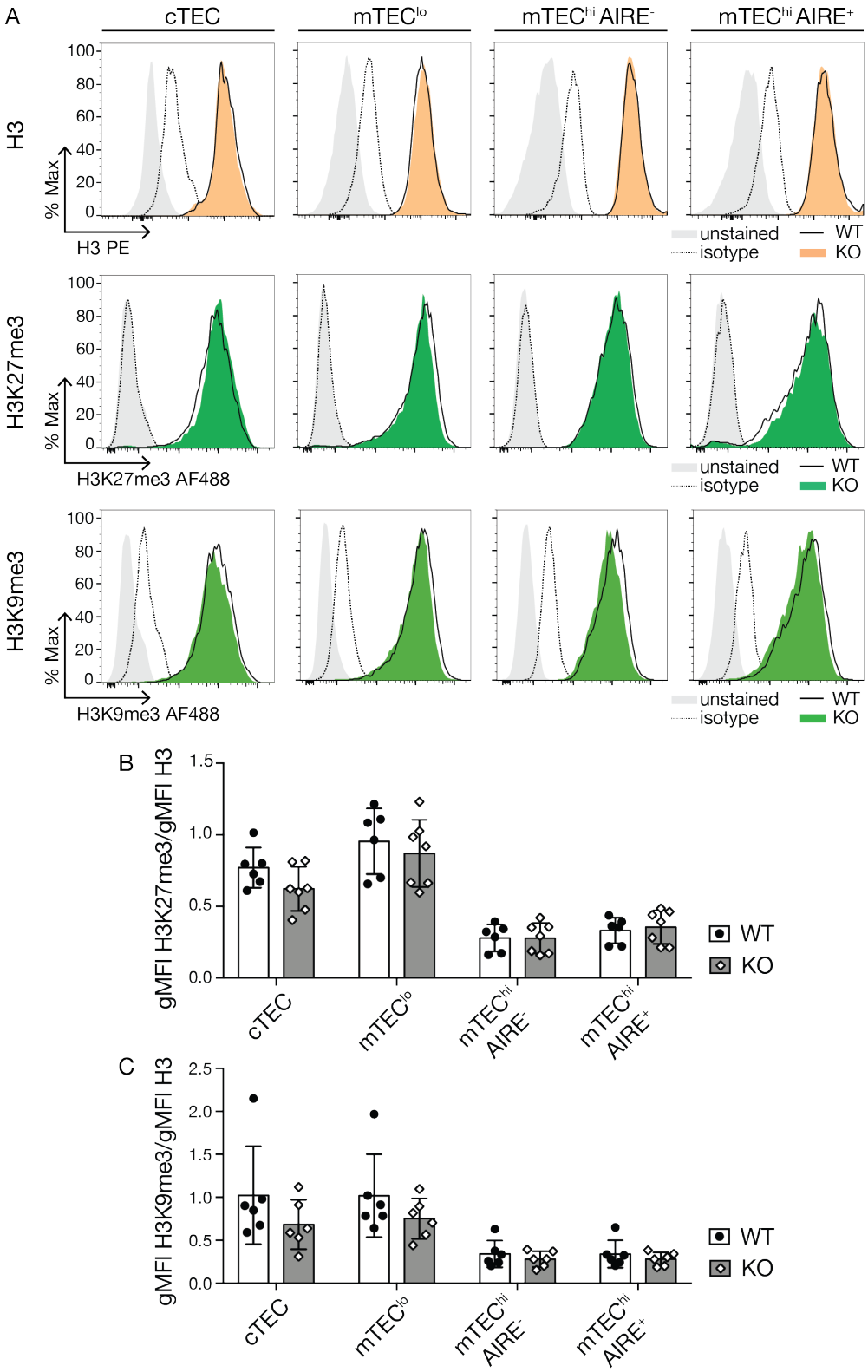

Figure 5.15: Unchanged global H3K27me3 and H3K9me3 levels in JARID2-deficient TEC. (A) Representative histograms show H3, H3K27me3 and H3K9me3 expression. Bar graphs depict gMFI of H3K27me3 **(B)** and H3K9me3 **(C)** normalised to H3. Data shown in graphs is pooled from two independent experiments: WT (*Jarid2*$^{fl/fl}$): n=6; KO (*Jarid2*$^{TEC-/-}$): n=7. Statistical analysis was done with multiple unpaired t-tests with correction for multiple comparisons.

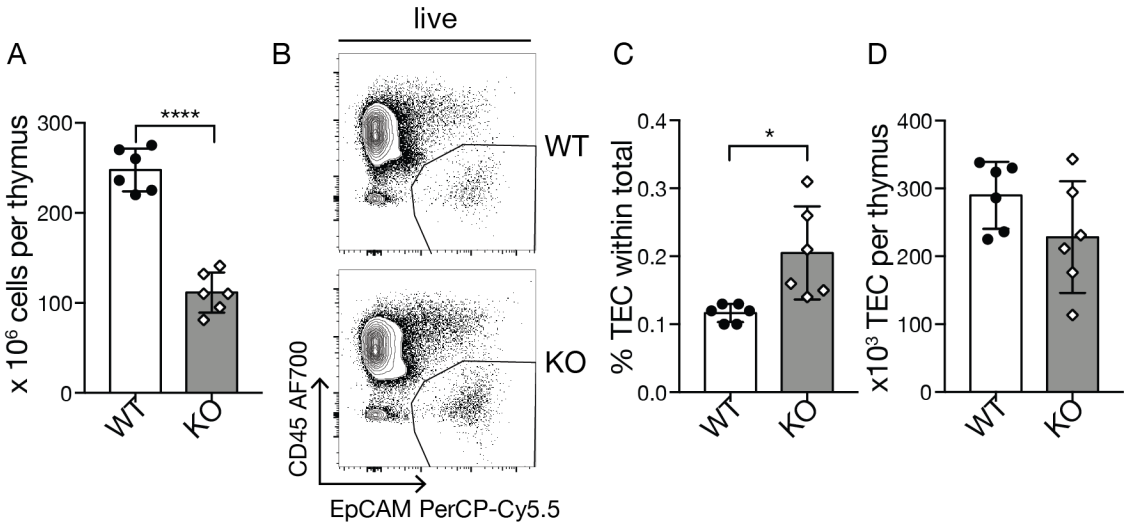

Figure 5.16: Thymic cellularity reduced at 16-18 weeks of age. (A) Bar graph depicts total thymus cellularity after enzymatic digestion. **(B)** Representative FACS plots show TEC ($EpCAM^+$ $CD45^-$) within live cells. **(C)** Bar graph depicts frequency of TEC within total cells. **(D)** Bar graph shows absolute TEC numbers. Data shown in graphs is pooled from two independent experiments. WT (*Jarid2*$^{fl/fl}$): n=6; KO (*Jarid2*$^{TEC-/-}$): n=6. Statistical analysis was done with two-tailed unpaired t-test. *p<0.05, **p<0.01, ***p<0.005.

Previous reports have noted that the KO of JARID2 affects the gene-specific distribution of H3K27me3, but not its global level [89, 199, 200]. The result of the histone methylation staining is therefore in line with these previously reported findings and future work will need to assess whether there are changes in the H3K27me3 and H3K9me3 distribution in TEC devoid of JARID2. The most informative assay to obtain such information is H3K27me3 and H3K9me3 ChIP-Seq.

5.3.5 Reduced total thymus cellularity and reduced mTEC cellularity at 16-18 weeks of age

In addition to the 5-week time point, I analysed the thymi of mice aged 16-18 weeks with the aim to assess whether a lack of JARID2 impacts the maintenance of a functional thymus. At this older age, the total thymic cellularity of *Jarid2*$^{TEC-/-}$ mice was reduced by half in comparison to that of age-matched WT animals (Fig. 5.16A), however, their total TEC cellularity was comparable (Fig. 5.16C-D), suggesting that the older JARID2-deficient TEC were functionally impaired and could not support normal thymopoiesis.

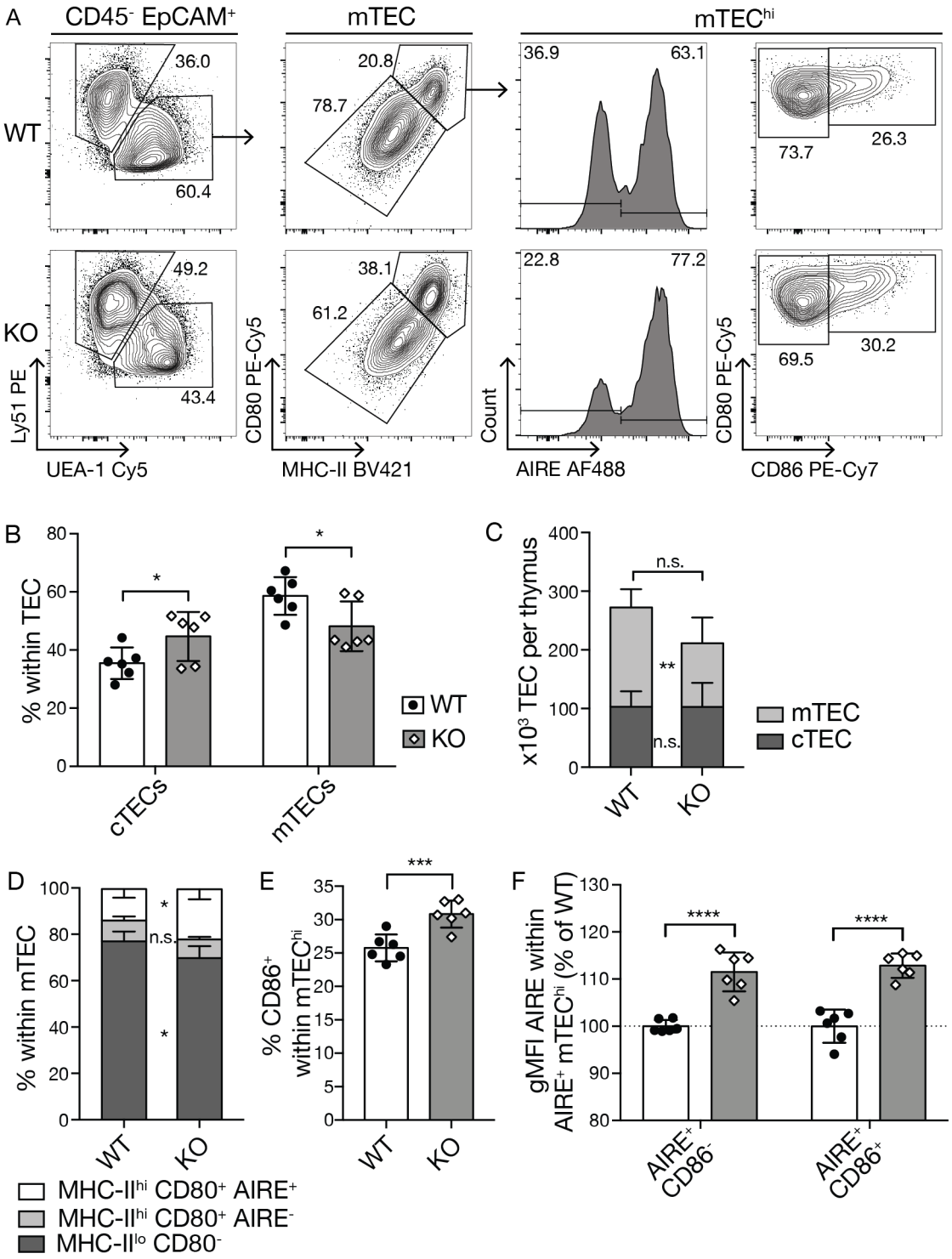

Figure 5.17: mTEC cellularity is reduced at 16-18 weeks of age. **(A)** Representative FACS plots show the gating strategy for TEC characterisation. Bar graph showing relative **(B)** and absolute **(C)** mTEC and cTEC numbers. **(D)** Bar graph depicts mTEC maturation according to MHC-II, CD80 and AIRE expression. **(E)** Bar graph shows relative frequency of $CD86^+$ cells within $mTEC^{hi}$. **(F)** Bar graph shows expression level of AIRE within $AIRE^+$ $CD86^-$ $mTEC^{hi}$ and $AIRE^+$ $CD86^+$ $mTEC^{hi}$ as measured by gMFI normalised to respective WT population. Data shown in graphs is pooled from two independent experiments: WT ($Jarid2^{fl/fl}$): n=6; KO ($Jarid2^{TEC-/-}$): n=6. Statistical analysis was done with two-tailed unpaired t-tests with correction for multiple comparisons. *p<0.05, **p<0.01, ***p<0.005, ****p<0.001.

Upon differentiating TEC into cortical and medullary phenotypes, a reduction of mTEC was observed in both relative and absolute numbers (Fig. 5.17B-C). The mTEC phenotype showed a similar pattern as that observed in 5 week old mice with a relative increase in AIRE^{+} mTEC^{hi} (Fig. 5.17D). Furthermore, an increase in AIRE protein expression in the AIRE^{+} mTEC^{hi} was again observed in 16-18 week old mice (Fig. 5.17F).

5.3.6 Brief summary of JARID2-deficient TEC

Taken together so far, mTEC maturation was altered in the absence of JARID2 expression targeted to thymic epithelia. This was most prominently revealed by the result that mature AIRE^{+} CD86^{+} mTEC^{hi} were more abundant in the mutant mice. Moreover, the AIRE expression level per cell, as measured by gMFI, was increased when compared to WT cells. Further, MHC-I expression was increased in mTEC, with the biggest change within the mTEC^{lo} population. cTEC did not display any phenotypic alterations in the *Jarid2*$^{TEC-/-}$ mice that set them apart of WT animals. With 16-18 weeks of age, the loss of JARID2 in TEC caused a reduction in mTEC cellularity accompanied by a drastic reduction in thymocyte cellularity reflective of an inability of JARID2-deficient TEC to maintain normal thymopoiesis at an older age.

5.4 Thymocyte development in *Jarid2*$^{TEC-/-}$ mice

The role of TEC is to provide a unique cellular and molecular microenvironment that allows thymocyte lineage commitment, maturation and selection. Functional and numerical changes in TEC are thus likely reflected in alterations in thymocyte differentiation. To identify the impact of an absence of JARID2 in TEC on thymocyte development, I used phenotyping by flow cytometry to determine the expression of defined thymocyte markers that reflect specific maturation and selection stages.

5.4.1 mSPCD8 are reduced in *Jarid2*$^{TEC-/-}$ mice

First, I analysed the initial maturation stages of thymocytes in the cortex after seeding to the thymus as ETP. To this end, I used a "dump" channel to exclude B cells (CD19), γδ T cells (GL3), dendritic cells (CD11b, CD11c), red blood cells (TER119), NK cells (NK1.1, CD49b), NK T cells (CD49b) and myeloid cells (F4/80, Gr-1) to assess the maturation stages of very immature DN thymocytes and their subsequent progeny of iCD8, DP, SPCD4 and mSPCD8 (Fig. 5.18).

A detailed analysis of the DN subpopulations as defined by expression of CD44 and CD25 revealed no changes in the early stages of thymocyte development (Fig. 5.18B). Subsequent thymocyte subpopulations were comparable for both mouse strains with the exception of a slight but consistent reduction in mSPCD8 (TCRβ^{+} CD8^{+} CD4^{-} lin^{-}) in the *Jarid2*$^{TEC-/-}$ mice (1.55 % ± 0.28) as compared to WT mice (2.35 % ± 0.44) (Fig. 5.18C). The frequency of iCD8 (TCRβ^{-} thymocytes that fall within the SPCD8 gate) was unchanged. These cells are not committed to the CD8 lineage, but are on the way to become DP thymocytes.

5.4.2 Positive selection is unaffected

After the rearrangement of the TCRα and TCRβ chain, the newly created TCR will be expressed on the surface, where it will be eventually tested for its ability to interact with pMHC complexes. Once a sufficiently strong activation signal is mediated, thymocytes are positively selected and upregulate the activation marker CD69 (see Figure 3.26). Positive selection happens at the DP stage once sufficient TCR/CD3 complexes are expressed on the cell surface [149]. Thymocytes that are unable to engage with pMHC will not receive the signal required to survive and consequently undergo apoptosis after 3-5 days during which this process needs to be completed. Programmed cell death due to the failure to receive this survival signal is referred to as "death by neglect".

To probe whether the observed reduction in TCRβ^{hi} SPCD8 in the *Jarid2*$^{TEC-/-}$ mice is the result of defective positive selection, the progression through different selection

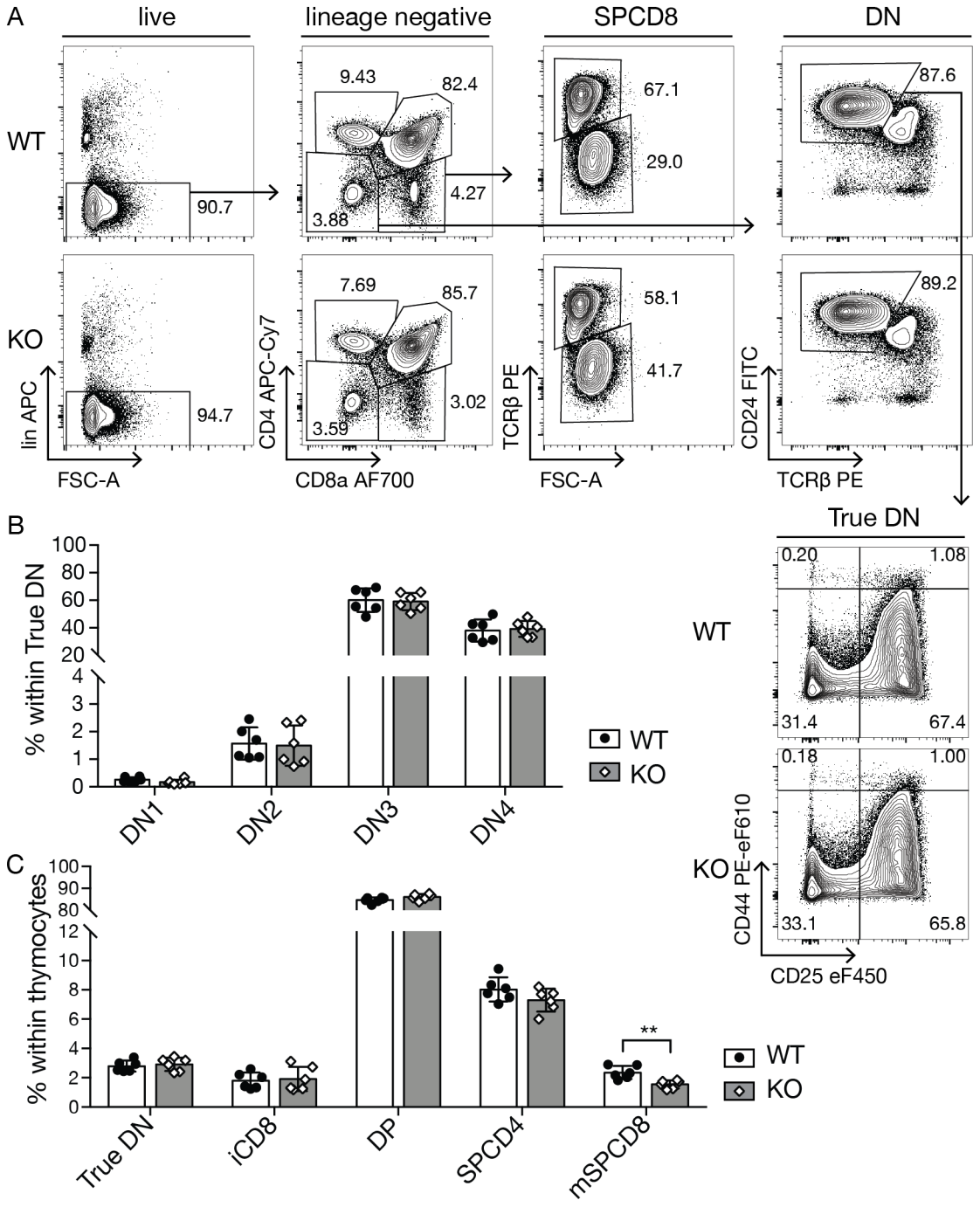

Figure 5.18: Reduction of mSPCD8 in thymi with TEC lacking JARID2. (A) Representative FACS plots show the gating strategy for defining True DN, iCD8, mSPCD8, DP and SPCD4. Lineage markers include antibodies against CD11b, CD11c, Gr-1, CD19, CD49b, F4/80, NK1.1, GL3 and TER119. "True DN" (lin$^-$ CD4$^-$ CD8$^-$ TCRβ^{lo} CD24$^+$) are further divided into DN1 (CD44^{hi} CD25$^-$), DN2 (CD44^{hi} CD25$^+$), DN3 (CD44^{lo} CD25$^+$) and DN4 (CD44^{lo} CD25$^-$). **(B)** Bar graph depicts frequencies of the defined subpopulations within "True DN". **(C)** Bar graph depicts the relative frequencies of the defined subpopulations within lin$^-$ thymocytes. Data in graphs is pooled from two independent experiments: WT (*Jarid2$^{fl/fl}$*): n=6; KO (*Jarid2$^{TEC-/-}$*): n=6. Statistical analysis was done with two-tailed unpaired t-tests. *p<0.05, **p<0.01, ***p<0.005, ****p<0.001.

stages was assessed, as defined by the differential expression of CD69 and TCRβ were assessed (Fig. 5.14A). Frequencies and the progression between the distinct cell stages were comparable between WT and *Jarid2*$^{TEC-/-}$ mice.

In a next analysis, I assessed the CD8 and CD4 expression within the individual stages of selection (Fig. 5.19D-E). Differences between WT and *Jarid2*$^{TEC-/-}$ mice could not be identified up to developmental stage S2. Thereafter, SPCD8 were significantly reduced in mutant thymi when compared to WT (PostS stage: 0.56 % ± 0.09 vs 0.94 % ± 0.17; Mature stage: 0.73 % ± 0.14 vs 1.14 % ± 0.14).

This analysis did not provide any indication that an altered positive selection process is the reason for the reduction in SPCD8 thymocytes, but it clearly identified that the reduction in SPCD8 thymocytes in *Jarid2*$^{TEC-/-}$ mice was isolated to the post selection stages and that SPCD8 thymocytes within the S1 and S2 stages remained identical for both stages. An unchanged positive selection process also fits in with the fact that the cTEC compartment of *Jarid2*$^{TEC-/-}$ mice did not have any phenotypic changes including unchanged levels of MHC-I and MHC-II cell surface expression.

5.4.3 Post selection maturation reveals partial block at DP^{dull} to immature SPCD8 stage

After positive selection DP cells slightly downregulate CD8 and CD4 to obtain a phenotype designated as DP^{dull} and then progress to adopt either SPCD4 or SPCD8 fate. According to their lineage choice CD8 or CD4 is differentially expressed and the cells progress to a mature SP phenotype. The positively selected cells also begin to upregulate the chemokine receptor CCR7, which enables them to migrate from the cortex to the medulla whilst eventually downregulating CD69 and CD24. This progression defines the stages of immature, semimature and mature thymocytes as illustrated in Figure 3.29 and the gating strategy is shown in representative FACS plots in Figure 5.20A for the SPCD8 lineage and in Figure 5.20E for the SPCD4 lineage. I thus assessed DP, SPCD4 and SPCD8 within TCRβ^{hi} CD5^{+} thymocytes and identified a small decrease (12.03 % ± 0.68 vs 13.82 %

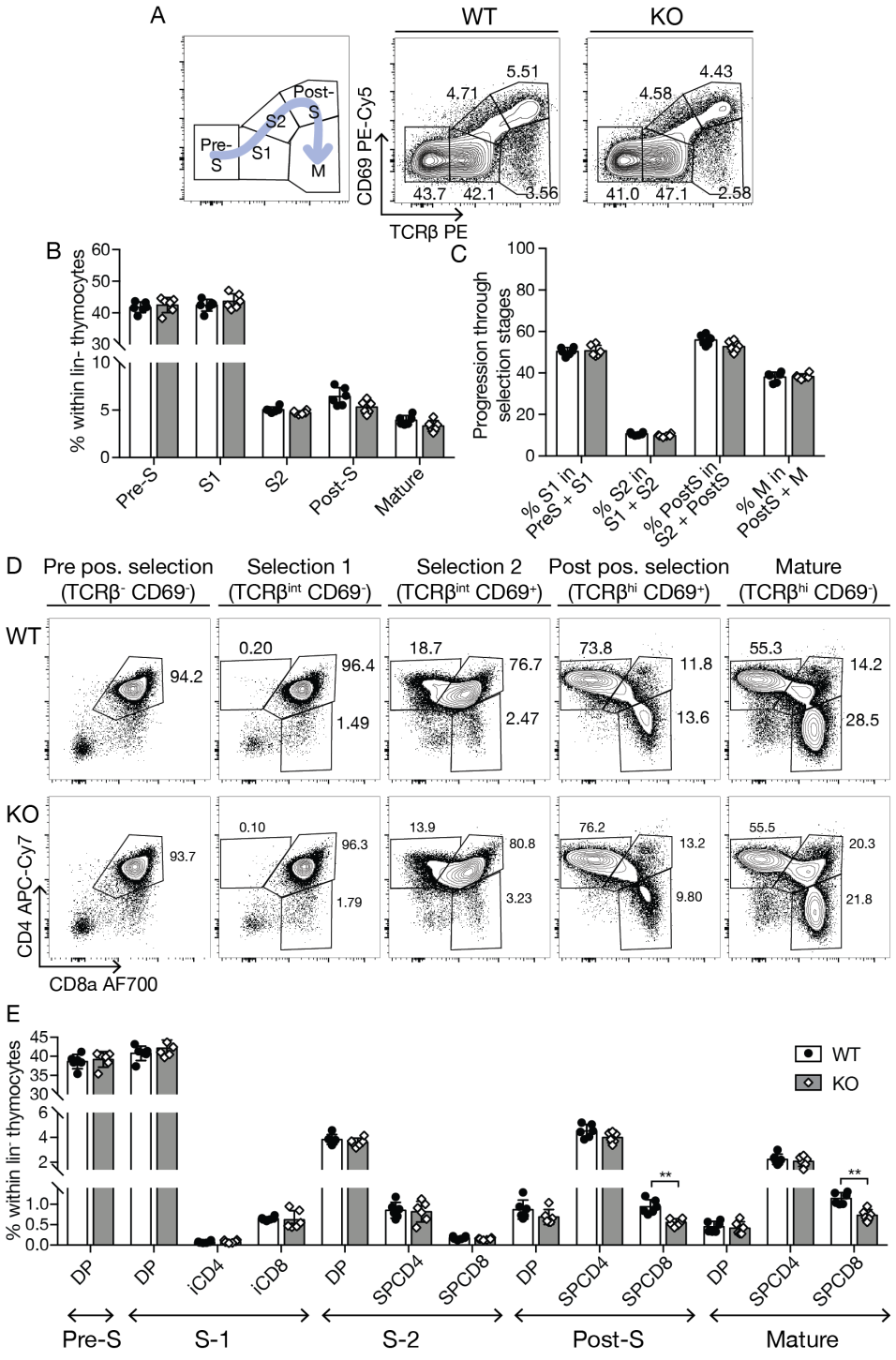

Figure 5.19: Reduction of SPCD8 in post selection stages in *Jarid2*$^{TEC-/-}$ mice. (A) Representative FACS plots define the different stages with regards to positive selection. **(B)** Bar graph shows relative frequencies of selection stages. **(C)** Bar graph shows progression through sequential selection stages. Calculation: (Stage B)/(Stage A+B)x100 where A is the maturation stage immediately before B. **(D)** Representative FACS plots for defining DP, SPCD4 and SPCD8 within different selection stages. **(E)** Bar graph shows the percentage of DP, SPCD4 and SPCD8 within PreS to M positive selection stages within lineage negative thymocytes. Data in graphs is pooled from two independent experiments: WT (*Jarid2*$^{fl/fl}$): n=6; KO (*Jarid2*$^{TEC-/-}$): n=6. Statistical analysis was done with two-tailed unpaired t-tests with correction for multiple comparisons. *p<0.05, **p<0.01, ***p<0.005, ****p<0.001.

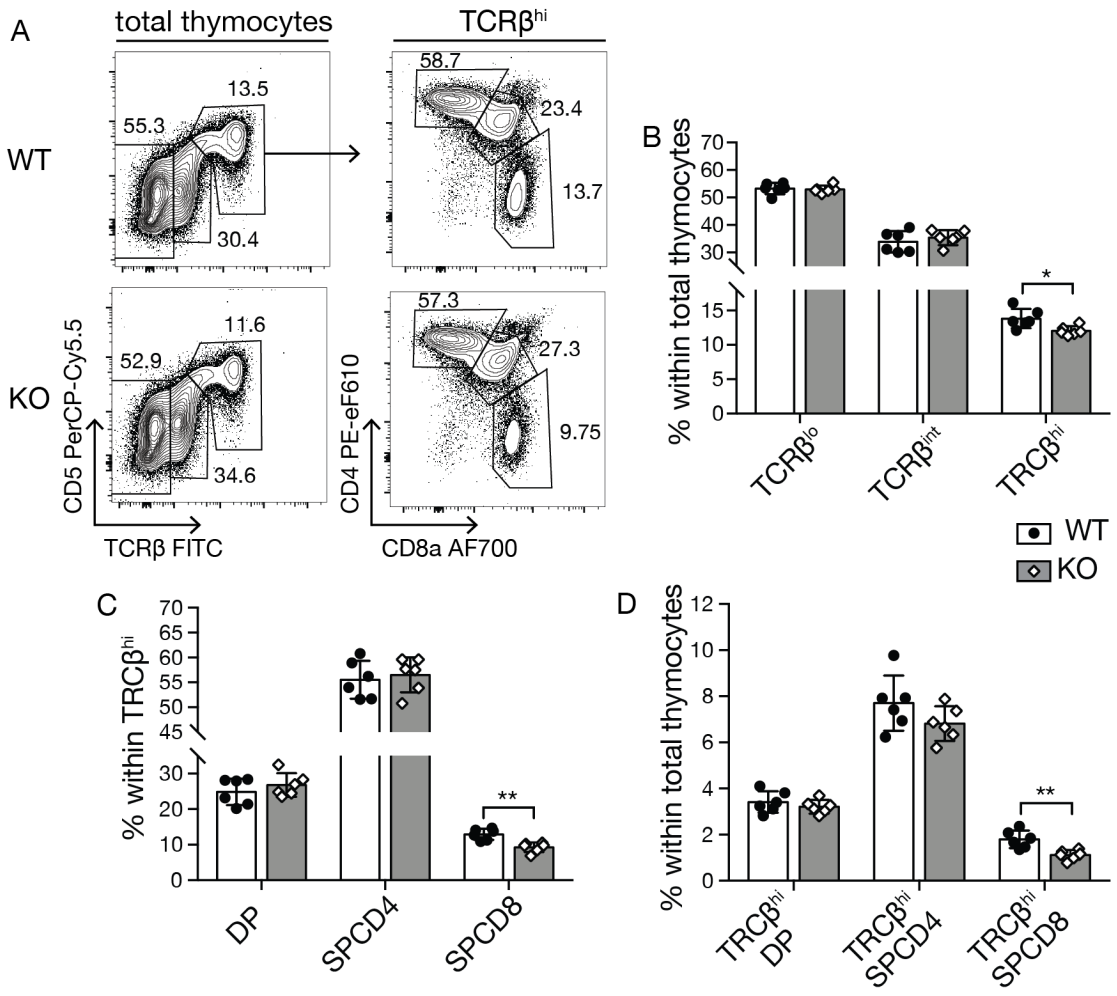

Figure 5.20: Lower frequency of TCRβ^{hi} cells due to reduced TCRβ^{hi} SPCD8 thymocytes in *Jarid2$^{TEC-/-}$* mice. **(A)** Representative FACS analysis shows the gating strategy for defining TCRβ^{lo}, TCRβ^{int} and TCRβ^{hi} populations using TCRβ and CD5 cell surface expression and gating for the DP, SPCD4 and SPCD8 subpopulations that are TCRβ^{hi}. **(B)** Bar graph shows relative frequencies of the indicated phenotypes within the population of total thymocytes. **(C-D)** Bar graphs show the relative frequencies of DP, SPCD4 and SPCD8 within TCRβ^{hi} thymocytes (C) and within the pool of total thymocytes (D). Data in graphs is pooled from two independent experiments: WT (*Jarid2$^{fl/fl}$*): n=6; KO (*Jarid2$^{TEC-/-}$*): n=6. Statistical analysis was done with two-tailed unpaired t-tests with correction for multiple comparisons. *p<0.05, **p<0.01, ***p<0.005, ****p<0.001.

± 1.4) in TCRβ^{hi} cells in the *Jarid2$^{TEC-/-}$* mice when compared to WT (Fig. 5.20B), which was accounted for by the decrease in SPCD8 thymocytes (Fig. 5.20C-D).

Within the CD8 lineage maturation, all stages, including immature (TCRβ^{hi} CCD7^{hi} CD8^{+} CD4^{lo}), semimature (CD24^{+} CD69^{+} SPCD8) to mature (CD24^{-} CD69^{-} SPCD8) stages, were reduced. Analysing the progression between the individual maturational stages, a significant yet partial block was identified at the transition from DP^{dull} to immature CD8

thymocytes in the *Jarid2*$^{TEC-/-}$ mice. A further, yet smaller partial developmental block was present at the transition from immature CD8 to semimature CD8. The transition from semimature to mature CD8 remained unchanged in the mice with TEC deficient in JARID2 expression. Contrary to the SPCD8 lineage, the post-selection maturation of SPCD4 thymocytes was not affected by the absence of JARID2 in TEC (Fig. 5.22A-D).

This analysis demonstrated that the reduced frequency in the CD8 lineage started once the cells had moved to the medulla and then remained low over subsequent maturational stages in the medulla with no compensational mechanisms, such as proliferative expansion, being able to correct the reduction.

This analysis also allows to assess the presence of mature T cells having recirculated from the periphery. The frequency of these cells in the thymus was unchanged between wild type and mutant mice (Fig. 5.22E).

5.4.4 Post selection maturation using MHC-I and CD69 expression confirms an equal reduction of SPCD8 across all their medullary developmental stages

There are different ways to analyse post-selection maturation. Hogquist et al. proposed using MHC-I and CD69 cell surface expression to define three sequential populations within the pool of TCRβ^{hi} SP thymocytes: SM, M1 and M2 [153]. SM are MHC-I^{lo} and CD69^{+}, M1 are MHC-I^{hi} and CD69^{+} and M2 are MHC-I^{hi}, CD69^{-}. M2 are the most mature SP thymocytes and are ready to leave the thymus. A scheme of the individual maturational stages is depicted in Figure 3.32.

I thus wanted to confirm the finding that the absence of JARID2 in TEC reduces the frequency of SPCD8 with this alternative analysis. The gating strategy is displayed in Figure 5.23A and F selecting a cut-off for TCRβ^{hi} cells that is higher in comparison to the previous analysis for post-positive selection maturation (Figs. 5.21 and 5.22). Thus, the DP^{dull} and immature stages of SP maturation are excluded from this analysis and only the later stages of medullary maturation are considered.

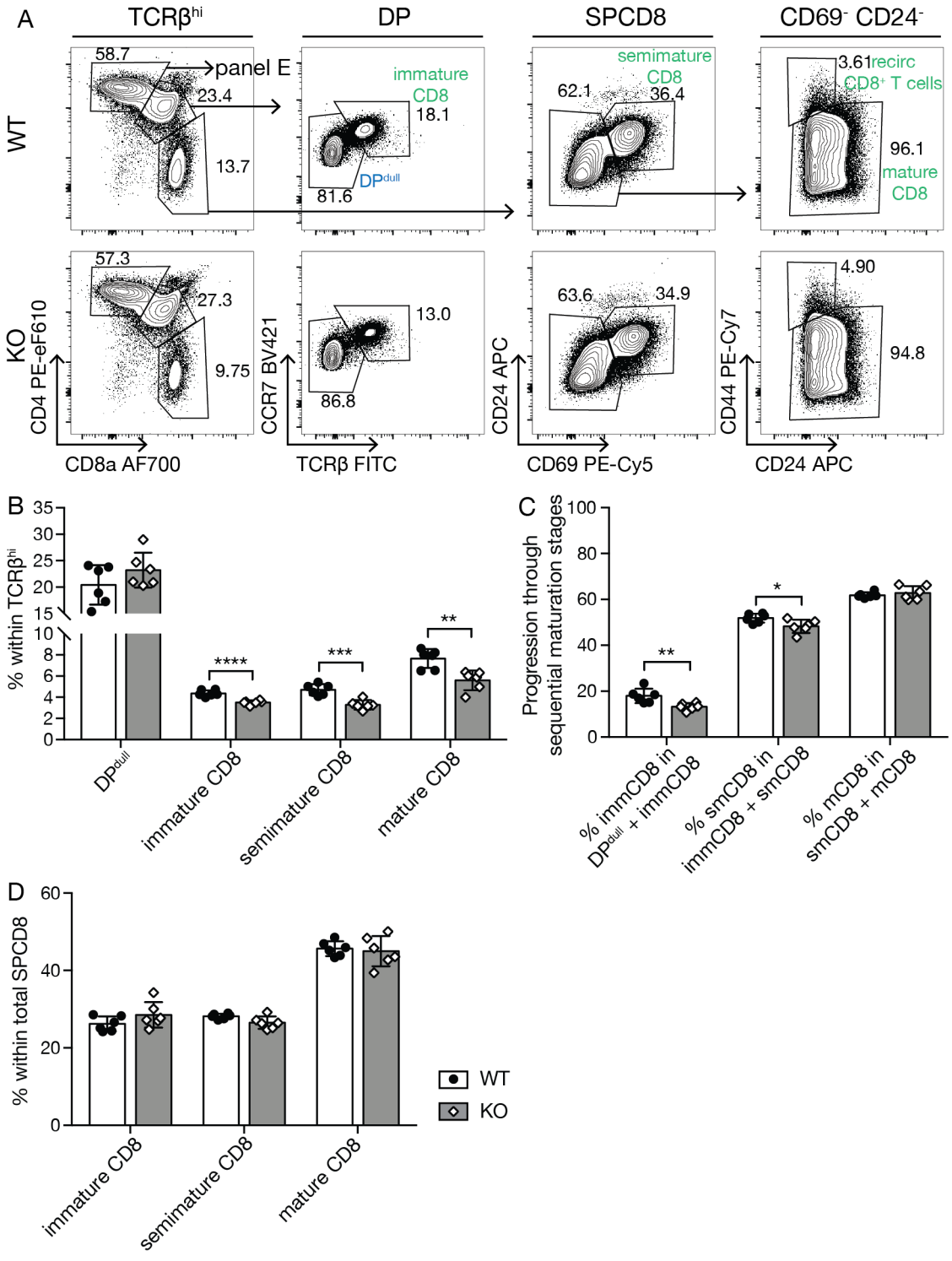

Figure 5.21: Partial maturational block in the progression of thymocytes from DP^{dull} to immature CD8 stage in *Jarid2*$^{TEC-/-}$ mice. **(A)** Representative FACS plots show the gating strategy for defining post selection maturation of SPCD8 within TCRβ^{hi} thymocytes. This was done according to the scheme depicted in Fig. 3.26 **(B)** Bar graph depicts the relative frequencies of the defined subpopulations within TCRβ^{hi} thymocytes. **(C)** Bar graph shows progression through sequential maturational stages as calculated by the following formula: (Stage B)/(Stage A+B)x100 where A is the maturation stage immediately before B. **(D)** Bar graph depicts relative frequencies of the defined subpopulations within the pool of total SPCD8 thymocytes. Data in graphs is pooled from two independent experiments: WT (*Jarid2*$^{fl/fl}$): n=6; KO (*Jarid2*$^{TEC-/-}$): n=6. Statistical analysis was done with two-tailed unpaired t-tests with correction for multiple comparisons. *p<0.05, **p<0.01, ***p<0.005, ****p<0.001.

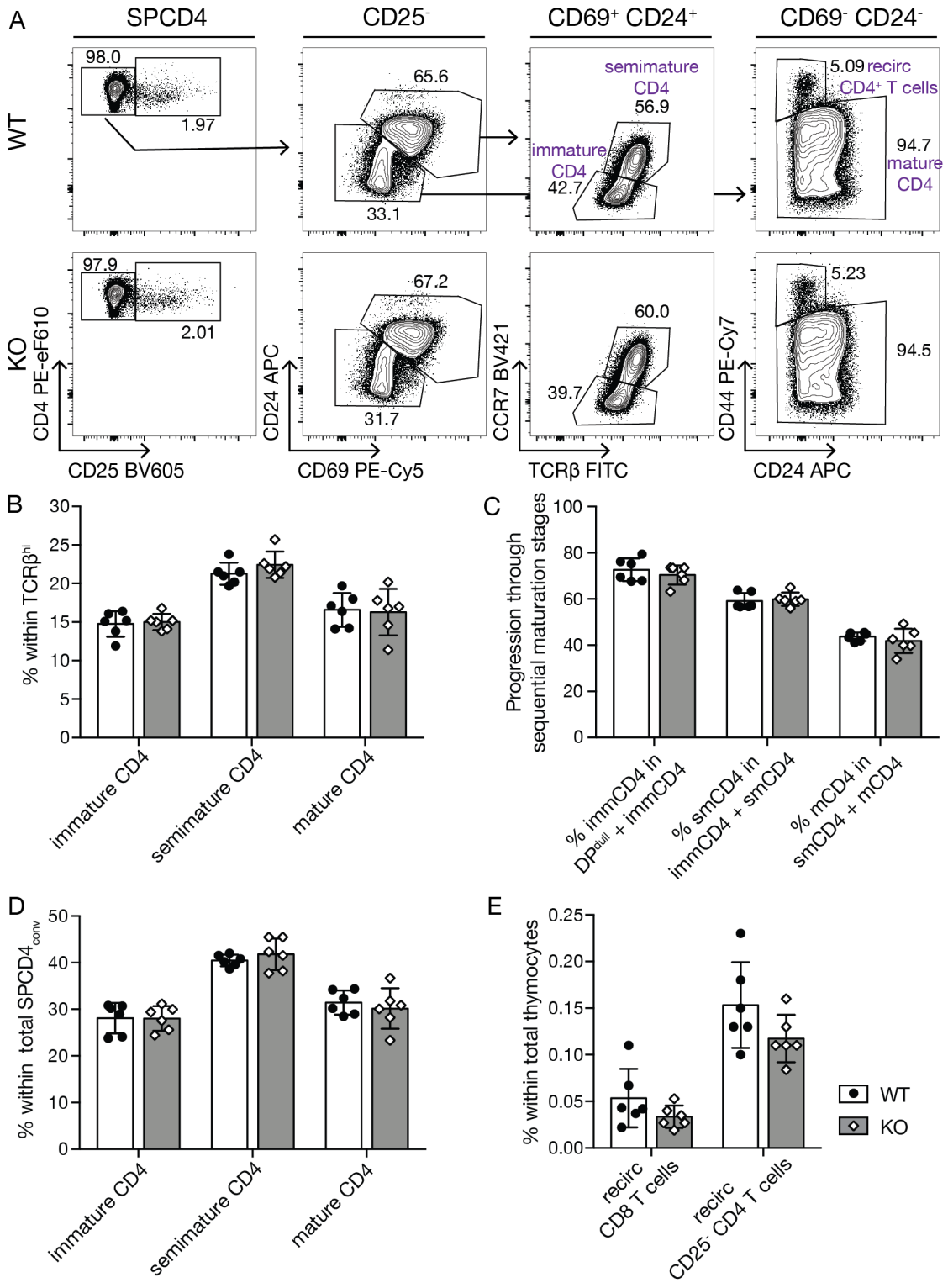

Figure 5.22: Unchanged maturation of SPCD4 in *Jarid2*$^{TEC-/-}$ mice. (A) Representative FACS plots show the gating strategy for defining post selection maturation of SPCD4 within TCRβ^{hi} thymocytes. **(B)** Bar graphs depict the relative frequencies within TCRβ^{hi} thymocytes. **(C)** Bar graph shows the progression through sequential maturation stages as calculated by the following formula: (Stage B)/(Stage A+B)x100 where A is the maturation stage immediately before B. (D) Bar graph shows the relative contribution of immature, semimature and mature SPCD4 to the total of CD25$^-$ SPCD4. **(E)** Bar graph shows the percentage of recirculating CD8 T cells and conventional (CD25$^-$) CD4 T cells within total thymocytes. Data in graphs is pooled from two independent experiments: WT (*Jarid2*$^{fl/fl}$): n=6; KO (*Jarid2*$^{TEC-/-}$): n=6. Statistical analysis was done with two-tailed unpaired t-tests with correction for multiple comparisons.

This different gating strategy demonstrated a reduction of maturational stages of the CD8 lineage in the medulla corroborating the previous result (Fig. 5.23). As all three populations were reduced, the progression from SM to M1 and M2 was undisturbed (Fig. 5.23E). In contrast, SPCD4 maturation in the medulla was unaffected by the lack of JARID2 expression in TEC (Fig. 5.23F). Taken together, these results confirm the analysis in Chapter 5.4.3 suggesting a reduction in CD8 lineage in the medulla.

Given the decreased frequency of SPCD8 thymocytes at all maturational stages in the medulla, I next determined the expression of genes known to control the progression of immature thymocytes to the M1 and M2 stages and responsible for thymic egress using qPCR [153]. For the M1 stage, the expression of *cFlip*, *Tak1*, *Nemo* and *Relb* was tested, as these genes are important for thymocyte survival [201–204], whereas for the M2 stage, the expression of genes essential for thymic egress, *Pak2*, *Foxo1*, *Klf2* and *S1pr1*, was determined [205].

As demonstrated in Figure 5.24, transcript copy numbers were comparable for WT and $Jarid2^{TEC-/-}$ SPCD4 and SPCD8 thymocytes at the M1 and M2 maturational stage. This suggests that despite being reduced in their frequency SPCD8 are maturing normally and are able to express the factors necessary for thymic egress.

5.4.5 TNFα licensing of SPCD8 is unchanged

In their last maturational stages before thymocytes egress from the thymus, they are licenced to express and secrete cytokines in response to TCR-mediated signals [206]. These mature thymocytes produce a broad range of cytokines including TNFα, IL-2, IL-4 and γ-IFN, albeit at a lower level than their counterpart of mature naïve peripheral T cells. Known as the cytokine licensing, this functional feature of mature thymocytes can be assessed by quantifying the frequency of thymocytes expressing TNFα after 5 h of stimulation with αCD3 and αCD28. Mature thymocytes can be classified by their surface expression of MHC-I and CD69 into SM, M1 and M2 stages (see Chapter 5.4.4),

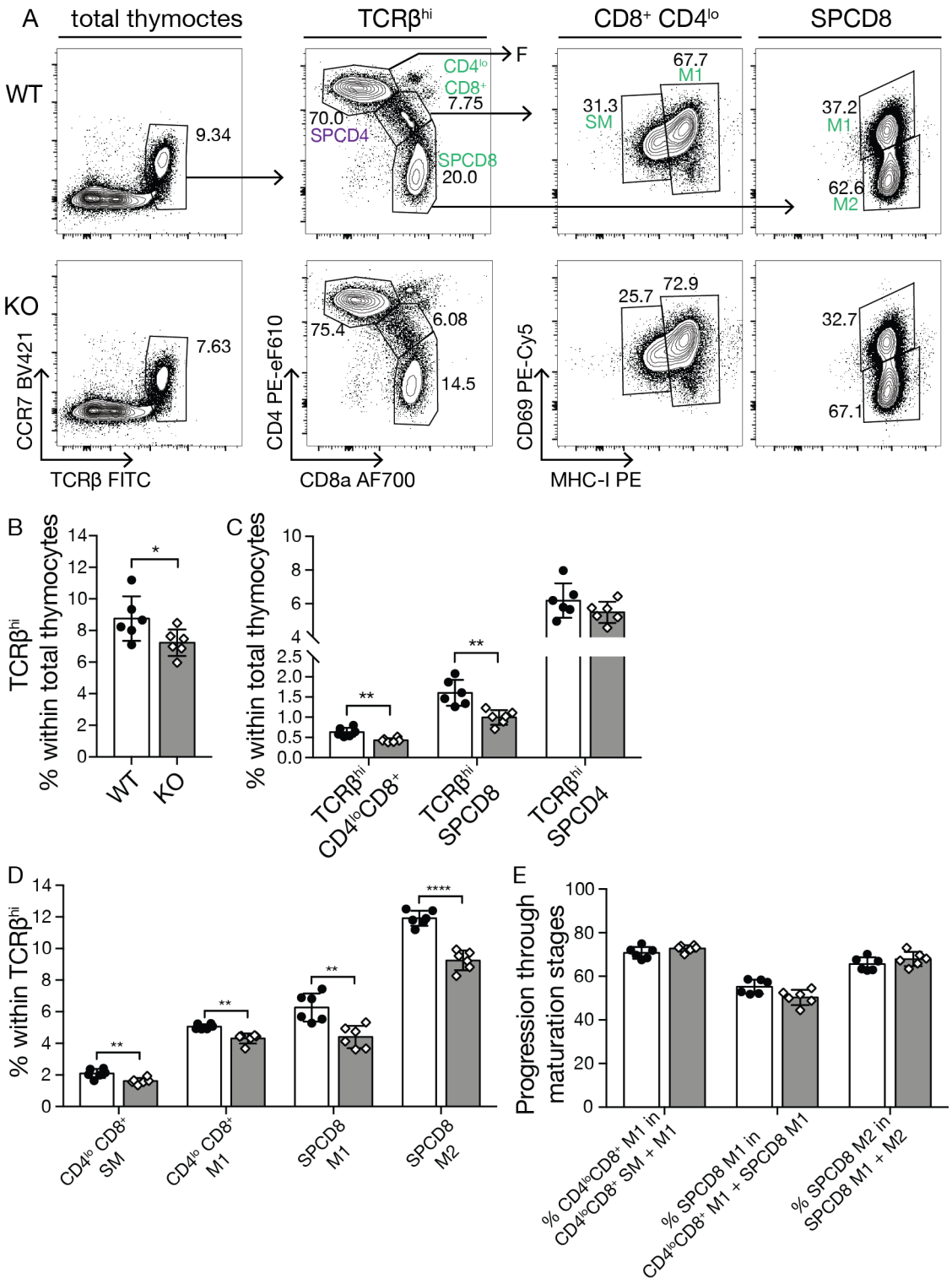
A
total thymoctes
TCRβhi
CD8+ CD4lo
SPCD8
WT
KO
9.34
7.63
CD4lo
CD8+
7.75
70.0
SPCD4
SPCD8
20.0
67.7
M1
31.3
SM
37.2
M1
62.6
M2
75.4
6.08
14.5
25.7
72.9
32.7
67.1
CCR7 BV421
TCRβ FITC
CD4 PE-eF610
CD8a AF700
CD69 PE-Cy5
MHC-I PE
B
% within total thymocytes
TCRβhi
WT
KO
C
% within total thymocytes
TCRβhi CD4loCD8+
TCRβhi SPCD8
TCRβhi SPCD4
D
% within TCRβhi
CD4lo CD8+ SM
CD4lo CD8+ M1
SPCD8 M1
SPCD8 M2
E
Progression through maturation stages
% CD4loCD8+ M1 in CD4loCD8+ SM + M1
% SPCD8 M1 in CD4loCD8+ M1 + SPCD8 M1
% SPCD8 M2 in SPCD8 M1 + M2

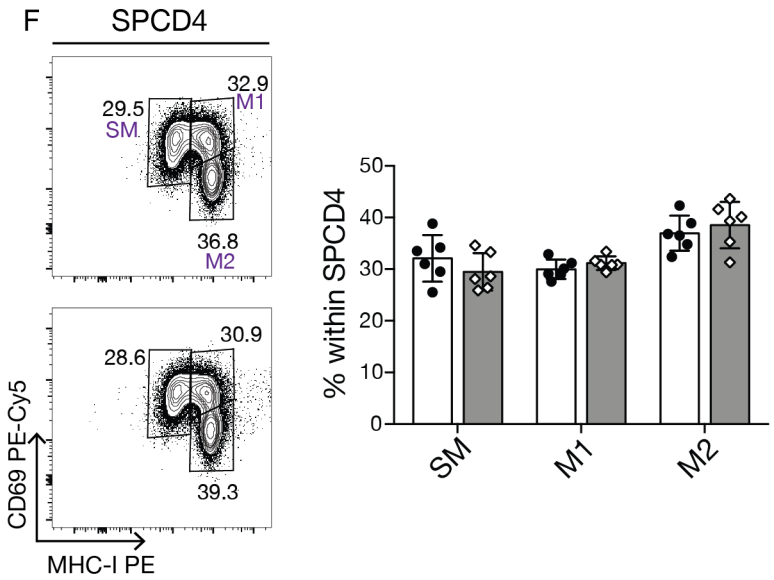

Figure 5.23: The Frequency of CD8 SM, M1 and M2 stages is reduced in *Jarid2*$^{TEC-/-}$ mice. **(A)** Representative FACS plots show the gating strategy to identify SM, M1, M2 post-selection maturation stages of SPCD8 within TCRβ^{hi}. **(B)** Bar graph displays the relative frequency of TCRβ^{hi} cells within the population of total thymocytes. **(C)** Bar graph displays relative frequencies of TCRβ^{hi} CD8^{+} CD4^{lo} , SPCD8 and SPCD4 within the population of total thymocytes. **(D)** Bar graphs display relative frequencies of SM CD8^{+} CD4^{lo}, M1 CD8^{+} CD4^{lo} M1 SPCD8 and M2 SPCD8 within TCRβ^{hi} thymocytes. **(E)** Bar graphs demonstrate the progression along sequential maturational stages of medullary CD8 T cells as calculated by the following formula: (Stage B)/(Stage A+B)x100 where A is the maturation stage immediately before B. **(F)** Representative FACS plots and bar graphs show relative frequencies of SM, M1 and M2 within SPCD4 TCRβ^{hi}. Data in graph is pooled from two independent experiments: WT (*Jarid2*$^{fl/fl}$): n=6; WT (*Jarid2*$^{TEC-/-}$): n=6. Statistical comparison was done with two-tailed unpaired t-tests. *p<0.05, **p<0.01, ***p<0.005, ****p<0.001.

whereby cells in the M2 stage and to a lesser extent in the M1 stage produce detectable amounts of TNFα [111].

The frequency of TNFα secreting SPCD8 thymocytes at the M1 and M2 was comparable for WT and *Jarid2*$^{TEC-/-}$ mice, suggesting that the post-selectional maturation of CD8 lineage thymocytes was not compromised with regards to the cells' function (Fig. 5.25). In contrast the corresponding analysis of CD4 lineage revealed a small statistically significant increase in TNFα production in the *Jarid2*$^{TEC-/-}$ mice when compared to the WT animals (M1: WT = 1.8 % vs KO = 2.1 %; M2: WT = 11.7 % vs KO = 13.1 %) (Fig. 5.26).

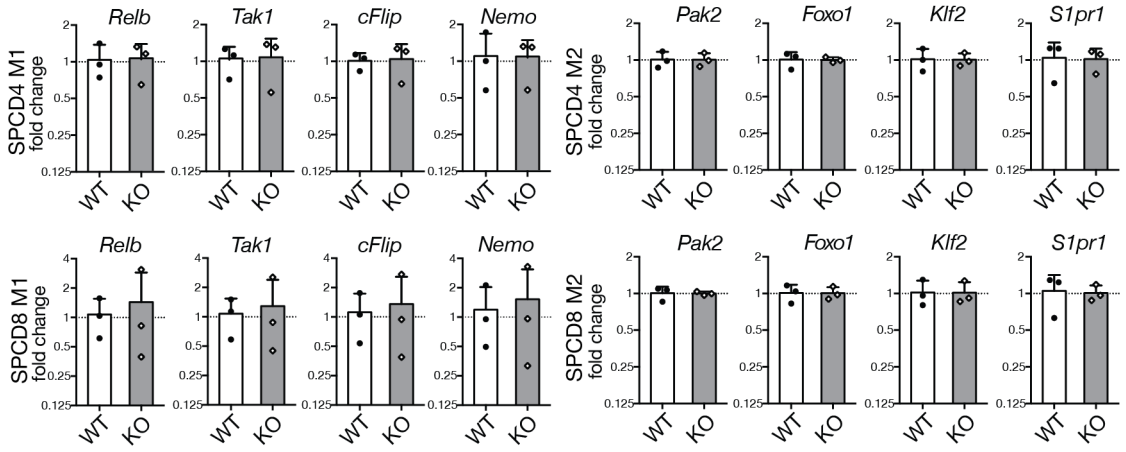

Figure 5.24: Expression of selected genes relevant for late stage thymocyte maturation and thymic egress were unchanged in *Jarid2*$^{TEC-/-}$ mice. M1 and M2 SPCD4 and SPCD8 thymocytes were sorted and analysed by qPCR for the expression of the indicated genes. Data was analysed using the $2^{-\Delta\Delta Ct}$ method with normalisation to *Gapdh* expression and setting expression in WT to 1. The experiment was done with mice at 5 weeks of age. Each data point represents an individual mouse: WT (*Jarid2*$^{fl/fl}$): n=3; KO (*Jarid2*$^{TEC-/-}$): n=3. Statistical analysis was done with two-tailed unpaired t-tests.

5.4.6 Medullary negative selection is increased in *Jarid2*$^{TEC-/-}$ affecting both SPCD4 and SPCD8 thymocytes.

T cells with a self-reactive TCR carry the risk of initiating autoimmune reactions once they encounter their cognate antigen in the periphery. It is one of the central tasks of the thymus to prevent the escape of self-reactive thymocytes into the periphery. This process – called negative selection – is effected in different sequential waves, which have been described in previous chapters (see Fig. 3.34). The first waves take place in the cortex (thus also referred to as cortical negative selection) while the second wave takes place in the medulla (knows as medullary negative selection).

Thymocytes that receive a strong signal through their TCR secondary to a high-affinity interaction with their cognate pMHC complex are negatively selected and consequently undergo programmed cell death. Thymocytes undergoing negative selection in the cortex (wave 1), can be identified by their expression of the markers PD-1 and HELIOS, whereas during wave 2, negatively selected thymocytes in the medulla express high levels of HELIOS [154]. The gating strategy to assess thymocytes undergoing wave 1 and wave 2 negative selection is displayed in Figure 5.27A-B.

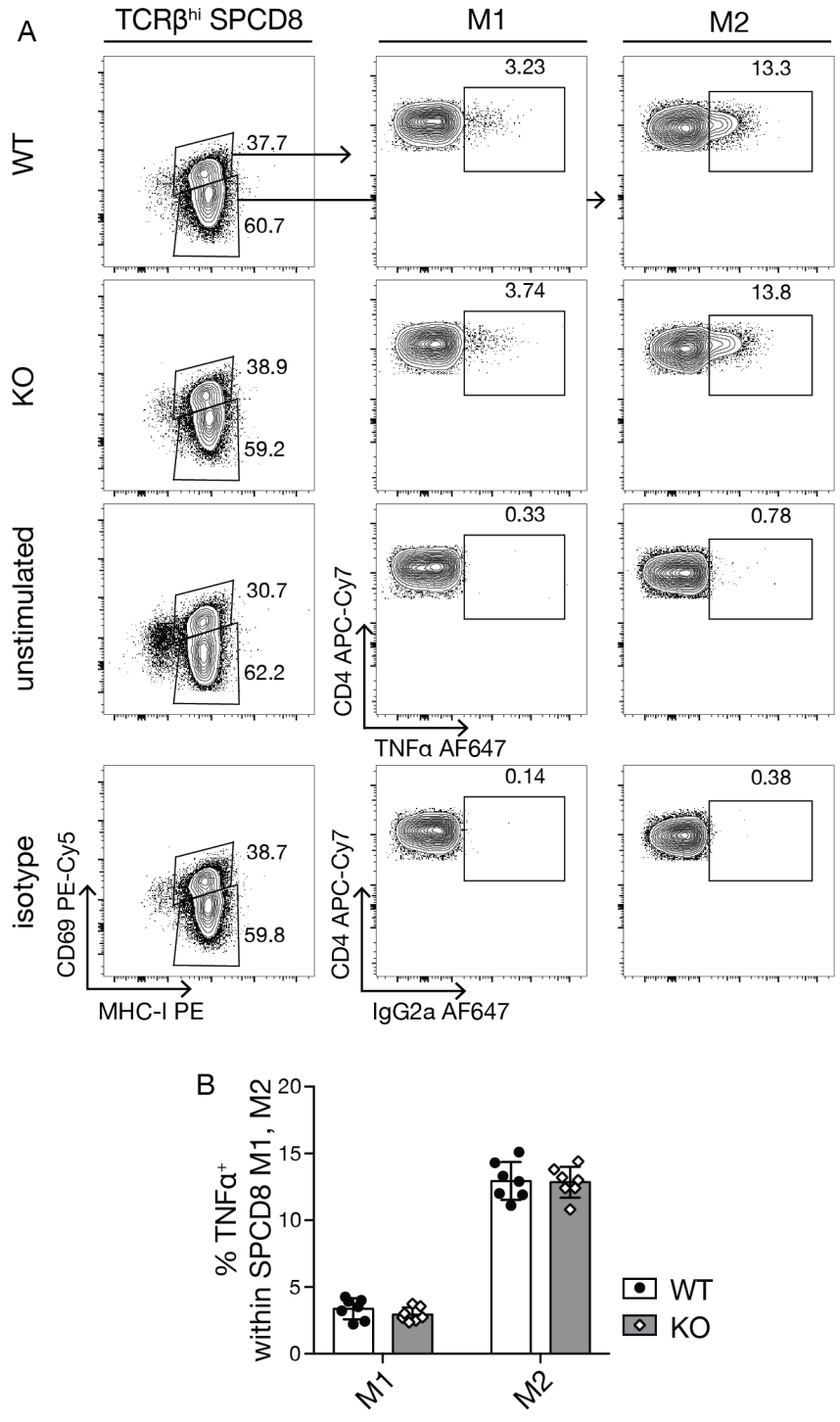

Figure 5.25: M1 and M2 SPCD8 educated on TEC with JARID2 KO are able to produce TNFα upon stimulation. (A) Representative FACS plots show the gating strategy to define M1 and M2 populations and their gating for TNFα expression. **(B)** Bar graphs show relative frequencies of TNFα$^+$ cells. Data in graph is pooled from two independent experiments: WT (*Jarid2*$^{fl/fl}$): n=7; KO (*Jarid2*$^{TEC-/-}$): n=7. Statistical comparison was done with two-tailed unpaired t-tests. *p<0.05, **p<0.01.

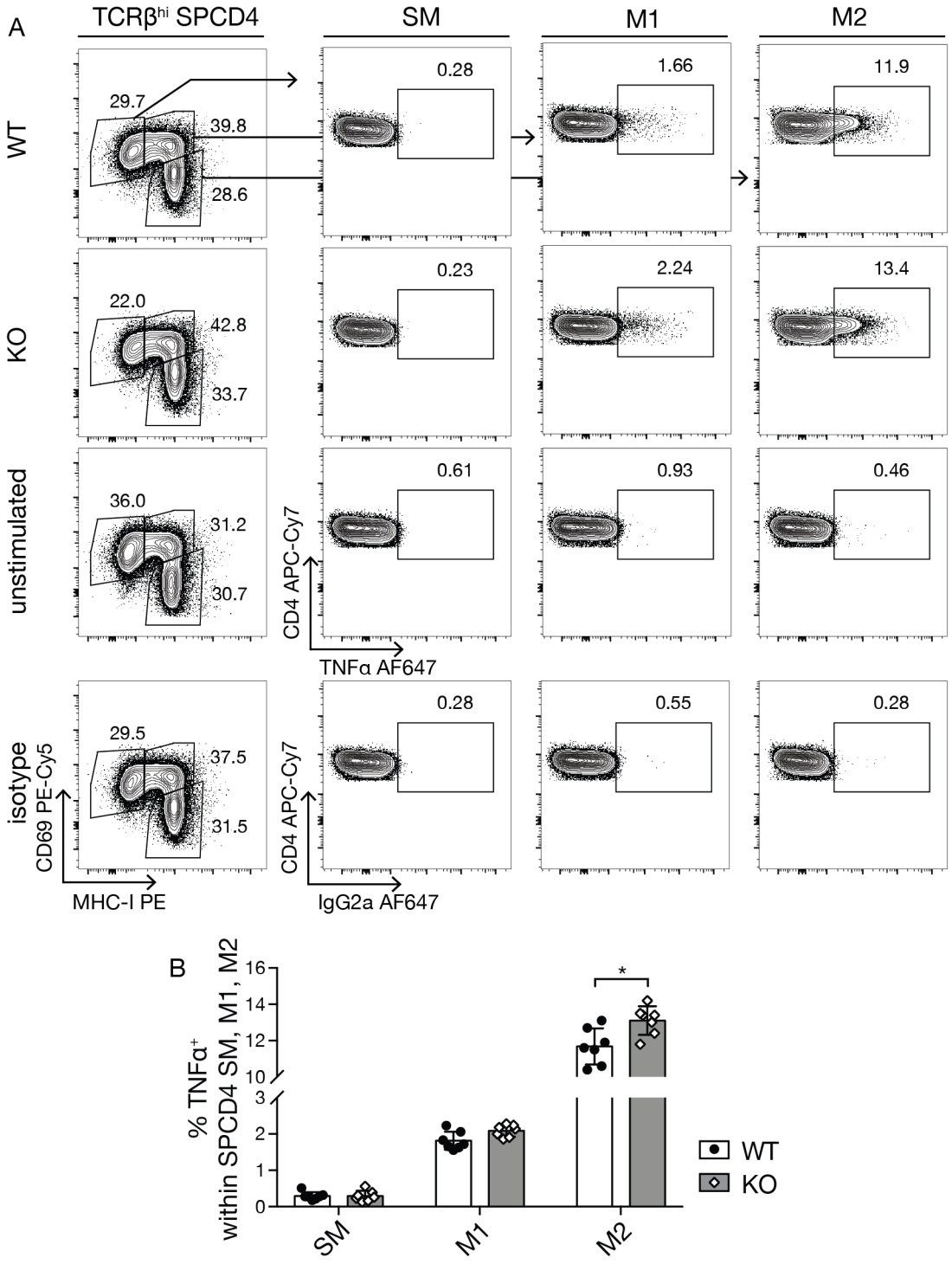

Figure 5.26: M2 SPCD4 educated on TEC with JARID2 KO are able to produce more TNFα upon stimulation. (A) Representative FACS plots show the gating strategy to define SM, M1 and M2 populations and their gating for TNFα expression. **(B)** Bar graphs show relative frequencies of TNFα$^+$ cells. Data in graph is pooled from two independent experiments: WT (*Jarid2*$^{fl/fl}$): n=7; KO (*Jarid2*$^{TEC-/-}$): n=7. Statistical comparison was done with two-tailed unpaired t-tests. *p<0.05, **p<0.01.

The aim of this analysis was to assess how a lack of JARID2 in TEC affects their capacity to enforce negative selection. No significant changes were detected in wave 1 of negative selection between WT and *Jarid2*$^{TEC-/-}$ animals (Fig. 5.27C). In contrast, wave 2 negative selection was increased in *Jarid2*$^{TEC-/-}$ mice for both CD4 and CD8 lineages (Fig. 5.27D-E).

This result suggests that the increased MHC-I expression within mTEC and the higher percentage of MHC-II^{hi} and AIRE^{+} cells with a higher expression level of AIRE protein per cell might provide a more efficient environment for medullary negative selection. The increased frequency of negatively selected cells in the medulla might explain the reduction in the SPCD8 in *Jarid2*$^{TEC-/-}$ thymi. However, even though medullary SPCD4 negative selection was increased as well, SPCD4 populations show no reduced cellularity. However, SPCD4 might have a higher potential to compensate for increased negative selection by increased cell proliferation.

5.4.7 T_{reg} cell generation in the thymus is unaltered, but there are more ICOS^{+} CD103^{+} cells within the recirculating T_{reg} cell population

Thymocytes with a high-affinity TCR recognising pMHC in the thymic microenvironment, can adopt a cell fate alternative to negative selection, namely differentiation into regulatory T (T_{reg}) cells. Given the increase in negative selection, I wanted to see if T_{reg} cell generation was altered as well.

Intrathymic T_{reg} cells are identified as FOXP3^{+} CD25^{+} SPCD4 thymocytes and their immediate precursors include FOXP3^{+} CD25^{-} and FOXP3^{-} CD25^{+} thymocytes. The pool of intrathymic T_{reg} cells is composed of two distinct subpopulations, namely the newly *in situ* generated T_{reg} cells and mature T_{reg} cells that have recirculated from the periphery to the thymus. Studies with genetically marked mice have shown that around half of FOXP3^{+} CD25^{+} SPCD4 thymocytes have recirculated from the periphery back to the thymus where a few of the latter can chose to adapt a FOXP3^{+} CD25^{-} and FOXP3^{-} CD25^{+} phenotype [159].

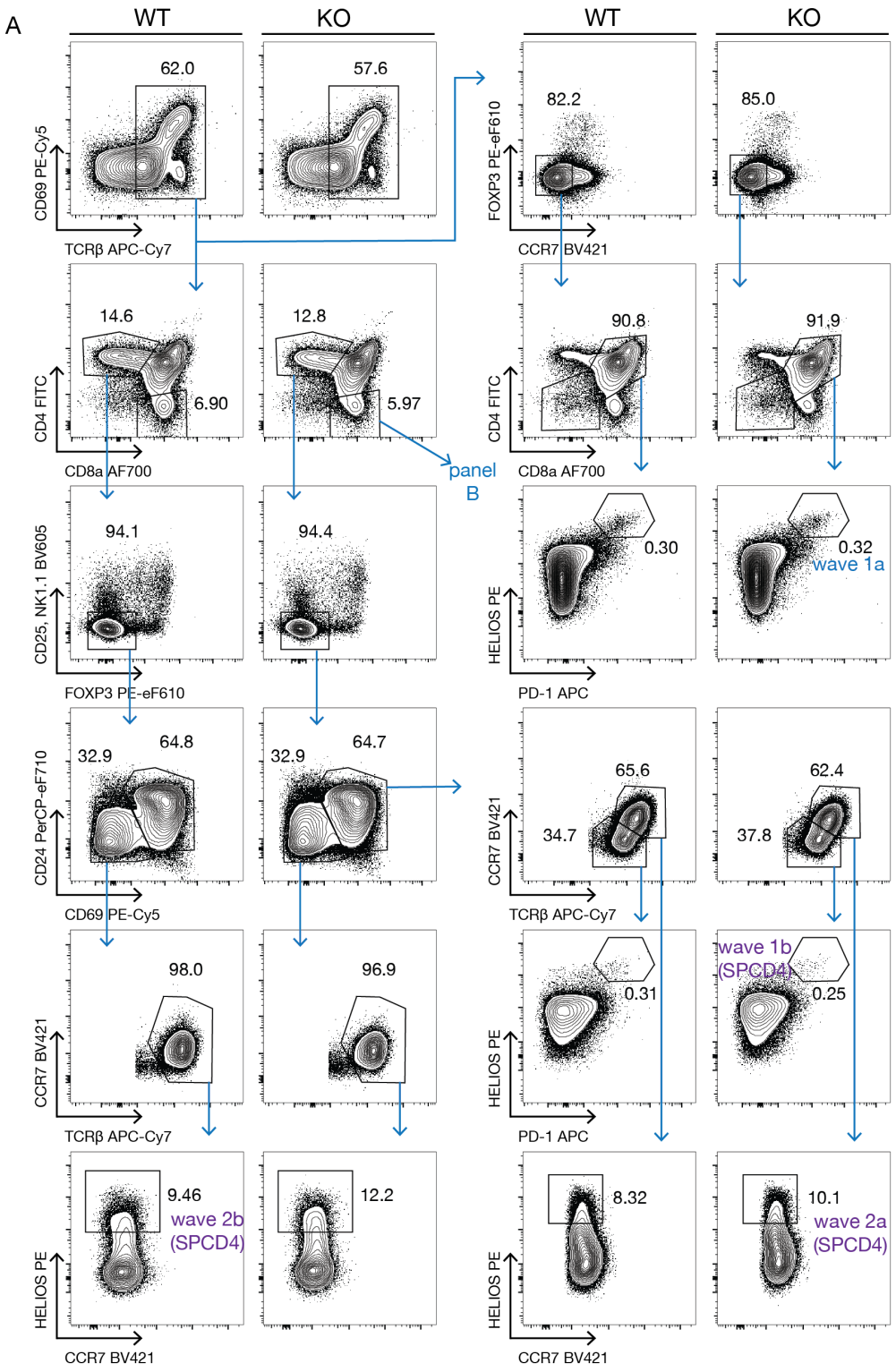
A
WT
KO
WT
KO
62.0
57.6
82.2
85.0
CD69 PE-Cy5
TCRβ APC-Cy7
FOXP3 PE-eF610
CCR7 BV421
14.6
6.90
12.8
5.97
90.8
91,9
CD4 FITC
CD8a AF700
panel B
94.1
94.4
0.30
0.32
wave 1a
CD25, NK1.1 BV605
FOXP3 PE-eF610
HELIOS PE
PD-1 APC
32.9
64.8
32.9
64.7
65.6
34.7
62.4
37.8
CD24 PerCP-eF710
CD69 PE-Cy5
CCR7 BV421
TCRβ APC-Cy7
98.0
96.9
0.31
wave 1b (SPCD4)
0.25
CCR7 BV421
TCRβ APC-Cy7
HELIOS PE
PD-1 APC
9.46
wave 2b (SPCD4)
12.2
8.32
10.1
wave 2a (SPCD4)
HELIOS PE
CCR7 BV421
CCR7 BV421

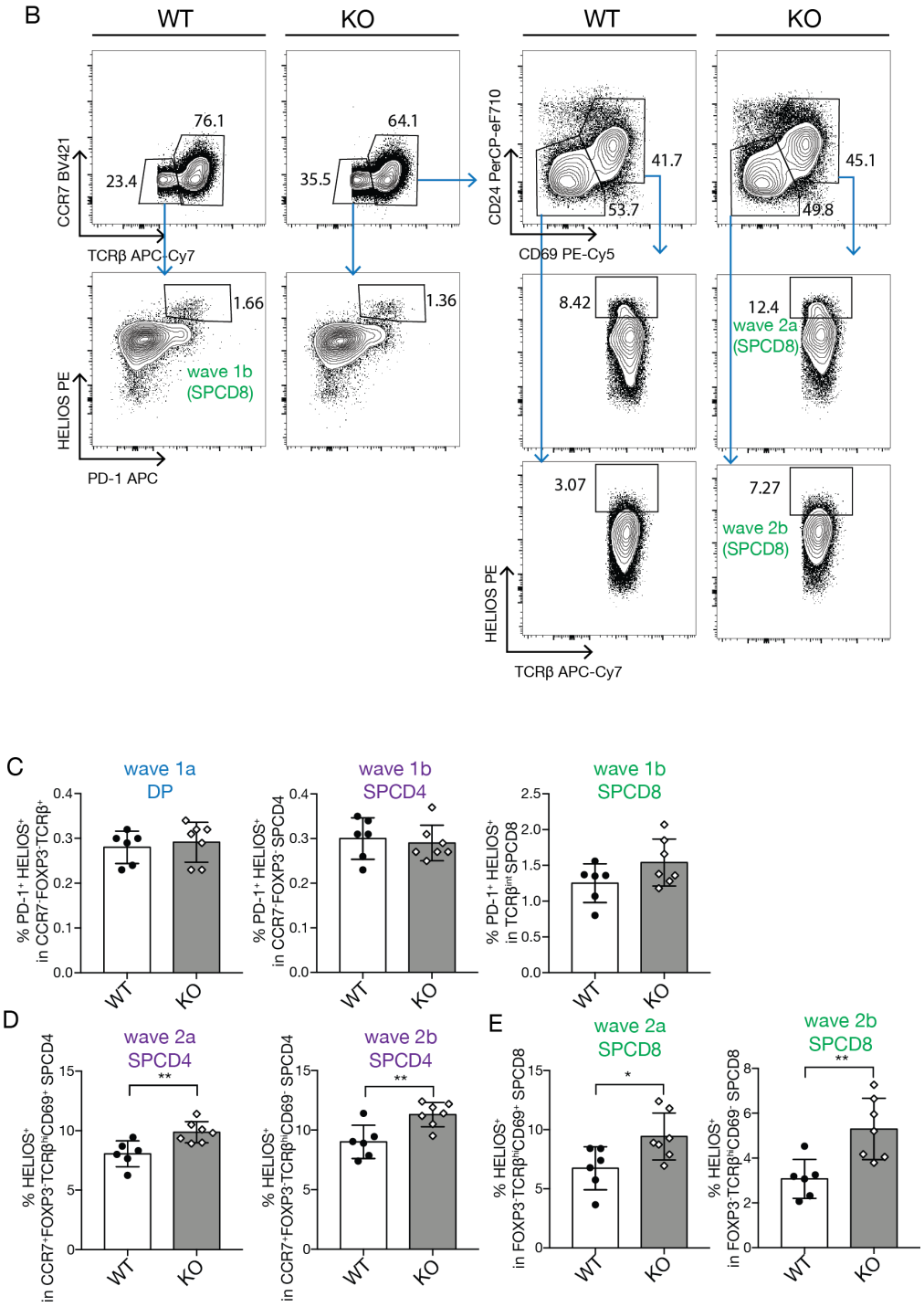

Figure 5.27: Frequency of negatively selected cells in medullary wave 2 is increased in *Jarid2*$^{TEC-/-}$ mice. (A, B) Representative FACS plots depict the gating strategy for defining the different waves of negative selection in the thymus. **(C)** Bar graphs show frequencies of wave 1. **(D)** Bar graphs depict frequencies of wave 2 in SPCD4 cells. **(D)** Bar graphs depict relative frequencies of wave 2 in SPCD8 cells. Data in graph is pooled from two independent experiments: WT (*Jarid2*$^{fl/fl}$): n=6; KO (*Jarid2*$^{TEC-/-}$): n=7. Statistical comparison was done with two-tailed unpaired t-tests. *p<0.05, **p<0.01, ***p<0.005.

The detection of recirculating T_{reg} cells has recently been simplified as the cell surface detection of the chemokine receptor CCR6 has been identified as a good marker for recirculated T_{reg} [161]. CCR6 senses CCL20 [162], which is expressed by mature mTEC in an AIRE-dependent fashion.

I therefore used the CCR6 expression on T_{reg} cells to determine their origin (Fig. 5.28), which I validated by probing for other markers, such as ICOS and CD103 that are only expressed in recirculating T_{reg} cells, and CD24 and CCR7 that are more highly expressed in newly generated T_{reg} cells [158, 207]. As expected, $ICOS^+$ $CD103^+$ were only present in $CCR6^+$ T_{reg} (Fig. 5.28A), while the expression levels of CD24 and CCR7 were higher in $CCR6^-$ T_{reg} as compared to $CCR6^+$ T_{reg} (Fig. 5.28B). Additionally, Figure 5.28C shows that the majority of $CCR6^+$ T_{reg} (in blue) falls within the gate of "recirculated" T cells as defined by CCR7 or CD24 and CD44.

The frequencies of T_{reg} cells and their immediate precursor populations ($FOXP3^+$ $CD25^-$, $FOXP3^-$ $CD25^+$) were unchanged when comparing WT and mutant animals (Fig. 5.29B). The fraction of recirculated and newly generated T_{reg} cells as defined by CCR6 was furthermore also unaltered (Fig. 5.29C). However, among the recirculating T_{reg} cells, there were slightly more $ICOS^+$ $CD103^+$ T_{reg} cells in mice with TEC devoid of JARID2 expression (15.37 % $\pm$ 2.55 vs 11.85 % $\pm$ 2.31) (Fig. 5.29D). The combined expression of ICOS and CD103 is characteristic for a lymph node specific differentiation stage characterised by a high suppressive function [158]. It remains to be determined which role activated T_{reg} cells with an $ICOS^+$ $CD103^+$ phenotype play in thymic function.

5.5 The peripheral T cell compartment in *Jarid2$^{TEC-/-}$* mice

The lack of JARID2 in TEC expression has caused detectable changes in thymocyte development in the medulla, namely an increase in negative selection and a reduction in SPCD8. I thus wanted to see if the alterations in the thymus impact the peripheral T cell compartment.

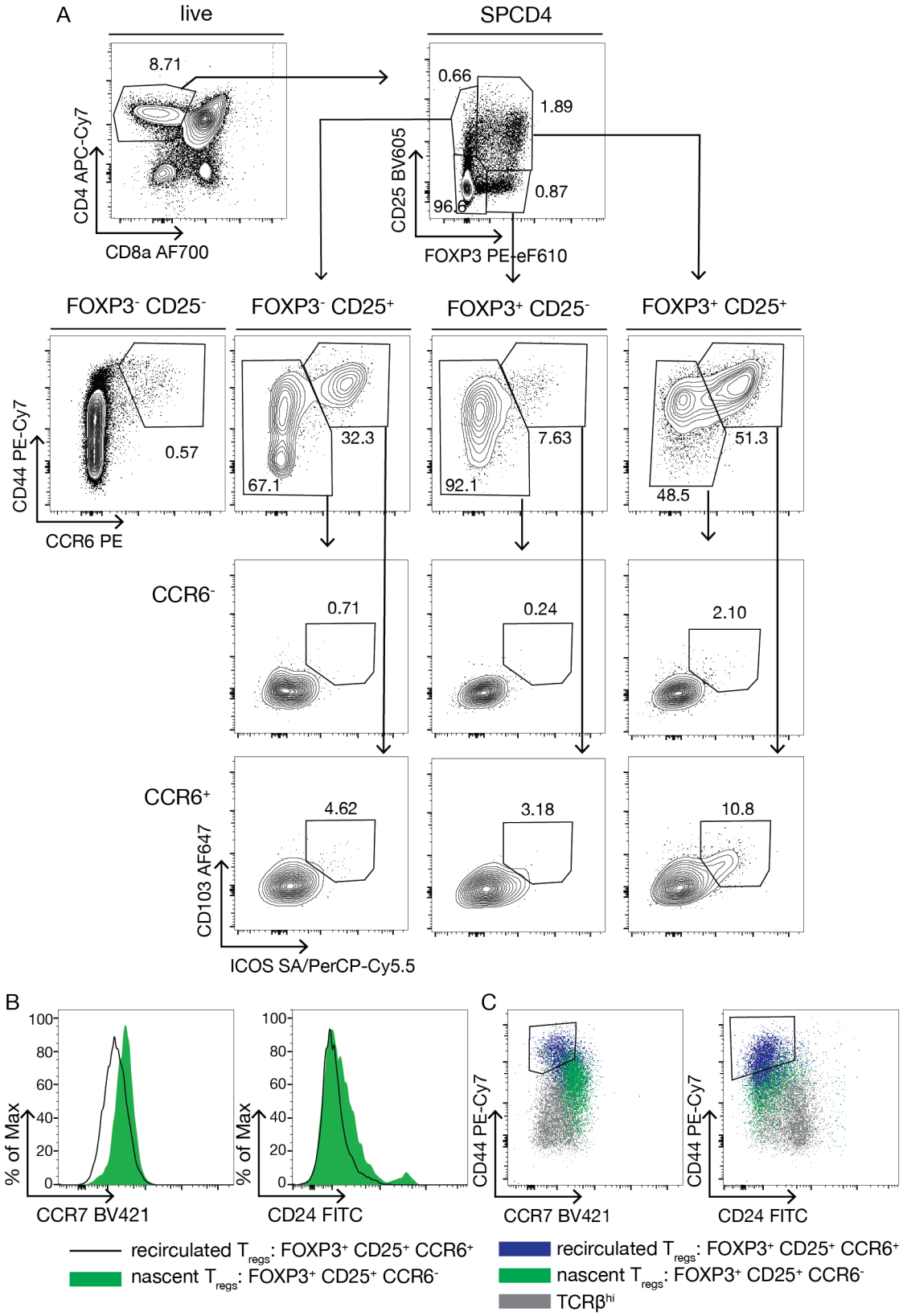

Figure 5.28: Gating strategy for identifying newly generated and recirculating T_{reg} cells. (A) Representative FACS plots show the gating of thymic T_{reg} cells using CCR6 expression to identify recirculating T_{reg} cells. **(B)** Represenative histograms for CCR7 and CD24 expression within the population of $CCR6^-$ and $CCD6^+$ T_{reg} cells. **(C)** FACS plots show total $TCR\beta^{hi}$ (gray), newly generated T_{reg} (green) and recirculated T_{reg} (blue).

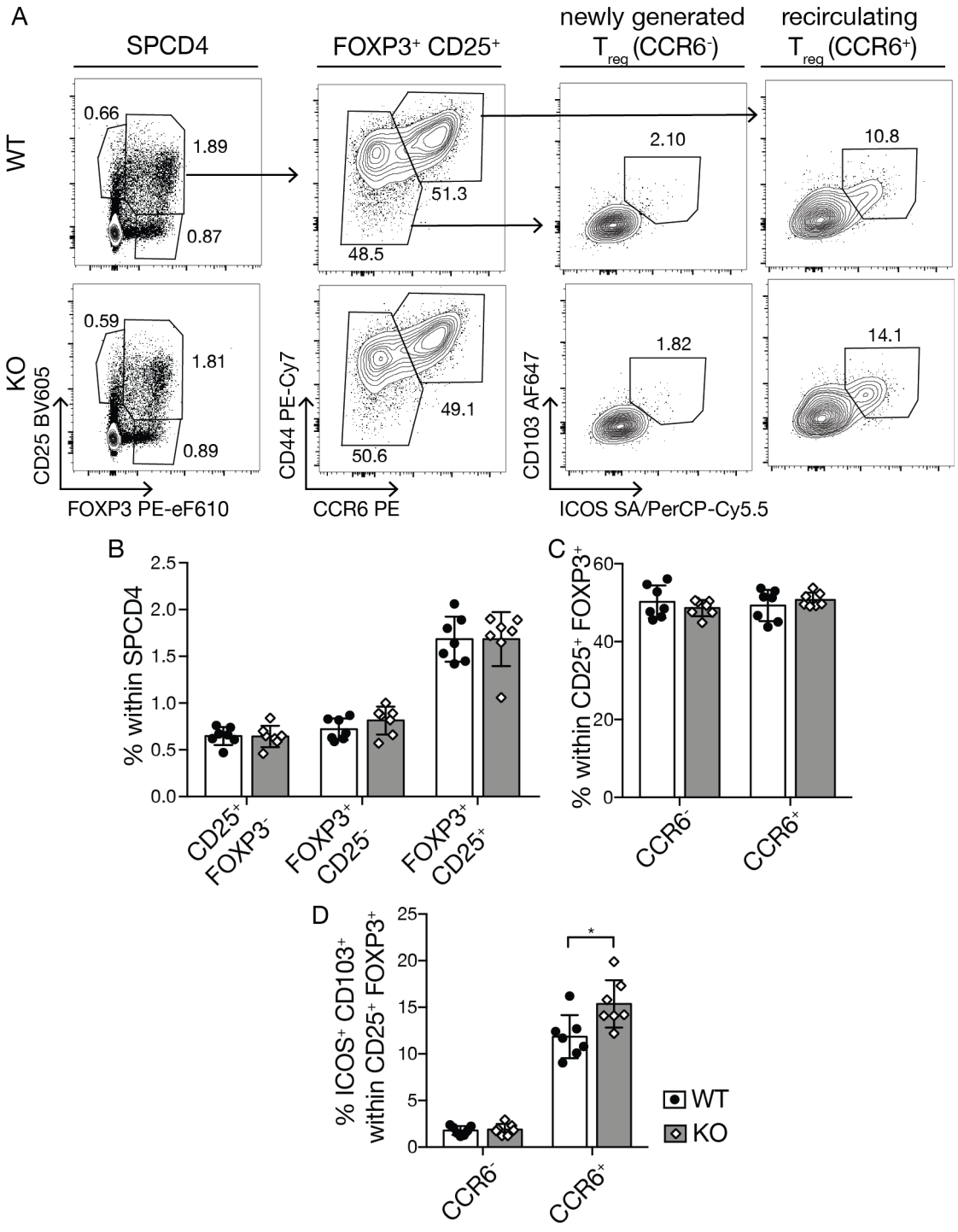

Figure 5.29: Increased population of ICOS$^+$ CD103$^+$ recirculating T$_{reg}$ cells in the thymus of *Jarid2$^{TEC-/-}$* mice. **(A)** Representative FACS plots show the gating strategy to define the different thymic T$_{reg}$ cell populations. **(B)** Bar graph shows the relative frequencies of T$_{reg}$ cells within SPCD4. **(C)** Bar graphs depicts the frequencies of newly generated (CCR6-) and recirculated (CCR6$^+$) cells within CD25$^+$ FOXP3$^+$ T$_{reg}$ cells. **(D)** Bar graph depicts relative frequencies of ICOS$^+$ CD103$^+$ cells within CCR6$^-$ (newly generated) and CCR6$^+$ (recirculated) CD25$^+$ FOXP3$^+$ T$_{reg}$ cells. Data in graph is pooled from two independent experiments: WT (*Jarid2$^{fl/fl}$*): n=6; KO (*Jarid2$^{TEC-/-}$*): n=7. Statistical comparison was done with two-tailed unpaired t-tests with correction for multiple comparisons. *p<0.05.

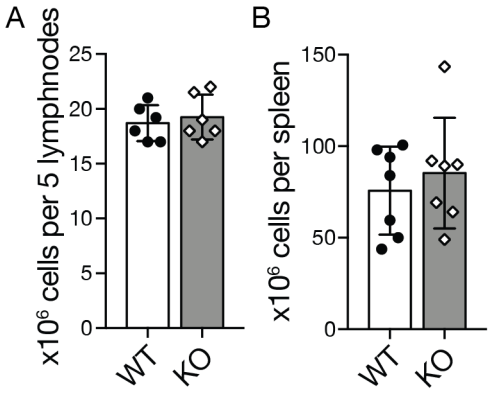

Figure 5.30: Cellularity of lymph nodes and spleen are unchanged in *Jarid2*$^{TEC-/-}$ mice. (A) Bar graph depicts cellularity of five lymph nodes combined after mechanic disruption and represents two independent experiments (WT (*Jarid2*$^{fl/fl}$): n=6; KO (*Jarid2*$^{TEC-/-}$): n=6). **(B)** Bar graph depicts the total splenic cellularity of the spleen after red blood cell lysis and represents two independent experiments (WT (*Jarid2*$^{fl/fl}$): n=7; KO (*Jarid2*$^{TEC-/-}$): n=7). Statistical comparison was done with two-tailed unpaired t-tests.

5.5.1 Reduction in CD8$^+$ T cells in the lymph nodes of mice with a TEC-specific JARID2 KO

To probe the peripheral T cell compartment in WT and *Jarid2*$^{TEC-/-}$, lymph nodes were isolated and analysed by flow cytometry. Though comparing the size of lymph nodes isolated from specific anatomical locations is not a quantitatively robust analysis, this did not reveal any apparent size differences between the lymph nodes isolated from WT and KO mice. Moreover, the cellularity of mechanically disrupted lymph nodes was comparable between the mouse lines (Fig. 5.30A), which was in keeping with the analysis of total splenic cellularity in the two mouse strains (Fig. 5.30).

The lymph nodes of mice with a TEC-specific loss of JARID2 expression had frequencies of T and B cells that were comparable to those of WT animals (Fig. 5.31B). Within the T cell compartment there was a skewing towards cells with a CD4$^+$ phenotype in lieu of CD8$^+$ T cells (36.22 % $\pm$ 2.76 vs 43.2 % $\pm$ 1.65) (Fig. 5.31C). The composition of naïve, central memory and effector memory cells within the pool of CD4$^+$ T cells was comparable for WT and *Jarid2*$^{TEC-/-}$ mice (Fig. 5.31D). In contrast, CD8$^+$ T cells displayed a skewing from naïve cells towards cells with a central memory phenotype (Fig. 5.31E), which may reflect a homeostatic mechanism to compensate for the lymphopenia of peripheral CD8$^+$ T cells.

In summary, these results suggest that the reduced frequencies of SPCD8 generated in the thymi with TEC lacking JARID2 expression, lead to reduced $CD8^+$ T cell frequencies in the periphery.

5.5.2 $CD103^+$ $ICOS^+$ T_{reg} cells are unchanged in the periphery

T_{reg} cells expressing concomitantly $ICOS^+$ $CD103^+$ cells were detected in the thymus at an increased frequency in *Jarid2*$^{TEC-/-}$ mice. ICOS and CD103 expression are acquired in peripheral lymphoid tissues in response to antigen driven activation [158]. It was therefore intriguing to establish whether T_{reg} cells positive for the expression of ICOS and CD103 could be detected at a higher frequency in the lymph nodes of mutant mice (Fig. 5.32).

The frequency of T_{reg} cells among lymph node cells was unchanged in *Jarid2*$^{TEC-/-}$ mice when compared to WT animals (Fig. 5.32B). Given the skew in the $CD4^+/CD8^+$ T cell ratio in *Jarid2*$^{TEC-/-}$ mice, the frequency of $CD4^+$ T cells was increased and the fraction of T_{reg} within $CD4^+$ T cells was slightly decreased (Fig. 5.32C).

The frequency of peripheral T_{reg} cells concomitantly expressing ICOS and CD103 was similar for WT and mutant mice. Thus, the increased presence of these cells in the thymus must reflect a preferential seeding to a stromal environment composed of TEC lacking JARID2 expression.

5.5.3 Fewer peripheral T cells in aged *Jarid2*$^{TEC-/-}$ mice

The cellularity of thymi from *Jarid2*$^{TEC-/-}$ mice aged 16-18 weeks was significantly reduced compared to WT animals reminiscent of a premature involution. I thus assessed the peripheral T cell compartment of aged *Jarid2*$^{TEC-/-}$ mice to investigate if there are detectable consequences of drastically reduced thymic cellularity. There were no apparent differences in size or cellularity between the lymph nodes isolated from WT and *Jarid2*$^{TEC-/-}$ mice (Fig. 5.32), a finding that reflects the result observed in 5 week old animals (see Fig. 5.16).

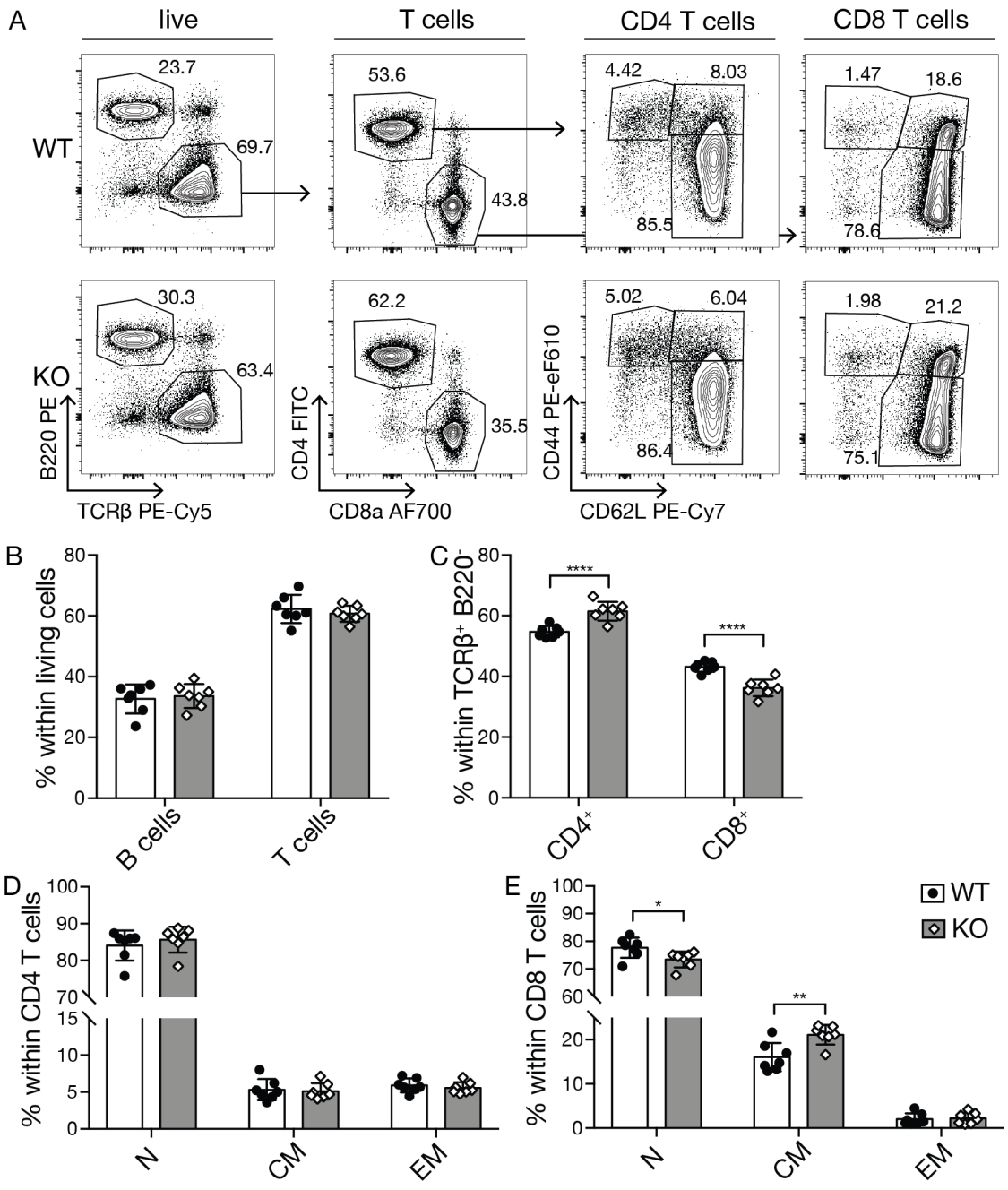

Figure 5.31: Changed ratio of CD4$^+$ to CD8$^+$ T cells in the periphery of *Jarid2$^{TEC-/-}$* mice. **(A)** Representative FACS plots display the gating strategy to assess T cells in lymph nodes. **(B)** Bar graph shows T and B cell frequencies within total lymph node cells. **(C)** Bar graph displays relative frequencies of CD4$^+$ and CD8$^+$ within the pool of T cells. **(D-E)** Bar graph depicts the frequency of CD62L$^+$ CD44^{lo} naïve (N), CD62L$^+$ CD44^{hi} central memory (CM) and CD62L$^-$ CD44^{hi} effector memory (EM) T cells within CD4$^+$ (D) and within CD8$^+$ **(E)**. Graphs represent the pooled data from two independent experiments. WT (*Jarid2$^{fl/fl}$*): n=7; KO (*Jarid2$^{TEC-/-}$*): n=7. Statistical comparison was done with two-tailed unpaired t-tests with correction for multiple comparisons. *p< 0.05, **p<0.01, ***p<0.005, ***p<0.001.

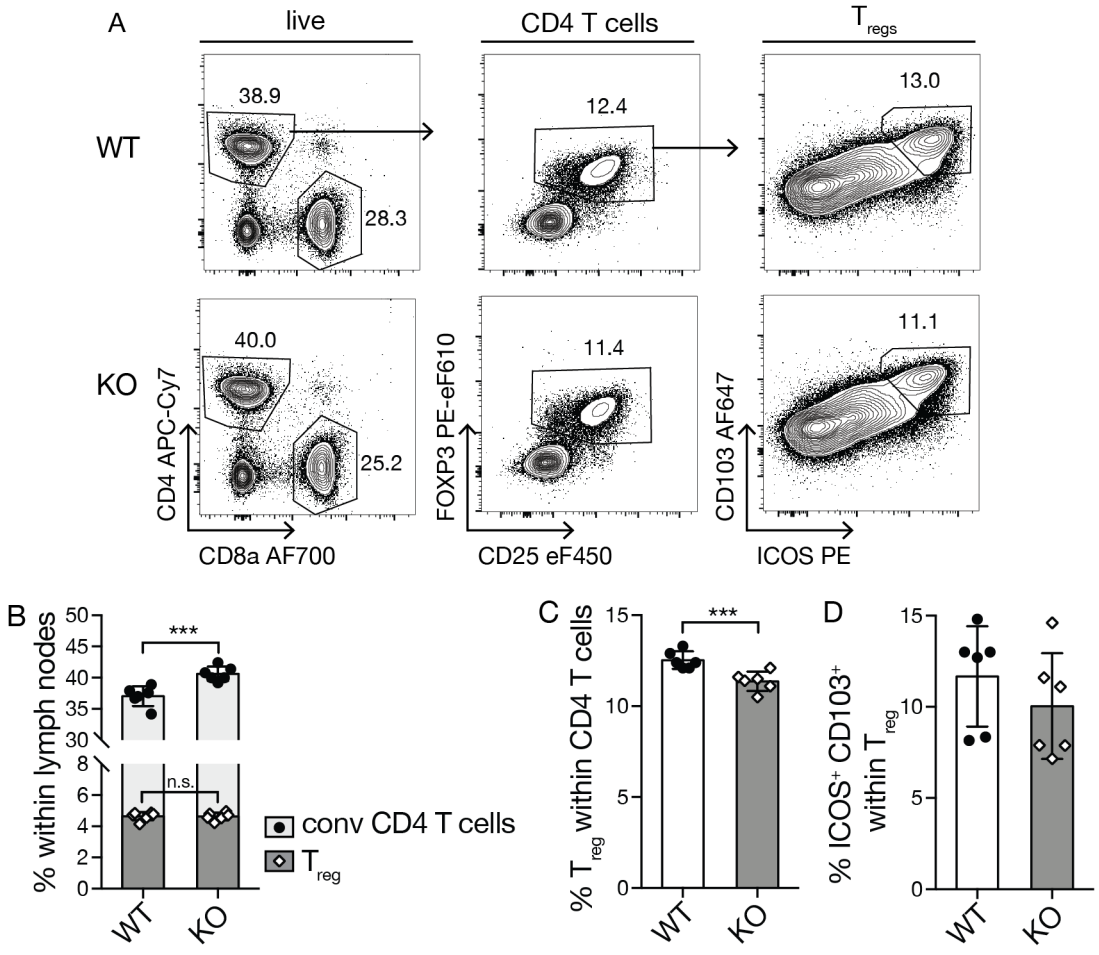

Figure 5.32: Small reduction in the frequency of T_{reg} cells within the pool of peripheral CD4$^+$ T cells in *Jarid2$^{TEC-/-}$* mice. **(A)** Representative FACS plots show the gating strategy to assess T_{reg} cells in lymph nodes. **(B)** Bar graph depicts the frequency of CD4$^+$ T cells and CD4$^+$ T_{reg} cells within total lymph node cells. **(C)** Bar graph shows the relative frequencies of T_{reg} within CD4$^+$ T cells. **(D)** Bar graph shows the relative frequencies of ICOS$^+$ CD103$^+$ T_{reg} cells within the pool of total T_{reg} cells. Graphs represent the pooled data from two independent experiments. WT (*Jarid2$^{fl/fl}$*): n=6; KO (*Jarid2$^{TEC-/-}$*): n=6. Statistical comparison was done with two-tailed unpaired t-test with correction for multiple comparisons. *p< 0.05, **p<0.01, ***p<0.005, ****p<0.001.

A closer analysis of the lymph node resident cells demonstrated a mildly reduced frequency of lymph node T cells in the aged *Jarid2$^{TEC-/-}$* animals (51.77 % ± 5.22 vs 60.23 % ± 5.07; p=0.034) (Fig. 5.33). This difference might be reflective of the decreased thymus size in aged mutant mice (see Fig. 5.16), which may correlate with a lower T cell output to the periphery.

The observed reduction of peripheral T cells in older *Jarid2$^{TEC-/-}$* animals was due to a slight decrease in both CD4$^+$ and CD8$^+$ T cells (Fig. 5.33C-D). Similar to the

result obtained in younger mice, $CD8^+$ T cells in older mutant mice displayed a skewed differentiation with fewer cell with a naïve phenotype but more central memory T cells (Fig. 5.33F). In contrast, the relative frequencies of naïve, central memory and effector memory $CD4^+$ T cells were comparable between WT and $Jarid2^{TEC-/-}$ mice (Fig. 5.33E). Peripheral T_{reg} cells could be detected at a frequency and cell surface phenotype with regards to the expression of ICOS and CD103 that was similar between WT and mutant mice (Fig. 5.34).

5.6 Summary

The lack of JARID2 expression in TEC impacts on the maturation of medullary epithelia, while cTEC remain phenotypically unchanged. Within mTEC, the frequency of $mTEC^{lo}$ is decreased while the frequency of $AIRE^+$ $mTEC^{hi}$ is increased. AIRE protein expression levels are increased in the $AIRE^+$ $mTEC^{hi}$. There is also an increased representation of the $CD86^+$ $mTEC^{hi}$ in *Jarid2*$^{TEC-/-}$ mice. mTEC with a deficiency in JARID2 further expressed higher levels of MHC-I on their surface. Taken together, the changes in mTEC maturation were mild and it remains to be elucidated whether these changes are due to alterations in differences in maturation, alteration in proliferation or cell death within the individual TEC populations.

The altered mTEC compartment in the *Jarid2*$^{TEC-/-}$ mice results in a higher frequency of negatively selected cells in the medulla affecting both SPCD4 and SPCD8. This might be due to the increased frequency of mature $AIRE^+$ mTEC, which could result in a more efficient negative selection process. T_{reg} cell generation is unchanged, however there are more $CD103^+$ $ICOS^+$ cells within the recirculating T_{reg} cells. These cells might be preferentially attracted by the higher frequency of mature mTEC and the chemokine ligands they express.

One of most prominent difference in thymocyte maturation between WT and *Jarid2*$^{TEC-/-}$ mice is the reduction of mature SPCD8 thymocytes in the medullary maturational stages, which might be caused by the increased negative selection. The functional maturation

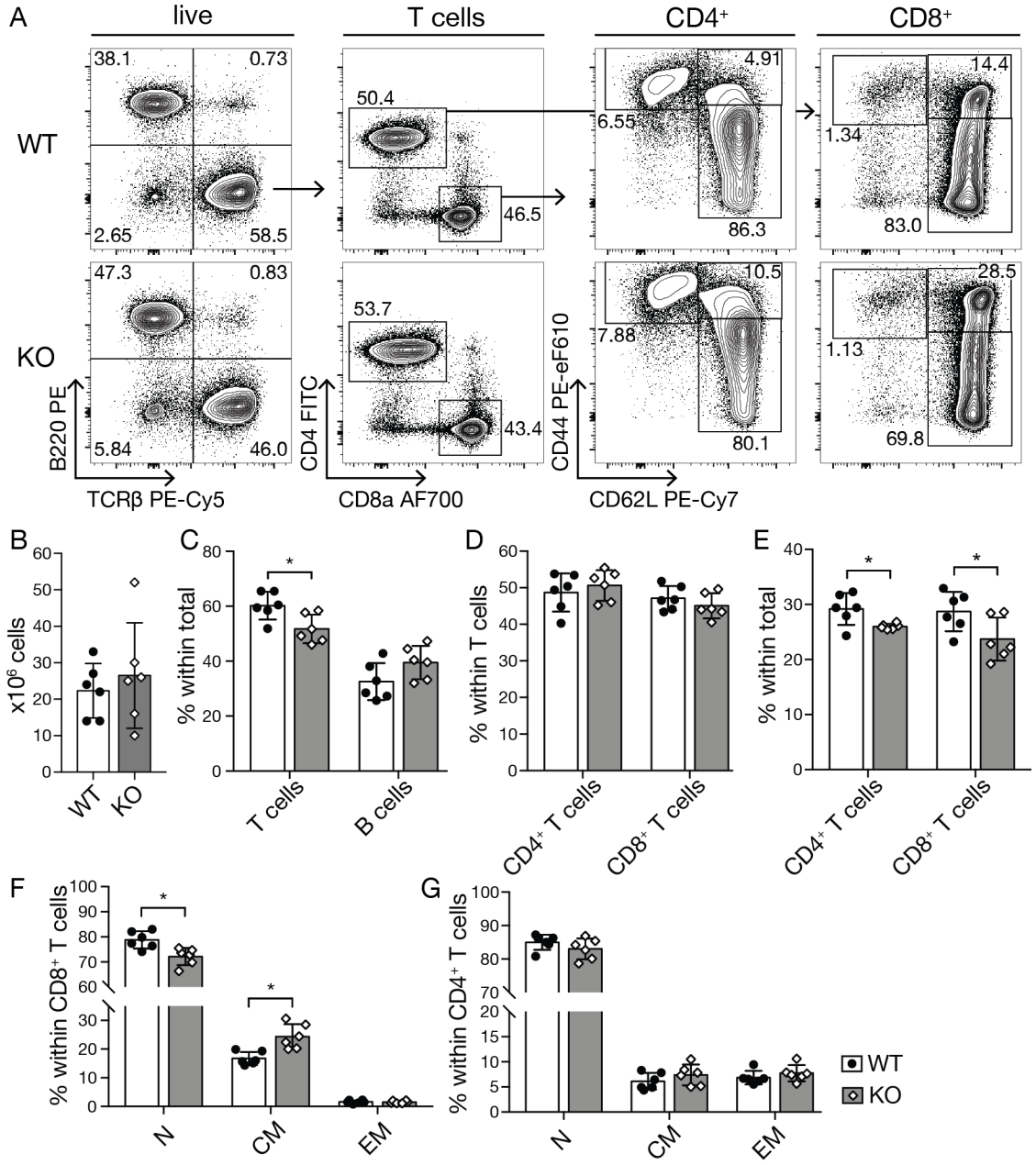

Figure 5.33: T cells are reduced in lymph nodes of 16-18 week old *Jarid2*$^{TEC-/-}$ mice. **(A)** Representative FACS plots show the gating strategy for peripheral T cell. **(B)** Bar graph shows absolute cell numbers isolated from a pool of six lymph nodes. **(C)** Bar graph shows the percentage of T and B cells within lymph nodes. **(D-E)** Bar graphs depict the frequencies of CD4$^+$ T cells and CD8$^+$ T cells within T cells (C) and within total live lymph node cells (D). **(F-G)** Bar graphs show CD62L$^+$ CD44^{lo} naïve (N), CD62L$^+$ CD44^{hi} central memory (CM) and CD62L$^-$ CD44^{hi} effector memory (EM) within CD8$^+$ (F) and CD4$^+$ (G) T cells, respectively. Graphs are pooled from 2 independent experiments. Graphs represent the pooled data from two independent experiments with mice at 16-18 weeks of age. WT (*Jarid2*$^{fl/fl}$): n=6; KO (*Jarid2*$^{TEC-/-}$): n=6). Statistical comparison was done with two-tailed unpaired t-test. *p< 0.05, **p<0.01.

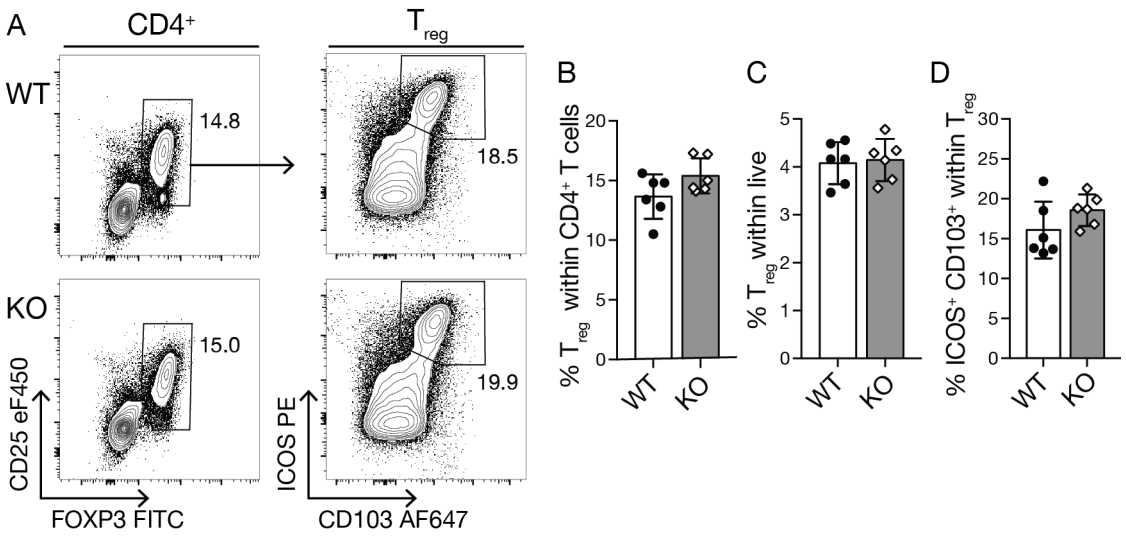

Figure 5.34: The frequency of T_{reg} cells in lymph nodes of 16-18 week old WT and *Jarid2*$^{TEC-/-}$ mice is comparable. (A) Representative FACS plots show the gating strategy to identify T_{reg} cells. **(B-C)** Bar graphs display percentage of T_{reg} cells within $CD4^+$ T cells (B) and within total live lymph node cells (C). **(D)** Bar graph demonstrates percentage of $ICOS^+$ $CD103^+$ cells within the T_{reg} cell population. Graphs represent the pooled data from two independent experiments with mice at 16-18 weeks of age. WT (*Jarid2*$^{fl/fl}$): n=6; KO (*Jarid2*$^{TEC-/-}$): n=6. Statistical comparison was done with two-tailed unpaired t-test.

of SPCD8 with regards to cytokine licensing and expression of key maturational genes is normal, which further supports the contention that the reduced frequencies are due to increased negative selection rather than due to perturbed maturation. The reduction in the CD8 lineage can also observed in the periphery of the mutant animals, where I detected a skewed distribution of T cell subsets with relatively fewer $CD8^+$ T cells in the lymph nodes. The $CD8^+$ cells in the periphery further showed a skewing towards a central memory phenotype. It is conceivable that the decreased frequency of SPCD8 leads to a reduced $CD8^+$ T cell export to the periphery, which needs to be compensated with homeostatic expansion; hence the increase in $CD8^+$ central memory cells.

The loss of JARID2 expression in TEC resulted in a reduction of total thymic cellularity in older mice, which was accompanied by a diminished mTEC cellularity and a small reduction in T cells within the lymph nodes. These changes would be in keeping with premature thymic involution and underline the importance of JARID2 expression in TEC to maintain proper thymic function over time.

			UTX/JMJD3 dKO	JARID2 KO
TEC	cTEC	Frequency within TEC	Down	-
	$mTEC^{lo}$	Frequency within mTEC	Down	Down
	$AIRE^{-}$ $mTEC^{hi}$	Frequency within mTEC	-	-
	$AIRE^{+}$ $mTEC^{hi}$	Frequency within mTEC	Up	Up
	$CD86^{+}$	Frequency within $mTEC^{hi}$	Up	Up
	AIRE expression	gMFI within $AIRE^{+}$	Down	Up
	MCHI expression	gMFI within cTEC	Down	-
		gMFI within $mTEC^{lo}$	-	Up
		gMFI within $mTEC^{hi}$	-	Up
Thymocytes	Negative selection	Wave 1a (DP)	Down	-
		Wave 1b (SPCD4)	Down	-
		Wave 1b (SPCD8)	-	-
		Wave 2a (SPCD4)	Down	Up
		Wave 2b (SPCD4)	Up	Up
		Wave 2a (SPCD8)	-	Up
		Wave 2b (SPCD8)	-	Up
	$CD103^{+}$ $ICOS^{+}$ cells	Frequency within T_{reg} cells	Up	Up
	SPCD8	Frequency of medullary SPCD8	Down	Down
	SPCD4	Frequency of medullary SPCD4	Down	-
T cells	$CD8^{+}$ T cells	Frequency within T cells	-	Down
	Central memory cells	Frequency within $CD8^{+}$ T cells	Up	Up

Table 5.1: Summary of changes caused by a TEC-specific loss of UTX/JMJD3 compared to a TEC-targeted loss of JARID2. A dash marks features that were not significantly changed. UTX/JMJD3 dKO: $Utx^{TEC-/-}$ $Jmjd3^{TEC-/-}$; JARID2 KO: $Jarid2^{TEC-/-}$.

5.7 Discussion

Epigenetic mechanisms are essential for establishing gene expression programmes that define a cell's identity. The importance of the epigenetic landscape in TEC development and function has recently become a focus of interest given the unique properties of these cells' gene expression programmes. This includes the study of histone post-translational methylation in the context of mTEC development and PGE [50, 103]. Two concepts have emerged from these studies. Firstly, in regards to PGE, it was observed that repressive histone modifications such as H3K27me3 and H3K9me3 are enriched while active marks such as H3K4me3 are depleted at the promoters of AIRE-regulated genes [50].

Furthermore, the chromatin landscape at AIRE-regulated genes is similar between mTEC^{lo} and mTEC^{hi}, which is reflected in the fact that machine learning algorithms are able to accurately predict AIRE dependency based on chromatin landmarks in both cell populations [103]. Secondly, even though the overall chromatin landscape between mTEC^{lo} and mTEC^{hi} is similar, the distribution of H3K27me3 modifications is different between these two maturational stages, reflective of H3K27me3 remodelling that might be important for mTEC maturation [103]. While these findings suggest that repressive histone modifications play a role for TEC development and biology, studies on the function of H3K27me3 have not been undertaken so far.

To investigate this question I studied mice with a TEC-targeted deficiency in histone modifiers. Additionally to the mice with a TEC-specific loss of the H3K27me2/me3 demethylases UTX and JMJD3 that I presented in the previous chapters, I also created a mouse model with a TEC-specific deficiency in JARID2. JARID2 is a cofactor of PRC2, which transfers methyl groups to H3K27 [199]. JARID2 has also been reported to associate with the H3K9 methyltransferases GLP/G9a and SETDB1 [196–198]. In the context of these complexes JARID2 is involved in establishing gene repression by either H3K27 or H3K9 methylation. The role of JARID2 mediated gene regulation has to date not been studied in the context of TEC biology. A global deficiency in JARID2 has been reported to cause thymic hypoplasia in embryos, but has not been followed up so far [92, 93].

Unpublished data from our group shows a drastic reduction of thymic cellularity and a block in mTEC maturation when core components of PRC2, i.e. EED and EZH1/2 are knocked out in TEC mediated by *Psmb11* promoter driven Cre recombinase. An even more dramatic impact on total thymic and TEC cellularity is observed when EED expression is disrupted by Cre recombinase under the control of the *Foxn1* promoter which leads to an EED deficiency one day earlier in TEC development than in the *Psmb11*-Cre system [17, 208, 209]. In contrast to these findings, the impact of a *Foxn1*-Cre-mediated loss of JARID2 expression on thymic biology was small with a normal total thymic and TEC cellularity at 5 weeks of age.

The milder impact of a JARID2 deficiency compared to a lack of the core components of the PRC2 can also be observed in embryogenesis: While a global lack of any of the core PRC2 components is early embryonically lethal [210–212], mice with a global JARID2 deficiency can survive up to birth, depending on their genetic background [88]. Further, the disruption of PRC2 function leads to a complete loss of H3K27me3 [213], while a lack in JARID2 causes changes in H3K27me3 distribution that has limited [214] to no [89, 199, 200] effect on global H3K27me3 levels.

The importance of JARID2 extends beyond the role during embryogenesis to the homeostasis of tissues. In thymocytes, *Jarid2* expression is upregulated during positive selection and a CD4-Cre driven deficiency in JARID2 decreases H3K9me3 at the *Zbtb16* locus and increases the expression of this gene, which lead to an increased generation of innate $CD8^+$ T cell development in the thymus [196]. In the case of muscle tissue, JARID2 has been shown to be crucial for the differentiation from myoblasts to myocytes through the PRC2 mediated influence on Wnt signalling, while it is dispensable for differentiated myocytes [215].

5.7.1 JARID2 as a negative regulator of mTEC maturation

Even though the changes caused by JARID2 deficiency were small in TEC, the findings were consistent and impacted thymocyte development. Thymi from $Jarid2^{TEC\text{-}/\text{-}}$ mice have a lower frequency of $mTEC^{lo}$ and higher frequency of $AIRE^+$ $mTEC^{hi}$. Thus, JARID2 can be seen as a negative regulator of mTEC maturation. It is conceivable that JARID2 inhibits the gene expression program for mTEC maturation through H3K27me3 or H3K9me3 deposition, similar to the increased differentiation in Jarid2 knockdown haematopoietic stem cells [216]. The expression of genes important for mTEC development [142] will be probed in transcriptomic data of $mTEC^{lo}$ and $mTEC^{hi}$ isolated from $Jarid2^{TEC\text{-}/\text{-}}$ mice that will be available soon.

In the older $Jarid2^{TEC\text{-}/\text{-}}$ mice, there is a small reduction in the frequency of mTEC, accompanied by a drastic reduction in total thymic cellularity compared to WT mice.

JARID2 is thus crucial for maintaining TEC integrity and function at an older age. It is possible that similar to an EED deficiency in adult haematopoietic stem cells [213], JARID2 deficiency causes an exhaustion of TEC progenitors causing a premature thymic involution in *Jarid2*$^{TEC-/-}$ mice.

The increase in more mature mTEC as a consequence of the loss of JARID2 contrasts to the effect seen in animals with a loss of EED or EZH1/2, where mTEC maturation is blocked (unpublished results). It is conceivable that the block in mTEC maturation in the EED or EZH1/2 deficiency is caused by the disruption of TEC physiology due to the complete loss of H3K27me3, while the milder effect on H3K27me3 due to the lack of JARID2 reveals the importance of PRC2 silencing during mTEC maturation. Alternatively, the contrasting effect on mTEC maturation can be interpreted as an indication that JARID2's function in TEC is potentially independent of PRC2, and maybe rather involves association with GLP/G9a.

Surprisingly, the TEC phenotype in the *Jarid2*$^{TEC-/-}$ mouse model is very similar to the one observed in the *Utx*$^{TEC-/-}$ *Jmjd3*$^{TEC-/-}$ animals which also have a lower frequency of mTEC^{lo} and more AIRE^{+} mTEC^{hi} (see Table 5.1). This seems paradoxical given that UTX/JMJD3 and JARID2 have an opposite effect on H3K27 methylation. However both the effect of JARID2 as well as UTX/JMJD3 are gene-specific. Therefore, a way to explain this finding is that JARID2 and UTX/JMJD3 control different gene sets. It is conceivable that while JARID2 negatively regulates the expression of genes that would drive maturation towards mTEC^{hi}, UTX and JMJD3 are important for a set of genes that negatively regulate mTEC maturation.

Unexpectedly, the changes induced in both mouse models attract a higher frequency of ICOS^{+} CD103^{+} T_{reg} cells to the thymus. Maybe the thymic stroma composed of more AIRE^{+} mTEC^{hi} creates more niches for this type of recirculating T_{reg} cells. It remains unclear what functions these cells have in the thymus and in both mouse models they do not have an impact on frequency of de-novo T_{reg} generation.

Despite their similar effect on mTEC maturation JARID2 and UTX/JMJD3 have an opposite effect on AIRE protein expression levels. Epigenetic mechanisms (i.e. DNA methylation and chromatin remodelling) of the *Aire* locus have been reported to be crucial for *Aire* expression [217]. Therefore, it is conceivable that histone modifiers might also be involved in the chromatin remodelling process, which would explain the finding that a loss of JARID2 enhances, while the loss of UTX/JMJD3 reduces *Aire* expression. It has to be kept in mind that the differences in AIRE expression are small, suggesting that neither UTX/JMJD3 nor JARID2 are key controllers. Further, the effect might also be caused by the regulation of other factors that are involved in regulating *Aire* expression, such as *Irf4*, *Irf8*, *Tbx21*, *Tcf7* and *Ctcfl* [217]. While the expression of these factors is unchanged in UTX/JMJD3-deficient mTEC^{hi}, they have not been probed yet in the JARID2-deficient TEC.

In the UTX/JMJD3-deficient mTEC^{hi}, AIRE-regulated gene expression was increased. Under the assumption that a lack of JARID2 decreases the H3K27me3 marks at AIRE-regulated TRA, the lack of JARID2 could have the opposite effect on PGE and lead to a reduction of AIRE-regulated PGE. As it is not expected that JARID2 deficiency causes H3K27me3 reduction across all genes, it will be important to specifically correlate transcriptomic changes with the chromatin landscape. Performing ChIP-Seq for H3K27me3 and H3K9me3 in these cells will enable to identify the mechanism of action of JARID2 in TEC. It is also conceivable that both H3K27me3 and H3K9me3 are changed simultaneously, as PRC2 and GLP/G9a have been reported to interact [218].

5.7.2 Negative selection is increased in *Jarid2$^{TEC-/-}$* mice

Even though the observed changes in TEC are small, the loss of JARID2 in TEC has an impact on thymocyte development, causing an increase in medullary negative selection and a reduced frequency of SPCD8 thymocytes. The selective reduction of CD8 thymocyte lineage reminds of the phenotype seen in mice with a TEC-specific β5t deficiency [39, 219], which causes problems in cTEC and their ability to present peptides that are important for CD8 lineage selection. However, in the *Jarid2$^{TEC-/-}$* mice, there are no phenotypic or

numerical changes in cTEC and also an assessment of the cortical steps of thymocyte development does not reveal any impact of the JARID2 deficiency. The reduction in the frequency of SPCD8 thymocytes begins in the medullary CCR7$^+$ stages and stays constant across all maturational stages until thymic egress. It is also in the medulla where there are phenotypic changes in the TEC compartment, reflected in a lower frequency of mTEC^{lo} and more mTEC^{hi} that express AIRE and CD86. Additionally, mTEC^{lo} and mTEC^{hi} express higher levels of MHC-I. Thus, the higher fraction of mature cells and the higher level of MHC-I surface expression in the medulla might provide more niches for negative selection, which in turn might be the explanation for the decreased frequency of SPCD8 thymocytes. The decrease in CD8 lineage can also be seen in the peripheral lymphoid organs.

However, the increased medullary negative selection does not only affect SPCD8 but also SPCD4 thymocytes. Since SPCD4 frequencies are not reduced in the *Jarid2*$^{TEC-/-}$ thymus, SPCD4 must be able to compensate for the increased negative selection for example by proliferating more.

5.7.3 Conclusion

The impact of a loss of JARID2 on TEC is small, especially when compared to a deficiency in the core components of PRC2. Nevertheless, JARID2 causes distinct and reproducible changes in the mTEC compartment potentially playing the role of a negative regulator of mTEC maturation. The altered JARID2-deficient TEC are unable to support proper CD8$^+$ T cell development potentially due to increased negative selection. The importance of having an intact JARID2 expression in TEC becomes even clearer in aged mice as mTEC and total thymus cellularity drop.

6

Conclusions and Future Work

Contents

6.1 Conclusions 180
6.2 Future Work 182
6.3 Final Remarks 185

6.1 Conclusions

The work presented in this thesis focused on the investigation of the role of H3K27me3 in TEC biology. This was addressed by studying two mouse models, one with a TEC-specific deficiency of the H3K27me3 demethylases UTX and JMJD3, and the other with a TEC-targeted loss of JARID2, a cofactor of the PRC2 methyltransferase complex. The aim of these mouse models was to cause changes in the H3K27me3 landscape in TEC that could then be correlated to its functional impact.

My results demonstrate that the targeted loss of UTX and JMJD3 increases AIRE-enhanced PGE. As UTX's and JMJD3's role is to demethylate H3K27me3, these results are indicative, albeit no proof, of a functional role of H3K27me3 in regulating AIRE-controlled gene expression programmes. It is possible that H3K27me3 plays a role in

targeting the AIRE protein complex to its loci and/or in stabilising it at the chromatin (see Figure 6.1). This mechanism could be similar to the role of H3K4me0, which is involved in stabilising AIRE itself at its target genes [104, 220]. However, since AIRE does not directly bind H3K27me3, the effect of this histone PTM would most likely be indirect via a binding partner of AIRE (like CHD6). In aggregate, this highlights the role of UTX and JMJD3 in negatively modulating AIRE-regulated gene expression programmes in TEC. Limiting the level of TRA expression might be advantageous to avoid adverse effects of the expression of a stochastically determined set of tissue specific genes on the cell's physiology. Notably, since the observed gene expression changes in the absence of UTX/JMJD3 were of small amplitude, it is plausible that these demethylases mainly play a role in fine-tuning the system and there are no fundamental H3K27me3 changes that UTX and JMJD3 have to establish for normal PGE.

Histone PTM as a targeting mechanism for AIRE-mediated gene transcription would account for the large variety of genes regulated by AIRE. Investigating the direct relationship of the H3K27me3 landscape and transcriptomic consequences in $mTEC^{hi}$ will provide us with valuable insight on this hypothesis. Work in progress on this aspect is summarised in the following chapter (see Chapter 6.2.1). Moreover, the role of JARID2 in the context of regulating the expression of AIRE-controlled genes will also be addressed with further experiments (see Chapter 6.2.2).

Both mouse models exhibit a normally sized and structured thymus at 4-5 weeks of age. This finding was somewhat unexpected, as UTX/JMJD3 and JARID2 have been reported to be important for establishing gene expression programmes during cell differentiation. This suggests that the transcriptional programmes allowing TEC development are largely independent of H3K27me3 regulation by these proteins. It is conceivable that alternative mechanisms to remove H3K27me3 might play a role in differentiating TEC not least because these cells are actively proliferating and are thus able to dilute the H3K27me3 marks during cell division.

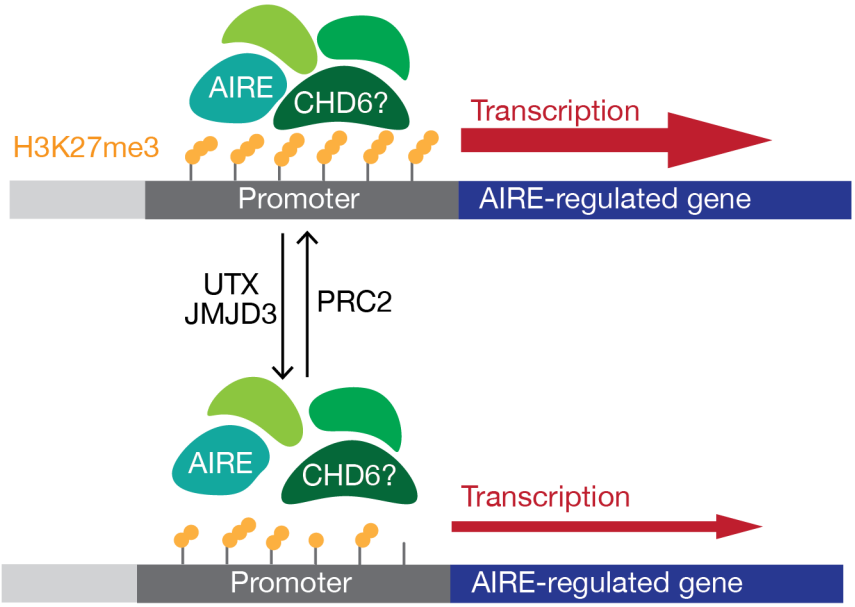

Figure 6.1: Hypothetical role of H3K27me3 in targeting or stabilising the AIRE protein complex. AIRE does not directly recognise H3K27me3 [68], however AIRE interaction partners (e.g. CHD6 [106]) may bind to H3K27me3 at the inactive promoters of genes with tissue-restricted expression. This interaction potentially targets or stabilises AIRE at its target genes and consequently the level of H3K27me3 (modulated by the demethylases UTX/JMJD3 and methyltransferase PRC2) determines the level of AIRE-regulated gene expression.

However, UTX/JMJD3 as well as JARID2 are relevant for mTEC maturation as both *Jarid2*$^{TEC-/-}$ and *Utx*$^{TEC-/-}$ *Jmjd3*$^{TEC-/-}$ mice had a small but significant increase in the frequency of mature mTEC. Given the opposite impact of UTX/JMJD3 and JARID2 on H3K27me3 it is surprising that their deficiency has a similar impact on mTEC maturation and most likely indicates that they control different sets of genes. In both mouse models, the relevance of these changes for TEC function is reflected in the fact that they cause alterations in thymocytes, affecting negative selection and decreasing the frequency of SP thymocytes. Additionally, JARID2 in TEC plays a crucial role for the maintenance of thymic function in aged *Jarid2*$^{TEC-/-}$ mice as they show a severe reduction in thymic cellularity and a decline in mTEC cellularity.

6.2 Future Work

Several question in regards to the role of H3K27me3 in TEC and in PGE require further investigation. I have outlined below how some of these questions will be or are currently

being addressed in order to follow up on the findings so far.

6.2.1 H3K27me3 ChIP-Seq in UTX/JMJD3-deficient TEC

The study on the UTX/JMJD3-deficient TEC will be extended to include H3K27me3 ChIP-Seq analysis on mTEC^{hi} and the results will be compared to the RNA-Seq dataset. This experiment will directly relate changes in the presence and distribution of H3K27me3 marks to the gene expression profile of UTX/JMJD3-deficient mTEC^{hi}. Specifically, this will demonstrate whether the increased expression of AIRE-regulated genes correlates with an alteration of H3K27me3 marks at the corresponding loci. Detecting changes in the abundance of H3K27me3 at the promoters of differentially expressed genes would give weight to the argument that transcriptomic changes are caused by the demethylase function of UTX and JMJD3. If however there are no detectable H3K27me3 changes at the loci of the differentially expressed genes, this might be reflective of demethylase-independent roles of the enzymes at these genes or an indirect mechanism that causes the gene expression change.

An important limitation of the planned analysis is that TRA are only expressed in a fraction of mTEC^{hi} and therefore population level analysis might not be reflective of the H3K27me3 landscape in cells expressing a certain gene. To get around this limitation we are considering using TRA that are expressed on the cell surface of mTEC^{hi} for cell sorting, which would allow the purification of a cell population expressing a specific TRA and a subsequent H3K27me3 ChIP-Seq analysis at bulk level. There are several AIRE-enhanced genes (e.g. *Ly6c1*) that encode surface molecules that are upregulated in their expression in the UTX/JMJD3-deficient mTEC^{hi} and could serve as potential markers for sorting cell populations that express this specific gene.

6.2.2 Transcriptomic analysis of TEC lacking JARID2 expression

Another dataset that will become available soon, but has not been sequenced in time for inclusion in the thesis, is the transcriptomic analysis of cTEC, mTEC^{lo} and mTEC^{hi}

isolated from *Jarid2*$^{TEC-/-}$ mice. With this dataset, I seek to establish which gene expression programmes are affected by the lack of JARID2 in TEC. A specific focus of this analysis will be to establish transcriptomic changes that might explain the increased frequency of mature mTEC and to reveal changes in AIRE-dependent, AIRE-enhanced and AIRE-independent PGE.

According to the proposed hypothesis, a loss of JARID2 is predicted to disrupt the expression of AIRE-regulated genes via the misplacement of H3K27me3 marks. Alternatively, it is possible that JARID2 associates with H3K9 methyltransferase complexes in TEC and thus a loss of JARID2 would lead to a reduced methylation of H3K9. Similar to H3K27me3, H3K9me3 marks are also enriched at the promoters of AIRE-regulated genes [50] and it is thus possible that either or both of these histone PTM play a role in the regulation of PGE. To differentiate between these two potential roles of JARID2 and to link transcriptional changes with changes in the histone PTM landscape, the RNA-Seq analysis of JARID2-deficient TEC will be followed up by assessing the presence of H3K27me3 and H3K9me3 marks by ChIP.

As transcriptomic changes do not always correlate to changes in protein levels, it will also be important to assess the latter by Liquid Chromatography coupled Tandem Mass Spectrometry (LC-MSMS) that has recently been established in our lab for low input TEC samples. Differences at the protein level will be more indicative of an altered repertoire for thymocyte selection.

6.2.3 Assessment of changed central tolerance

Alterations in negative selection were detected in both the *Utx*$^{TEC-/-}$ *Jmjd3*$^{TEC-/-}$ and the *Jarid2*$^{TEC-/-}$ mouse models. The relevance of a lack of UTX/JMJD3 and JARID2 in TEC for T cell repertoire selection and the establishment of central tolerance will be followed up.

To this end, these mice will be assessed for their susceptibility to autoimmunity. Since UTX/JMJD3-deficient TEC express more AIRE-enhanced TRA, it is possible that *Utx*$^{TEC-/-}$ *Jmjd3*$^{TEC-/-}$ mice have a lower susceptibility to disease when compared to

WT animals. An option to assess protection against autoimmunity is to investigate the outcome of T_{reg} depletion in *Utx*$^{TEC-/-}$ *Jmjd3*$^{TEC-/-}$ mice. To this end, bone marrow from Foxp3-DTR knock-in mice would be transplanted into sublethally irradiated RAG2-deficient *Utx*$^{TEC-/-}$ *Jmjd3*$^{TEC-/-}$ mice [221]. This allows the ablation of T_{reg} cells by injecting doxycycline. Treated mice will be monitored for the occurrence of weight loss (as a sign of autoimmunity) and organ-specific T cell infiltrates.

6.3 Final Remarks

The thymus plays the crucial role in providing functionally competent T cells which need to express antigen receptors that respond preferentially to foreign antigens but are tolerant to the body's own antigens. Any significant disturbance in the capacity of the thymus to effectively support T cell generation and select its TCR repertoire risks eliciting autoimmunity. In this thesis, the role of enzymes that impact H3K27 methylation in TEC and in the vital process of PGE has been investigated for the first time. The data presented provide an insight into the role of UTX/JMJD3 and JARID2 for mTEC maturation and function, and subsequently for thymocyte selection.

This study contributes to advancing our molecular understanding of how PGE is achieved and whether congenital or drug-mediated changes in the H3K27me3 landscape might account for an altered susceptibility to autoimmune diseases. A better understanding of the molecular mechanism directing PGE will greatly assist the design of novel diagnostic options and therapeutic opportunities, like small drug molecules that can edit central tolerance and ultimately aid the treatment of autoimmune diseases.

References

[1] J. Janeway C. A. and R. Medzhitov. “Innate immune recognition”. *Annu Rev Immunol* 20 (2002), pp. 197–216.

[2] L. Alexopoulou, A. C. Holt, R. Medzhitov, and R. A. Flavell. “Recognition of double-stranded RNA and activation of NF-kappaB by Toll-like receptor 3”. *Nature* 413.6857 (2001), pp. 732–8.

[3] L. Peiser, S. Mukhopadhyay, and S. Gordon. “Scavenger receptors in innate immunity”. *Curr Opin Immunol* 14.1 (2002), pp. 123–8.

[4] T. Boehm and J. B. Swann. “Origin and evolution of adaptive immunity”. *Annu Rev Anim Biosci* 2 (2014), pp. 259–83.

[5] S. Tonegawa, C. Steinberg, S. Dube, and A. Bernardini. “Evidence for somatic generation of antibody diversity”. *Proc Natl Acad Sci U S A* 71.10 (1974), pp. 4027–31.

[6] M. M. Davis and P. J. Bjorkman. “T-cell antigen receptor genes and T-cell recognition”. *Nature* 334.6181 (1988), pp. 395–402.

[7] J. S. Blum, P. A. Wearsch, and P. Cresswell. “Pathways of antigen processing”. *Annu Rev Immunol* 31 (2013), pp. 443–73.

[8] D. Kagi, F. Vignaux, B. Ledermann, K. Burki, V. Depraetere, S. Nagata, H. Hengartner, and P. Golstein. “Fas and Perforin Pathways as Major Mechanisms of T-Cell-Mediated Cytotoxicity”. *Science* 265.5171 (1994), pp. 528–530.

[9] I. Raphael, S. Nalawade, T. N. Eagar, and T. G. Forsthuber. “T cell subsets and their signature cytokines in autoimmune and inflammatory diseases”. *Cytokine* 74.1 (2015), pp. 5–17.

[10] A. Lanzavecchia. “Antigen-Specific Interaction between T-Cells and B-Cells”. *Nature* 314.6011 (1985), pp. 537–539.

[11] I. V. Hutchinson and H. Zola. “Antigen-reactive cell opsonization: a mechanism of antibody-mediated immune suppression”. *Cell Immunol* 36.1 (1978), pp. 161–9.

[12] J. R. Dunkelberger and W. C. Song. “Complement and its role in innate and adaptive immune responses”. *Cell Res* 20.1 (2010), pp. 34–50.

[13] G. Anderson, P. J. Lane, and E. J. Jenkinson. “Generating intrathymic microenvironments to establish T-cell tolerance”. *Nat Rev Immunol* 7.12 (2007), pp. 954–63.

[14] J. Gordon, A. R. Bennett, C. C. Blackburn, and N. R. Manley. “Gcm2 and Foxn1 mark early parathyroid- and thymus-specific domains in the developing third pharyngeal pouch”. *Mech Dev* 103.1-2 (2001), pp. 141–3.

[15] N. R. Manley and B. G. Condie. “Transcriptional regulation of thymus organogenesis and thymic epithelial cell differentiation”. *Prog Mol Biol Transl Sci* 92 (2010), pp. 103–20.

[16] C. C. Blackburn and N. R. Manley. “Developing a new paradigm for thymus organogenesis”. *Nat Rev Immunol* 4.4 (2004), pp. 278–89.

[17] G. Balciunaite, M. P. Keller, E. Balciunaite, L. Piali, S. Zuklys, Y. D. Mathieu, J. Gill, R. Boyd, D. J. Sussman, and G. A. Hollander. “Wnt glycoproteins regulate the expression of FoxN1, the gene defective in nude mice”. *Nat Immunol* 3.11 (2002), pp. 1102–8.

[18] H. J. Vaidya, A. Briones Leon, and C. C. Blackburn. "FOXN1 in thymus organogenesis and development". *Eur J Immunol* 46.8 (2016), pp. 1826–37.

[19] M. Itoi, H. Kawamoto, Y. Katsura, and T. Amagai. "Two distinct steps of immigration of hematopoietic progenitors into the early thymus anlage". *Int Immunol* 13.9 (2001), pp. 1203–11.

[20] M. Riemann, N. Andreas, M. Fedoseeva, E. Meier, D. Weih, H. Freytag, R. Schmidt-Ullrich, U. Klein, Z. Q. Wang, and F. Weih. "Central immune tolerance depends on crosstalk between the classical and alternative NF-kappa B pathways in medullary thymic epithelial cells". *Journal of Autoimmunity* 81 (2017), pp. 56–67.

[21] T. Akiyama, Y. Shimo, H. Yanai, J. Qin, D. Ohshima, Y. Maruyama, Y. Asaumi, J. Kitazawa, H. Takayanagi, J. M. Penninger, M. Matsumoto, T. Nitta, Y. Takahama, and J. Inoue. "The tumor necrosis factor family receptors RANK and CD40 cooperatively establish the thymic medullary microenvironment and self-tolerance". *Immunity* 29.3 (2008), pp. 423–37.

[22] E. Van Vliet, E. J. Jenkinson, R. Kingston, J. J. Owen, and W. Van Ewijk. "Stromal cell types in the developing thymus of the normal and nude mouse embryo". *Eur J Immunol* 15.7 (1985), pp. 675–81.

[23] D. H. Gray, N. Seach, T. Ueno, M. K. Milton, A. Liston, A. M. Lew, C. C. Goodnow, and R. L. Boyd. "Developmental kinetics, turnover, and stimulatory capacity of thymic epithelial cells". *Blood* 108.12 (2006), pp. 3777–85.

[24] Y. Takahama. "Journey through the thymus: stromal guides for T-cell development and selection". *Nature Reviews Immunology* 6.2 (2006), pp. 127–135.

[25] E. F. Lind, S. E. Prockop, H. E. Porritt, and H. T. Petrie. "Mapping precursor movement through the postnatal thymus reveals specific microenvironments supporting defined stages of early lymphoid development". *J Exp Med* 194.2 (2001), pp. 127–34.

[26] F. M. Rossi, S. Y. Corbel, J. S. Merzaban, D. A. Carlow, K. Gossens, J. Duenas, L. So, L. Yi, and H. J. Ziltener. "Recruitment of adult thymic progenitors is regulated by P-selectin and its ligand PSGL-1". *Nat Immunol* 6.6 (2005), pp. 626–34.

[27] M. A. Oettinger, D. G. Schatz, C. Gorka, and D. Baltimore. "RAG-1 and RAG-2, adjacent genes that synergistically activate V(D)J recombination". *Science* 248.4962 (1990), pp. 1517–23.

[28] S. Yamasaki and T. Saito. "Molecular basis for pre-TCR-mediated autonomous signaling". *Trends Immunol* 28.1 (2007), pp. 39–43.

[29] T. Ueno, F. Saito, D. H. Gray, S. Kuse, K. Hieshima, H. Nakano, T. Kakiuchi, M. Lipp, R. L. Boyd, and Y. Takahama. "CCR7 signals are essential for cortex-medulla migration of developing thymocytes". *J Exp Med* 200.4 (2004), pp. 493–505.

[30] S. R. Schwab, J. P. Pereira, M. Matloubian, Y. Xu, Y. Huang, and J. G. Cyster. "Lymphocyte sequestration through S1P lyase inhibition and disruption of S1P gradients". *Science* 309.5741 (2005), pp. 1735–1739.

[31] J. E. Cowan, S. M. Parnell, K. Nakamura, J. H. Caamano, P. J. Lane, E. J. Jenkinson, W. E. Jenkinson, and G. Anderson. "The thymic medulla is required for Foxp3+ regulatory but not conventional CD4+ thymocyte development". *J Exp Med* 210.4 (2013), pp. 675–81.

[32] C. S. Hsieh, H. M. Lee, and C. W. Lio. "Selection of regulatory T cells in the thymus". *Nat Rev Immunol* 12.3 (2012), pp. 157–67.

[33] B. Kyewski and L. Klein. "A central role for central tolerance". *Annu Rev Immunol* 24 (2006), pp. 571–606.

[34] L. Klein, B. Kyewski, P. M. Allen, and K. A. Hogquist. "Positive and negative selection of the T cell repertoire: what thymocytes see (and don't see)". *Nat Rev Immunol* 14.6 (2014), pp. 377–91.

[35] S. W. Rossi, W. E. Jenkinson, G. Anderson, and E. J. Jenkinson. "Clonal analysis reveals a common progenitor for thymic cortical and medullary epithelium". *Nature* 441.7096 (2006), pp. 988–91.

[36] C. C. Bleul, T. Corbeaux, A. Reuter, P. Fisch, J. S. Monting, and T. Boehm. "Formation of a functional thymus initiated by a postnatal epithelial progenitor cell". *Nature* 441.7096 (2006), pp. 992–6.

[37] I. Ohigashi, S. Zuklys, M. Sakata, C. E. Mayer, Y. Hamazaki, N. Minato, G. A. Hollander, and Y. Takahama. "Adult Thymic Medullary Epithelium Is Maintained and Regenerated by Lineage-Restricted Cells Rather Than Bipotent Progenitors". *Cell Reports* 13.7 (2015), pp. 1432–1443.

[38] C. E. Mayer, S. Zuklys, S. Zhanybekova, I. Ohigashi, H. Y. Teh, S. N. Sansom, N. Shikama-Dorn, K. Hafen, I. C. Macaulay, M. E. Deadman, C. P. Ponting, Y. Takahama, and G. A. Hollander. "Dynamic spatio-temporal contribution of single beta5t+ cortical epithelial precursors to the thymus medulla". *Eur J Immunol* 46.4 (2016), pp. 846–56.

[39] S. Murata, K. Sasaki, T. Kishimoto, S. Niwa, H. Hayashi, Y. Takahama, and K. Tanaka. "Regulation of CD8+ T cell development by thymus-specific proteasomes". *Science* 316.5829 (2007), pp. 1349–53.

[40] T. Nakagawa, W. Roth, P. Wong, A. Nelson, A. Farr, J. Deussing, J. A. Villadangos, H. Ploegh, C. Peters, and A. Y. Rudensky. "Cathepsin L: critical role in Ii degradation and CD4 T cell selection in the thymus". *Science* 280.5362 (1998), pp. 450–3.

[41] K. Honey, T. Nakagawa, C. Peters, and A. Rudensky. "Cathepsin L regulates CD4+ T cell selection independently of its effect on invariant chain: a role in the generation of positively selecting peptide ligands". *J Exp Med* 195.10 (2002), pp. 1349–58.

[42] J. Gommeaux, C. Gregoire, P. Nguessan, M. Richelme, M. Malissen, S. Guerder, B. Malissen, and A. Carrier. "Thymus-specific serine protease regulates positive selection of a subset of CD4+ thymocytes". *Eur J Immunol* 39.4 (2009), pp. 956–64.

[43] J. Derbinski, A. Schulte, B. Kyewski, and L. Klein. "Promiscuous gene expression in medullary thymic epithelial cells mirrors the peripheral self". *Nature Immunology* 2.11 (2001), pp. 1032–1039.

[44] C. N. Miller, I. Proekt, J. von Moltke, K. L. Wells, A. R. Rajpurkar, H. Wang, K. Rattay, I. S. Khan, T. C. Metzger, J. L. Pollack, A. C. Fries, W. W. Lwin, E. J. Wigton, A. V. Parent, B. Kyewski, D. J. Erle, K. A. Hogquist, L. M. Steinmetz, R. M. Locksley, and M. S. Anderson. "Thymic tuft cells promote an IL-4-enriched medulla and shape thymocyte development". *Nature* 559.7715 (2018), pp. 627–631.

[45] C. Bornstein, S. Nevo, A. Giladi, N. Kadouri, M. Pouzolles, F. Gerbe, E. David, A. Machado, A. Chuprin, B. Toth, O. Goldberg, S. Itzkovitz, N. Taylor, P. Jay, V. S. Zimmermann, J. Abramson, and I. Amit. "Single-cell mapping of the thymic stroma identifies IL-25-producing tuft epithelial cells". *Nature* 559.7715 (2018), pp. 622–626.

[46] C. Koble and B. Kyewski. "The thymic medulla: a unique microenvironment for intercellular self-antigen transfer". *J Exp Med* 206.7 (2009), pp. 1505–13.

[47] A. M. Gallegos and M. J. Bevan. "Central tolerance to tissue-specific antigens mediated by direct and indirect antigen presentation". *J Exp Med* 200.8 (2004), pp. 1039–49.

[48] T. Brocker. "The role of dendritic cells in T cell selection and survival". *J Leukoc Biol* 66.2 (1999), pp. 331–5.

[49] Z. Sarang, E. Garabuczi, G. Joos, B. Kiss, K. Toth, R. Ruhl, and Z. Szondy. "Macrophages engulfing apoptotic thymocytes produce retinoids to promote selection, differentiation, removal and replacement of double positive thymocytes". *Immunobiology* 218.11 (2013), pp. 1354–60.

[50] S. N. Sansom, N. Shikama-Dorn, S. Zhanybekova, G. Nusspaumer, I. C. Macaulay, M. E. Deadman, A. Heger, C. P. Ponting, and G. A. Hollander. "Population and single-cell genomics reveal the Aire dependency, relief from Polycomb silencing, and distribution of self-antigen expression in thymic epithelia". *Genome Research* 24.12 (2014), pp. 1918–1931.

[51] P. Brennecke, A. Reyes, S. Pinto, K. Rattay, M. Nguyen, R. Kuchler, W. Huber, B. Kyewski, and L. M. Steinmetz. "Single-cell transcriptome analysis reveals coordinated ectopic gene-expression patterns in medullary thymic epithelial cells". *Nat Immunol* 16.9 (2015), pp. 933–41.

[52] M. Meredith, D. Zemmour, D. Mathis, and C. Benoist. "Aire controls gene expression in the thymic epithelium with ordered stochasticity". *Nat Immunol* 16.9 (2015), pp. 942–9.

[53] K. Rattay, H. V. Meyer, C. Herrmann, B. Brors, and B. Kyewski. "Evolutionary conserved gene co-expression drives generation of self-antigen diversity in medullary thymic epithelial cells". *J Autoimmun* 67 (2016), pp. 65–75.

[54] M. S. Anderson, E. S. Venanzi, L. Klein, Z. B. Chen, S. P. Berzins, S. J. Turley, H. von Boehmer, R. Bronson, A. Dierich, C. Benoist, and D. Mathis. "Projection of an immunological self shadow within the thymus by the aire protein". *Science* 298.5597 (2002), pp. 1395–1401.

[55] D. Mathis and C. Benoist. "Aire". *Annu Rev Immunol* 27 (2009), pp. 287–312.

[56] A. Liston, S. Lesage, J. Wilson, L. Peltonen, and C. C. Goodnow. "Aire regulates negative selection of organ-specific T cells". *Nat Immunol* 4.4 (2003), pp. 350–4.

[57] K. Nagamine, P. Peterson, H. S. Scott, J. Kudoh, S. Minoshima, M. Heino, K. J. Krohn, M. D. Lalioti, P. E. Mullis, S. E. Antonarakis, K. Kawasaki, S. Asakawa, F. Ito, and N. Shimizu. "Positional cloning of the APECED gene". *Nat Genet* 17.4 (1997), pp. 393–8.

[58] F.-G. A. Consortium. "An autoimmune disease, APECED, caused by mutations in a novel gene featuring two PHD-type zinc-finger domains". *Nat Genet* 17.4 (1997), pp. 399–403.

[59] K. Arulanantham, J. M. Dwyer, and M. Genel. "Evidence for defective immunoregulation in the syndrome of familial candidiasis endocrinopathy". *N Engl J Med* 300.4 (1979), pp. 164–8.

[60] P. Bjorses, J. Aaltonen, N. Horelli-Kuitunen, M. L. Yaspo, and L. Peltonen. "Gene defect behind APECED: a new clue to autoimmunity". *Hum Mol Genet* 7.10 (1998), pp. 1547–53.

[61] C. Ramsey, O. Winqvist, L. Puhakka, M. Halonen, A. Moro, O. Kampe, P. Eskelin, M. Pelto-Huikko, and L. Peltonen. "Aire deficient mice develop multiple features of APECED phenotype and show altered immune response". *Human Molecular Genetics* 11.4 (2002), pp. 397–409.

[62] J. Abramson, M. Giraud, C. Benoist, and D. Mathis. "Aire's partners in the molecular control of immunological tolerance". *Cell* 140.1 (2010), pp. 123–35.

[63] J. Abramson and Y. Goldfarb. "AIRE: From promiscuous molecular partnerships to promiscuous gene expression". *European Journal of Immunology* 46.1 (2016), pp. 22–33.

[64] M. Gaetani, V. Matafora, M. Saare, D. Spiliotopoulos, L. Mollica, G. Quilici, F. Chignola, V. Mannella, C. Zucchelli, P. Peterson, A. Bachi, and G. Musco. "AIRE-PHD fingers are structural hubs to maintain the integrity of chromatin-associated interactome". *Nucleic Acids Res* 40.22 (2012), pp. 11756–68.

[65] M. Giraud, H. Yoshida, J. Abramson, P. B. Rahl, R. A. Young, D. Mathis, and C. Benoist. "Aire unleashes stalled RNA polymerase to induce ectopic gene expression in thymic epithelial cells". *Proc Natl Acad Sci U S A* 109.2 (2012), pp. 535–40.

[66] K. Zumer, K. Saksela, and B. M. Peterlin. "The mechanism of tissue-restricted antigen gene expression by AIRE". *J Immunol* 190.6 (2013), pp. 2479–82.

[67] A. S. Koh, A. J. Kuo, S. Y. Park, P. Cheung, J. Abramson, D. Bua, D. Carney, S. E. Shoelson, O. Gozani, R. E. Kingston, C. Benoist, and D. Mathis. "Aire employs a histone-binding module to mediate immunological tolerance, linking chromatin regulation with organ-specific autoimmunity". *Proc Natl Acad Sci U S A* 105.41 (2008), pp. 15878–83.

[68] T. Org, A. Rebane, K. Kisand, M. Laan, U. Haljasorg, R. Andreson, and P. Peterson. "AIRE activated tissue specific genes have histone modifications associated with inactive chromatin". *Human Molecular Genetics* 18.24 (2009), pp. 4699–4710.

[69] O. Ucar and K. Rattay. "Promiscuous Gene Expression in the Thymus: A Matter of Epigenetics, miRNA, and More?" *Front Immunol* 6 (2015), p. 93.

[70] H. Takaba, Y. Morishita, Y. Tomofuji, L. Danks, T. Nitta, N. Komatsu, T. Kodama, and H. Takayanagi. "Fezf2 Orchestrates a Thymic Program of Self-Antigen Expression for Immune Tolerance". *Cell* 163.4 (2015), pp. 975–87.

[71] J. Abramson and G. Anderson. "Thymic Epithelial Cells". *Annu Rev Immunol* (2017).

[72] S. L. Berger, T. Kouzarides, R. Shiekhattar, and A. Shilatifard. "An operational definition of epigenetics". *Genes Dev* 23.7 (2009), pp. 781–3.

[73] G. Egger, G. Liang, A. Aparicio, and P. A. Jones. "Epigenetics in human disease and prospects for epigenetic therapy". *Nature* 429.6990 (2004), pp. 457–63.

[74] C. Wu and J. R. Morris. "Genes, genetics, and epigenetics: a correspondence". *Science* 293.5532 (2001), pp. 1103–5.

[75] A. Meissner. "Epigenetic modifications in pluripotent and differentiated cells". *Nat Biotechnol* 28.10 (2010), pp. 1079–88.

[76] K. Luger, A. W. Mader, R. K. Richmond, D. F. Sargent, and T. J. Richmond. "Crystal structure of the nucleosome core particle at 2.8 angstrom resolution". *Nature* 389.6648 (1997), pp. 251–260.

[77] C. Martin and Y. Zhang. "The diverse functions of histone lysine methylation". *Nature Reviews Molecular Cell Biology* 6.11 (2005), pp. 838–849.

[78] T. Jenuwein and C. D. Allis. "Translating the histone code". *Science* 293.5532 (2001), pp. 1074–80.

[79] R. Bonasio, S. Tu, and D. Reinberg. "Molecular signals of epigenetic states". *Science* 330.6004 (2010), pp. 612–6.

[80] T. I. Lee, R. G. Jenner, L. A. Boyer, M. G. Guenther, S. S. Levine, R. M. Kumar, B. Chevalier, S. E. Johnstone, M. F. Cole, K. Isono, H. Koseki, T. Fuchikami, K. Abe, H. L. Murray, J. P. Zucker, B. Yuan, G. W. Bell, E. Herbolsheimer, N. M. Hannett, K. Sun, D. T. Odom, A. P. Otte, T. L. Volkert, D. P. Bartel, D. A. Melton, D. K. Gifford, R. Jaenisch, and R. A. Young. "Control of developmental regulators by Polycomb in human embryonic stem cells". *Cell* 125.2 (2006), pp. 301–13.

[81] H. Santos-Rosa, R. Schneider, A. J. Bannister, J. Sherriff, B. E. Bernstein, N. C. T. Emre, S. L. Schreiber, J. Mellor, and T. Kouzarides. "Active genes are tri-methylated at K4 of histone H3". *Nature* 419.6905 (2002), pp. 407–411.

[82] K. Hyun, J. Jeon, K. Park, and J. Kim. "Writing, erasing and reading histone lysine methylations". *Exp Mol Med* 49.4 (2017), e324.

[83] S. M. Kooistra and K. Helin. "Molecular mechanisms and potential functions of histone demethylases". *Nat Rev Mol Cell Biol* 13.5 (2012), pp. 297–311.

[84] A. H. F. M. Peters, J. E. Mermoud, D. O'Carroll, M. Pagani, D. Schweizer, N. Brockdorff, and T. Jenuwein. "Histone H3 lysine 9 methylation is an epigenetic imprint of facultative heterochromatin". *Nature Genetics* 30.1 (2002), pp. 77–80.

[85] B. E. Bernstein, T. S. Mikkelsen, X. H. Xie, M. Kamal, D. J. Huebert, J. Cuff, B. Fry, A. Meissner, M. Wernig, K. Plath, R. Jaenisch, A. Wagschal, R. Feil, S. L. Schreiber, and E. S. Lander. "A bivalent chromatin structure marks key developmental genes in embryonic stem cells". *Cell* 125.2 (2006), pp. 315–326.

[86] T. S. Mikkelsen, M. Ku, D. B. Jaffe, B. Issac, E. Lieberman, G. Giannoukos, P. Alvarez, W. Brockman, T. K. Kim, R. P. Koche, W. Lee, E. Mendenhall, A. O'Donovan, A. Presser, C. Russ, X. Xie, A. Meissner, M. Wernig, R. Jaenisch, C. Nusbaum, E. S. Lander, and B. E. Bernstein. "Genome-wide maps of chromatin state in pluripotent and lineage-committed cells". *Nature* 448.7153 (2007), pp. 553–60.

[87] A. Kuzmichev, K. Nishioka, H. Erdjument-Bromage, P. Tempst, and D. Reinberg. "Histone methyltransferase activity associated with a human multiprotein complex containing the Enhancer of Zeste protein". *Genes Dev* 16.22 (2002), pp. 2893–905.

[88] D. Landeira and A. G. Fisher. "Inactive yet indispensable: the tale of Jarid2". *Trends Cell Biol* 21.2 (2011), pp. 74–80.

[89] S. Sanulli, N. Justin, A. Teissandier, K. Ancelin, M. Portoso, M. Caron, A. Michaud, B. Lombard, S. T. da Rocha, J. Offer, D. Loew, N. Servant, M. Wassef, F. Burlina, S. J. Gamblin, E. Heard, and R. Margueron. "Jarid2 Methylation via the PRC2 Complex Regulates H3K27me3 Deposition during Cell Differentiation". *Mol Cell* 57.5 (2015), pp. 769–83.

[90] C. Cifuentes-Rojas, A. J. Hernandez, K. Sarma, and J. T. Lee. "Regulatory Interactions between RNA and Polycomb Repressive Complex 2". *Molecular Cell* 55.2 (2014), pp. 171–185.

[91] O. Oksuz, V. Narendra, C. H. Lee, N. Descostes, G. LeRoy, R. Raviram, L. Blumenberg, K. Karch, P. P. Rocha, B. A. Garcia, J. A. Skok, and D. Reinberg. "Capturing the Onset of PRC2-Mediated Repressive Domain Formation". *Mol Cell* 70.6 (2018), 1149–1162 e5.

[92] J. Motoyama, K. Kitajima, M. Kojima, S. Kondo, and T. Takeuchi. "Organogenesis of the liver, thymus and spleen is affected in jumonji mutant mice". *Mechanisms of Development* 66.1-2 (1997), pp. 27–37.

[93] J. Jung, M. R. Mysliwiec, and Y. Lee. "Roles of JUMONJI in mouse embryonic development". *Developmental Dynamics* 232.1 (2005), pp. 21–32.

[94] S. H. Hong, Y. W. Cho, L. R. Yu, H. Yu, T. D. Veenstra, and K. Ge. "Identification of JmjC domain-containing UTX and JMJD3 as histone H3 lysine 27 demethylases". *Proceedings of the National Academy of Sciences of the United States of America* 104.47 (2007), pp. 18439–18444.

[95] K. Agger, P. A. Cloos, J. Christensen, D. Pasini, S. Rose, J. Rappsilber, I. Issaeva, E. Canaani, A. E. Salcini, and K. Helin. "UTX and JMJD3 are histone H3K27 demethylases involved in HOX gene regulation and development". *Nature* 449.7163 (2007), pp. 731–4.

[96] T. Swigut and J. Wysocka. "H3K27 demethylases, at long last". *Cell* 131.1 (2007), pp. 29–32.

[97] R. Margueron and D. Reinberg. "The Polycomb complex PRC2 and its mark in life". *Nature* 469.7330 (2011), pp. 343–9.

[98] D. B. Yap, J. Chu, T. Berg, M. Schapira, S. W. G. Cheng, A. Moradian, R. D. Morin, A. J. Mungall, B. Meissner, M. Boyle, V. E. Marquez, M. A. Marra, R. D. Gascoyne, R. K. Humphries, C. H. Arrowsmith, G. B. Morin, and S. A. J. R. Aparicio. "Somatic mutations at EZH2 Y641 act dominantly through a mechanism of selectively altered PRC2 catalytic activity, to increase H3K27 trimethylation". *Blood* 117.8 (2011), pp. 2451–2459.

[99] J. Villasenor, W. Besse, C. Benoist, and D. Mathis. "Ectopic expression of peripheral-tissue antigens in the thymic epithelium: probabilistic, monoallelic, misinitiated". *Proc Natl Acad Sci U S A* 105.41 (2008), pp. 15854–9.

[100] M. Guerau-de-Arellano, D. Mathis, and C. Benoist. "Transcriptional impact of Aire varies with cell type". *Proc Natl Acad Sci U S A* 105.37 (2008), pp. 14011–6.

[101] R. Perniola and G. Musco. "The biophysical and biochemical properties of the autoimmune regulator (AIRE) protein". *Biochim Biophys Acta* 1842.2 (2014), pp. 326–37.

[102] I. Liiv, A. Rebane, T. Org, M. Saare, J. Maslovskaja, K. Kisand, E. Juronen, L. Valmu, M. J. Bottomley, N. Kalkkinen, and P. Peterson. "DNA-PK contributes to the phosphorylation of AIRE: importance in transcriptional activity". *Biochim Biophys Acta* 1783.1 (2008), pp. 74–83.

[103] A. E. Handel, N. Shikama-Dorn, S. Zhanybekova, S. Maio, A. N. Graedel, S. Zuklys, C. P. Ponting, and G. A. Holländer. "Comprehensively Profiling the Chromatin Architecture of Tissue Restricted Antigen Expression in Thymic Epithelial Cells Over Development". *Frontiers in Immunology* 9 (2018), p. 2120.

[104] A. S. Koh, R. E. Kingston, C. Benoist, and D. Mathis. "Global relevance of Aire binding to hypomethylated lysine-4 of histone-3". *Proc Natl Acad Sci U S A* 107.29 (2010), pp. 13016–21.

[105] R. E. Mansfield, C. A. Musselman, A. H. Kwan, S. S. Oliver, A. L. Garske, F. Davrazou, J. M. Denu, T. G. Kutateladze, and J. P. Mackay. "Plant homeodomain (PHD) fingers of CHD4 are histone H3-binding modules with preference for unmodified H3K4 and methylated H3K9". *J Biol Chem* 286.13 (2011), pp. 11779–91.

[106] R. Alfonso, T. Lutz, A. Rodriguez, J. P. Chavez, P. Rodriguez, S. Gutierrez, and A. Nieto. "CHD6 chromatin remodeler is a negative modulator of influenza virus replication that relocates to inactive chromatin upon infection". *Cellular Microbiology* 13.12 (2011), pp. 1894–1906.

[107] A. S. Koh, E. L. Miller, J. D. Buenrostro, D. M. Moskowitz, J. Wang, W. J. Greenleaf, H. Y. Chang, and G. R. Crabtree. "Rapid chromatin repression by Aire provides precise control of immune tolerance". *Nat Immunol* 19.2 (2018), pp. 162–172.

[108] S. Manna, J. K. Kim, C. Bauge, M. Cam, Y. Zhao, J. Shetty, M. S. Vacchio, E. Castro, B. Tran, L. Tessarollo, and R. Bosselut. "Histone H3 Lysine 27 demethylases Jmjd3 and Utx are required for T-cell differentiation". *Nat Commun* 6 (2015), p. 8152.

[109] C. I. Rodriguez, F. Buchholz, J. Galloway, R. Sequerra, J. Kasper, R. Ayala, A. F. Stewart, and S. M. Dymecki. "High-efficiency deleter mice show that FLPe is an alternative to Cre-loxP". *Nature Genetics* 25.2 (2000), pp. 139–140.

[110] S. Zuklys, J. Gill, M. P. Keller, M. Hauri-Hohl, S. Zhanybekova, G. Balciunaite, K. J. Na, L. T. Jeker, K. Hafen, N. Tsukamoto, T. Amagai, M. M. Taketo, W. Krenger, and G. A. Hollander. "Stabilized beta-catenin in thymic epithelial cells blocks thymus development and function". *J Immunol* 182.5 (2009), pp. 2997–3007.

[111] B. Priyadharshini, R. M. Welsh, D. L. Greiner, R. M. Gerstein, and M. A. Brehm. "Maturation-dependent licensing of naive T cells for rapid TNF production". *PLoS One* 5.11 (2010), e15038.

[112] S. Picelli, A. K. Bjorklund, O. R. Faridani, S. Sagasser, G. Winberg, and R. Sandberg. "Smart-seq2 for sensitive full-length transcriptome profiling in single cells". *Nat Methods* 10.11 (2013), pp. 1096–8.

[113] H. E. Lynch and G. D. Sempowski. "Molecular measurement of T cell receptor excision circles". *Methods Mol Biol* 979 (2013), pp. 147–59.

[114] A. M. Bolger, M. Lohse, and B. Usadel. "Trimmomatic: a flexible trimmer for Illumina sequence data". *Bioinformatics* 30.15 (2014), pp. 2114–20.

[115] A. Dobin, C. A. Davis, F. Schlesinger, J. Drenkow, C. Zaleski, S. Jha, P. Batut, M. Chaisson, and T. R. Gingeras. "STAR: ultrafast universal RNA-seq aligner". *Bioinformatics* 29.1 (2013), pp. 15–21.

[116] Y. Liao, G. K. Smyth, and W. Shi. "featureCounts: an efficient general purpose program for assigning sequence reads to genomic features". *Bioinformatics* 30.7 (2014), pp. 923–30.

[117] N. Kryuchkova-Mostacci and M. Robinson-Rechavi. "A benchmark of gene expression tissue-specificity metrics". *Brief Bioinform* 18.2 (2017), pp. 205–214.

[118] M. Lizio, J. Harshbarger, H. Shimoji, J. Severin, T. Kasukawa, S. Sahin, I. Abugessaisa, S. Fukuda, F. Hori, S. Ishikawa-Kato, C. J. Mungall, E. Arner, J. K. Baillie, N. Bertin, H. Bono, M. de Hoon, A. D. Diehl, E. Dimont, T. C. Freeman, K. Fujieda, W. Hide, R. Kaliyaperumal, T. Katayama, T. Lassmann, T. F. Meehan, K. Nishikata, H. Ono, M. Rehli, A. Sandelin, E. A. Schultes, P. A. t Hoen, Z. Tatum, M. Thompson, T. Toyoda, D. W. Wright, C. O. Daub, M. Itoh, P. Carninci, Y. Hayashizaki, A. R. Forrest, H. Kawaji, and F. consortium. "Gateways to the FANTOM5 promoter level mammalian expression atlas". *Genome Biol* 16 (2015), p. 22.

[119] H. Li and R. Durbin. "Fast and accurate short read alignment with Burrows-Wheeler transform". *Bioinformatics* 25.14 (2009), pp. 1754–60.

[120] G. Lunter and M. Goodson. "Stampy: a statistical algorithm for sensitive and fast mapping of Illumina sequence reads". *Genome Res* 21.6 (2011), pp. 936–9.

[121] A. T. Lun, K. Bach, and J. C. Marioni. "Pooling across cells to normalize single-cell RNA sequencing data with many zero counts". *Genome Biol* 17 (2016), p. 75.

[122] F. Lan, P. E. Bayliss, J. L. Rinn, J. R. Whetstine, J. K. Wang, S. Chen, S. Iwase, R. Alpatov, I. Issaeva, E. Canaani, T. M. Roberts, H. Y. Chang, and Y. Shi. "A histone H3 lysine 27 demethylase regulates animal posterior development". *Nature* 449.7163 (2007), pp. 689–94.

[123] N. Mosammaparast and Y. Shi. "Reversal of histone methylation: biochemical and molecular mechanisms of histone demethylases". *Annu Rev Biochem* 79 (2010), pp. 155–79.

[124] T. Sengoku and S. Yokoyama. "Structural basis for histone H3 Lys 27 demethylation by UTX/KDM6A". *Genes Dev* 25.21 (2011), pp. 2266–77.

[125] L. J. Walport, R. J. Hopkinson, M. Vollmar, S. K. Madden, C. Gileadi, U. Oppermann, C. J. Schofield, and C. Johansson. "Human UTY(KDM6C) Is a Male-specific N-epsilon-Methyl Lysyl Demethylase". *Journal of Biological Chemistry* 289.26 (2014), pp. 18302–18313.

[126] S. A. Miller, S. E. Mohn, and A. S. Weinmann. "Jmjd3 and UTX play a demethylase-independent role in chromatin remodeling to regulate T-box family member-dependent gene expression". *Mol Cell* 40.4 (2010), pp. 594–605.

[127] M. R. Hubner and D. L. Spector. "Role of H3K27 demethylases Jmjd3 and UTX in transcriptional regulation". *Cold Spring Harb Symp Quant Biol* 75 (2010), pp. 43–9.

[128] C. Morales Torres, A. Laugesen, and K. Helin. "Utx is required for proper induction of ectoderm and mesoderm during differentiation of embryonic stem cells". *PLoS One* 8.4 (2013), e60020.

[129] T. Burgold, N. Voituron, M. Caganova, P. P. Tripathi, C. Menuet, B. K. Tusi, F. Spreafico, M. Bevengut, C. Gestreau, S. Buontempo, A. Simeone, L. Kruidenier, G. Natoli, S. Casola, G. Hilaire, and G. Testa. "The H3K27 demethylase JMJD3 is required for maintenance of the embryonic respiratory neuronal network, neonatal breathing, and survival". *Cell Rep* 2.5 (2012), pp. 1244–58.

[130] C. Wang, J. E. Lee, Y. W. Cho, Y. Xiao, Q. Jin, C. Liu, and K. Ge. "UTX regulates mesoderm differentiation of embryonic stem cells independent of H3K27 demethylase activity". *Proc Natl Acad Sci U S A* 109.38 (2012), pp. 15324–9.

[131] T. Satoh, O. Takeuchi, A. Vandenbon, K. Yasuda, Y. Tanaka, Y. Kumagai, T. Miyake, K. Matsushita, T. Okazaki, T. Saitoh, K. Honma, T. Matsuyama, K. Yui, T. Tsujimura, D. M. Standley, K. Nakanishi, K. Nakai, and S. Akira. "The Jmjd3-Irf4 axis regulates M2 macrophage polarization and host responses against helminth infection". *Nat Immunol* 11.10 (2010), pp. 936–44.

[132] A. A. Mansour, O. Gafni, L. Weinberger, A. Zviran, M. Ayyash, Y. Rais, V. Krupalnik, M. Zerbib, D. Amann-Zalcenstein, I. Maza, S. Geula, S. Viukov, L. Holtzman, A. Pribluda, E. Canaani, S. Horn-Saban, I. Amit, N. Novershtern, and J. H. Hanna. "The H3K27 demethylase Utx regulates somatic and germ cell epigenetic reprogramming". *Nature* 488.7411 (2012), pp. 409–13.

[133] K. B. Shpargel, T. Sengoku, S. Yokoyama, and T. Magnuson. "UTX and UTY demonstrate histone demethylase-independent function in mouse embryonic development". *PLoS Genet* 8.9 (2012), e1002964.

[134] A. Greenfield, L. Carrel, D. Pennisi, C. Philippe, N. Quaderi, P. Siggers, K. Steiner, P. P. Tam, A. P. Monaco, H. F. Willard, and P. Koopman. "The UTX gene escapes X inactivation in mice and humans". *Hum Mol Genet* 7.4 (1998), pp. 737–42.

[135] R. Bosselut. "Pleiotropic Functions of H3K27Me3 Demethylases in Immune Cell Differentiation". *Trends Immunol* 37.2 (2016), pp. 102–113.

[136] X. P. Wang, M. Laan, R. Bichele, K. Kisand, H. S. Scott, and P. Peterson. "Post-Aire maturation of thymic medullary epithelial cells involves selective expression of keratinocyte-specific autoantigens". *Frontiers in Immunology* 3 (2012).

[137] T. C. Metzger, I. S. Khan, J. M. Gardner, M. L. Mouchess, K. P. Johannes, A. K. Krawisz, K. M. Skrzypczynska, and M. S. Anderson. "Lineage tracing and cell ablation identify a post-Aire-expressing thymic epithelial cell population". *Cell Rep* 5.1 (2013), pp. 166–79.

[138] S. Guerder, C. Viret, H. Luche, L. Ardouin, and B. Malissen. "Differential processing of self-antigens by subsets of thymic stromal cells". *Curr Opin Immunol* 24.1 (2012), pp. 99–104.

[139] H. S. Teh, P. Kisielow, B. Scott, H. Kishi, Y. Uematsu, H. Bluthmann, and H. von Boehmer. "Thymic major histocompatibility complex antigens and the alpha beta T-cell receptor determine the CD4/CD8 phenotype of T cells". *Nature* 335.6187 (1988), pp. 229–33.

[140] R. N. Germain. "T-cell development and the CD4-CD8 lineage decision". *Nat Rev Immunol* 2.5 (2002), pp. 309–22.

[141] J. Gerdes, H. Lemke, H. Baisch, H. H. Wacker, U. Schwab, and H. Stein. "Cell cycle analysis of a cell proliferation-associated human nuclear antigen defined by the monoclonal antibody Ki-67". *J Immunol* 133.4 (1984), pp. 1710–5.

[142] P. M. Rodrigues, P. Peterson, and N. L. Alves. "Setting Up the Perimeter of Tolerance: Insights into mTEC Physiology". *Trends Immunol* 39.1 (2018), pp. 2–5.

[143] R. J. Miragaia, X. Zhang, T. Gomes, V. Svensson, T. Ilicic, J. Henriksson, G. Kar, and T. Lonnberg. "Single-cell RNA-sequencing resolves self-antigen expression during mTEC development". *Sci Rep* 8.1 (2018), p. 685.

[144] J. A. Dahl and G. D. Gilfillan. "How low can you go? Pushing the limits of low-input ChIP-seq". *Brief Funct Genomics* 17.2 (2018), pp. 89–95.

[145] D. A. Orlando, M. W. Chen, V. E. Brown, S. Solanki, Y. J. Choi, E. R. Olson, C. C. Fritz, J. E. Bradner, and M. G. Guenther. "Quantitative ChIP-Seq normalization reveals global modulation of the epigenome". *Cell Rep* 9.3 (2014), pp. 1163–70.

[146] L. P. O'Neill, M. D. VerMilyea, and B. M. Turner. "Epigenetic characterization of the early embryo with a chromatin immunoprecipitation protocol applicable to small cell populations". *Nature Genetics* 38.7 (2006), pp. 835–841.

[147] H. O'Geen, L. Echipare, and P. J. Farnham. "Using ChIP-Seq Technology to Generate High-Resolution Profiles of Histone Modifications". *Epigenetics Protocols, Second Edition* 791 (2011), pp. 265–286.

[148] R. Ceredig and T. Rolink. "A positive look at double-negative thymocytes". *Nat Rev Immunol* 2.11 (2002), pp. 888–97.

[149] C. J. V. Van de Wiele, J. H. Marino, B. W. Murray, S. S. Vo, M. E. Whetsell, and T. K. Teague. "Thymocytes between the beta-selection and positive selection checkpoints are nonresponsive to IL-7 as assessed by STAT-5 phosphorylation". *Journal of Immunology* 172.7 (2004), pp. 4235–4244.

[150] J. S. Hale and P. J. Fink. "Back to the thymus: peripheral T cells come home". *Immunol Cell Biol* 87.1 (2009), pp. 58–64.

[151] J. S. Hale, T. E. Boursalian, G. L. Turk, and P. J. Fink. "Thymic output in aged mice". *Proc Natl Acad Sci U S A* 103.22 (2006), pp. 8447–52.

[152] N. Bosco, F. Agenes, A. G. Rolink, and R. Ceredig. "Peripheral T cell lymphopenia and concomitant enrichment in naturally arising regulatory T cells: the case of the pre-Talpha gene-deleted mouse". *J Immunol* 177.8 (2006), pp. 5014–23.

[153] K. A. Hogquist, Y. Xing, F. C. Hsu, and V. S. Shapiro. "T Cell Adolescence: Maturation Events Beyond Positive Selection". *J Immunol* 195.4 (2015), pp. 1351–7.

[154] S. R. Daley, D. Y. Hu, and C. C. Goodnow. "Helios marks strongly autoreactive CD4+ T cells in two major waves of thymic deletion distinguished by induction of PD-1 or NF-kappaB". *J Exp Med* 210.2 (2013), pp. 269–85.

[155] D. Y. Hu, R. C. Wirasinha, C. C. Goodnow, and S. R. Daley. "IL-2 prevents deletion of developing T-regulatory cells in the thymus". *Cell Death Differ* 24.6 (2017), pp. 1007–1016.

[156] X. Tai, B. Erman, A. Alag, J. Mu, M. Kimura, G. Katz, T. Guinter, T. McCaughtry, R. Etzensperger, L. Feigenbaum, D. S. Singer, and A. Singer. "Foxp3 transcription factor is proapoptotic and lethal to developing regulatory T cells unless counterbalanced by cytokine survival signals". *Immunity* 38.6 (2013), pp. 1116–28.

[157] S. Sakaguchi, T. Yamaguchi, T. Nomura, and M. Ono. "Regulatory T cells and immune tolerance". *Cell* 133.5 (2008), pp. 775–87.

[158] T. Barthlott, A. J. Bosch, C. Berkemeier, R. Nogales-Cadenas, L. T. Jeker, M. P. Keller, A. Pascual-Montano, and G. A. Hollander. "A subpopulation of CD103(pos) ICOS(pos) Treg cells occurs at high frequency in lymphopenic mice and represents a lymph node specific differentiation stage". *Eur J Immunol* 45.6 (2015), pp. 1760–71.

[159] J. E. Cowan, N. I. McCarthy, and G. Anderson. "CCR7 Controls Thymus Recirculation, but Not Production and Emigration, of Foxp3(+) T Cells". *Cell Rep* 14.5 (2016), pp. 1041–1048.

[160] N. Thiault, J. Darrigues, V. Adoue, M. Gros, B. Binet, C. Perals, B. Leobon, N. Fazilleau, O. P. Joffre, E. A. Robey, J. P. van Meerwijk, and P. Romagnoli. "Peripheral regulatory T lymphocytes recirculating to the thymus suppress the development of their precursors". *Nat Immunol* 16.6 (2015), pp. 628–34.

[161] J. E. Cowan, S. Baik, N. I. McCarthy, S. M. Parnell, A. J. White, W. E. Jenkinson, and G. Anderson. "Aire controls the recirculation of murine Foxp3(+) regulatory T-cells back to the thymus". *Eur J Immunol* 48.5 (2018), pp. 844–854.

[162] T. Yamazaki, X. O. Yang, Y. Chung, A. Fukunaga, R. Nurieva, B. Pappu, N. Martin-Orozco, H. S. Kang, L. Ma, A. D. Panopoulos, S. Craig, S. S. Watowich, A. M. Jetten, Q. Tian, and C. Dong. "CCR6 Regulates the Migration of Inflammatory and Regulatory T Cells". *Journal of Immunology* 181.12 (2008), pp. 8391–8401.

[163] O. Boyman, S. Letourneau, C. Krieg, and J. Sprent. "Homeostatic proliferation and survival of naive and memory T cells". *Eur J Immunol* 39.8 (2009), pp. 2088–94.

[164] O. Boyman, J. F. Purton, C. D. Surh, and J. Sprent. "Cytokines and T-cell homeostasis". *Curr Opin Immunol* 19.3 (2007), pp. 320–6.

[165] J. Nikolich-Zugich. "Ageing and life-long maintenance of T-cell subsets in the face of latent persistent infections". *Nature Reviews Immunology* 8.7 (2008), pp. 512–522.

[166] A. W. Goldrath and M. J. Bevan. "Low-affinity ligands for the TCR drive proliferation of mature CD8+ T cells in lymphopenic hosts". *Immunity* 11.2 (1999), pp. 183–90.

[167] T. E. Boursalian, J. Golob, D. M. Soper, C. J. Cooper, and P. J. Fink. "Continued maturation of thymic emigrants in the periphery". *Nat Immunol* 5.4 (2004), pp. 418–25.

[168] T. J. Friesen, Q. Ji, and P. J. Fink. "Recent thymic emigrants are tolerized in the absence of inflammation". *J Exp Med* 213.6 (2016), pp. 913–20.

[169] F. C. Hsu, M. J. Shapiro, M. W. Chen, D. C. McWilliams, L. M. Seaburg, S. N. Tangen, and V. S. Shapiro. "Immature recent thymic emigrants are eliminated by complement". *J Immunol* 193.12 (2014), pp. 6005–15.

[170] C. J. Cooper, M. T. Orr, C. J. McMahan, and P. J. Fink. "T cell receptor revision does not solely target recent thymic emigrants". *Journal of Immunology* 171.1 (2003), pp. 226–233.

[171] M. D. Hazenberg, J. A. Borghans, R. J. de Boer, and F. Miedema. "Thymic output: a bad TREC record". *Nat Immunol* 4.2 (2003), pp. 97–9.

[172] P. Ye and D. E. Kirschner. "Reevaluation of T cell receptor excision circles as a measure of human recent thymic emigrants". *J Immunol* 168.10 (2002), pp. 4968–79.

[173] C. S. Hsieh, Y. Liang, A. J. Tyznik, S. G. Self, D. Liggitt, and A. Y. Rudensky. "Recognition of the peripheral self by naturally arising CD25+ CD4+ T cell receptors". *Immunity* 21.2 (2004), pp. 267–77.

[174] D. L. Mueller. "Mechanisms maintaining peripheral tolerance". *Nat Immunol* 11.1 (2010), pp. 21–7.

[175] R. J. Martinez, N. Zhang, S. R. Thomas, S. L. Nandiwada, M. K. Jenkins, B. A. Binstadt, and D. L. Mueller. "Arthritogenic self-reactive CD4+ T cells acquire an FR4hiCD73hi anergic state in the presence of Foxp3+ regulatory T cells". *J Immunol* 188.1 (2012), pp. 170–81.

[176] L. A. Kalekar, S. E. Schmiel, S. L. Nandiwada, W. Y. Lam, L. O. Barsness, N. Zhang, G. L. Stritesky, D. Malhotra, K. E. Pauken, J. L. Linehan, M. G. O'Sullivan, B. T. Fife, K. A. Hogquist, M. K. Jenkins, and D. L. Mueller. "CD4(+) T cell anergy prevents autoimmunity and generates regulatory T cell precursors". *Nat Immunol* 17.3 (2016), pp. 304–14.

[177] S. Zuklys, C. E. Mayer, S. Zhanybekova, H. E. Stefanski, G. Nusspaumer, J. Gill, T. Barthlott, S. Chappaz, T. Nitta, J. Dooley, R. Nogales-Cadenas, Y. Takahama, D. Finke, A. Liston, B. R. Blazar, A. Pascual-Montano, and G. A. Hollander. "MicroRNAs control the maintenance of thymic epithelia and their competence for T lineage commitment and thymocyte selection". *J Immunol* 189.8 (2012), pp. 3894–904.

[178] M. W. Dobenecker, J. K. Kim, J. Marcello, T. C. Fang, R. Prinjha, R. Bosselut, and A. Tarakhovsky. "Coupling of T cell receptor specificity to natural killer T cell development by bivalent histone H3 methylation". *J Exp Med* 212.3 (2015), pp. 297–306.

[179] C. Z. Jiang and B. F. Pugh. "Nucleosome positioning and gene regulation: advances through genomics". *Nature Reviews Genetics* 10.3 (2009), pp. 161–172.

[180] T. Tamura, M. Smith, T. Kanno, H. Dasenbrock, A. Nishiyama, and K. Ozato. "Inducible deposition of the histone variant H3.3 in interferon-stimulated genes". *J Biol Chem* 284.18 (2009), pp. 12217–25.

[181] P. Iglesias and J. J. Diez. "Management of endocrine disease: a clinical update on tumor-induced hypoglycemia". *Eur J Endocrinol* 170.4 (2014), R147–57.

[182] A. Rotem, O. Ram, N. Shoresh, R. A. Sperling, A. Goren, D. A. Weitz, and B. E. Bernstein. "Single-cell ChIP-seq reveals cell subpopulations defined by chromatin state". *Nat Biotechnol* 33.11 (2015), pp. 1165–72.

[183] F. Tie, R. Banerjee, P. A. Conrad, P. C. Scacheri, and P. J. Harte. "Histone demethylase UTX and chromatin remodeler BRM bind directly to CBP and modulate acetylation of histone H3 lysine 27". *Mol Cell Biol* 32.12 (2012), pp. 2323–34.

[184] E. L. Pearce, A. C. Mullen, G. A. Martins, C. M. Krawczyk, A. S. Hutchins, V. P. Zediak, M. Banica, C. B. DiCioccio, D. A. Gross, C. A. Mao, H. Shen, N. Cereb, S. Y. Yang, T. Lindsten, J. Rossant, C. A. Hunter, and S. L. Reiner. "Control of effector CD8+ T cell function by the transcription factor Eomesodermin". *Science* 302.5647 (2003), pp. 1041–3.

[185] K. M. Arcipowski, C. A. Martinez, and P. Ntziachristos. "Histone demethylases in physiology and cancer: a tale of two enzymes, JMJD3 and UTX". *Curr Opin Genet Dev* 36 (2016), pp. 59–67.

[186] W. Zhao, Q. Li, S. Ayers, Y. Gu, Z. Shi, Q. Zhu, Y. Chen, H. Y. Wang, and R. F. Wang. "Jmjd3 inhibits reprogramming by upregulating expression of INK4a/Arf and targeting PHF20 for ubiquitination". *Cell* 152.5 (2013), pp. 1037–50.

[187] L. Yang, L. S. Song, X. F. Liu, Q. Xia, L. G. Bai, L. Gao, G. Q. Gao, Y. Wang, Z. Y. Wei, C. L. Bai, and G. P. Li. "The Maternal Effect Genes UTX and JMJD3 Play Contrasting Roles in Mus musculus Preimplantation Embryo Development". *Sci Rep* 6 (2016), p. 26711.

[188] S. Lee, J. W. Lee, and S. K. Lee. "UTX, a Histone H3-Lysine 27 Demethylase, Acts as a Critical Switch to Activate the Cardiac Developmental Program". *Developmental Cell* 22.1 (2012), pp. 25–37.

[189] F. Zhang, L. Xu, L. Xu, Q. Xu, G. Karsenty, and C. D. Chen. "Histone demethylase JMJD3 is required for osteoblast differentiation in mice". *Sci Rep* 5 (2015), p. 13418.

[190] F. De Santa, M. G. Totaro, E. Prosperini, S. Notarbartolo, G. Testa, and G. Natoli. "The histone H3 lysine-27 demethylase Jmjd3 links inflammation to inhibition of polycomb-mediated gene silencing". *Cell* 130.6 (2007), pp. 1083–94.

[191] J. A. Anderton, S. Bose, M. Vockerodt, K. Vrzalikova, W. Wei, M. Kuo, K. Helin, J. Christensen, M. Rowe, P. G. Murray, and C. B. Woodman. "The H3K27me3 demethylase, KDM6B, is induced by Epstein-Barr virus and over-expressed in Hodgkin's Lymphoma". *Oncogene* 30.17 (2011), pp. 2037–2043.

[192] F. De Santa, V. Narang, Z. H. Yap, B. K. Tusi, T. Burgold, L. Austenaa, G. Bucci, M. Caganova, S. Notarbartolo, S. Casola, G. Testa, W. K. Sung, C. L. Wei, and G. Natoli. "Jmjd3 contributes to the control of gene expression in LPS-activated macrophages". *EMBO J* 28.21 (2009), pp. 3341–52.

[193] P. Ntziachristos, A. Tsirigos, G. G. Welstead, T. Trimarchi, S. Bakogianni, L. Xu, E. Loizou, L. Holmfeldt, A. Strikoudis, B. King, J. Mullenders, J. Becksfort, J. Nedjic, E. Paietta, M. S. Tallman, J. M. Rowe, G. Tonon, T. Satoh, L. Kruidenier, R. Prinjha, S. Akira, P. Van Vlierberghe, A. A. Ferrando, R. Jaenisch, C. G. Mullighan, and I. Aifantis. "Contrasting roles of histone 3 lysine 27 demethylases in acute lymphoblastic leukaemia". *Nature* 514.7523 (2014), pp. 513–7.

[194] J. Van der Meulen, V. Sanghvi, K. Mavrakis, K. Durinck, F. Fang, F. Matthijssens, P. Rondou, M. Rosen, T. Pieters, P. Vandenberghe, E. Delabesse, T. Lammens, B. De Moerloose, B. Menten, N. Van Roy, B. Verhasselt, B. Poppe, Y. Benoit, T. Taghon, A. M. Melnick, F. Speleman, H. G. Wendel, and P. Van Vlierberghe. "The H3K27me3 demethylase UTX is a gender-specific tumor suppressor in T-cell acute lymphoblastic leukemia". *Blood* 125.1 (2015), pp. 13–21.

[195] G. G. Welstead, M. P. Creyghton, S. Bilodeau, A. W. Cheng, S. Markoulaki, R. A. Young, and R. Jaenisch. "X-linked H3K27me3 demethylase Utx is required for embryonic development in a sex-specific manner". *Proceedings of the National Academy of Sciences of the United States of America* 109.32 (2012), pp. 13004–13009.

[196] R. M. Pereira, G. J. Martinez, I. Engel, F. Cruz-Guilloty, B. A. Barboza, A. Tsagaratou, C. W. J. Lio, L. J. Berg, Y. Lee, M. Kronenberg, H. S. Bandukwala, and A. Rao. "Jarid2 is induced by TCR signalling and controls iNKT cell maturation". *Nature Communications* 5 (2014).

[197] H. Shirato, S. Ogawa, K. Nakajima, M. Inagawa, M. Kojima, M. Tachibana, Y. Shinkai, and T. Takeuchi. "A jumonji (Jarid2) protein complex represses cyclin D1 expression by methylation of histone H3-K9". *J Biol Chem* 284.2 (2009), pp. 733–9.

[198] M. R. Mysliwiec, C. D. Carlson, J. Tietjen, H. Hung, A. Z. Ansari, and Y. Lee. "Jarid2 (Jumonji, AT rich interactive domain 2) regulates NOTCH1 expression via histone modification in the developing heart". *J Biol Chem* 287.2 (2012), pp. 1235–41.

[199] G. Li, R. Margueron, M. Ku, P. Chambon, B. E. Bernstein, and D. Reinberg. "Jarid2 and PRC2, partners in regulating gene expression". *Genes Dev* 24.4 (2010), pp. 368–80.

[200] X. Shen, W. Kim, Y. Fujiwara, M. D. Simon, Y. Liu, M. R. Mysliwiec, G. C. Yuan, Y. Lee, and S. H. Orkin. "Jumonji modulates polycomb activity and self-renewal versus differentiation of stem cells". *Cell* 139.7 (2009), pp. 1303–14.

[201] N. Zhang and Y. W. He. "An essential role for c-FLIP in the efficient development of mature T lymphocytes". *J Exp Med* 202.3 (2005), pp. 395–404.

[202] H. H. Liu, M. Xie, M. D. Schneider, and Z. J. Chen. "Essential role of TAK1 in thymocyte development and activation". *Proc Natl Acad Sci U S A* 103.31 (2006), pp. 11677–82.

[203] S. Sato, H. Sanjo, T. Tsujimura, J. Ninomiya-Tsuji, M. Yamamoto, T. Kawai, O. Takeuchi, and S. Akira. "TAK1 is indispensable for development of T cells and prevention of colitis by the generation of regulatory T cells". *International Immunology* 18.10 (2006), pp. 1405–1411.

[204] M. Schmidt-Supprian, G. Courtois, J. Tian, A. J. Coyle, A. Israel, K. Rajewsky, and M. Pasparakis. "Mature T cells depend on signaling through the IKK complex". *Immunity* 19.3 (2003), pp. 377–389.

[205] M. Matloubian, C. G. Lo, G. Cinamon, M. J. Lesneski, Y. Xu, V. Brinkmann, M. L. Allende, R. L. Proia, and J. G. Cyster. "Lymphocyte egress from thymus and peripheral lymphoid organs is dependent on S1P receptor 1". *Nature* 427.6972 (2004), pp. 355–60.

[206] Y. Xing, X. Wang, S. C. Jameson, and K. A. Hogquist. "Late stages of T cell maturation in the thymus involve NF-kappaB and tonic type I interferon signaling". *Nat Immunol* 17.5 (2016), pp. 565–73.

[207] D. Y. Hu, J. Y. Yap, R. C. Wirasinha, D. R. Howard, C. C. Goodnow, and S. R. Daley. "A timeline demarcating two waves of clonal deletion and Foxp3 upregulation during thymocyte development". *Immunol Cell Biol* 94.4 (2016), pp. 357–66.

[208] N. Singarapu, H. F. Xie, S. Orkin, and E. Richie. "Targeted deletion of Eed arrests thymus development". *Journal of Immunology* 194 (2015).

[209] A. M. Ripen, T. Nitta, S. Murata, K. Tanaka, and Y. Takahama. "Ontogeny of thymic cortical epithelial cells expressing the thymoproteasome subunit beta5t". *Eur J Immunol* 41.5 (2011), pp. 1278–87.

[210] D. O'Carroll, S. Erhardt, M. Pagani, S. C. Barton, M. A. Surani, and T. Jenuwein. "The polycomb-group gene Ezh2 is required for early mouse development". *Mol Cell Biol* 21.13 (2001), pp. 4330–6.

[211] C. Faust, A. Schumacher, B. Holdener, and T. Magnuson. "The eed mutation disrupts anterior mesoderm production in mice". *Development* 121.2 (1995), pp. 273–85.

[212] D. Pasini, A. P. Bracken, M. R. Jensen, E. Lazzerini Denchi, and K. Helin. "Suz12 is essential for mouse development and for EZH2 histone methyltransferase activity". *EMBO J* 23.20 (2004), pp. 4061–71.

[213] H. Xie, J. Xu, J. H. Hsu, M. Nguyen, Y. Fujiwara, C. Peng, and S. H. Orkin. "Polycomb repressive complex 2 regulates normal hematopoietic stem cell function in a developmental-stage-specific manner". *Cell Stem Cell* 14.1 (2014), pp. 68–80.

[214] D. Pasini, P. A. C. Cloos, J. Walfridsson, L. Olsson, J. P. Bukowski, J. V. Johansen, M. Bak, N. Tommerup, J. Rappsilber, and K. Helin. "JARID2 regulates binding of the Polycomb repressive complex 2 to target genes in ES cells". *Nature* 464.7286 (2010), 306–U193.

[215] E. Cho, M. R. Mysliwiec, C. D. Carlson, A. Ansari, R. J. Schwartz, and Y. Lee. "Cardiac-specific developmental and epigenetic functions of Jarid2 during embryonic development". *J Biol Chem* 293.30 (2018), pp. 11659–11673.

[216] S. A. Kinkel, R. Galeev, C. Flensburg, A. Keniry, K. Breslin, O. Gilan, S. Lee, J. Liu, K. Chen, L. J. Gearing, D. L. Moore, W. S. Alexander, M. Dawson, I. J. Majewski, A. Oshlack, J. Larsson, and M. E. Blewitt. "Jarid2 regulates hematopoietic stem cell function by acting with polycomb repressive complex 2". *Blood* (2015).

[217] Y. Herzig, S. Nevo, C. Bornstein, M. R. Brezis, S. Ben-Hur, A. Shkedy, M. Eisenberg-Bord, B. Levi, M. Delacher, Y. Goldfarb, E. David, L. Weinberger, S. Viukov, S. Ben-Dor, M. Giraud, J. H. Hanna, A. Breiling, F. Lyko, I. Amit, M. Feuerer, and J. Abramson. "Transcriptional programs that control expression of the autoimmune regulator gene Aire". *Nature Immunology* 18.2 (2017), pp. 161–172.

[218] C. Mozzetta, J. Pontis, L. Fritsch, P. Robin, M. Portoso, C. Proux, R. Margueron, and S. Ait-Si-Ali. "The histone H3 lysine 9 methyltransferases G9a and GLP regulate polycomb repressive complex 2-mediated gene silencing". *Mol Cell* 53.2 (2014), pp. 277–89.

[219] T. Nitta, I. Ohigashi, and Y. Takahama. "The development of T lymphocytes in fetal thymus organ culture". *Methods Mol Biol* 946 (2013), pp. 85–102.

[220] A. J. Ruthenburg, C. D. Allis, and J. Wysocka. "Methylation of lysine 4 on histone H3: intricacy of writing and reading a single epigenetic mark". *Mol Cell* 25.1 (2007), pp. 15–30.

[221] J. M. Kim, J. P. Rasmussen, and A. Y. Rudensky. "Regulatory T cells prevent catastrophic autoimmunity throughout the lifespan of mice". *Nat Immunol* 8.2 (2007), pp. 191–7.

A

Appendix

Supplementary Figures

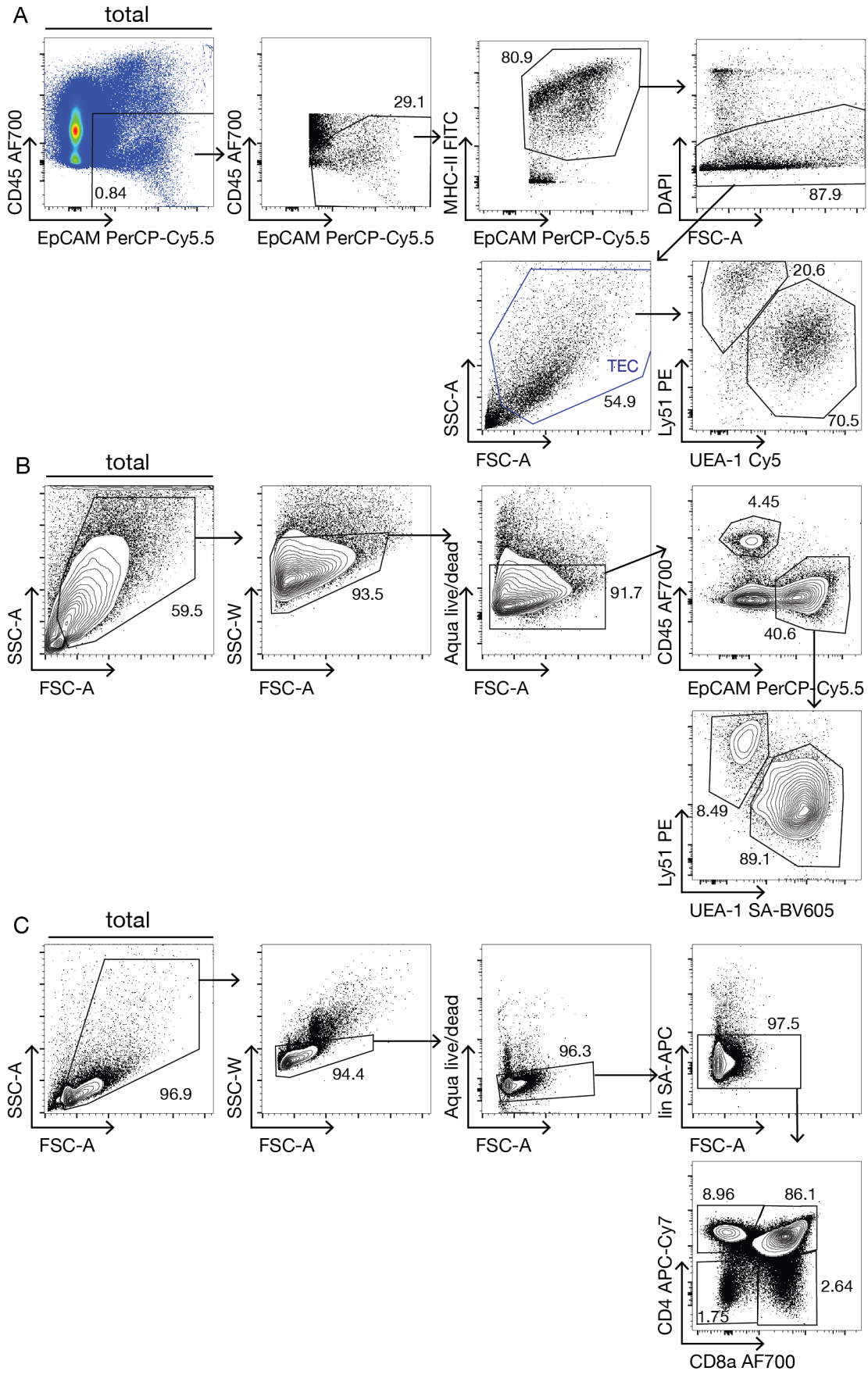
A
total
CD45 AF700
EpCAM PerCP-Cy5.5
0.84
29.1
80.9
MHC-II FITC
DAPI
87.9
FSC-A
SSC-A
TEC
54.9
20.6
Ly51 PE
70.5
UEA-1 Cy5
B
total
SSC-A
FSC-A
59.5
SSC-W
93.5
Aqua live/dead
91.7
4.45
CD45 AF700
40.6
8.49
89.1
UEA-1 SA-BV605
C
total
96.9
94.4
96.3
lin SA-APC
97.5
CD4 APC-Cy7
8.96
86.1
2.64
1.75
CD8a AF700

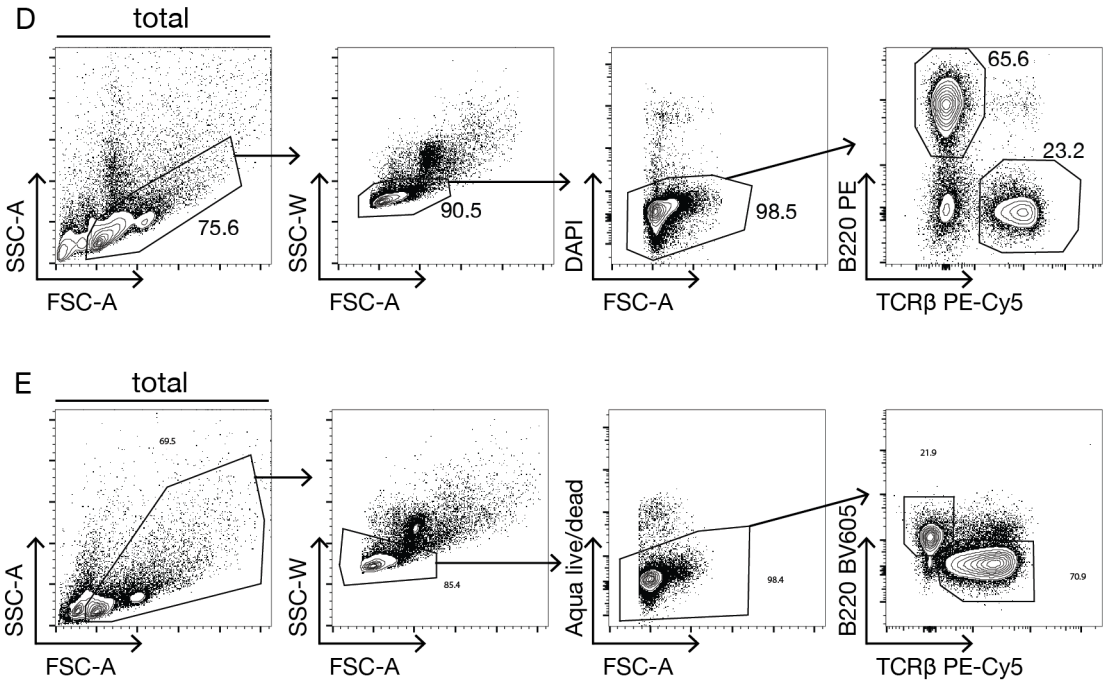

Figure A.1: Basic gating strategies. **(A)** Basic gating strategy for TEC without $CD45^+$-depletion: Total cells were gated for $EpCAM^+$ $CD45^-$, then for $MHC\text{-}II^+$. Dead cells were excluded by DAPI. Subsequently, cells were gated according to FSC-A and SSC-A. **(B)** Basic gating strategy for $CD45^+$ depleted TEC: Total cells were gated according to FSC-A and SSC-A, doublets were excluded with SSC-W. Aqua live/dead was used to exclude dead cells. Subsequently, TEC were identified by gating for $EpCAM^+$ $CD45^-$. **(C)** Basic gating strategy for thymocytes: Total cells were gated according to FSC-A and SSC-A, doublets were excluded with SSC-W. When possible Aqua live/dead was used to exclude dead cells. A lineage dump channel was used in the FACS panel for assessing DN cells. Dump channel included antibodies against CD11b, CD11c, Gr-1, CD19, CD49b, F4/80, NK1.1, GL3 and TER119. **(D)** Basic gating strategy for splenocytes: Total cells were gated according to FSC-A and SSC-A, doublets were excluded with SSC-W. DAPI or Aqua live/dead was used to exclude dead cells. **(E)** Basic gating strategy for lymph nodes: Total cells were gated according to FSC-A and SSC-A, doublets were excluded with SSC-W. Aqua live/dead was used to exclude dead cells. Gating strategies show representative FACS plots from WT female mice 4-5 weeks of age.